THE CHEMISTRY OF ATHEROGENIC HIGH DENSITY LIPOPROTEIN

A Dissertation

by

D'VESHARRONNE J. MOORE

Submitted to the Office of Graduate Studies of
Texas A&M University
in partial fulfillment of the requirements for the degree of

DOCTOR OF PHILOSOPHY

May 2011

Major Subject: Chemistry

The Chemistry of Atherogenic High Density Lipoprotein

THE CHEMISTRY OF ATHEROGENIC HIGH DENSITY LIPOPROTEIN

A Dissertation

by

D'VESHARRONNE J. MOORE

Submitted to the Office of Graduate Studies of
Texas A&M University
in partial fulfillment of the requirements for the degree of

DOCTOR OF PHILOSOPHY

Approved by:

Chair of Committee,	Ronald Macfarlane
Committee Members,	Rosemary Walzem
	David Barondeau
	Christian Hilty
Head of Department,	David Russell

May 2011

Major Subject: Chemistry

ABSTRACT

The Chemistry of Atherogenic High Density Lipoprotein. (May 2011)

D'Vesharronne J. Moore, B.S., Texas Southern University

Chair of Advisory Committee: Dr. Ronald Macfarlane

An array of analytical methods including density gradient ultracentrifugation, capillary electrophoresis, and matrix-assisted laser desorption ionization mass spectrometry (MALDI-MS), were utilized to analyze serum high density lipoprotein (HDL) subfractions from two cohorts of normolipidemic individuals, which included subjects with diagnosed coronary artery disease (CAD), and angiographically proven non-CAD controls. These methods collectively provided characteristic information about the two populations of individuals including composition, electrophoretic mobilities, molecular weights, isoforms, and post-translational modifications of HDL apolipoproteins. This information proved useful in identifying potential biomarkers for CAD risk and understanding the biological functions of a novel atherogenic HDL phenotype in individuals with CAD.

Through the implementation of the aforementioned methodologies, new isoforms of apoC-I were identified. MALDI-MS detected a shifting of approximately 90 Da in the mass to charge ratios corresponding to apoC-I peaks in the serum subfractions from all CAD cohort patients. This shifting was not observed in the non-CAD cohort which displayed apoC-I peaks in accordance with the known mass of this protein. In addition to the shifting observed in the CAD cohort, some CAD patients showed further modifications of apoC-I that were indicative of oxidative processes.

Interestingly, one patient, who has not been diagnosed with CAD and has a family history of the disease, contained the apoC-I isoforms. This feature could underlie

this subject's known family history of CAD and serve as an initial screening that could indicate the future development of CAD in this individual.

Through collaborative work with Johns Hopkins University, it was initially observed that apoC-I enriched HDL induced apoptosis of aortic smooth muscle cells. Conversely, apoC-I depleted HDL induced minimal to no apoptosis which led to the hypothesis that apoC-I is a contributor to atherogenic HDL and is a potential risk factor for CAD. Further collaborative work with Johns Hopkins assessed the apoptosis levels induced by HDL from both cohorts of patients. A distinct difference in apoptosis was identified between the two cohorts. High density lipoprotein subfractions from subjects in the CAD cohort, all of which contained the apoC-I isoforms, induced marked apoptosis compared to the non-CAD controls. These results further supported the hypothesis that apoC-I compromises the functionality of HDL and showed that through the induction of apoptosis, apoC-I can contribute to the destabilization of atherosclerotic plaque and the acceleration of CAD.

DEDICATION

"And whatsoever ye do, do it heartily, as to the Lord and not unto men; knowing that of the Lord ye shall receive the reward of inheritance for ye serve the Lord Christ."
Colossians 3:23 – 24, KJV

To my parents David and Sharon Moore and brother David Jr., for their enormous support, constant encouragement, and for providing me with a strong academic foundation upon which I could build. In memory of my loving grandfather Oscar Milling Jr., whose battle against heart disease fueled my passion to investigate the disease.

ACKNOWLEDGEMENTS

I, first and foremost, acknowledge God for the strength and determination to work for years to accomplish this goal through His grace. I would like to express my appreciation to all of the individuals and organizations that allowed this research to be possible. I would like to acknowledge my research advisor Dr. Ronald Macfarlane for his involvement in my graduate work. I would like to thank my committee member Dr. Walzem for her willingness to assist in understanding the scientific processes occurring with regards to lipids and for her encouragement. I am also thankful for my committee members Dr. Barondeau and Dr. Hilty for their availability, support, feedback, and assistance throughout the course of this research.

I would like to acknowledge Dr. Dangott for his knowledge regarding proteins and generosity in allowing me to utilize his facilities and supplies. I would like to thank my former colleague Sandy Lester for her assistance during the early stages of my research and Candace Hayes and Aydee Alvarado for their laboratory assistance. Thanks also to Dr. Yohannes Rezenom and the Laboratory for Biological Mass Spectrometry for the acquisition of MALDI spectra. I acknowledge Johns Hopkins University for the collaborative apoptosis work, Dr. Robert Brocia at Roar Biomedical for transfer protein activity assays, and the collaboration with Scott & White Hospital which provided patient samples.

I also extend my gratitude to the Department of Chemistry and NASA University Research Center at Texas Southern University for providing me with a superior undergraduate education, research experiences which prepared me for the rigorous graduate school curriculum and workload, and a support system that spanned beyond my undergraduate years.

I sincerely appreciate Aaron McGriff for his time, assistance, support, and electronic expertise. Lastly, I thank my family and friends for their support and motivation.

LIST OF ABBREVIATIONS

ACN	Acetonitrile
Apo	Apolipoprotein
BGE	Background electrolyte
BSA	Bovine serum albumin
bTRL	Bouyant triglyceride-rich lipoprotein
C_{18}	Carbon tail of eighteen atoms
CE	Capillary electrophoresis
CETP	Cholesterol ester transfer protein
CM	Chylomicrons
CsCdY	dicesium cadmium ethylenediaminetetraacetic acid
CAD	Coronary artery disease
CVD	Cardiovascular disease
DGU	Density gradient ultracentrifugation
I-DGU	Immunospecific-density gradient ultracentrifugation
DMSO	Dimethyl sulfoxide
DS	Dextran sulfate
dTRL	Dense triglyceride rich lipoprotein
EDTA	Ethyelenediaminetetraacetic acid
HDL	High density lipoprotein
HSA	Human serum albumin
IDL	Intermediate density lipoprotein
LCAT	Lecithin: cholesterol acyltransferase
LDL	Low density lipoprotein
LP	Lipoprotein
Lp(a)	Lipoprotein a
LPL	Lipoprotein lipase
MALDI-MS	Matrix-assisted laser desorption ionization mass spectrometry

NaBiY	Sodium bismuth ethylenediaminetetraacetic acid
NBD	7-nitro-2,1,3-benz-oxadiazol-4-yl
pI	Isoelectric point
PLTP	Phospholipid transfer protein
SAA	Serum amyloid A
SDS	Sodium dodecyl sulfate
TAG	Triglycerides or triacylglycerol
TFA	Trifluoroacetic acid
TOF	Time of flight
TRL	Triglyceride rich lipoprotein
UC	Ultracentrifugation
VLDL	Very low density lipoprotein
Y	EDTA

TABLE OF CONTENTS

CHAPTER Page

CHAPTER Page

LIST OF FIGURES

FIGURE Page

FIGURE Page

FIGURE Page

FIGURE Page

FIGURE Page

FIGURE Page

FIGURE Page

FIGURE Page

FIGURE Page

FIGURE Page

LIST OF TABLES

TABLE Page

TABLE Page

TABLE Page

TABLE Page

TABLE Page

TABLE Page

TABLE Page

TABLE Page

TABLE Page

TABLE Page

CHAPTER I

INTRODUCTION

HDL in Health and Disease

High Density Lipoprotein Cholesterol and Coronary Artery Disease

Coronary artery disease (CAD) is the leading cause of morbidity and mortality in the developed world.[1] It is well established that there is a powerful inverse correlation between circulating high density lipoprotein cholesterol (HDL-C) levels and CAD risk.[2] High density lipoprotein cholesterol is determined as the amount of cholesterol in high density lipoprotein (HDL) particles per 100mL of plasma.[3] High density lipoprotein cholesterol levels greater than or equal to 60 mg/dL are considered protective, while those below 40mg/dL in men and below 50mg/dL in women, are independent risk factors for future cardiovascular events.[4] There is an elevation in CAD risk of approximately 3% in women and 2% in men for each decrement of 0.0259mM (1mg/dL) in HDL-C.[5,6] With this established relationship between HDL-C and CAD risk, the medical community has historically tailored diagnosis, treatment, and prevention around HDL-C levels.

Atheroprotective Properties of HDL

In addition to the correlation between HDL-C levels and CAD risk, HDL is also known for its many anti-atherogenic or atheroprotective properties. The primary atheroprotective property of HDL is its ability to promote the efflux of cholesterol from macrophage and peripheral cells in a process known as reverse cholesterol transport.[7, 8] Peripheral cells are unable to catabolize cholesterol, thus the mechanism of reverse cholesterol transport provides the pathway by which excess cholesterol in the vessel wall and in macrophages, can be scavenged and returned to the liver for removal.[9] This

---

This dissertation follows the style of *Analytical Chemistry*.

mechanism beneficially prevents systemic vascular cholesterol retention and accumulation.9 High density lipoprotein displays a number of atheroprotective properties independent of reverse cholesterol transport, including antioxidant[10], anti-inflammatory[11], and anti-thrombotic properties.[12, 13] The antioxidant properties of HDL are typically observed as the inhibition of low density lipoprotein (LDL) oxidation.[14, 15] High density lipoprotein associated proteins and enzymes contribute to its antioxidant functions. These associated proteins and enzymes can prevent or delay LDL oxidation by the removal of oxidized phospholipids from LDL and artery wall cells, and by hydrolyzing LDL-derived oxidized phospholipids.[15] The anti-inflammatory properties of HDL include decreasing cytokine-induced expression of adhesion molecules on endothelial cells, the inhibition of monocyte adhesion to these cells, and altering other aspects of endothelial function.[16, 17] The anti-thrombotic properties of HDL are observed as inhibitory actions on factors that promote blood coagulation and may be related to HDL particle phospholipids containing potent anticoagulant properties. [18, 19] High density lipoprotein has also been shown to possess anti-apoptotic, vasodilatory, and anti-infectious properties. [20, 21] High density lipoprotein potently inhibits apoptosis in endothelial cells induced by oxidized LDL,[22, 23] this effect is also accompanied by decreased generation of reactive oxygen species suggesting a relation to the intracellular anti-oxidative properties of HDL.[24] High density lipoprotein vasodilatory properties may be related to the stimulation of nitric oxide release by endothelial cells.[25, 26] Likewise, increased production of nitric oxide may form a basis for the inhibitory properties of HDL on platelet aggregation.[27] The multifaceted functions and properties of HDL demonstrate its complexity and provide insight as to why its functionality and role in health and disease has not been completely elucidated.

Atherogenic High Density Lipoprotein

Given the complexity of HDL, it is not unforeseen that a single assay of plasma steady-state HDL-C levels does not absolutely correlate with HDL function. Although high serum levels of HDL-C have been correlated with longevity and decreased CAD

risk,[28, 29] recent evidence suggests that elevated HDL-C levels may also portend increased risk for CAD and related events.[30] There is also evidence that low HDL-C levels are associated with no increase or even reduced CAD risk.[30] The apolipoprotein A-I (apoA-I) Milano mutation for example, is a rare, naturally occurring genetic point mutation in apoA-I that leads to low HDL-C levels but does not confer an increased CAD risk.3, [31] Despite the many atheroprotective properties of HDL, there have been several populations of individuals identified with disease despite elevated levels of HDL-C such as the clinical trials involving cholesterol ester transfer protein (CETP) deficiencies.[32, 33] The recently published results of outcome trials with CETP inhibitor torcetrapib[34, 35, 36, 37] showed no apparent impact on atherosclerosis and increased morbidity and mortality despite significant raising of HDL-C levels.[34] Trials were terminated prematurely due to a 25% increase in major CAD events and a 40% increase in death from CAD causes in the active treatment arm.[37] These adverse events occurred despite a 72% increase in HDL-C and a 25% reduction in LDL-C.[34] Contrary to its many atheroprotective properties, it is seen that dysfunctional or atherogenic HDL contains properties that add to CAD risk and development. In many patients with atherosclerosis, the hardening of arteries which occurs along with the progression of CAD, it appears that HDL is not only ineffectual as an antioxidant, but paradoxically increases lipid peroxide formation.[38] In the setting of systemic inflammation, the anti-atherogenicity of HDL can markedly diminish, to the extent where it even becomes proinflammatory.[39, 40] This inflammatory situation can lead to a proinflammatory phenotype of HDL that increases LDL oxidation, increases vascular inflammation, promotes expression of cellular adhesion molecules, and is less, if at all, effective in reverse cholesterol transport.[17, 41] The many studies reporting CAD despite elevated HDL-C levels as well as longevity and health despite low HDL-C levels, suggest that the anti-atherogenicity of elevated HDL-C is strongly influenced by specific genetic and metabolic backgrounds.

Therapeutic Strategies to Improve High Density Lipoprotein

Strategies to increase HDL-C levels have been the target of HDL therapeutics, given the strong epidemiological associations between HDL-C and CAD. Substantial experimental evidence suggest that augmenting the levels and or functions of HDL and its associated components can have major vascular protective effects, independent of total or non-HDL-C levels. [42] A number of therapeutic strategies are being developed to target elevated HDL-C levels in an attempt to inhibit the progression or induce regression of atherosclerosis, reduce CAD events, normalize the intravascular metabolism and physicochemical properties of HDL, and improve anti-atherogenic efficacy. [43] Nicotinic acid, also known as niacin, is the most effective HDL-C raising agent currently available and can increase HDL-C by up to 35%.4 Several clinical studies have demonstrated niacin's ability to reduce CAD events and slow the progression of atherosclerosis in patients with CAD and lower HDL-C levels.[44] Niacin reduces triglyceride hydrolysis in adipose tissue by inhibition of hormone-sensitive lipase via HM74 receptors. [45] Plasma levels of triglyceride-rich lipoproteins and LDL-C are decreased and levels of HDL-C are raised primarily as a result of diminished hepatic uptake of HDL with enhanced lipidation of apoA-I.[46] Cholesterol ester transfer protein (CETP), is a plasma protein that mediates transfer of cholesteryl esters from HDL to apoB-containing lipoproteins in exchange for triglycerides.[47] The interest in CETP inhibition was sparked after the discovery of Japanese individuals with extremely high levels of HDL-C who were genetically deficient in CETP.[48, 49] This genetic association led to the concept that pharmacological inhibition of CETP might be an approach to raise HDL-C. Unfortunately, trials involving CETP inhibitor torcetrapib provided surmountable challenges in the search for effective strategies, and were terminated prematurely due to substantial mortality rates in the active treatment arm.[37] Fibrates are peroxisome proliferative-activated receptor α agonists that exert multiple effects on lipid metabolism, increasing plasma HDL-C by 10% and decreasing triglycerides by 36% (averages for 53 randomized trials).[50] Though the primary use of fibrates target lowering triglyceride levels, the modest HDL-C raising effect of these agents may also

translate into a reduction in clinical CAD events.[51, 52] Statins' major effect is to decrease the number of atherogenic apoB-containing lipoprotein particles. In addition, these agents raise levels of HDL-C typically by 5 – 10%, reduce CETP activity and possess pleiotropic effects, which include anti-inflammatory and anti-oxidative activities.[53] While statin treatment is associated with a limited effect on HDL-C concentration, changes in HDL's anti-inflammatory or inflammatory properties may be greater. Consistent with these data, treatment of CAD patients with simvastatin increases HDL functionality, rendering HDL anti-inflammatory.[38] Recently, reconstituted HDL, consisting of apoA-I and phospholipids, is stimulating significant therapeutic interest. [54] Intravenous injection of reconstituted HDL is followed by a rapid elevation in HDL-C levels, facilitation of reverse cholesterol transport, as well as multiple anti-atherogenic effects.[55] Short apoA-I mimicking peptides equally increase HDL levels, reduce atherosclerosis, activate reverse cholesterol transport, and exhibit other anti-atherogenic properties.[56] Other drug classes in development include novel PPAR alpha agonists, liver-X receptor agonists, ABCA1 upregulators, SR-B1 inhibitors, protein mimetics and gene therapy.[43] All of these approaches will require proof of long-term safety as well as clinical efficacy. Different HDL-C raising agents may function complementarily or in series, and have additive effects, thus, combined use of such agents has also been proposed.[44] For example, nicotinic acid combined with simvastatin potently elevates plasma HDL-C, lowers triglycerides, reduces the frequency of CAD events and slows the progression of CAD in patients with low HDL-C levels.[45] Actions of statins on HDL functionality involve cooperation with CETP inhibitors,[57,58] and apoA-I mimetic peptides.[59] Table 1 reports information on HDL raising drugs. There are currently many therapeutic hypotheses and agents under investigation. The success of each however, will depend on the biological variability of those to which they are administered, and the outcomes of extensive clinical trials.

Table 1. HDL raising drugs

Drug Class	Mechanism of Action for HDL Elevation	Elevation of HDL-C
Nicotinic acid	Suppresses triglyceride hydrolysis in adipose tissue by inhibition by hormone-sensitive lipase, thereby decreasing VLDL-triglyceride levels; stimulates cholesterol efflux by activating ABCA1.	Up to 35%
Fibrates	Upregulation of apoA-I, apoA-II, lipoprotein lipase, SR-B1 and ABCA1 expression through binding and activation of PPARα; increase lipolysis of VLDL, with enhanced release of surface fragments to HDL, via increase in lipoprotein lipase activity.	Up to 16%
Statins	Lower plasma CETP concentration; reduce CETP-mediated transfer of cholesteryl esters to apoB-containing lipoproteins via reductions in acceptor particle number; enhance hepatic apoA-I production.	Up to 15%
CETP Inhibitor Torcetrapib	Inhibition of CETP by enhancing its association with its lipoprotein substrates; preferential elevation of large HDL.	Up to 106%
Reconstituted HDL	Rapid formation of small HDL; apoA-I_{Milano}, elevated efficiency as a cellular cholesterol acceptor through Arg173→Cys substitution.	Transient
ApoA-I mimetics	Rapid formation of small HDL particles, which subsequently mature to large HDL particles.	Transient

Apoptosis and Coronary Artery Disease

Apoptosis is the highly regulated, energy requiring process by which cells are terminated in the human body. In this form of cell death, damaged cells are removed without causing inflammation or damage to surrounding tissue.[60] Apoptosis was

initially characterized by its morphological characteristics which include chromatin condensation, DNA fragmentation, plasma membrane blebbing, formation of apoptotic bodies, and cell shrinkage due to reduction in cytoplasm and organelles.[61] Membrane bound apoptotic bodies containing cytosol and processed organelles are formed and subsequently removed by macrophages via phagocytosis.[62] In relation to CAD, studies have shown that apoptosis plays a key role in pathogenesis.[63] Apoptosis occurs in myocardial tissue samples from patients suffering from myocardial infarction or heart disease, dilated cardiomyopathy, and end stage heart failure.[64] Apoptosis is activated by various stressors that are commonly seen in CAD such as cytokine production,[65] increased oxidative stress,[66] and DNA damage.[67] Apoptosis can be initiated by mitochondria, which release cytochrome c into the cytosol in response to extrinsic stimuli such as oxidative insults.[68] Alternatively, the apoptotic pathway can be initiated via endogenous death receptors, leading to internal death signaling that promotes coordinated and specific cell death.[69] Both pathways converge on a common downstream pathway, which mediates the final morphological and biochemical alterations that are characteristic of apoptosis. Due to the limitations on the regenerative capacity of the myocardium, there is intense interest in the prevention of cardiomyocyte loss in coronary artery disease to prevent development of heart failure.[63]

When it comes to the topic of HDL in health and disease, there are several unanswered questions that will take years to investigate. The evidence supports the need to increase HDL-C in patients at risk for CAD events.9 High density lipoprotein cholesterol however, does not directly assess the rate of centripetal cholesterol flux from peripheral foam cells to the liver, which is influenced by factors other than HDL-C alone. Additionally, HDL-C values fail to provide information regarding the anti-inflammatory, antioxidant, anti-thrombotic, and endothelial function promoting benefits of HDL, despite increasing evidence supporting the clinical significance of these functions. Biochemically innovative approaches to raising HDL-C, controlling HDL particle size and functionality, atherogenicity, and preventing the formation of dysfunctional HDL, offer greater insight and direction for reducing the risk of CAD than

currently available drug therapy. The multiple actions and properties of HDL make it a complex therapeutic target albeit one with an abundance of anti-atherogenic potential.

High Density Lipoprotein Particles

Lipoprotein Particles

Lipoproteins are biochemical assemblies of lipids and proteins which serve to carry nonpolar lipids throughout the body in aqueous blood and extracellular fluid. These particles facilitate lipid exchange between lipoprotein classes and cells, and are instrumental in the metabolism and transportation of triglycerides, phospholipids, cholesteryl esters, and cholesterol. These water-soluble macromolecules are composed of a surface monolayer made of amphipathic phospholipids, free cholesterol, and apolipoproteins surrounding a central core containing nonpolar lipids, mainly triglycerides and cholesteryl esters (Figure 1).[70]

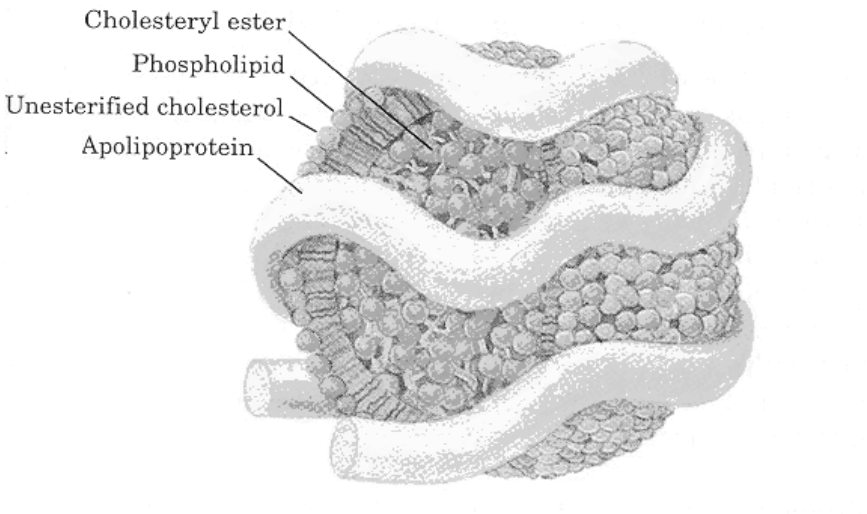

Figure 1. Lipoprotein structure and composition.

These particles are classified based upon their hydrated densities, and comprise a heterogeneous spectrum of particles that differ in size, density, lipid, and apolipoprotein composition. This system of classification gives way to the five lipoprotein subclasses: low density lipoprotein (LDL), very low density lipoprotein (VLDL), intermediate density lipoprotein (IDL), high density lipoprotein (HDL), and chylomicrons (Table 2).[71]

Table 2. Lipoprotein characteristics

Lipoprotein Class	Density (g/mL)	Size (nm)	Major Lipids	Major Apolipoproteins
Chylomicrons	>0.93	100 – 500	Dietary TAG	B-48, C-II, E
VLDL	0.93 – 1.006	30 – 80	Endogenous TAG	B-100, C-II, E
IDL	1.006 – 1.019	25 – 50	CE and TAG	B-100, E
LDL	1.019 – 1.063	18 – 28	CE and TAG	B-100
HDL	1.063 – 1.210	5 – 15	CE and PL	A-I, A-II, C-II, E

High Density Lipoprotein Particles

High density lipoprotein (HDL) particles are the most dense lipoprotein subclass and have been classically defined as a group of pseudomicellar, quasi-spherical, protein and lipid complexes with hydrated densities between 1.063 – 1.210g/mL.[71] High density lipoprotein particles can vary tremendously in size, density, composition, and functional properties, potentially affecting their relationship to CAD. These particles are characterized by their structural and metabolic heterogeneity, caused by their diverse metabolic origin and continuous remodeling by lipolytic enzymes, lipid transporters, and furthermore by lipid and apolipoprotein exchange with other circulating tissues and lipoproteins.3, [70] High density lipoprotein particles can be further divided into two distinct subfractions, HDL_2 and HDL_3. HDL_2 spans the density range between 1.063 – 1.125g/mL while HDL_3 spans the range between 1.125 – 1.210g/mL. [72] The larger and

more buoyant HDL_2 is formed by enzymatic action upon the smaller and denser HDL_3. Overall, HDL is protein rich compared to other lipoprotein subclasses, with a protein to lipid ratio ranging from 1:2 in HDL_2 to 10:1 in HDL_3.[73] Progressive reduction in HDL particle size with increasing hydrated density is associated with elevation in protein content and in surface to core ratio accompanied by reduction in core lipid content, consistent with the predominance of surface components in small, dense HDL_3.[74] A lower HDL_2 to HDL_3 ratio, typically involving decreased HDL_2 with constant or increased HDL_3 has been associated with increased CAD risk.[75] Coronary artery disease patients were also found to have less HDL with apoA-I within the more buoyant HDL_2 subclass, and more HDL with apoA-I and apoA-II within the denser HDL_3 subclass compared with healthy controls.[76, 77] Within the population of individuals with CAD, HDL subclasses also show prediction regarding disease. The HDL_{2b} subclass is inversely related to disease severity on coronary angiograms and progression of coronary lesions between repeated angiographies.[78, 79] HDL_{3b} also has been associated with a lipoprotein profile indicative of increased risk of CAD independent of HDL_{2b}.[76]

High Density Lipoprotein Metabolism

Lipoprotein metabolism involves the collaborative work of all five lipoprotein subclasses, and involves the transportation of dietary or exogenous fat, endogenous fat, and reverse cholesterol transport. Reverse cholesterol transport and HDL metabolism are two pathways with significant overlap, only the final step of reverse cholesterol transport, bile acid formation and excretion, is unrelated to HDL. The metabolism of HDL, involves a variety of factors regulating HDL synthesis, intravascular remodeling, and catabolism. In HDL metabolism, the individual lipid and apolipoprotein components of HDL are mostly assembled following secretion, frequently exchanged with or transferred to other lipoproteins, actively remodeled within the plasma compartment, and cleared at least in part independent from each other. HDL metabolism begins with cholesterol efflux. This process underlies the formation of HDL from lipid-free apoA-I and cellular lipids, cholesterol, and or phospholipids. Cholesterol efflux

occurs at the plasma membranes of cells as a result of the action of ATP binding cassette A-I (ABCA1),[80] resulting in small, lipid-poor, discoidal HDL particles.[81] These nascent particles are effective acceptors of cellular cholesterol, although other pathways involving ABCG1 and scavenger receptor B1 (SR-B1) mediate this step which results in large, lipid-rich discoidal particles.[80] Upon reaching the appropriate size and composition, discoidal HDL particles become a substrate for lecithin:cholesterol acyltransferase (LCAT). Lecithin:cholesterol acyltransferase esterifies free cholesterol and forms the hydrophobic core, transforming HDL from discoidal to spherical particles. These particles acquire additional cholesterol and apolipoproteins from other lipoproteins in the plasma and fuse with each other. The products of this step are mature, large, cholesterol-rich, spherical particles.[82] These spherical particles, upon reaching the appropriate size and composition, become substrates for a number of enzymes and transfer factors. These include SR-B1 and the LDL-receptor related protein (LRP) at the surfaces of hepatocytes, which ensure delivery of HDL-C to the liver either by selective cholesteryl ester uptake or through HDL holoparticle uptake, respectively.[83] Additionally, cholesterol ester transfer protein (CETP) facilitates the exchange of HDL cholesteryl esters for triglycerides in apoB-containing lipoproteins.[84] Other factors include phospholipid transfer protein (PLTP)[85] and endothelial and hepatic lipases,[86] which transfer and hydrolyze HDL phospholipids and triglycerides. The rate of HDL remodeling and the proportion of cholesterol delivered to the liver versus that delivered to apoB-containing lipoproteins depends on the activities of SR-B1 and LRP, and the levels of triglycerides and activity of CETP. The products of this step are small, lipid-poor spherical HDL particles and lipid-free apoA-I released during remodeling. The lipid poor spherical HDL particles join the cycle at the stage of maturation, while the lipid-free apoA-I can undergo a new cycle of lipidation and HDL formation.

High Density Lipoprotein Associated Apolipoproteins

Apolipoproteins attach to the surface of lipoprotein particles and facilitate the formation of lipoproteins, modulate the activity of enzymes and lipid transfer factors

involved in lipoprotein remodeling in circulation, and modulate receptor-mediated binding and endocytosis of lipoproteins and or their remnants. [87] High density lipoprotein associated apolipoproteins have a domain structure with amphipathic α-helices that orient themselves with their nonpolar, lipid-binding surfaces interacting with polar and nonpolar regions of the particle surface lipids, while the opposite surfaces, rich in charged amino acid side chains, are in contact with the aqueous environment. The major apolipoproteins of HDL are apoA-I and apoA-II, while others including apos A-IV, A-V, C-I, C-II, C-III, D, E, F, H, J, L, M, O, and P are also attached. Recent studies have identified up to 75 distinct proteins associated with centrifugally-isolated HDL.[88] The plasma abundance of these associated proteins however is insufficient to permit one copy per HDL particle, indicating that specific proteins may be bound to distinct particle species which are differentially distributed across the HDL density spectrum. The potential for distinct particle subpopulations is consistent with the fact that HDL exerts various biological activities.

ApoA-I is present in the majority of HDL particles and constitutes approximately 70% of the apolipoprotein content of HDL particles; consequently, plasma apoA-I concentrations correlate closely with plasma HDL-C. [89] ApoA-I is secreted predominantly by the liver and intestine as lipid-poor apoA-I and nascent phospholipid-rich cholesterol poor HDL particles. ApoA-I is a 28kDa protein found in plasma at a concentration of 100 – 150 mg/dL.[89] Research studies have shown that overexpression of apoA-I leads to enhanced macrophage-specific reverse cholesterol transport, [90] increases HDL-C, reduces atherosclerosis progression, and can even induce plaque regression.[91, 92] ApoA-I infusion studies have shown temporary increases in total plasma apoA-I concentrations without any adverse effects,[93] as well as rapid increases in plasma apoA-I and HDL followed by increases in HDL cholesteryl esters and apoA-I.[94] An additional approach uses apoA-I mimetics, peptides that are structurally related to apoA-I and mimic its effects. Currently, several small amphipathic peptides containing 18 – 22 amino acids have been created and shown to significantly reduce the progression of

aortic atherosclerosis and reduced inflammation when injected into cholesterol fed mice without causing significant changes in lipoprotein levels.[95]

ApoC-I is an HDL associated apolipoprotein which is emerging as a potential atherogenic component of HDL. ApoC-I is a 6.6kDa serum protein, found in plasma at a concentration of 6mg/dL, and consists of 57 amino acids. [96] Synthesized in the liver and intestine, apoC-I is secreted following a co-translational cleavage of a 26-residue signal peptide from the N-terminal end, and does not contain a propeptide upon secretion.[97] Due to its high lysine content, human apoC-I has the highest isoelectric point of all apolipoproteins, approximately 6.5, a feature often used for the purification of the protein from other apolipoproteins.[98] ApoC-I contains alpha-helix regions contributing to lipid binding,[99] and has been shown to activate LCAT in vitro resulting in increased formation of cholesteryl esters.[100, 101] Thus, it has the potential to participate in the esterification of the cholesterol that is transferred to HDL as a part of the excess surface components generated during lipolysis of VLDL and chylomicrons or that is transferred to HDL from cells. The ability of apoC-I to activate LCAT may account for the normal serum levels of esterified cholesterol in individuals with apoA-I deficiencies. ApoC-I has also been shown to inhibit cholesteryl ester transfer protein (CETP).[102, 103] ApoC-I is important in the regulation of cholesterol transport; and is presently a possible independent risk factor for premature coronary artery disease. Prior studies also demonstrated the existence of an elevated large HDL particle enriched in apoC-I found in infants of lower birth weight and younger gestational age.[104] Although this apoC-I enriched particle disappears soon after birth, these infants have increased risk of heart disease in adulthood.[105] The molecular mechanism behind this association remains to be elucidated, however, studies also indicate that apoC-I plays a role in apoptosis of vascular smooth muscle cells via recruitment of neutral sphingomyelinase.[106]

The amino acid sequences of apoC-I and its truncated form apoC-I', derived from the DNA sequence are shown in Figure 2. The mature forms of these apolipoproteins are capable of binding lipids due to the presence of two dynamic class A amphipathic helices.[107]

Prepeptide
MRLFLSLPVL VVVLSIVLEG PAPAQG

Mature ApoC-I
1 10 20 30 40
TPDVSSALDK LKEFGNTLED KARELISRIK QSELSAKMRE
WFSETFQKVK EKLKIDS

Truncated ApoC-I
DVSSALDKLK EFGNTLEDKA RELISRIKQS ELSAKMREWF
SETFQKVKEK LKIDS

Figure 2. Amino acid sequence of apolipoprotein C-I and its pre-peptide.[108] The single letter amino acid notations are defined as: A=Ala, R=Arg, N=Asn, D=Asp, C=Cys, E=Glu, Q=Gln, G=Glyc, H=His, I=Ile, L=Leu, K=Lys, M=Met, F=Phe, P=Pro, S=Ser, T=Thr, W=Tryp, Y=Tyr, V=Val.

Residues 7-24 and 35-53 of apoC-I consist of amphipathic helices which are connected by a short linker region, contribute to lipid binding, and are stabilized by interhelical interactions.[109, 110] The flexible linker region, allows helices to adopt many orientations. The non-polar face contains hydrophobic amino acids and interacts with fatty acid lipid chains. The polar face contains hydrophilic amino acids that extend toward lipid groups and aqueous milieu. Hydrophobic interactions between nonpolar residues of the amphipathic protein and lipid fatty acid chains are hypothesized to stabilize lipoprotein association. The ability of apoC-I to associate with lipids is due to hydrophobic clusters formed by side chains of leucine and isoleucine as well as aromatic residues of tryptophan and phenylalanine.[111]

The genes coding for human apoC-I are members of a 48-kb gene cluster on chromosome 19 which also includes the *APOE* and *APOC2* gene,[112] and is located either 4.3[113] or 5.3[114]kb downstream from the *APOE* gene in the same transcriptional orientation. Mostly expressed in the liver, *APOC1* is also expressed in the lung, skin, testes, adipose tissue, brain, and spleen.[114] The *pseudo-APOC1* gene resulted from the duplication of *APOC1* and is located 7.5kb downstream from *APOC1*, between *APOC1 and APOC4* genes.[114] The regulation of human *APOC1* gene expression, is under the

control of an array of elements found throughout the whole gene cluster. The hepatic control region (HCR), located approximately 9kb downstream from the *APOC1* gene was found to regulate the expression of the gene in the liver.[115] The majority of apolipoprotein genes are comprised of four exons and three introns, with the first exon being non coding. Exon 2 of human apoC-I encodes 20 of the 26 residues in the 26 amino acid signal sequence and exon 3 encodes the remaining segment of the signal sequence plus the first 39 amino acids of the mature protein. Exon 4 encodes the final segment of the mature protein. There is not substantial information known regarding naturally occurring mutations in the *APOC1* gene. There has been a study reporting the case of apoC-I deficiency in patients with familial chylomicronemia, which may not directly implicate apoC-I as patients had both apoC-II and apoC-I deficiency.[116] Restriction fragment length polymorphisms (RFLPs) in or around the human *APOC* genes have been identified that are associated with lipoprotein disorders or altered plasma lipid concentrations in humans. Human studies have not shown polymorphisms in the *APOC1* gene leading to functional variants, an *HpaI* polymorphism in the promoter region has been shown to lead to 57% increased expression of this gene.[117,118]

High Density Lipoprotein Associated Enzymes

Many enzymes are associated with HDL particles and facilitate the synthesis and functionality of this heterogeneous group of particles. Lecithin:cholesterol acyltransferase (LCAT) plays a significant role in the maturation of HDL. This enzyme catalyzes the transfer of 2-acyl groups from lecithin to free cholesterol, generating cholesteryl esters and lysolecithin.[119] Hydrophobic cholesteryl esters are retained in the HDL core forming larger mature HDL. The activity of LCAT is critical to normal HDL metabolism. In humans, genetic LCAT deficiency syndromes are associated with markedly reduced HDL-C and apoA-I levels,[82] and rapid catabolism of cholesteryl ester poor apoA-I.[120] Overexpression of LCAT in animal studies increases HDL-C levels, leading to decreased atherosclerosis in rabbits[121] whereas in LDL-deficient mice, LCAT overexpression was reported to increase atherosclerosis unless co-expressed with

CETP.[122] Although activation of LCAT would be expected to increase HDL-C, the effectiveness of this approach remains unspecific.

Cholesteryl ester transfer protein (CETP), is a hydrophobic glycoprotein synthesized in the liver, spleen, small intestine, and adipose tissue, that circulates attached to lipoproteins.[123] It promotes the redistribution and equilibration of hydrophobic cholesteryl esters and triglycerides packaged within the lipoprotein core between HDL and apoB containing lipoproteins, chylomicrons, and remnants. [124] The net effect of CETP action on HDL is depletion of cholesteryl esters and enrichment with triglycerides, with an overall net reduction in HDL particle size. CETP is found in circulation with a normal serum concentration ranging from 0.18 – 0.27 mg/dL; CETP concentration correlates directly with LDL-C and negatively with HDL-C.[123] Detected in foam cells in atherosclerotic lesions, the enzyme may promote cholesterol efflux from the lesions.[134] Increased concentration of CETP has been found in individuals with chylomicronemia and dysbetalipoproteinemia.[125] Decreased levels of CETP activity however, are associated with the risk of CAD despite higher HDL levels.[126] Low CETP levels increase the proportion of triglycerides in VLDL and LDL and promote the formation of small atherogenic and oxidized LDL particles.[127]

Phospholipid transfer protein (PLTP) is an enzyme associated with HDL and LDL particles, responsible for the transfer of phospholipids between lipoproteins, and synthesized in liver and adipose tissue.[128] PLTP mediates the transfer of phospholipids from triglyceride rich lipoproteins to HDL following the hydrolysis of triglyceride rich lipoproteins by lipoprotein lipase.[129] The activity of the enzyme increases during inflammation to maintain homeostasis by transferring and neutralizing inflammatory mediator, lipopolysaccharide.[130] Normal serum levels for this protein range between 1.2 – 1.5 mg/dL.[128] PLTP may also serve a protective role in HDL metabolism specifically during an acute phase response.[131]

In total, HDL associated enzymes, including paraoxonase 1, platelet-activating factor acetylhydrolase and lecithin:cholesterol acyltransferase, can become dysfunctional, depleted or both under inflammatory conditions in CAD.[38] Reduced

function of HDL apolipoproteins and enzymes might result from covalent modification, such as oxidation by arterial wall cells and nonenzymatic glycation in the presence of high levels of glucose.[132] It is hypothesized that modified HDL leads to changes in its anti-atherogenic properties and possibly results in the promotion of atherogenic events.[133] Recent data suggest that HDL can be modified and lose its anti-atherogenic properties through several mechanisms. Examples of some of these hypothesized mechanisms include oxidative modification due to the presence of free radicals and free metal ions in the atherosclerotic plaques[134]; enzyme-induced modification including myeloperoxidase, chymase-tryptase, matrix metalloproteinases, PMN-associated enzyme and endothelial lipase which degrade or oxidize apolipoproteins without substantial changes in lipid moiety or alternatively induce apolipoprotein cross-linking and lipid oxidation[135]; and acute phase reactants-induced modification during inflammation.[136] Overall, HDL represents a complex and diverse class of biomolecules. The physical characteristics, functions, and metabolism of these particles display various implications in health and disease. Progress in understanding the properties will aid in identifying biomarkers for heart disease.

Analytical Chemistry to Investigate Coronary Artery Disease

The physical and chemical properties of HDL particles provide clues regarding their atherogenic potential. Analytical methods can be used to identify various properties of HDL particles including but not limited to density, charge, size, and electrophoretic mobility. The collaborative results of such methods serve as invaluable tools in the discovery of biomarkers for CAD and further characterization of the heterogeneous HDL lipoprotein subclass.

Ultracentrifugation of Lipoproteins

Ultracentrifugation is regarded as the gold standard of lipoprotein subclass separation, as these particles are classified and defined based upon their densities. This

method relies on the ability of lipoprotein subclasses to separate when subjected to high gravitational forces and is useful as lipoproteins are relatively less dense than other serum proteins due to their lipid content. Ultracentrifugation techniques facilitate an analysis of density properties of lipoprotein particles, which may provide clues regarding their atherogenic properties. Sequential flotation[137] and density gradient[138] ultracentrifugation are two commonly used preparatory ultracentrifugation techniques for the separation of lipoprotein subclasses.

In sequential flotation, lipoprotein classes, sequentially float to the top of the sample tube after adjusting the solvent density to the lower limit of the fraction required using sodium chloride, potassium bromide, or mixtures of these salts.[139] Each major lipoprotein class may be sequentially isolated by adjusting the density of the resulting infranatant solution to successively higher values.[139] The reports of deLalla, Gofman, and Lindgren led to the key publications of Havel, Eder, and Bragdon describing how sequential ultracentrifugation of human plasma or serum in solutions of neutral salts such as KBr and NaI can be used to obtain defined lipoprotein subfractions.[71, 140] Modifications of this procedure have been used globally in lipoprotein research and are commonly used for isolation of lipoprotein classes and subclasses. During ultracentrifugation in neutral salts, however, HDL and other lipoprotein classes are exposed to ionic strengths of 5 to 20 times above those of human plasma and lymph. This condition subsequently has the potential to alter the lipoprotein complement by dissociation of molecules bound by charge-charge interactions. This occurrence of possible modification of lipoprotein apolipoproteins and associated proteins by high salt concentration as also shown in increased lipoprotein density, has been documented and recognized in several studies.[141, 142] Other disadvantages of sequential flotation ultracentrifugation include long spin times which can take up to several days for complete preparative fractionation. To minimize the possibility of protein stripping by high ionic strength, several laboratories have developed differential and isopycnic gradient ultracentrifugation procedures in buffers of deuterium oxide (D_2O) and sucrose, which maintain the lipoproteins at physiological ionic strength and pH. These solutions

allow isolation of homogeneous lipoprotein classes with reproducible content of apolipoproteins, associated proteins, and lipid content and composition.[143, 144]

Density gradient ultracentrifugation (DGU), has been the standard analytical method for lipoprotein profiling and uses solvent density gradients which are formed during ultracentrifugation. Compared to other methods such as sequential flotation ultracentrifugation, DGU allows lipoproteins to be fractionated in one spin rather than multiple steps. Density gradient ultracentrifugation techniques are more time efficient and expose lipoprotein particles to less centrifugal force which may lessen distortion in structure and composition. Though DGU offers several advantages over many ultracentrifugation techniques, it has also been deemed tedious and time-consuming compared to other profiling methods.[145] An additional disadvantage of DGU has been the difficulty in obtaining reproducible gradient forming solutes to generate a sufficient gradient from a homogenous solution. For example, alkali metal halide salts have been used for separations but require extensive centrifugation times and a pre-formed gradient.[146] Likewise, sucrose has been used as a gradient but is accompanied by decreased separation due to its high viscosity.[147] As an improvement to the aforementioned gradients, Nycodenz and Iodixanol, derivatives of triiodobenzoic acid were shown to provide for the quicker formation of a density gradient.[148] Yee and colleagues reported a novel iodixanol density gradient for composition, density, and phenotype analysis.[138] Unlike traditional sequential flotation ultracentrifugation, the use of iodixanol as a density gradient does not require extensive ultracentrifugation time, salt density adjustments or dialysis. Additionally, this novel gradient provides advantages of improved resolution of lipoproteins and their separation from plasma proteins as well as the ability to sub-fractionate individual lipoprotein density classes when compared to sequential flotation ultracentrifugation. Though the triiodobenzoic acid derivatives provided a better option than sucrose and alkali halide salts, they are accompanied by disadvantages including high concentration, large partial volume, and low diffusion force.[149]

In a response to the need for improved gradients for DGU, Hosken and colleagues in the Laboratory for Cardiovascular Chemistry at Texas A&M University, found a useful solution in a novel class of solutes based on metal ion complexes.[149] Complexing a heavy metal ion to a highly soluble organic ligand provided a compact but high molecular weight solute. Additionally, the modification of the metal ion, ligand, or counter ion provides a customizable gradient for specific separations. What resulted was a drastic improvement in DGU with novel tunable gradients with advantages including high solubility, low concentration, rapid gradient formation, high molecular weight, small partial volume, low viscosity, and high resolution. From this work, Hosken and colleagues first identified a cesium salt of bismuth ethylenediaminetetraacetic acid (BiEDTA) as an ideal gradient forming solute.[149] Despite its high UV absorbance and ability to be overloaded by high serum volumes, CsBiEDTA offered a significant improvement to the field by improving the quantity of information obtained from previous DGU separations while simultaneously simplifying sample preparation and analysis times. Shortly thereafter, Johnson and colleagues in the Laboratory for Cardiovascular Chemistry at Texas A&M University, expanded on the concept of metal ion complexes of EDTA as solutes for DGU by investigating the differences observed from changing both complexing and counter ions.[150] By measuring and comparing the density profiles of EDTA complexes of copper, iron, cadmium, lead, and bismuth using cesium and sodium counter ions, the link between solute molecular weight and the shape of the density gradient curve was understood. This useful work aided in the establishment of a group of density gradients that could highlight specific regions of a lipoprotein density profile. In addressing the issue of high UV absorbance, which prevents the measurement of protein at 280nm, it was observed that cadmium complexes had comparatively low UV absorbance, with a single maximum absorbance between 204 and 206nm.[150] Likewise, since the cadmium EDTA complexes are doubly charged and have a relatively low absorptivity it was perceived that they may serve as better density-gradient forming solutes, particularly for preparative work which uses larger serum volumes. It was also seen that NaBiEDTA provided a near-baseline separation among

all profile lipoprotein regions and would be an ideal gradient for analytical work or lipoprotein profiling.[150] Through the expanded work of Johnson and colleagues, preferential separation of lipoprotein subclasses by modifying the metal ions in the density gradient was achieved, adding even more flexibility and improvement to the field of lipoprotein profiling.

The current lipoprotein separation and profiling method in the laboratory is an isopycnic ultracentrifugation technique, which uses a homogenous solution composed of the density gradient solute, encompassing the range of densities expected in a serum sample (1.00–1.20g/mL), as well as the serum sample. During the process of ultracentrifugation, the solute forms a concentration gradient with a slope depending on the relative strengths of opposing diffusion and sedimentation forces.[151] As the gradient forms, individual serum sample components sediment or float to the position in the ultracentrifugation tube, where their hydrated density matches that of the density gradient. This particular position is known as the isopycnic point and is a fixed property of a particular molecule. By modifying the density gradient solution, however, the relative position of a particle's isopycnic point in a tube can be altered. When the homogenous solution of the density gradient forming solute is spun; the density of the solution increases exponentially as the solution depth proceeds away from the meniscus. This results in the meniscus of the solution having a lower tube coordinate and density, while the bottom of the UC tube has a higher tube coordinate and density. This density versus tube coordinate relationship can be fitted to an exponential curve function. The slope of the density curve can be obtained by spinning a solution of the desired density gradient forming solute and measuring the refractive index as a function of tube depth. The resulting density curve is essential in equilibrium isopycnic DGU experiments because it enables the determination of the density of the components of a sample based on their position in the ultracentrifugation tube. Lipoprotein molecules in serum samples are fluorescently labeled by NBD (C_6-ceramide), a lipophilic fluorophore, prior to density gradient ultracentrifugation. This fluorophore consists of a hydrophilic head and a hydrophobic tail and fluoresces when the polar head is embedded into a non-polar

environment such as the hydrophobic lipid core of a lipoprotein particle. In such an environment, the NBD-lipoprotein complex will exhibit characteristic excitation and emission spectra with excitation at 450 nm and emission at 520 nm. After incubation of serum samples with this molecule for thirty-five minutes, samples are subjected to DGU. Upon completion of the spin the fluorescence of the NBD-lipoprotein complex allows for the generation of a lipoprotein density profile that enables the distribution of lipoprotein particles to be visualized. The lipoprotein density profile shows the distribution of triglyceride rich, VLDL, LDL, and HDL particles and their subclasses. For fingerprint lipoprotein profiling, NaBiEDTA is used, in total 11 subclasses are observed including: TRL, LDL_1, LDL_2, LDL_3, LDL_4, LDL_5, HDL_{2b}, HDL_{2a}, HDL_{3a}, HDL_{3b}, and HDL_{3c}. For preparative HDL work, $Cs_2CdEDTA$ is used to separate HDL adequately for secondary analysis which is followed by excision of HDL serum subfractions. Though the described use of metal EDTA complexes in DGU offers several advantages compared to other methods, one of the drawbacks includes the contamination of albumin in denser lipoprotein subclasses, which is a common disadvantage of gradient ultracentrifugation methods.[138]

Mass Spectrometry of Apolipoproteins

Mass spectrometry (MS) is an analytical tool which separates and identifies apolipoproteins according to mass to charge ratio. Mass determination by MS requires the conversion of proteins or peptides into gas-phase ions with an ionization source. The ions are separated based on their mass and charge using a mass analyzer with detection occurring via an electronic multiplier.[152] The resulting spectra are represented as ion intensity versus the *m/z* value. There are several different types of mass spectrometers, which are classified according to the ionization source and mass analyzer employed.[153] One of the most widely used ionization sources is matrix-assisted laser desorption ionization (MALDI).[154] MALDI sources are most frequently coupled to time-of-flight (TOF) mass analyzers.[152] In the MALDI technique, samples containing peptides and proteins are dried on a plate together with a light absorbing matrix molecule.

Vaporization of the mixture of protein and matrix by a laser releases ionized protein molecules, often with a single charge, which can be analyzed in a TOF mass spectrometer. Intact molecular ions are formed from individual peptide chains, allowing accurate determination of polypeptide mass.[155] Since the mass of an intact protein offers limited diagnostic information, this method is generally limited to identifying known proteins.[156] Protein quantification by MALDI-TOF-MS can also be problematic, and suffers from a limited dynamic range. Thus, this technique is typically limited to relatively abundant proteins associated with lipoproteins such as C, A, and E apolipoproteins, and their isoforms. Several studies have identified new isoforms of many apolipoproteins.[157, 158, 159] Mass spectrometry is also ideal for identifying post-translational modifications, as these alterations involve a change in molecular mass, which is reflected in the mass of any peptide carrying the modified amino acid(s). Post-translational modifications refer to the chemical alteration of proteins following translation. Post-translational modifications result in the attachment or addition of biochemical functional groups such as carbohydrates, lipids, phosphates, and acetates to amino acids, and may also result in structural changes. These modifications are observed due to increased and or decreased molecular weight. Some changes are easily identified such as +16 Da for the addition of oxygen, but it may be unclear whether this is the common formation of methionine sulfoxide or another scenario. Other modifications are ambiguous such as +80 Da which could indicate phosphorylation or sulfation, though these may be elucidated through the detection of anions at m/z 70 versus 80 respectively. [160] The oxidation of lipoproteins is implicated in atherogenesis. [161] It has been observed, that HDL isolated from humans with CAD contains elevated levels of oxidized amino acids chlorotyrosine and nitrotyrosine when compared to healthy human HDL samples.[132] Chlorotyrosine is a direct oxidation product of the heme protein myeloperoxidase[162] and macrophages in atherosclerotic lesions express high levels of this enzyme.[163] When specific apoA-I methionine and tyrosine residues are oxidized by myeloperoxidase, HDL loses its ability to remove cholesterol from cells by the ABCAI pathway.[164] As the interaction between apoA-I and ABCA1 is imperative

in protecting macrophages from cholesterol accumulation and atherosclerosis, impairment of this pathway may generate dysfunctional HDL. These findings suggest that inflamed atherosclerotic lesions may be where oxidative damage of proteins occurs. Shao and colleagues showed post-translational modifications of apoA-I due to reactive carbonyls which subsequently impaired cholesterol transport.[165] This modification was seen through MALDI-TOF-MS spectral shifting of approximately 350 Da. Isoforms of C apolipoproteins have been identified in biological samples as a result of glycosylation and deglycosylation and proteolytic activity at the post-translational levels.[166, 167, 168] The truncated apoC-I isoform apoC-I′ was first identified by Bondarenko and colleagues and lacks Thr-Pro residues from the N terminus.[169] In 2006, Wroblewski and colleagues identified a functional polymorphism of apoC-I detected by mass spectrometry.[170] This polymorphism was found only in individuals of American Indian or Mexican ancestry. Tandem mass spectrometry showed the alteration to consist of a T45S variation which forms part of the lipid interacting surface of apoC-I. This study reported the first case of a structural variant of apoC-I as well as some protein properties that suggest the functional significance of this residue change. The individuals in this study showing the polymorphism had apoC-I double peaks for each of the two forms. More recently, Puppione and colleagues detected two distinct isoforms of apoC-I in great apes.[171] They designated these forms as acidic (apoC-IA), and basic (apoC-IB) based upon their calculated pI values. It is hypothesized that the anomaly observed in the discovery of the acidic form of this protein is due to oxidation with a methionine converted to methionine sulfoxide.[171] Other post translational modifications such as phosphorylation are part of common mechanisms for controlling protein behavior such as enzyme activation and inhibition. Thus phosphorylation is of interest in regards to apoC-I post-translational modifications in that apoC-I has been shown to inhibit the enzyme cholesterol ester transfer protein (CETP).[102] Inhibition of this enzyme by apoC-I may subsequently influence the ability of HDL to effectively remove cholesterol from the periphery resulting in the acceleration of atherosclerosis.

Capillary Electrophoresis of Lipoprotein Apolipoproteins

Capillary electrophoresis (CE) is used to analyze intact and delipidated lipoproteins, and analyzes the differences in charge/mass ratio, molecular size, and shape properties of lipoproteins and apolipoproteins. The application of a direct current causes ions to move within the electric field of a fine capillary at a rate dependent upon the force of the field, and impeding effects between the sample and the surrounding media. In the cardiovascular field, CE applications include analysis of apolipoproteins,[172] lipoproteins,[173] and modified lipoproteins.[174] Due to rapid separation, high resolution and high sensitivity, CE is an invaluable analytical tool. Capillary electrophoresis also exhibits advantages over other techniques such as HPLC for protein analysis in areas such as speed and affordability. In the past two decades, substantial progress has been made in the separation of serum proteins by CE using fused silica capillaries. In the analysis of intact lipoproteins, electrophoretic separations under nondenaturing conditions can be used to determine differences in LDL particle size. High density lipoprotein particles, on the other hand, are more heterogeneous with varying apolipoprotein composition. Attempts to directly analyze intact lipoproteins by CE have had minimal success, this is most likely attributed to interaction between lipoproteins and capillary walls. This problem is prevented through the use of detergents and organic solvent buffer modifiers which disrupt lipoprotein particles. In the application of CE for apolipoprotein characterization, Stocks and colleagues demonstrated the capability of CE to resolve apoA-I and A-II in human HDL following UC and delipidation.[175] This technique provided quantitative values of apoA-I and A-II which were comparable to those obtained by immunoassay. Tadey, Purdy and colleagues, also demonstrated the use of CE in uncoated capillaries to resolve apoA-I in human plasma or apoA-I and A-II in HDL.[176] Their technique involves electrophoresis in sodium dodecyl sulfate (SDS) containing buffers to overcome protein-capillary wall interactions. Separation depends on differences in the amount of SDS bound by hydrophobic interaction to individual proteins, resulting in differences in charge to mass ratio. In the absence of the detergent, the apolipoproteins eluted as a single peak. The effect of SDS was attributed

to the presence of discrete, non-interacting detergent binding sites on the apolipoproteins. Capillary electrophoresis offers incentives over conventional electrophoresis including its speed and instrumental format which removes the need for labor-intensive steps such as gel preparation and staining.

Overall, ultracentrifugation provides separation and isolation of lipoprotein subclasses while MALDI-MS and CE provide subsequent characterization of the apolipoprotein content of these subclasses. Through the development, modification, and implementation of these novel techniques, more information regarding how and why coronary artery disease develops will be obtained.

Research Aims

Ultimately, the aim of this research was to utilize several analytical methods for analyzing human serum HDL subfractions. In doing so, the information obtained assisted in the assessment of CAD risk. Through applying the methodologies to human serum samples from individuals with and without CAD, a better understanding between the two patient cohorts was enabled, along with the identification of potential biomarkers. With HDL being such an important factor in the quest for knowledge regarding the development and acceleration of CAD, its composition and subcomponents were the focus of this work. The methodologies reported here, sought to look closely at the apolipoprotein content of the HDL subfractions from two cohorts of patients to identify striking differences. It is possible that the effects and functions of HDL are highly controlled by these surface proteins. Combining DGU both as a primary analysis method and a preparative tool for secondary analysis, with techniques capable of secondary analysis separation such as MALDI-MS, enabled a multi-dimensional examination of the various subfractions of serum HDL. In addition, this combination of methods yielded important information regarding the character and distribution of apolipoproteins. Collectively, this information contributed to the ongoing effort to

identify features of HDL and HDL associated apolipoproteins that contribute to CAD risk, and to understand the chemistry of atherogenic HDL.

CHAPTER II

MATERIALS AND METHODS

Materials

NBD (C_6-ceramide) was purchased from Molecular Probes (Eugene, OR). Sodium bismuth ethylenediaminetetraacetic acid (NaBiY) was purchased from TCI America (Portland,OR). Cesium hydroxide, cesium carbonate, cadmium carbonate, ethylenediaminetetraacetic acid (H_4EDTA), sodium carbonate, bovine serum albumin, tricholoracetic acid, trifluoroacetic acid (TFA), ferulic acid, sinapinic acid, sodium borate, sodium dodecyl sulfate (SDS), Dextralip® 50, and magnesium chloride hexahydrate were purchased from Sigma Aldrich (St. Louis, MO). Acetonitrile (ACN), dimethyl sulfoxide (DMSO), glycerol, phosphoric acid, and methanol were purchased from EM Science (Gibbstown, NJ). Strata C18-E solid phase extraction cartridges and syringe adapter caps were purchased from Phenomenex (Torrance, CA). Cyanogen bromide (CNBr) activated Sepharose 4B was purchased from Amersham Biosciences. Anti-apoC-I IgY microbeads were purchased from GenWay Biotech, Inc. (San Diego, CA). ApoA-I and apoC-I standards, and anti apoC-I were purchased from Academy Biomedical (Houston, TX).

Analytical Methods

Serum Collection

Serum samples were obtained from human subjects by blood draw following a 12 hour fast into 9.5 mL Vacutainer™ tubes treated with a polymer gel and silica activator from Beckton Dickinson Systems (Franklin Lakes, NJ). The serum was subsequently separated from erythrocytes by centrifugation at 3200 rpm for 20 minutes at 5°C, followed by aspiration of the supernatant into 500µL Eppendorf tubes for storage at -80°C prior to analysis.

Patient Selection

Serum samples were selected from the laboratory serum library and consisted of CAD patients and non-CAD control patients. The serum library consists of donated serum from Scott & White Hospital (Temple, TX) patients. Informed consent was obtained from all donors.

The serum collected from the 8 control subjects without CAD included a 48 year old Caucasian female (patient 1), 77 year old Caucasian female (patient 3), 44 year old Caucasian female (patient 7), 66 year old Hispanic female (patient 13), 75 year old Caucasian female (patient 14), 73 year old Caucasian female (patient 16), 68 year old Caucasian female (patient 24), and a 50 year old African-American male (patient 25).

The serum collected from the 7 CAD patients included a 75 year old Caucasian female (patient 10), 72 year old Caucasian male (patient 41), 37 year old Caucasian female (patient 84), a 54 year old Caucasian male (patient 143), a 77 year old Caucasian female (patient 146), a 75 year old Caucasian male (patient 170), and a 72 year old Caucasian female who was also a low birth weight infant (patient 195).

One patient, a 56 year old Caucasian female with normal to high HDL (patient 49), was also used in this study. This individual did not have diagnosed CAD, however, did have a family history of premature CAD and also displayed marked apoptosis of aortic smooth muscle cells in addition to an enrichment of apoC-I.

Ultracentrifugation of Serum Samples

Density gradient ultracentrifugation of serum samples incorporated the use of heavy metal density gradient forming solutes, NaBiY and Cs_2CdY. The term "Y" symbolizes an "EDTA" molecule when complexed with a metal ion. NaBiY and Cs_2CdY complexes were synthesized by stoichiometric combination of H_4EDTA, the appropriate alkali carbonate or alkali hydroxide, and the appropriate heavy metal carbonate in 100mL of deionized water, followed by a two hour reflux yielding a clear density gradient solution.[79]

Serum density profiling was performed to obtain a fingerprint of the lipoprotein distribution of a serum sample. Six microliters of serum and 184µL of 0.18M NaBiY were added to an 1100µL solution of the NaBiY density gradient forming solute, followed by the addition of 10µL of a 1.000 mg/mL solution of NBD (C_6-ceramide) dissolved in DMSO. An 1150µL aliquot of this solution was then added to a UC tube and spun in an Optima TLX UC with a TLA 120.2 fixed angle rotor and in 1.5mL thick-walled polycarbonate UC tube from Beckman-Coulter (Palo Alto, CA) at a rotor speed of 120,000 rpm for 6 hours at 5°C. (Figure 3)

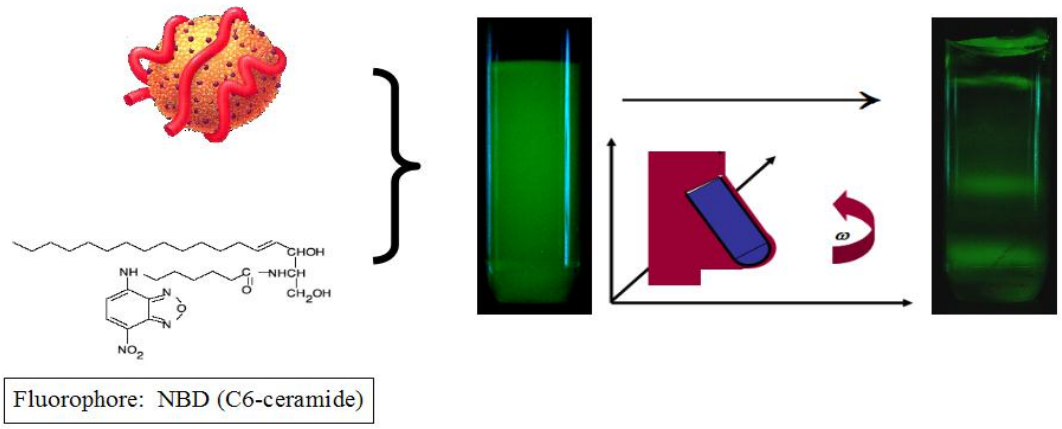

Figure 3. Density gradient ultracentrifugation schematic.

Preparative UC utilized larger serum volumes and preceded serum lipoprotein fraction studies. This work focused on HDL subclasses and to eliminate interferences from apoB containing lipoproteins, serum was first treated with dextran sulfate (DS) and magnesium chloride hexahydrate in 100mL of deionized water. The final solution had a concentration of 10.0g/L of DS and 0.500M magnesium chloride. This working solution was added to a sample of serum at a volume of 10% of the serum volume. This solution was mixed briefly by vortexing and left to stand at room temperature for 10 minutes. A

tabletop centrifuge spun at 12,000g for 5 minutes was used to sediment out the apoB containing lipoprotein particles. The supernatant was prepared for UC as a normal serum sample. Sixty to two hundred microliters of serum after dextran sulfate treatment, was added to an 1100µL solution of a 0.300M solution of Cs_2CdY, followed by the addition of 10µL of a 1.000 mg/mL solution of NBD (C_6-ceramide) dissolved in DMSO. From this mixture, a 1000µL aliquot was added to a UC tube and spun according to the conditions previously described.

Fluorescent Imaging Analysis

A digital color microscope camera, Microfire S99808, purchased from Optronics (Goleta, CA) with Fiber-Lite MH100A Illuminator from Edmund Industrial Optics (Barrington, NJ) was used to image each UC tube following DGU. The light source consists of a metal halide continuous light source. The camera and light source were positioned orthogonally to each other on an optical bench to illuminate the sample. Filters matching the excitation and emission properties of the fluorophore, NBD (C_6-ceramide), were purchased from Schott Glass (Elmsford, NY). The respective filters for excitation and emission were a blue-violet filter (BG-12) with a bandwidth centered about 407nm and a yellow filter (OG-515) with a bandwidth centered about 570nm. Specific settings for the Microfire camera software included an exposure time of 53.3mS for serum density profiling and 41mS for preparative UC. A gain of 1.000 and a target intensity of 30% were also applied.

Following fluorescence imaging, a density profile was generated from the image capture of each UC tube. Using Origin 7.0 software, the image was first converted into grayscale intensity values as a function of pixels in two dimensions, subsequently, the grayscale intensity from a small strip of 10 pixels oriented in the center of the UC tube was averaged. This averaged grayscale intensity was plotted as a function of tube coordinate (0-34mm) to give the final lipoprotein density profile.

Lipoprotein Fraction Collection

An in-laboratory developed freeze/slice method was used to collect serum lipoprotein fractions following preparative UC and fluorescence imaging. Ultracentrifugation tubes were slowly frozen in liquid nitrogen by placement into a custom 10-slot holder and lowering the holder into a Dewar of liquid nitrogen, causing the liquid in the tubes to freeze from the bottom to the top. In this manner, the expansion of water to ice could be accounted for by the following : (Eq. 1)

$$mm_s = \rho_l/\rho_s \times mmL - 10.405 \qquad \text{Eq. 1}$$

The tube coordinate in the solid state is represented by mm_s, while mmL corresponds to the tube coordinate in the liquid state, the state in which the image of the UC tube was captured. The term ρ_l/ρ_s corresponds to the ratio of the density of water in its liquid state ρl to its density in its solid state ρ_s. Since water is denser in its liquid state, this ratio gives a correction factor greater than unity and the equation can be simplified to: (Eq. 2)

$$mm_s = 1.058 \times mmL - 10.405$$

Eq. 2

10.405mm was also subtracted from the solid state tube coordinate to correct for the calibration of the micrometer/tube holder assembly that was used to dial in the correct cut points. This micrometer/tube holder assembly contained a micrometer head, which functioned to advance the position of the UC tube relative to the location of the notch for the saw blade. A Dremel® scroll saw (Racine, WI) was fitted with 0.25mm blades for the cutting of the tubes. The volumes of non HDL, HDL_2, HDL_3, and protein fractions were 212 ± 8 µL, 329 ± 8 µL, 249 ± 13 µL, and 60 ± 5 µL, respectively. The freeze/slice method is depicted in Figure 4.

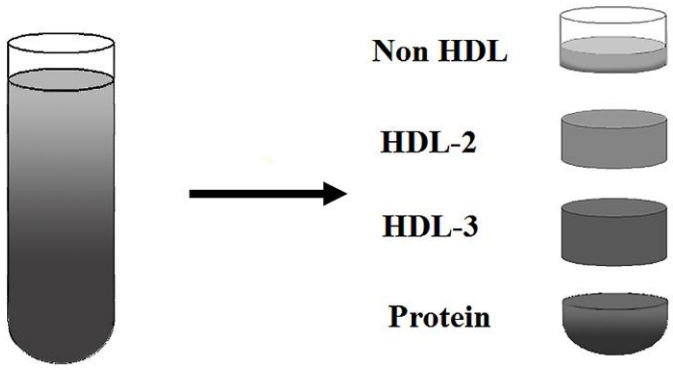

Figure 4. Freeze/slice method for excising lipoprotein fractions.

Gravimetric Density Determination

After sample excision and thawing, the density of each fraction was determined gravimetrically. A 100µL aliquot of each non HDL, HDL_2, and HDL_3 fraction and a 50µL aliquot of each protein fraction was added to a zeroed 1.5mL Eppendorf. An analytical balance was used to obtain the mass of each aliquot. The ratio of mass to volume was used to determine the density of each fraction.

C_{18} Solid Phase Extraction, Desalting, and Delipidation

After gravimetric density determination, delipidation and desalting was accomplished by means of a solid phase extraction (SPE) cartridge from Phenomenex, Strata C18-E (Torrance, CA). Delipidation of samples was based on a published method.[177]

The cartridge was conditioned drop wise with three 1mL rinses of 0.1% (v/v) TFA in acetonitrile (ACN), allowing no air to enter the cartridge. The cartridge was then conditioned drop wise with three 1mL rinses of 0.1% (v/v) TFA in deionized water, allowing no air to enter the cartridge. The sample to be delipidated was first acidified

with a sample volume of 0.1% (v/v) TFA in deionized water, then slowly added to the cartridge, allowing no air to enter the cartridge. The cartridge was washed with three 1mL rinses of 0.1% (v/v) TFA in deionized water to remove the density gradient solute, non-specifically bound apolipoproteins, and water soluble components of the serum sample. One milliliter of air was then pushed through the cartridge to remove any remaining liquid. Isocratic elution was performed with four 100µL aliquots of 0.1% (v/v) TFA in acetonitrile, purging with 1mL of air in between each aliquot and allowing at least one minute for the sorbent to soak prior to purging with air. The first aliquot contained all serum proteins (verified by MALDI-MS) and was the only aliquot retained. The C_{18} cartridge additionally served as a filter for any residual polycarbonate particulates remaining following tube cutting.

Following solid phase extraction, the samples were evaporated to dryness through the use of a SVC-100H Speed-Vac concentrator with a refrigerated condensation trap from Savant Instruments (Farmingdale, NY) which was connected to a 5KC36PN435AX vacuum pump from General Electric (Fort Wayne, IN). Dried apolipoprotein fractions were then reconstituted in suitable solvents for the method of investigation which included 0.1% (v/v) TFA in deionized water for MS experiments.

MALDI-MS Analysis of Apolipoproteins

The matrix assisted laser desorption ionization mass spectrometry (MALDI-MS) analysis was used to analyze serum HDL subfractions for qualitative analysis and standard solutions to assess purity. A commercial Voyager-DE STR, MALDI-TOF mass spectrometer equipped with a 2m flight tube from Applied Biosystems (Foster City, CA, USA) and a mass range of 500 – 300,000 Da was used for the analyses (Figure 5). The MALDI matrix consisted of a 10mg/dL solution of sinapinic acid in a 1:1 mixture of acetonitrile and 0.1% TFA in water. Serum samples underwent a thin-layer sample preparation method in which a MALDI plate was first spotted with the desired MALDI matrix and allowed to dry, and then a mixture of the sample and matrix (1:1 ratio) was deposited atop the original spot. Calibration was performed with bovine

insulin, bovine serum albumin, and *Escherichia coli* thioredoxin, 1µL of the standard was added to 24µL of the matrix. For the lower mass range, the acceleration potential was held at 25kV, the grid potential was at 93% and delay time was 575ns. Approximately 100 shots per spectrum were collected.

Capillary Electrophoresis Analysis of Apolipoproteins

Preparation of the Capillary

The capillaries were prepared using the Beckman capillary cartridge assembly (Beckman Instruments, Fullerton, CA, USA) and untreated fused silica capillaries (Polymicro Technologies, Phoenix, AZ, USA) preceding the capillary electrophoresis (CE) experiments. The capillaries had an inner diameter (i.d.) of 75µm and an outer diameter (o.d.) of 365µm. Briefly, approximately 80cm in length of capillary, was cut from the spool of capillary tubing by scoring with a cleaving stone (Beckman) and gently pulling in opposite directions on both sides of the score. Care was taken not to bend the capillary to avoid uneven breakage on the ends of the capillary. The total length of the cut capillary was measured with a precision of ± 1mm. Using a fine tipped pen, a mark was placed 12cm away from one end of the capillary. To prepare the capillary window, the capillary tubing was then inserted into a small metal coil attached to a power supply so the mark was within the coil. The power supply was turned on for approximately 10 seconds to heat the coil while the capillary was rotated to burn off the polyimide coating from the outside of the capillary tubing. The capillary was then removed from the coil and the burnt polyimide coating was gently removed by wiping the capillary with a Kim Wipe™ and methanol. The window was examined using a tabletop microscope to ensure that all of the coating was removed from the capillary window. The capillary window was no longer than 3mm in length. From this point on, extreme care was used when handling the capillary as the window region was fragile and finger oils can reduce detection sensitivity. The distance from the detector end of the capillary to the middle of the capillary window was measured to the nearest mm.

The capillary was then inserted into the cartridge according to the Beckman cartridge assembly guide and was assembled as follows. The capillary end farthest from the capillary window was inserted into the outlet side of the cartridge. The capillary was carefully pushed and twisted through the cartridge until it appeared at the cartridge inlet. The capillary was then pulled through the cartridge until the capillary window appeared centered in the cartridge window. From the back side of the cartridge, the center groove of the aperture clip was carefully aligned with the capillary window and pressed in place. From the front side of the cartridge, the retainer O-ring was placed in the aperture clip hole. Using the O-ring insertion tool, the tool was pressed carefully until the O-ring was seated in the aperture clip. The capillary seal retainer clips were then inserted over the capillary at each end and pressed to snap in place, being sure to clip both front and back edges into place for each clip. Once snapped, the capillary ends were inspected visually to verify that they were straight. The cartridge was then positioned against the capillary length template. Holding the capillary against the template, each end was scored at the cross mark on the capillary-length template with the cleaving stone. Each cut piece of capillary was measured to the nearest ± 0.5 mm. The pieces removed from both ends were subtracted from the total length of capillary initially cut to determine the corrected length of the capillary or L_c. In addition, the piece removed from the detector or outlet end of the capillary was subtracted from the distance from the detector end of the capillary to the window and was then subtracted from the initially measured length of the capillary to determine the length of the capillary to the detector or L_d.

The total length L_c of the capillaries were approximately 60cm with an effective length L_d of approximately 50cm. Precise measurements (±1mm) of the individual capillary distance parameters used in each experiment were used for calculating effective electrophoretic mobilities.

Capillary Electrophoresis Analysis of Samples

Following solid phase extraction and evaporation to dryness, as stated previously, dried protein samples were reconstituted in 100µL of the background electrolyte (BGE), which was a buffer solution consisting of 12.5mM sodium borate, 3.5mM SDS (70%) and 20% (v/v) acetonitrile prior to CE analysis. On initial use, the newly prepared capillary was rinsed with 1M NaOH for ten minutes, 0.1M NaOH for ten minutes and buffer for ten minutes, to condition the column. The neutral marker consisted of a 0.5% (v/v) solution of DMSO in deionized water. Capillary electrophoresis analyses were performed on a Beckman P/ACE™ MDQ system (Fullerton,CA) that was equipped with a diode array detector. Run parameters for a separation consisted of a rinse with buffer for two minutes, the injection of the neutral marker at 0.5psi for five seconds, injection of the sample at 0.5psi for five seconds and the application of 17.5kV for thirty-five minutes. Before each use, the BGE was degassed by vacuum sonication until bubbles were no longer observed within the solution. All solutions were filtered with a 0.22µm cellulose acetate membrane sterile syringe filter by Millipore (Billerica, MA) to remove microbes and blanketed with mineral oil (Amersham Biosciences) to eliminate sample evaporation.

Analysis was performed at a wavelength of 214nm. The capillary and sample tray of the instrument were thermostated at 25°C. Migration times and corrected peak areas were automatically obtained using the data analysis feature of the Beckman P/ACE Station Migration software. Identification of other apolipoprotein peaks was accomplished by comparison to previously published results.[178, 179] The resulting electropherograms were analyzed by 24 Karat software from Beckman (Fullerton, CA).

ApoA-I, ApoC-I and BSA Calibration Curves by Capillary Electrophoresis

Prior to CE analysis of samples, calibration curves for major serum proteins were constructed to enable identification of serum subfraction components. An apoA-I solution (100.0mg/dL; Academy Biomedical) was used in the preparation of a calibration curve. The apoA-I standard was diluted with BGE through serial dilutions in

a 1:1 ratio to yield concentrations of 80.0mg/dL, 40.0mg/dL, 20.0mg/dL, 10.0mg/dL, and 5.0mg/dL apoA-I. An apoC-I solution (80.0mg/dL; Academy Biomedical) was used in the preparation of a calibration curve. The apoC-I standard was diluted with BGE through serial dilutions in a 1:1 ratio to yield concentrations of 40.0mg/dL, 20.0mg/dL, 10.0mg/dL, and 5.0mg/dL apoC-I. A 200.0mg/dL solution of bovine serum albumin (BSA) (Sigma) was prepared by dissolving 2.000g in 1L of 0.1% TFA in deionized water and was used in the preparation of a calibration curve. The BSA stock solution was diluted with BGE to yield concentrations of 80.0mg/dL, 40.0 mg/dL, 20.0mg/dL, 10.0mg/dL, and 5.0mg/dL BSA. Each solution was analyzed by CE in triplicate and data analysis was carried out at 214nm to create calibration curves. The standard corrected peak areas (CPA) were plotted as a function of the concentration of each solution injected into the CE.

Collaborative Studies

The collaborative studies provided the opportunity to obtain additional information from samples by shipping them to other laboratories for further analysis. These studies enabled the ability to assess apoptosis levels from fractionated serum and apoC-I immunodepleted and apoC-I immunorecovered samples through cell culture studies with the Chatterjee Laboratory at Johns Hopkins University (Baltimore, MD). The studies additionally enabled the analysis of the transfer protein rates of whole serum through CETP and PLTP assays performed by Roar Biomedical (New York, NY).

ApoC-I Isolation by Immunoprecipitation

Immunoprecipitation was performed in order to obtain apoC-I depleted and apoC-I recovered serum which was subsequently analyzed using DGU and fluorescence imaging as described previously. ApoC-I enriched and apoC-I depleted HDL fractions,

as well as whole serum HDL fractions, were prepared and sent to collaborating laboratories for analysis.

Throughout the course of this study, two different methods were utilized in order to accomplish this goal. The first of which incorporated commercial beads with the antibody conjugated to a Sepharose resin and the second consisted of an in-laboratory procedure to make the beads.

Immunoprecipitation Using GenWay Anti ApoC-I IgY Beads

Using the commercial beads, 60µL of serum was added to 500µL of anti-apoC-I IgY microbeads (GenWay Biotech, Inc. San Diego, CA). Upon serum addition the mixture was incubated for 30 minutes at room temperature with shaking to suspend the microbeads. Following incubation, the beads were spun down by centrifugation. The supernatant which consisted of the apoC-I depleted serum was then carefully transferred into a new Eppendorf and stored at -85°C until needed for secondary analysis. The microbeads were then washed three times with 500µL of dilution buffer (10mM Tris-HCl, 0.15M NaCl, pH = 7.4). A volume of 250µL of stripping buffer (0.1M Glycine-HCl, pH = 2.5) was then added to the microbeads and incubated for 4 minutes at room temperature with shaking to suspend the microbeads. Following incubation, the beads were spun down. The supernatant which consisted of recovered apoC-I serum was then removed and transferred into a new Eppendorf for secondary analysis; this process was repeated two additional times for a total recovered volume of 750µL. Upon completion of immunorecovery, the recovered apoC-I sample was neutralized with 70µL of neutralization buffer (1M Tris-HCl, pH=8) and stored at -85°C freezer until analyzed.

Immunoprecipitation Using “In-house” Anti ApoC-I Beads

The in-laboratory method involved swelling the Sepharose beads and conjugating the antibody to the swollen beads. In this procedure, the following solutions were prepared and used during the binding of antibody to the Sepharose beads and the binding of serum to the antibody-Sepharose gel: coupling buffer, which consisted of 0.1M

$NaHCO_3$ and 0.5M NaCl, pH 9.0; 1mM HCl; blocking buffer, which consisted of 1M Tris-Base, pH 9.0 in coupling buffer; a low pH wash buffer, which consisted of 0.1M HCl, 0.5M NaCl; and 0.05M Tris-HCl.

An optical density reading at 280nm (OD_{280}) of the antibody solution was taken to determine the protein concentration in the antibody solution. A volume of 62.5µL of coupling buffer (0.1M $NaHCO_3$ and 0.5M NaCl, pH 9.0) was then added to the 125µL antibody solution. The Sepharose beads were mixed and allowed to swell in 1mM HCl for approximately 15 minutes at room temperature. The supernatant was then removed, and the Sepharose beads were washed with 1mM HCl solution for 1 minute, with the washing step repeated twice.

The next two steps were done without pausing in between. Washing with 5mL coupling buffer, the gel was prepped for the addition of the antibody-coupling buffer solution, and after the addition, the tube was rotated gently at room temperature for 4 hours. After the beads settled, the supernatant was removed, and the OD_{280} was taken. If the OD_{280} was at least 10-fold lower than before coupling, coupling was successful. If OD_{280} was not at least 10-fold lower than in step 1, coupling did not proceed as expected, mainly caused by not transferring gel to antibody solution quickly enough and had to be repeated.

Following successful coupling, the resin was washed twice with 1mL coupling buffer. One milliliter of blocking buffer (1M Tris-Base, pH 9.0 in coupling buffer) was added and allowed to stand for 2 hours at room temperature. The supernatant was then removed, and the gel was washed four times, alternating between low pH wash buffer (0.1M HCl, 0.5M NaCl) and high pH wash buffer (coupling buffer). The first and fourth washes were saved, and the OD_{280} of each was checked to verify that the antibody was no longer present in solution, which was demonstrated in an OD_{280} reading below ~0.01.

The AB-Sepharose gel, that was freshly made and washed with coupling buffer, was mixed with 50µL serum and 600µL 0.05M Tris-HCl in a 1.5mL Eppendorf tube. The tube was gently rotated for 4 hours at 1400rpm at room temperature. After rotation, the Sepharose gel was allowed to settle and the depleted serum, approximately 600µL,

was removed. Using a 3,000 MWCO filter the supernatant, containing everything that did not bind to the AB, was concentrated for UC use.

After removing the depleted serum from the AB-Sepharose gel, the beads were washed twice with coupling buffer to ensure that there was no residual serum left in the Eppendorf tube. Afterwards, 600µL of 1mM HCl was added to the beads. The tube was gently rotated at 1400rpm for 5 hours at 37°C. After rotation, the Sepharose gel was allowed to settle and the recovered serum, approximately 600µL, was removed.

The Sepharose-AB gel was washed with coupling buffer twice and then stored in 20% ethanol to prevent microbial growth at 4°C.

Desalting and Purification of Intact Lipoproteins

For the analysis of intact lipoproteins, samples must be desalted while retaining the lipid components. This procedure utilizes micro-concentration of the sample in place of solid phase extraction. Micro-concentration results in the replacement of the EDTA solute with deionized water. Micro-concentration decreased sample volume from 500µL to 50µL and then reconstituted the sample volume to 500µL for each cycle. Following micro-concentration, samples were sterilized using a 0.22µm syringe filter from Millipore (Billerica, MA) to remove microbes.

Smooth Muscle Cell Apoptosis

Selected samples of intact HDL_2 and HDL_3 were isolated using the freeze/slice method following preparative UC and immunospecific DGU. Samples were subjected to micro-concentration using filter units from Millipore (Billerica, MA) with a 30,000 molecular weight cutoff in order to remove the EDTA solute which would otherwise interfere with the apoptosis assay. Samples were then sterilized by a means of a 0.22µm sterile filter unit from Millipore (Billerica, MA). Following purification, samples were submitted to the Chatterjee Laboratory at Johns Hopkins University for apoptosis cell culture studies. Submitted HDL fractions were analyzed for apoptotic effects on cells in order to gain understanding of the functionality of HDL subfractions from patients.

Human aortic smooth muscle cells (ASMC) (Cambrex, Walkersville, MD) were grown on sterilized glass cover slips in 6-well trays and treated with the various lipoprotein fractions isolated from human subjects, pure apoC-I (2.5µg/µL medium).

Transfer Protein Assays

The effect of serum apolipoproteins on cholesteryl ester transfer protein rates and phospholipids transfer protein rates were determined through collaboration with Roar Biomedical.

Cholesteryl Ester Transfer Protein

Cholesteryl ester transfer protein, CETP, is a member of the lipid transfer/lipopolysaccharide binding protein gene family. This protein transfers neutral lipids from HDL to VLDL and is present in normal human plasma and serum. Playing an important role in lipoprotein metabolism, CETP influences the reverse cholesterol transport pathway. The Roar CETP Activity Assay is useful for measuring the CETP activity in human plasma and serum in other species that express CETP. The Roar CETP Activity Assay Kit uses a proprietary substrate that enables the detection of CETP-mediated transfer of neutral lipid from the substrate to a physiological acceptor. The transfer activity results in an increase in fluorescence intensity. In a total volume of 200µL, the assay is linear from 0.200 to 0.800µL of normal human plasma with a 3 hour incubation at 37°C. Advantages of the assay include: results that are not affected by endogenous plasma HDL, LDL, or VLDL concentration; the Roar donor particle is the preferred substrate by CETP over HDL, thus eliminating competition from endogenous HDL present in the plasma sample; and the addition of excess exogenous acceptor normalizes endogenous acceptor lipoprotein concentration present in the sample, whereas other methods including radioisotopic methods are affected by endogenous HDL concentration. Additionally, an increasing plasma HDL concentration in the sample decreases the specific activity of the labeled HDL substrate due to the equal preference by CETP for either labeled or unlabeled HDL; intra and inter assay

coefficients of variation are less than 3%; and assay components are stable for up to one year and assay substrates are stable at high DMSO concentrations greater than 10% v/v. The CETP Activity Assay Kit uses a donor molecule containing a fluorescent self-quenched neutral lipid that is transferred to an acceptor molecule in the presence of CETP. The CETP-mediated transfer of the fluorescent neutral lipid to the acceptor molecule results in an increase in fluorescence. (Excitation 465nm; Emission 535nm). For the CETP assay, a standard curve was prepared by making serial dilutions of the donor molecule in isopropanol and subsequently recording the fluorescence intensity of each dilution, using isopropanol alone as a blank. The fluorescence intensity values of the standard curve were applied directly to the results to express activity of the plasma sample. For each reaction in the assay procedure, the following components were added: 10µL of the donor molecule, 10µL of the acceptor molecule, 20µL of the 10X CETP Assay Buffer, 1-3µL of serum sample and deionized water to a total of 200µL. These materials were incubated for 30 - 60 minutes at 37°C. The fluorescence intensity of the blank, samples, and positive control were then measured and the fluorescence intensity from each sample was corrected by subtracting the blank fluorescence intensity. The following equation was used to calculate the activity of the plasma sample (Eqn. 3):

$$y = mx + b \qquad \text{Eqn. 3}$$

Where y corresponds to the fluorescence intensity of the sample subtracted from the fluorescence intensity of the blank, m corresponds to the slope of the standard curve, x corresponds to the concentration of the serum sample, and b corresponds to the intercept.

The Roar Ex Vivo CETP Activity Assay is useful for evaluating the non-reversible or reversible inhibitors on plasma CETP activity. The assay is not affected by changes in HDL concentration or other endogenous lipoproteins. The procedure follows

that described for the CETP assay, however, in the EVAK assay, the concentration of serum is 200µL with 5µL substrate compared to 0.5µL serum in 200µL substrate in the CETP assay.

Phospholipid Transfer Protein

Plasma phospholipid transfer protein (PLTP) is thought to play a major role in the facilitated transfer of phospholipids between lipoproteins and in the modulation HDL particle size and composition. PLTP-facilitated lipid transfer activity is related to HDL and LDL metabolism, as well as lipoprotein lipase activity, adiposity, and insulin resistance. The Roar PLTP Activity Assay Kit includes proprietary substrates to detect PLTP mediated transfer of the fluorescent substrate. Transfer activity results in increased fluorescent emission intensity from the assay. The PLTP Activity Assay Kit uses a donor molecule containing a fluorescent self-quenched phospholipid that is transferred to an acceptor molecule in the presence of PLTP. Phospholipid transfer protein-mediated transfer of the fluorescent phospholipid to the acceptor molecule results in an increase in fluorescence (Excitation: 465nm; Emission: 535nm). For the PLTP assay, a standard curve was prepared by making serial dilutions of the donor molecule in isopropanol and subsequently recording the fluorescence intensity of each dilution, using isopropanol alone as a blank. The fluorescence intensity values of the standard curve were applied directly to the results to express activity of the plasma sample. For each reaction in the assay procedure, the following components were added: 10µL of the donor molecule, 10µL of the acceptor molecule, 20µL of the 10X PLTP Assay Buffer, 1-3µL of serum sample, and deionized water to a total of 200µL. These materials were incubated for 30 - 60 minutes at 37°C. The fluorescence intensity of the blank, samples, and positive control were then measured and the fluorescence intensity from each sample was corrected by subtracting the blank fluorescence intensity. Equation 3 was used to calculate the activity of the plasma sample.

CHAPTER III

RESULTS AND DISCUSSION

Overview

Ultimately, the aim of this research was to utilize novel analytical methods for analyzing human serum HDL subfractions. Various method development studies were conducted to establish a reliable protocol, which would provide a comprehensive understanding of serum HDL subfractions. The serum volumes reported here, were 200µL, to adequately visualize all relevant apolipoprotein peaks via secondary analysis methods. Serum was also treated with dextran sulfate, which eliminated all apoB containing lipoproteins, removing the possible influence from these lipoproteins in the analysis and interpretation of HDL subfraction results. In the developmental stages of this method, samples were excised following DGU and re-spun to visualize the location of the excised fractions in the lipoprotein profiles. Upon re-spinning, lipoprotein subfractions were within their defined density ranges demonstrating the accuracy and precision of the method. Capillary electrophoresis analysis of these subfractions also resulted in accurate apolipoprotein distributions.

Mass spectrometry was utilized for the analysis of commercial standards and human serum subfractions. This method validated the serum subfraction elution patterns following solid phase extraction as well as HDL fraction composition. For serum fractions, MALDI-MS provided the molecular weights of the major proteins present in patient HDL fractions. This technique also enabled the visualization of isoforms of apolipoproteins as well as post-translational modifications in the two patient cohorts.

Capillary electrophoresis was also used to analyze commercial standards and human subfraction composition. This method provided electrophoretic mobilities of the standards and also showed reproducible subfraction composition between cohorts.

Collaborative studies providing lipid levels, aortic smooth muscle cell apoptosis levels, and transfer protein activity rates provided further information regarding HDL

subfractions. Apoptosis studies indicated that there was a distinct difference in apoptosis levels between the two cohorts. Transfer protein rates provided additional information regarding the possible influence of cholesteryl ester transfer protein (CETP) and phospholipid transfer protein (PLTP) activity rates on CAD risk.

Overall, an array of analytical methods was used to successfully isolate, purify, and analyze HDL subfractions from two cohorts of patients. In doing so, distinct differences in apolipoproteins were observed and provided strong evidence of possible biomarkers for CAD.

Method Accuracy and Precision Studies

Ultracentrifugation Studies

Preparative UC was used as a primary analysis technique to separate the HDL region of the lipoprotein profile and facilitate excision for secondary analysis. At a concentration of 0.300M the solute dicesium cadmium ethylenediaminetetraacetic acid (Cs_2CdY), effectively broadens HDL particle distribution, allowing for excision of HDL subfractions while also providing ideal resolution of the HDL region from neighboring regions. It was beneficial to remove all apoB containing lipoproteins such as VLDL, LDL, IDL, Lp(a) and chylomicrons. The removal of apoB containing lipoproteins prior to ultracentrifugation minimized interferences particularly from LDL and Lp(a). This process involved precipitation of apoB containing lipoproteins by the addition of a dextran sulfate reagent to whole serum prior to UC as described in the methods chapter.[180] A superimposed comparison between lipoprotein density profiles using human serum spun in a 0.18M NaBiY density gradient solution with and without dextran sulfate treatment verified that the procedure cleanly removed all apoB-containing lipoproteins from the serum profile prior to sample analysis (Figure 5). By merging treatment of serum with dextran sulfate with a UC spin using 0.300M Cs_2CdY, it was possible to freeze serum samples following DGU, maintain their spatial arrangement, and subsequently excise them for secondary analyses.

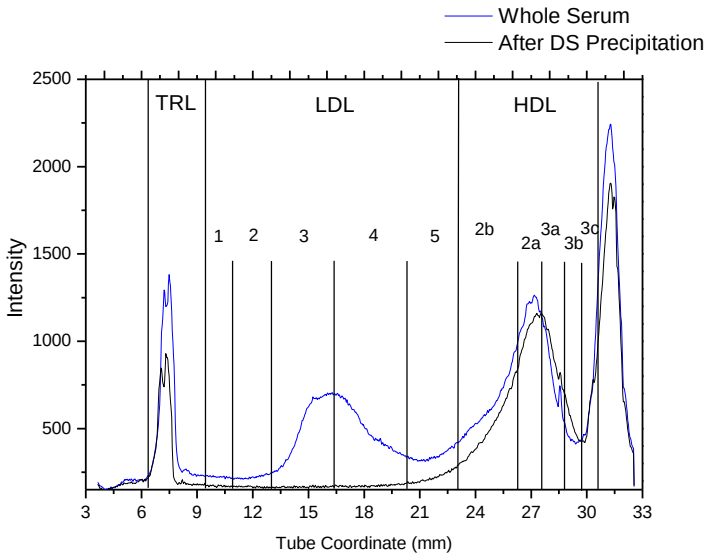

Figure 5. Superimposed lipoprotein density profiles corresponding to 6µL of whole serum (blue) and 6µL of serum following treatment with dextran sulfate (black) in a 0.18M solution of NaBiY, spun for 6 hours at 120,000rpm at 5°C.

Analysis of Re-Spun Fraction Lipoprotein Profiles

For preparative ultracentrifugation, it was determined that previously used density ranges were not ideal for the conditions used during DGU to obtain lipoprotein profiles and accurately excised serum subfractions. The formerly used ranges were obtained from literature sources which utilized an alternative method known as rate zonal ultracentrifugation. Upon re-spinning fractions using the former density ranges, the HDL_3 fractions consistently appeared in the HDL_2 region of the lipoprotein density profile. Upon review of the literature, more accurate definitions for the density ranges including 1.063 – 1.125g/mL for HDL_2 and 1.125 – 1.210g/mL for HDL_3 were used.[181] All particles in the aggregated distribution in the density range below 1.063g/mL were designated as the top or non-HDL fraction, while those in the density range above 1.210g/mL were designated as the bottom or protein fraction. To investigate the redefined density boundaries, serum was spun in replicate to obtain DGU lipoprotein

profiles, subfractions were excised, the average densities were determined, and these subfractions were re-spun. Figure 6 shows a lipoprotein profile from a 200µL serum sample following treatment with dextran sulfate. The cut points for the HDL fractions were based upon the defined boundaries of the density regions for HDL_2 and HDL_3, and are represented by the blue vertical lines in the lipoprotein profile. The first peak in the profile, is an imaging artifact that corresponds to the reflection of fluorescence radiation emanating from the lipoprotein layers to the meniscus in the UC tube. As the density increased leading into the HDL_2 region, there appeared to be overlap of the HDL_2 peak into the non HDL fraction, spanning the density range of approximately 1.050 – 1.063g/mL. This observation is likely due to the use of the 200µL serum volume which was used in order to effectively analyze fractions by secondary methods. Two hundred microliters of serum, is beyond the volume required for saturation. Saturation is achieved using 10µL of the fluorophore NBD and 6µL of serum; thus the relatively large volume of serum used, is likely responsible for the appearance of the HDL_2 peak outside of its defined boundary. This result in turn indicated that minimal amounts of HDL would be present in the neighboring non HDL fraction. Likewise, beyond the upper boundary of the HDL_2 region proceeding into the HDL_3 region, there was overlap of HDL_2 into the HDL_3 region spanning the density range of approximately 1.125 – 1.175g/mL. This result is also likely due the large serum volume used and indicated that HDL_2 would be present in the HDL_3 fraction following excision. The degree of overlap between the HDL_3 and protein fraction was inconclusive prior to re-spinning. The profile intensity suggested that there would be overlap between these fractions. Overlap between the HDL_3 and protein subfractions could be due to aggregation of HDL_3 with protein fraction components, which may have caused the majority of the HDL_3 peak to shift to the denser protein fraction though a shoulder remained in the HDL_3 density region. It is also important to note that the seam of the UC tube coincides with the density range between the HDL_3 and protein fractions. As this is the bottom of the UC tube, it is also possible that separation was limited in this region due to UC tube length. This seam or reference line in the wall of the UC tube, appears consistently between 28 –

29mm and is also a measurement of the reproducibility of the method. The distribution above 1.210g/mL consists of free proteins which sediment to the bottom of the UC tube. The intensity of this region however indicated that there may also be a substantial amount of lipid in this region, since the fluorophore utilized in DGU is lipophilic and fluoresces in a hydrophobic environment. Such fluorescence supports the hypothesis that there may be overlap of HDL_3 in this region and may also be due to aggregation of HDL_3 with protein, in addition to separation limitations due to the UC tube length.

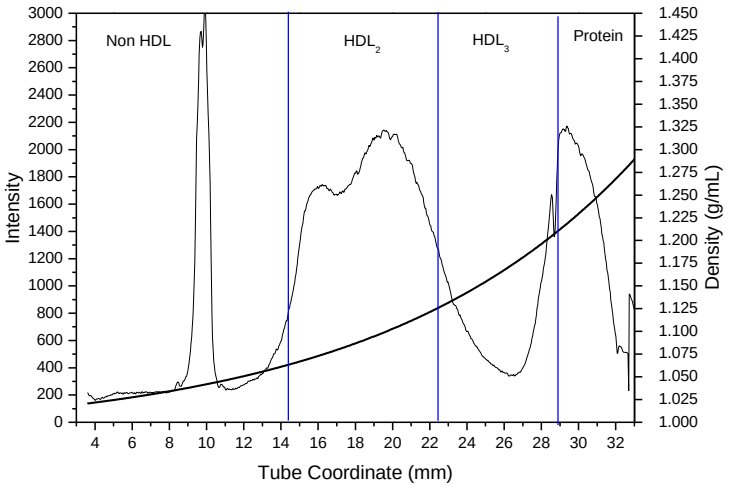

Figure 6. DGU lipoprotein profile of a 200µL serum sample after treatment with dextran sulfate using 0.300M Cs_2CdY density gradient.

Following the acquisition of the total lipoprotein profile, each non HDL, HDL_2, HDL_3, and protein fraction was excised and re-spun. Figure 7 shows the resulting lipoprotein density profile following re-spinning the excised non HDL fraction. This result supported the hypothesis that there would be overlap between the non HDL and HDL_2 regions; and that the non HDL region would as a result, contain minimal amounts of HDL_2. The peak present in the re-spun non HDL fraction spanned a density range of 1.050 – 1.063g/mL which is slightly greater than the range of overlap approximated

from the total lipoprotein profile shown in Figure 6. The non HDL fraction contained an average density of 1.034 ± 0.004 g/mL which was within the defined density range of this fraction, however, as Figure 7 shows, this fraction contained a particle which appeared in the density range corresponding to HDL_2. Further analysis by secondary methods would elucidate the composition of this peak.

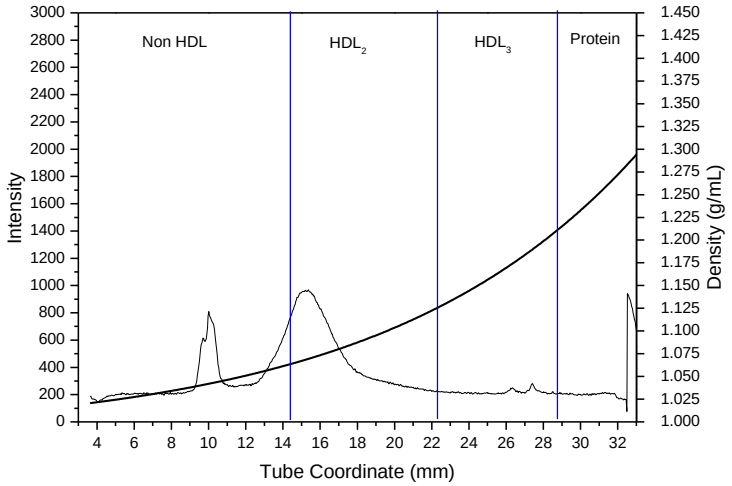

Figure 7. DGU lipoprotein profile of the re-spun non HDL fraction from a previously spun 200µL serum sample after treatment with dextran sulfate using 0.300M Cs_2CdY density gradient.

Figure 8 shows the resulting lipoprotein density profile following re-spinning the excised HDL_2 fraction. The resulting profile closely resembled the serum profile shown in Figure 6 prior to subfraction excision. Figure 8 shows overlap into the neighboring non HDL and HDL_3 density regions, with a total HDL_2 re-spun fraction spanning the density range of 1.050 – 1.160g/mL. The HDL_2 fraction contained an average density of 1.070 ± 0.004 g/mL. As there is an enrichment of HDL_2 in the total lipoprotein profile from this sample, it was observed that this fraction overlapped into neighboring density regions. Additionally, the aggregation of HDL_2 with HDL_3 or perhaps other serum

proteins may contribute to the HDL_2 having higher density which spans beyond the defined HDL_2 density range into the defined HDL_3 density range.

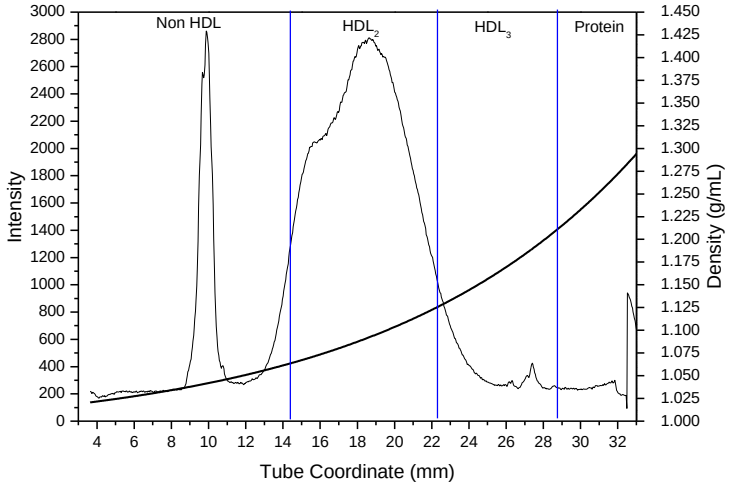

Figure 8. DGU lipoprotein profile of the re-spun HDL_2 fraction from a previously spun sample of 200µL serum after treatment with dextran sulfate using 0.300M Cs_2CdY density gradient.

Figure 9 shows the lipoprotein density profile following re-spinning the excised HDL_3 fraction. The resulting profile provided a much clearer understanding of the composition of this serum subfraction. As hypothesized from the visual distribution of HDL_2 in Figure 6, the re-spun HDL_3 contained a peak in the density range between 1.063 – 1.150g/mL which may correspond to HDL_2 and be due to overflow of HDL_2 into the HDL_3 region due to the large serum volume used. It is also possible that this peak is an artifact or possibly a fragment which dissociated from the HDL_3 particle during ultracentrifugation and possesses a density within the HDL_2 density range. It is also possible that there may be aggregation of HDL_2 with HDL_3, and that re-spinning cut fractions provided the force to separate joined lipoprotein particles. Most importantly, the HDL_3 peak was visualized within its defined boundary at a high intensity. There was overlap between the HDL_3 and bottom or protein regions, with a peak appearing in the

density range between 1.150 – 1.126g/mL which was also hypothesized from Figure 6. This overlap may be due to the HDL_3/protein fraction boundary being in such close proximity to the bottom of the UC tube. The HDL_3 fraction contained an average density of 1.128 ± 0.016g/mL.

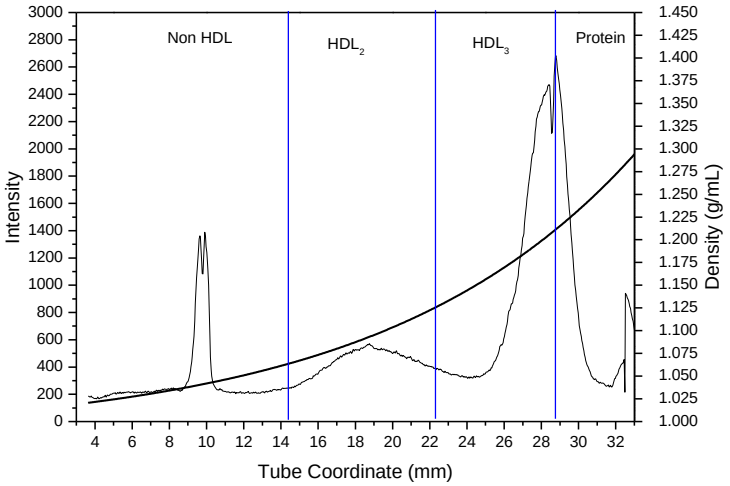

Figure 9. DGU lipoprotein profile of the re-spun HDL_3 fraction from a previously spun 200µL serum sample after treatment with dextran sulfate using 0.300M Cs_2CdY density gradient.

Figure 10 shows the resulting lipoprotein density profile following re-spinning the protein fraction. As hypothesized from the serum profile shown in Figure 6, this fraction contained overlap with the HDL_3 region. The HDL_3/protein fraction boundary appears near the bottom of the UC tube, limiting further separation of HDL_3 from protein beyond this point. The peak visualized in the re-spun protein fraction spanned a density range between 1.150 – 1.126g/mL which is the same as the re-spun HDL_3 fraction profile. This result supported the hypothesis that the protein fraction fluoresces due to HDL_3 contamination or overlap. The protein fraction contained an average density of 1.245 ± 0.016 g/mL which is within the defined range for the protein fraction, however, near the lower limits of the range influenced most likely by the HDL_3 content

of this fraction. Table 3 provides the average densities of each cut fraction from the replicate samples.

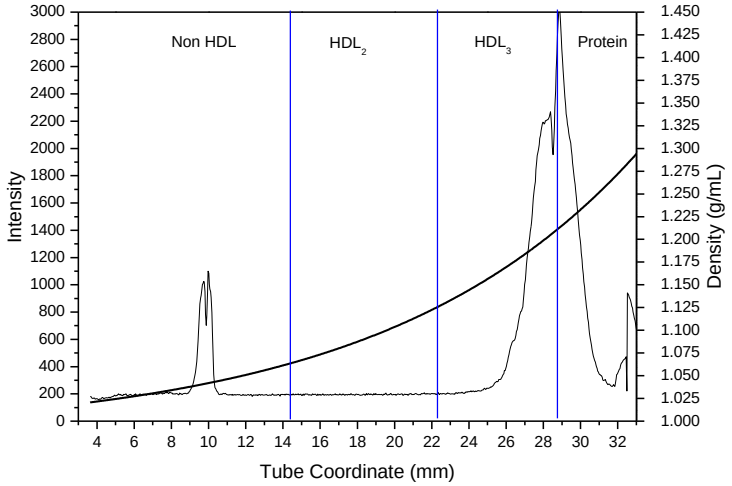

Figure 10. DGU lipoprotein profile of the re-spun protein fraction from a previously spun 200µL serum sample after treatment with dextran sulfate using 0.300M Cs_2CdY density gradient.

Table 3. Average density data corresponding to the cut fractions from the 200µL DS serum sample shown in Figures 6 through 9.

Fraction	Average Weight (g)	Average Volume (µL)	Average Density (g/mL)	Literature Values (g/mL)
Non HDL	0.1030 ± 0.0004	100 ± 0.1	1.034 ± 0.004	<1.063
HDL_2	0.1070 ± 0.0004	100 ± 0.1	1.070 ± 0.004	1.063 – 1.125
HDL_3	0.1130 ± 0.0016	100 ± 0.1	1.128 ± 0.016	1.125 – 1.210
Protein	0.0620 ± 0.0019	50 ± 0.1	1.245 ± 0.038	1.210<

Overall, re-spinning excised serum subfractions provided a closer look into the actual composition and densities of the subfractions. The redefined boundaries did result in an improvement in the accuracy of obtaining the desired subfractions. All

subfractions with the exception of HDL_2 showed the presence of additional peaks outside of the fraction's defined density range. It is possible that these fractions were contaminated by neighboring density region subfractions, which can be expected in a liquid state sample system with closely defined boundaries. Such overlap may be attributed to the limitations of the current laboratory fractionation technology and equipment as well. The cryogenic procedure used to freeze serum samples, saw used to excise fractions, and the fact that the HDL_3/protein fraction boundary is near the bottom of the UC tube, may introduce further error into the fractionation process. The major contributing factor to any possible overlapping of fractions however, is hypothesized to be due to the fact that the 200µL serum volume is over 30 times greater than the serum volume needed for saturation. The densities of each excised fraction were obtained in triplicate and the average densities of each were within their defined ranges despite the possible mixing that occurred between the subfractions. Most importantly, the results demonstrate the capability of the methodology to excise serum fractions accurately and precisely within the defined density ranges. As our current procedure incorporates a novel solute system unlike those predominantly reported in the literature, it has been shown that the heavy metal density gradient system does not substantially compromise the integrity or density of lipoproteins. Due to the fact that the subfractions possibly contained neighboring serum subfractions particularly the non HDL and protein fractions, all four fractions were excised, retained and analyzed in subsequent experiments to obtain a comprehensive analysis of the each serum sample.

C_{18} Solid Phase Extraction Delipidation Studies

Purified apolipoproteins were prepared from lipoprotein fractions obtained from preparative UC using a delipidation procedure described in the methods chapter which incorporated a reversed phase SPE cartridge. This purification facilitated the preparation of apolipoproteins for high resolution MALDI-MS and capillary electrophoresis. Serum HDL subfractions must be subjected to delipidation prior to secondary analysis to both remove lipids and de-salt the sample following UC. Solid phase extraction served to

retain the most nonpolar lipid components and elute the polar components of each sample. Using capillary electrophoresis, all four 100µL elutions were retained separately and analyzed following solid phase extraction to investigate the composition of each elution.

Figure 11 shows the resulting electropherograms following the analysis of the first 100µL elution after solid phase extraction. The major apolipoproteins and serum proteins were observed in the first elution.

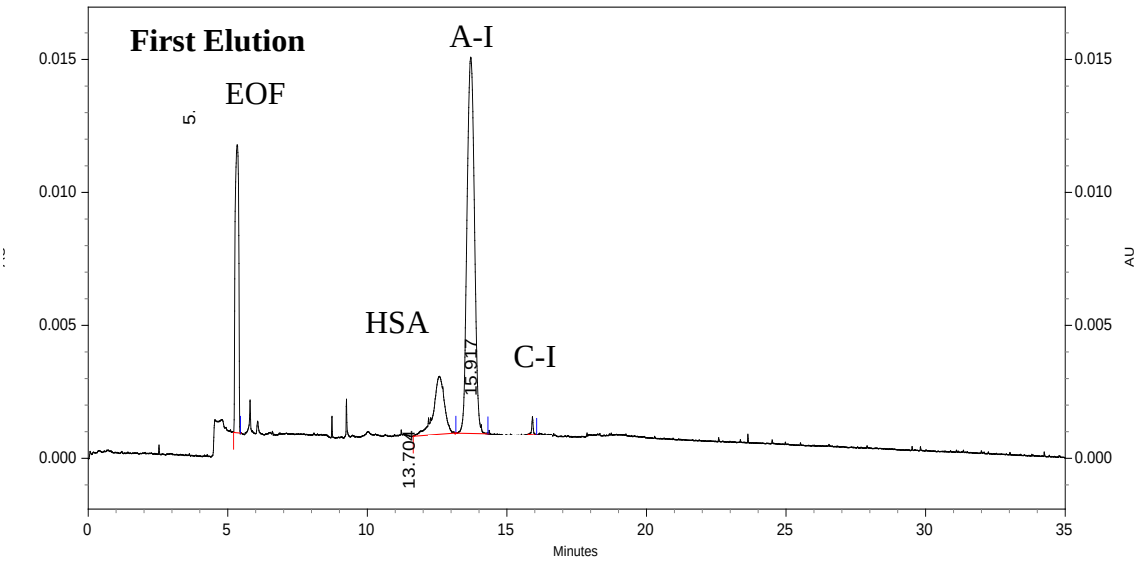

Figure 11. Electropherogram corresponding to the first elution following solid phase extraction of an HDL_2 fraction from a 200µL serum sample.

Figure 12 shows the resulting electropherograms following the analysis of the second, third, and fourth 100µL elutions following solid phase extraction. There were no analyte peaks in the second, third, or fourth elutions. This experiment was repeated in replicate, with reproducible results and that were observed in patient sample elutions as well.

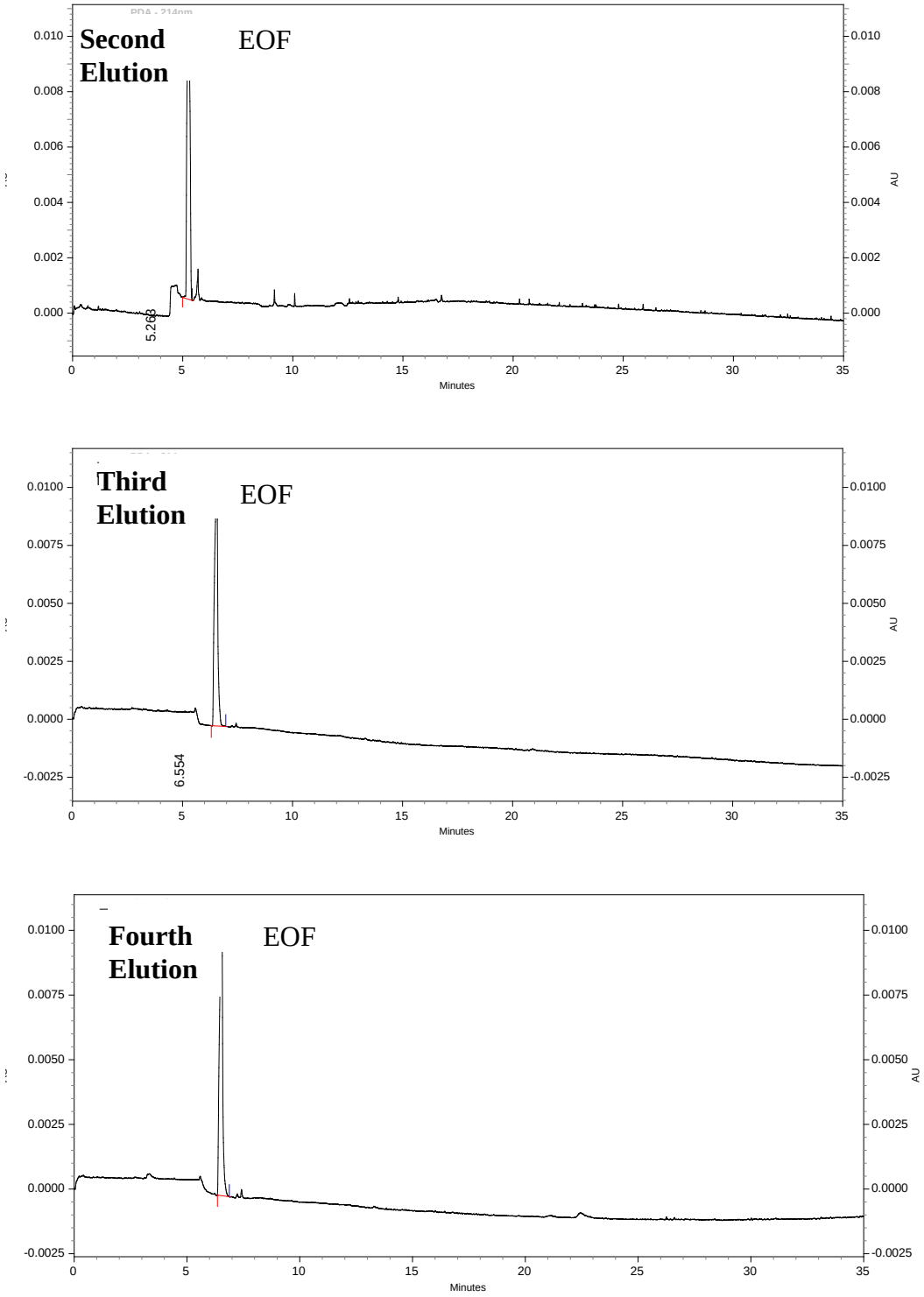

Figure 12. Electropherograms corresponding to the second, third, and fourth elutions following solid phase extraction of an HDL_2 fraction from a 200µL serum sample.

This result was quite different from previous elution pattern experiments which reported analytes in all four 100µL eluents.[79] This difference is most likely due to the modifications to the solid phase extraction procedure which included increasing the amount of time that the eluent interacted with the sorbent bed prior to elution, and decreasing flow rates to the rate of gravity. Mass spectrometry was also used to investigate and confirm the elution profile from the solid phase extraction cartridge. Four aliquots of 100µL eluents were individually obtained and prepared for MALDI-MS as described in the methods chapter. Figure 13 corresponds to the first through fourth elutions following solid phase extraction of an excised HDL_2 fraction. This sample contained several apolipoprotein peaks including apoA-I, C-I, C-II/C-III isoforms, and albumin. The second through fourth 100µL elutions of the excised HDL_2 fraction following solid phase extraction, showed no detectable analyte peaks.

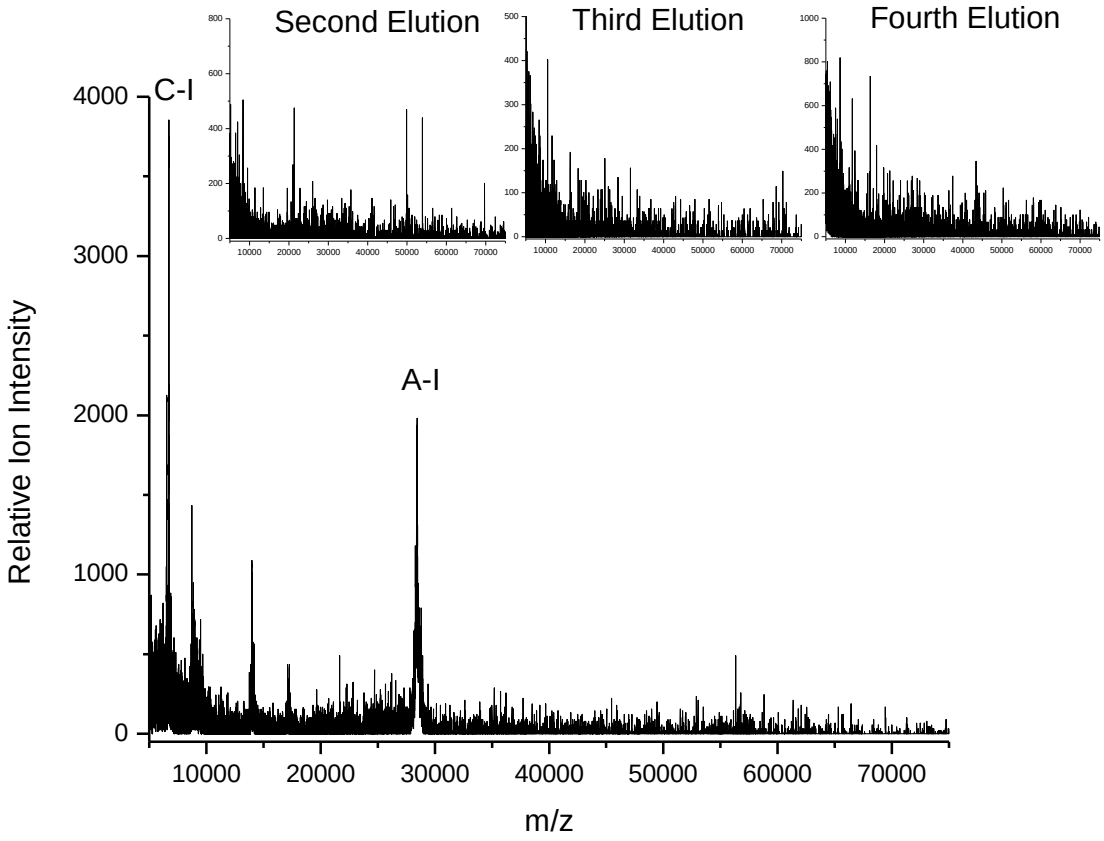

Figure 13. MALDI-MS spectra corresponding to the first (large) through fourth elutions of an HDL_2 serum subfraction following solid phase extraction.

The results obtained from MALDI-MS analysis supported the results obtained by capillary electrophoresis and indicated that the elution of analyte peaks was completed in the first 100µL elution. In Figure 11 the peaks are identified as human serum albumin, apoA-I, and apoC-I, with effective mobilities which all correspond with the mobility determination experimental results which will be presented in the following section. Overall, the C_{18}-SPE desalting/delipidating method provided purified apolipoproteins from the HDL fractions in an analyte matrix amenable to a variety of analytical methods.

Serum Subfraction Composition Studies

High density lipoprotein as a whole contains a higher protein content and lower lipid content than less buoyant fractions such as LDL, VLDL, and chylomicrons. This fraction likewise contains many apolipoproteins and varying ratios of these surface proteins between HDL subfractions. Several studies were conducted to investigate the composition of HDL subfractions to identify differences between the two cohorts. Prior to analyzing serum subfractions, several studies were conducted using commercial protein standards.

Commercial Protein Standards: Electrophoretic Mobility and Purity Determination

Protein mobility experiments were conducted to determine the effective mobilities of commercial standards. These commercial standards were used in order to identify apolipoprotein serum fraction composition and elution patterns based on electrophoretic mobilities and molecular weight. Each commercial standard solution was analyzed in triplicate by CE and the effective mobility of each was calculated. For the CE electropherograms, the absorbance at 214nm was plotted as a function of the effective mobility (μ_{eff} x 10^{-5} $cm^2/V*s$). In the electropherograms, the mobilities were in the opposite direction of the electroosmotic flow, giving the effective mobilities a negative charge. Calibration curves were prepared at a wavelength of 214nm as described in the methods section to enable quantitation by CE. Briefly, a series of solutions including apoA-I, apoC-I, and bovine serum albumin, containing varying standard solution concentrations was analyzed in triplicate by CE. Linear regression was done for each of the calibration curves and the resulting equations were used for subsequent concentration calculations. The MALDI-MS analysis assessed the purity of the commercial standards. The MALDI-MS spectra are presented as the relative ion intensity plotted as a function of the mass to charge (*m/z*) ratio. The commercial specifications for purity of the apolipoproteins were ≥ 99% by SDS-PAGE.

The electropherogram of the 80.0mg/dL bovine serum albumin (BSA) solution in the presence of 0.1% aqueous TFA is shown in Figure 14. Only one peak was observed in addition to the EOF marker in the electropherogram. This indicated that the solution was relatively pure for BSA. The mobility of the bovine serum albumin peak was -20.869 ± 0.069 x 10^{-5} $cm^2/V*s$ and the corrected peak area (CPA) was 78463 ± 3317. The corrected peak area was calculated using an algorithm in the Beckman P/ACE Station Migration software and accounted for the band broadening due to the duration of time required for the peak to pass by the detector.

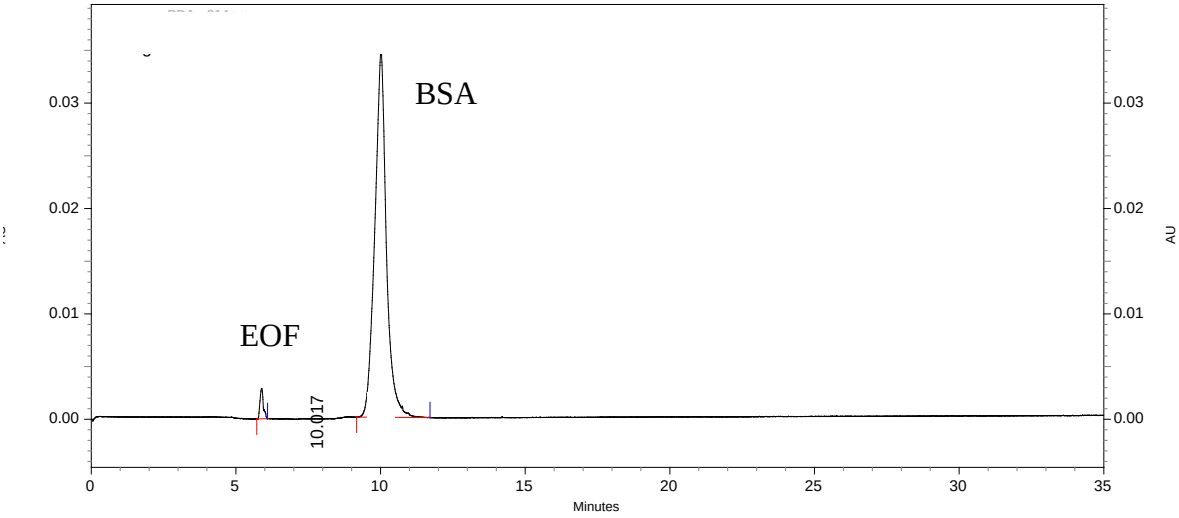

Figure 14. Electropherogram corresponding to 80.0mg/dL bovine serum albumin.

Figure 15 is the MALDI mass spectrum of the bovine serum albumin solution. One major peak was observed in the spectrum corresponding to bovine serum albumin. An additional peak was observed corresponding to doubly protonated bovine serum albumin. In all MALDI spectra, the protonated molecule was designated by the apolipoprotein and the doubly protonated molecule was identified by a superscript charge. To assess the effect of solid phase extraction on samples, the bovine serum albumin standard was subjected to solid phase extraction and analyzed by MALDI-MS.

Figure 15 corresponds to the resulting MALDI spectrum obtained following solid phase extraction. There was no fragmentation observed in the bovine serum albumin standard.

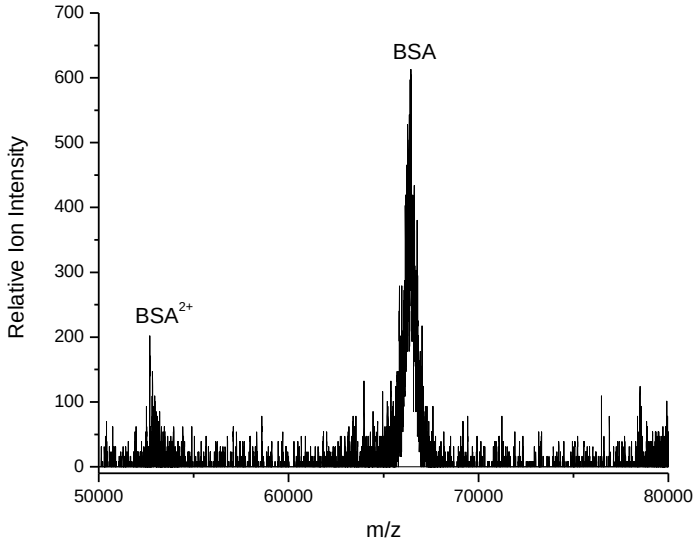

Figure 15. MALDI-MS spectrum corresponding to 80.0mg/dL bovine serum albumin in 0.1% (v/v) TFA.

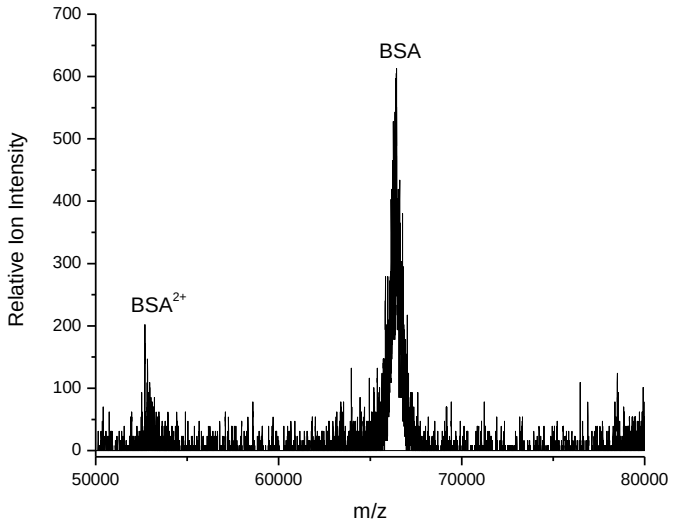

Figure 16. MALDI-MS spectrum corresponding to 80.0mg/dL bovine serum albumin in 0.1% (v/v) TFA after solid phase extraction.

Overall, the MALDI-MS and CE data indicated that the standard bovine serum albumin solution was of high purity, and was not compromised following solid phase extraction. Figure 17 corresponds to the bovine serum albumin calibration curve. From the derived linear regression of the CPA in Figure 17, bovine serum albumin concentration from CPA values could be calculated according as follows: (Eq. 4)

Calculated bovine serum albumin concentration = CPA/993.13. Eq. 4

The average electrophoretic mobility corresponding to bovine serum albumin was $-20.914 \pm 0.0961 \times 10^{-5}$ $cm^2/V*s$ and the average elution time of bovine serum albumin was 10.139 ± 0.0789 min. Table 4 provides the average effective mobilities, corrected peak areas (CPA) and elution times for each of the standard dilutions.

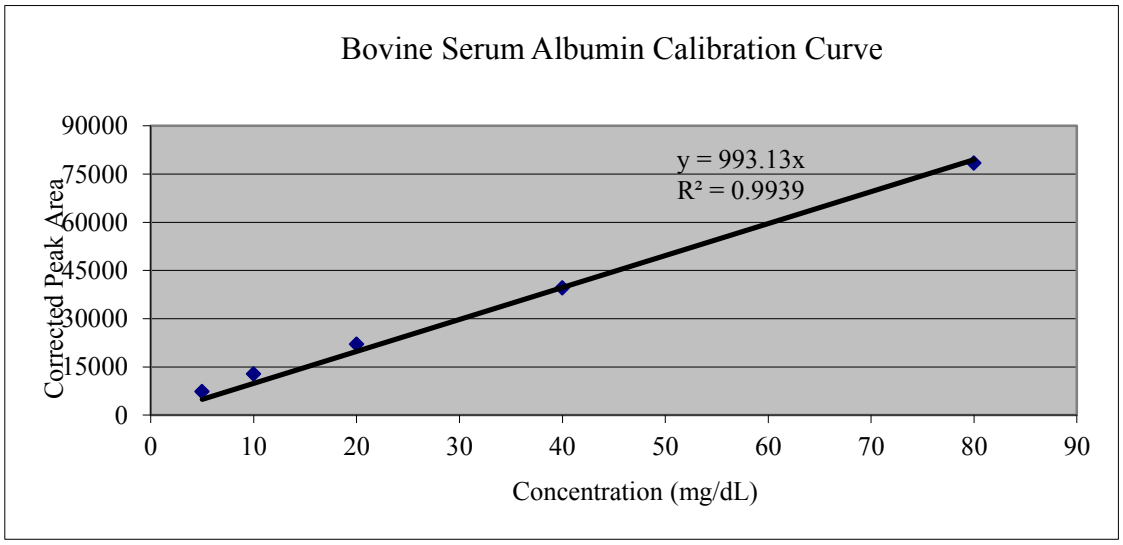

Figure 17. Calibration curve generated from the corrected peak area (CPA) of bovine serum albumin standard dilutions versus the concentration of the bovine serum albumin standard dilutions by capillary electrophoresis at 214nm.

Table 4. BSA data corresponding to each dilution of the bovine serum albumin standard.

BSA Concentration (mg/dL)	Area	Calculated Concentration (mg/dL)	Mobility ($x10^{-5}cm^2/Vs$)	Elution Time (min)
80.0	78463 ± 3317	78.98 ± 0.005	-20.869 ± 0.149	10.061 ± 0.062
40.0	39570 ± 3747	38.31 ± 0.185	-20.852 ± 0.136	10.121 ± 0.030
20.0	22080 ± 1433	21.86 ± 0.004	-20.906 ± 0.065	10.131 ± 0.068
10.0	12794 ± 1272	12.34 ± 0.007	-20.917 ± 0.033	10.159 ± 0.083
5.0	7406 ± 1726	6.42 ± 0.014	-21.029 ± 0.037	10.225 ± 0.106

The electropherogram of the 80.0mg/dL apoA-I solution in the presence of 0.1% aqueous TFA is shown in Figure 18. Two additional peaks were observed in the electropherogram besides the EOF marker and the apoA-I peak indicating possible impurities in the standard. The mobility of the apoA-I peak was -24.758 ± 0.295 x 10^{-5} cm^2/V*s and the corrected peak area (CPA) was 28110 ± 2252.

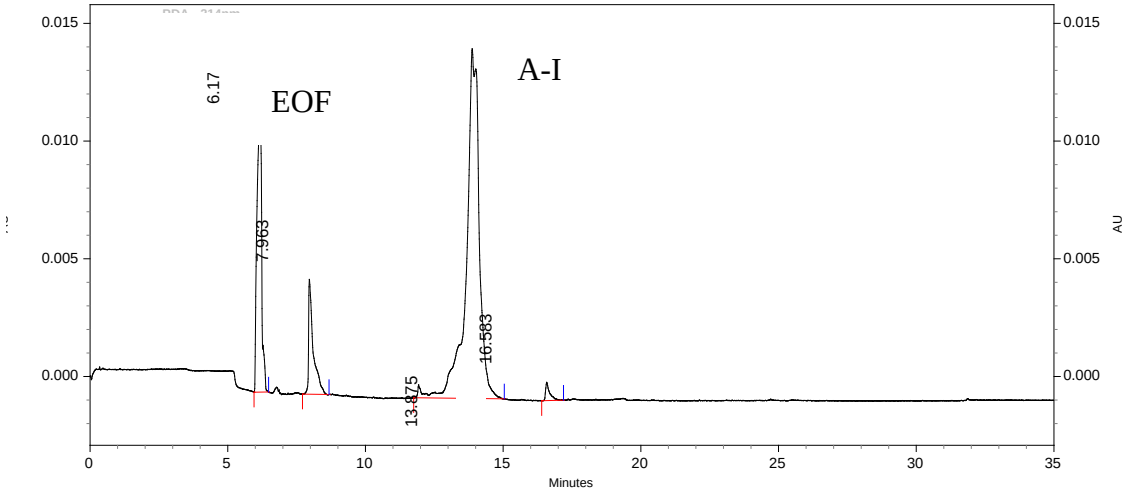

Figure 18. Electropherogram corresponding to 80.0mg/dL apo A-I.

Figure 19 is the MALDI mass spectrum corresponding to apoA-I. Two major peaks were observed in the spectrum corresponding to singly and doubly protonated

apoA-I. A third peak was observed on the shoulder of the protonated molecule designated A-I_{add} +98. This peak was likely attributed to the addition of phosphoric acid and or sulfuric acid molecules originating from the commercial sample purification procedure, as also observed in previous studies.[182] Figure 20 corresponds to the resulting MALDI-MS spectrum following solid phase extraction. There was no fragmentation of the commercial apoA-I standard following solid phase extraction. The results obtained from the commercial apoA-I standard solutions by MALDI-MS and CE indicated that the standard was of high purity. The MALDI-MS findings also verified that the predominant peak in the electropherogram corresponded to apoA-I.

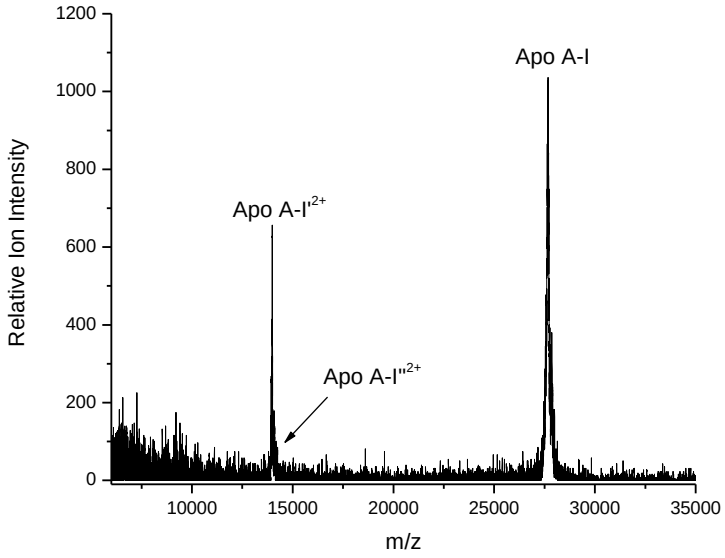

Figure 19. MALDI-MS spectrum corresponding to 80.0mg/dL apoA-I in 0.1%(v/v) TFA.

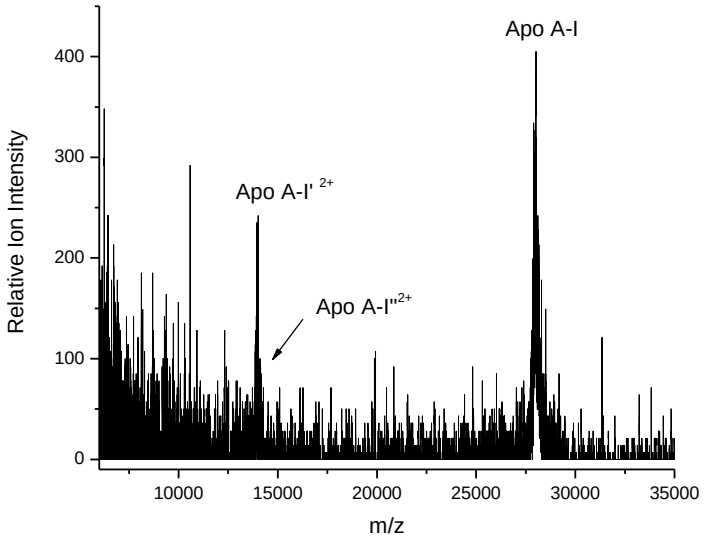

Figure 20. MALDI-MS spectrum corresponding to 80.0mg/dL apoA-I in 0.1%(v/v) TFA after solid phase extraction.

Figure 21 corresponds to the apoA-I calibration curve. From the derived linear regression of the CPA in Figure 21, apoA-I concentration from CPA values could be calculated according as follows: (Eq. 5)

Calculated apoA-I concentration = CPA/360.40. Eq. 5

The average electrophoretic mobility corresponding to apoA-I was -24.776 ± 0.2649 x 10^{-5} cm^2/V*s and the average elution time of apoA-I was 13.610 ± 0.5612 min. Table 5 provides the average effective mobilities, corrected peak areas (CPA) and elution times for each of the standard dilutions.

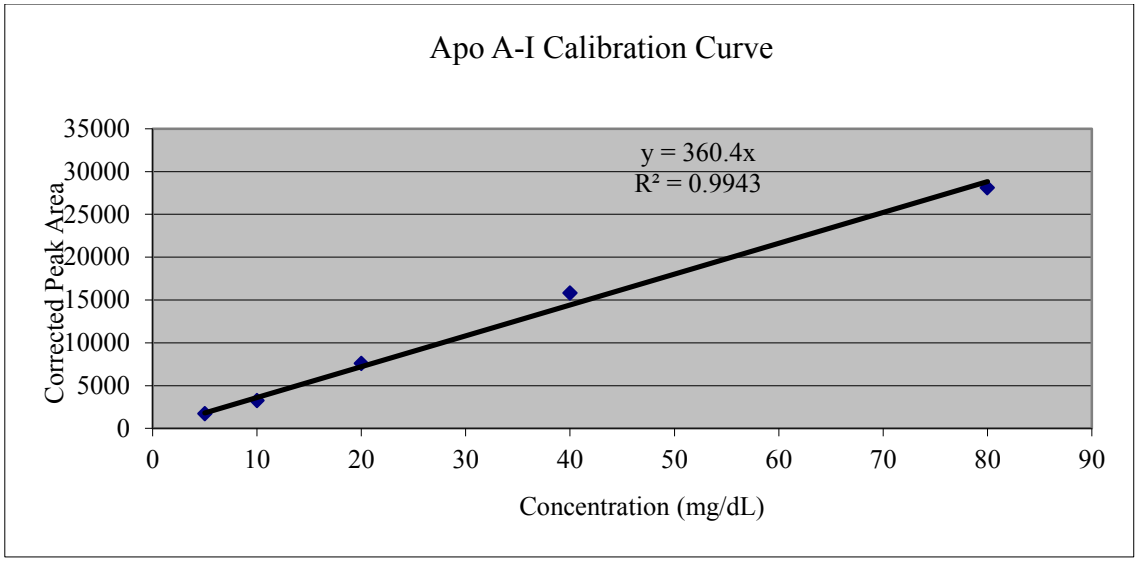

Figure 21. Calibration curve generated from the corrected peak area (CPA) of apoA-I standard dilutions versus the concentration of the apoA-I standard dilutions by capillary electrophoresis at 214nm.

Table 5. ApoA-I data corresponding to each dilution of the apoA-I standard.

ApoA-I Concentration (mg/dL)	**Area**	**Calculated Concentration (mg/dL)**	**Mobility ($x10^{-5}cm^2/Vs$)**	**Elution Time (min)**
80.0	28110 ± 2252	77.32 ± 0.013	-24.758 ± 0.295	13.325 ± 0.778
40.0	15788 ± 372	48.71 ± 0.035	-24.740 ± 0.313	13.429 ± 0.890
20.0	7596 ± 90	22.36 ± 0.004	-24.752 ± 0.733	13.362 ± 0.926
10.0	3245 ± 303	10.62 ± 0.009	-24.445 ± 0.586	14. 611 ± 2.808
5.0	1704 ± 59	5.64 ± 0.012	-25.187 ± 1.661	13.321 ± 0.884

The electropherogram of apoC-I is observed in Figure 22. The major peak observed at a mobility of -31.325 ± 0.279 x 10^{-5} $cm^2/V*s$ with a CPA of 32017 ± 2988 was identified as apoC-I. Additional peaks were observed, eluting before and after apoC-I which were likely impurities in the standard.

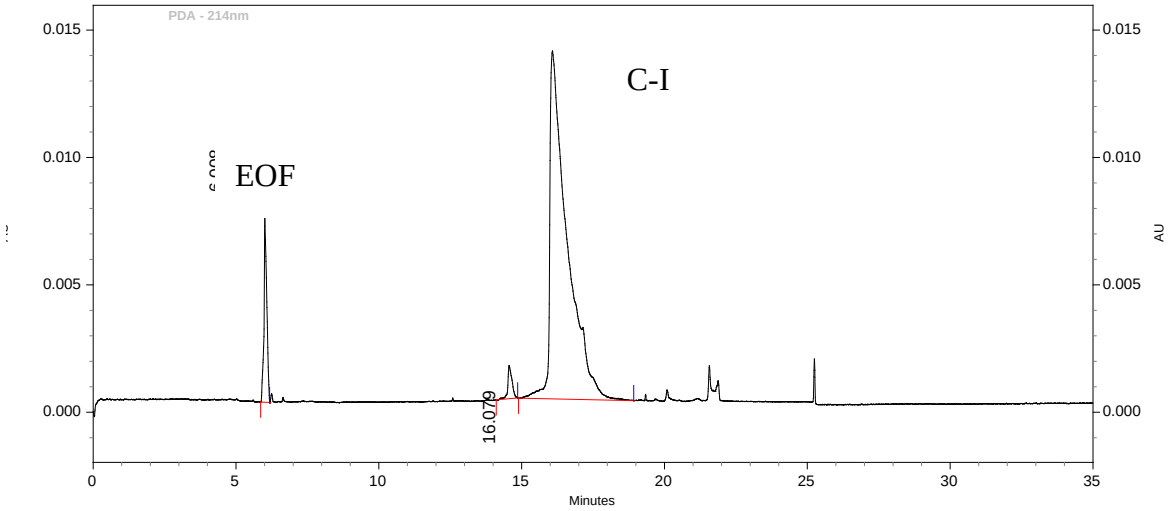

Figure 22. Electropherogram corresponding to 80.0mg/dL apoC-I.

The MALDI spectrum of the apoC-I solution is seen in Figure 23. The primary peak observed was due to the protonated molecule of apoC-I. The shorter peak in front of the primary peak was identified as apoC-I' and corresponds to the truncated protein missing the last two N-terminal amino acids, threonine and proline. As observed in the MALDI spectrum for apoA-I these two peaks were detected along with the addition of a +98 adduct which is likely attributed to the addition of phosphoric acid or sulfuric acid molecules originating from the commercial sample purification procedure.[182] Figure 24 shows the MALDI-MS spectrum corresponding to the apoC-I standard following solid phase extraction, and shows no fragmentation.

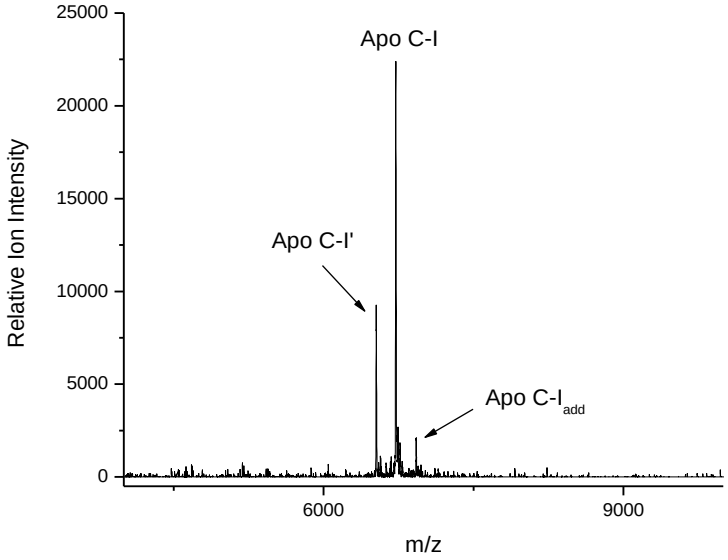

Figure 23. MALDI-MS spectra corresponding to 80.0mg/dL apoC-I in 0.1% (v/v) TFA.

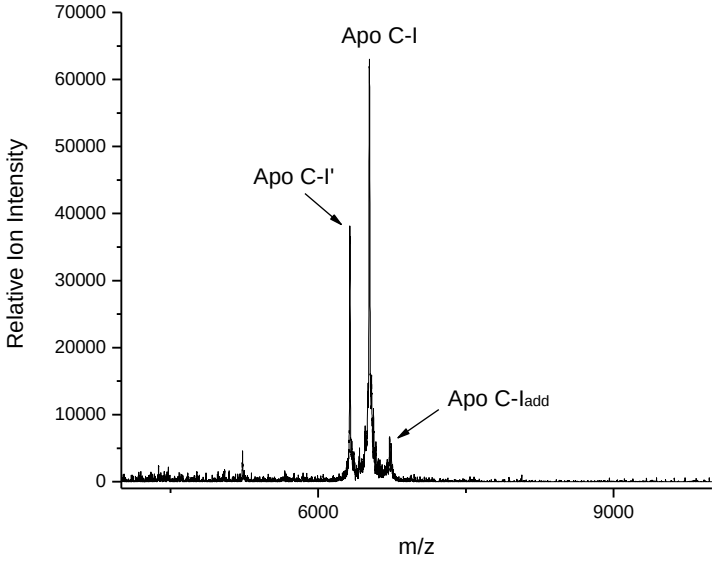

Figure 24. MALDI-MS spectra corresponding to 80.0mg/dL apoC-I in 0.1% (v/v) TFA after solid phase extraction.

Figure 25 corresponds to the apoC-I calibration curve. From the derived linear regression of the CPA in Figure 25, apoC-I concentration from CPA values could be calculated as follows: (Eq. 6)

Calculated apoC-I concentration = CPA/423.26. Eq. 6

The average electrophoretic mobility corresponding to apoC-I was -31.929 ± 0.4782 x 10^{-5} $cm^2/V*s$ and the average elution time of apoC-I was 17.038 ± 0.7272 min. Table 6 provides the average effective mobilities, corrected peak areas (CPA) and elution times for each of the standard dilutions.

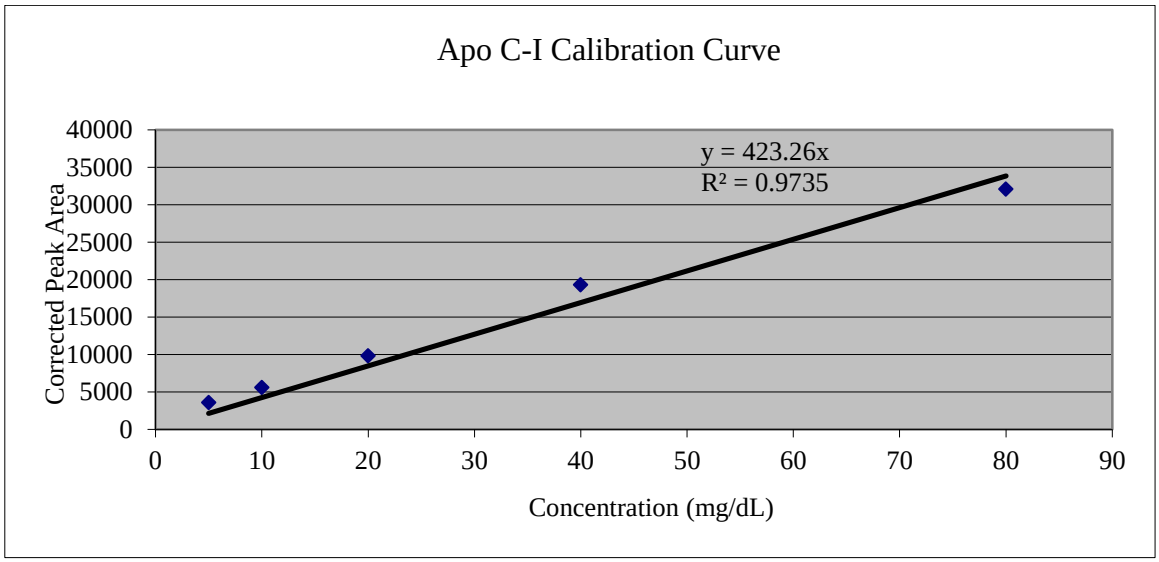

Figure 25. Calibration curve generated from the corrected peak area (CPA) of apoC-I standard dilutions versus the concentration of the apoC-I standard dilutions by capillary electrophoresis at 214nm.

Table 6. ApoC-I data corresponding to each dilution of the apoC-I standard.

ApoC-I Concentration (mg/dL)	**Area**	**Calculated Concentration (mg/dL)**	**Mobility ($x10^{-5}cm^2/Vs$)**	**Elution Time (min)**
0.800	32017 ± 2988	78.84 ± 0.0340	-31.325 ± 0.279	15.996 ± 0.117
0.400	19313 ± 1052	47.61 ± 0.042	-31.891 ± 0.354	16.611 ± 0.004
0.200	9812 ± 1249	24.06 ± 0.004	-32.328 ± 0.337	17.240 ± 0.021
0.100	1003 ± 5593	13.67 ± 0.005	-31.573 ± 0.292	17.631 ± 0.003
0.050	3560 ± 173	8.78 ± 0.008	-32.440 ± 0.708	17.713 ± 0.312

The calibration curves showed a strong linear relationship between concentration and UV absorbance over the selected concentration range for both apolipoproteins. The corrected area of peaks that migrated past the detector was calculated as a function of the integrated area and velocity of the peaks, length to the detector, and the migration time of the peaks as they eluted through the capillary.

MALDI-MS Accuracy and Precision

Replicate commercial bovine insulin samples were used to assess the accuracy and precision of the MALDI-MS instrumentation. This would in turn provide further confidence in the mass measurements that were detected in the actual serum samples. Ten 100.0mg/dL bovine serum insulin samples were ran and analyzed by MALDI-MS.

The results of this experiment further demonstrated the accuracy and precision of the MALDI-MS procedure and instrumentation. The known mass of bovine insulin is 5734.59 Da as verified by the LBMS instrument database. The results of this experiment showed the exceptional precision and accuracy of the MALDI-MS instrumentation from the closeness of each measured insulin standard mass to the known mass, as well as to the other standard sample masses. Figures 26 and 27 show the MALDI-MS spectra corresponding to each of the ten samples. The intensities of the samples were comparable with the exception of two samples with relatively lower intensities. The fluctuation in intensities is due to the fact that the MALDI-MS analysis is qualitative as opposed to quantitative. Fluctuations in intensity also may be attributed to the heterogeneity of the electromagnetic fields on the MALDI plate.

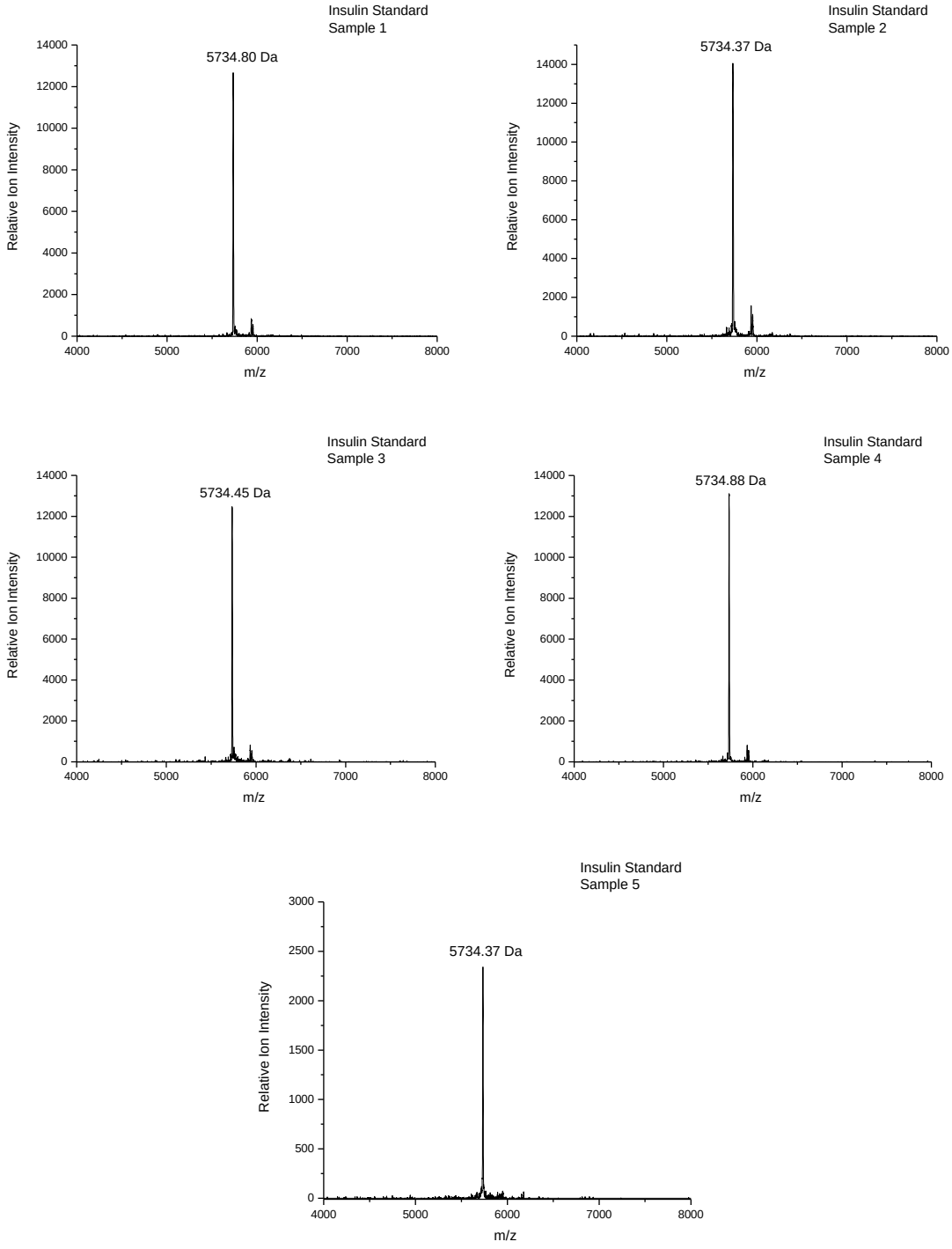

Figure 26. MALDI-MS spectra corresponding to the first through fifth 100.0mg/dL bovine insulin standard samples.

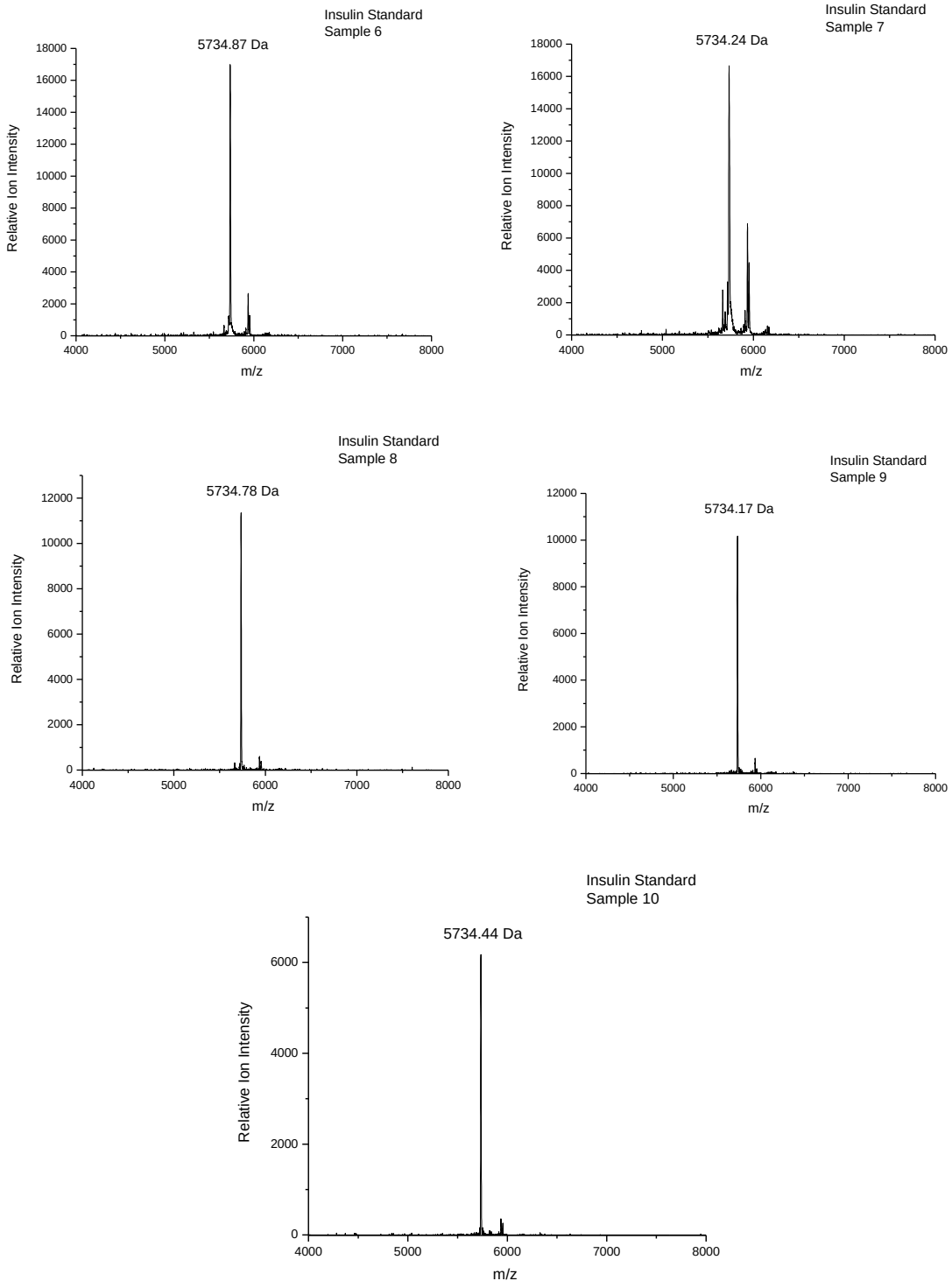

Figure 27. MALDI-MS spectra corresponding to the sixth through tenth 100.0mg/dL bovine insulin standard samples.

From the calculation shown in Equation 7, it could be assumed that 95 times out of 100, the true mean, μ, would be within ± 0.192 Da for bovine insulin. Overall, as hypothesized, the results of this experiment demonstrated the repeatability and accuracy of the MALDI instrumentation. Table 7 shows the average mass of all ten insulin standards as well as the standard deviation.

Table 7. Comparison of bovine insulin known and experimental masses.

Bovine Insulin (known mass)	5734.59 Da
Bovine Insulin (average experimental mass)	5734.54 Da
Bovine Insulin (standard deviation)	0.269Da

Student's T Equation (at the 95% confidence level) t = 2.26

$$\mu = \bar{x} \pm \frac{ts}{\sqrt{N}} \qquad \text{Eq. 7}$$

$\mu = 5734.54 \pm 0.192$ Da

Clinical Studies

Overview

To further investigate apolipoprotein composition of HDL subfractions and to correlate with and verify the apolipoprotein peaks observed and identified by CE, MALDI-MS was used as a qualitative method. Although quantitation was not sought from MALDI-MS analysis, the relative intensities of the apo peaks following MALDI-MS analysis was of interest. The MALDI-MS spectra from all patients were obtained for the non HDL, HDL_2, HDL_3, and protein fractions.

Capillary electrophoresis (CE) was also used for secondary analysis following preparative UC to investigate potential differences in electrophoretic properties in non-CAD control and CAD cohort subfractions. The C_{18} solid phase extraction method of delipidation with subsequent CE was implemented as part of a comprehensive apolipoprotein analysis using both cohorts of patient samples. Data obtained was also compared to MALDI-MS data to verify the identities of analyte peaks and to determine whether post-translational modifications could be detected by changes in the inherent mobility of the HDL apolipoproteins in these samples. Following solid phase extraction and evaporation to dryness the subfractions were reconstituted in 100µL of the capillary electrophoresis buffer consisting of 12.5mM sodium borate, 3.5mM SDS, and 20% (v/v) acetonitrile. This buffer system was chosen in order to provide a strong electroosmotic force due to the high pH of the buffer which was approximately 9.00, and to ensure significant negative charge on the apolipoproteins due their interaction with the anionic surfactant. These conditions served to minimize apolipoprotein-apolipoprotein interactions and apolipoprotein-wall interactions. The electrophoresis experiment was performed in normal polarity, such that the electroosmotic flow moved from the anode to the cathode. Integration of peak areas was performed manually.

Following the MALDI-MS analysis of both patient cohorts, a distinct difference was observed in the apoC-I peaks. The apoC-I peaks were observed in detail in the mass range spanning 6300 – 6800m/z where these protein peaks were expected to be found. The HDL_2 spectra from the control cohort are shown in Figures 28 and 29.

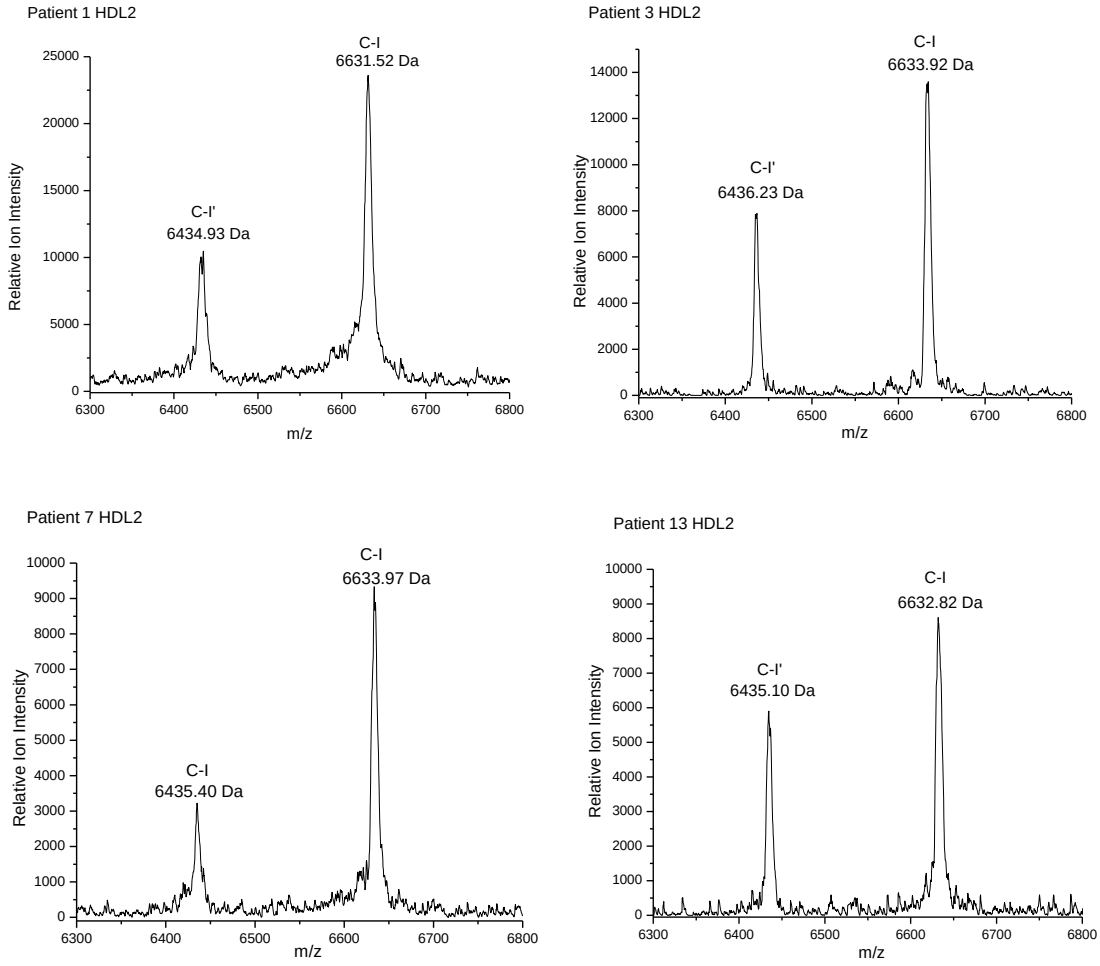

Figure 28. MALDI-MS HDL_2 apoC-I spectra from control cohort patients 1, 3, 7, and 13.

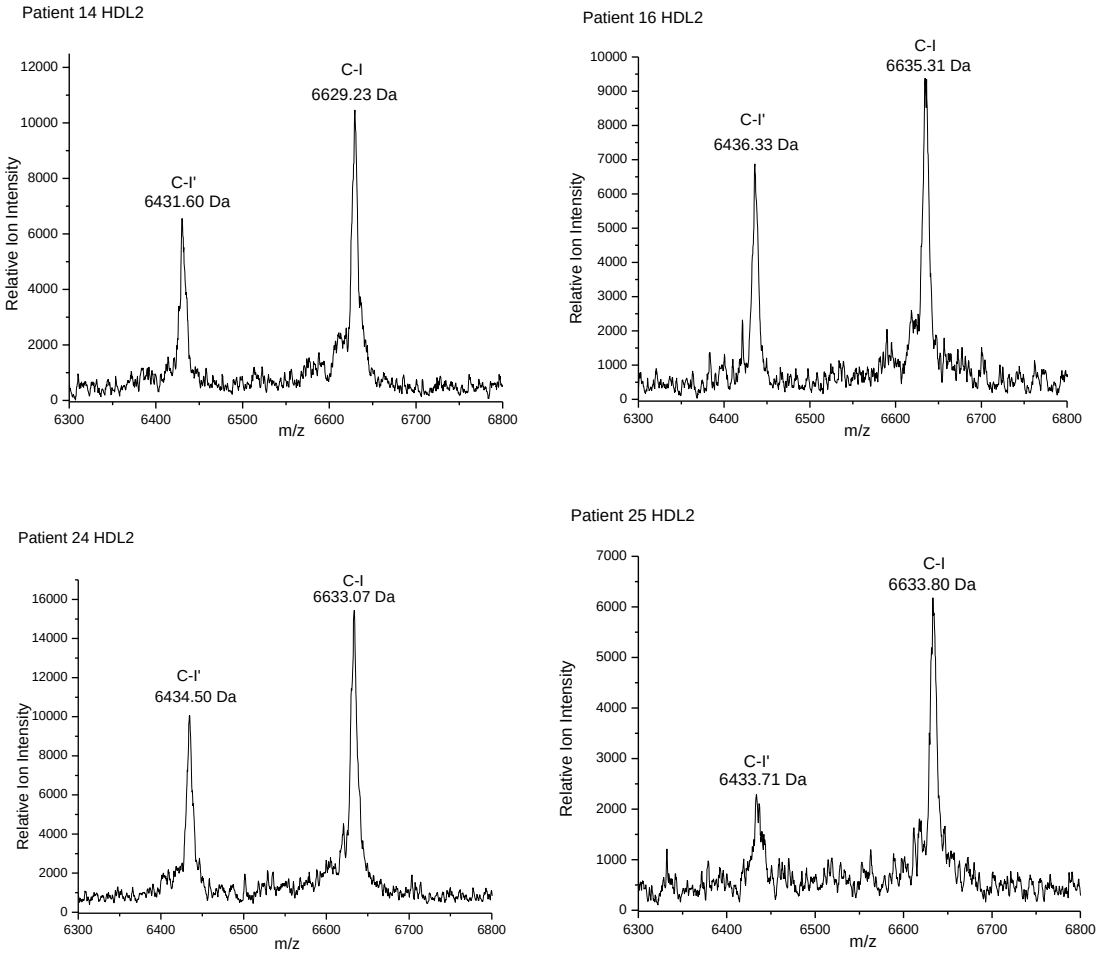

Figure 29. MALDI-MS HDL_2 apoC-I spectra from control cohort patients 14, 16, 24 and 25.

The HDL_3 subfraction apoC-I peaks are shown for the control cohort in Figures 30 and 31. In the control cohort, apoC-I' and apoC-I were both observed and identified based upon their molecular weights which are 6432.50 Da and 6630.60 Da respectively. Due to the consistent detection of apoC-I peaks in all patient HDL fractions, the mass accuracy of the apoC-I peaks was determined by averaging the masses of each peak from the control cohort, and calculating the standard deviation at the 95% confidence level.

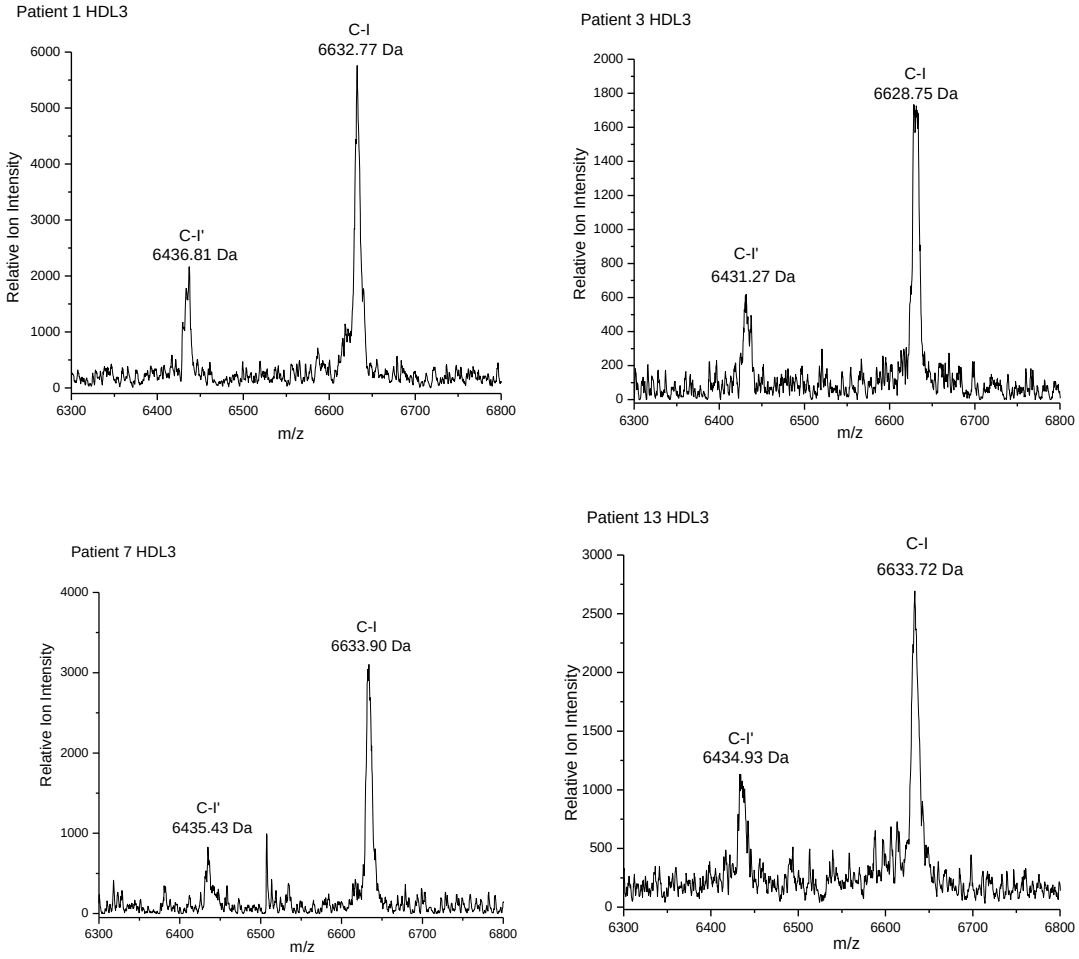

Figure 30. MALDI-MS HDL_3 apoC-I spectra from control cohort patients 1, 3, 7, and 13.

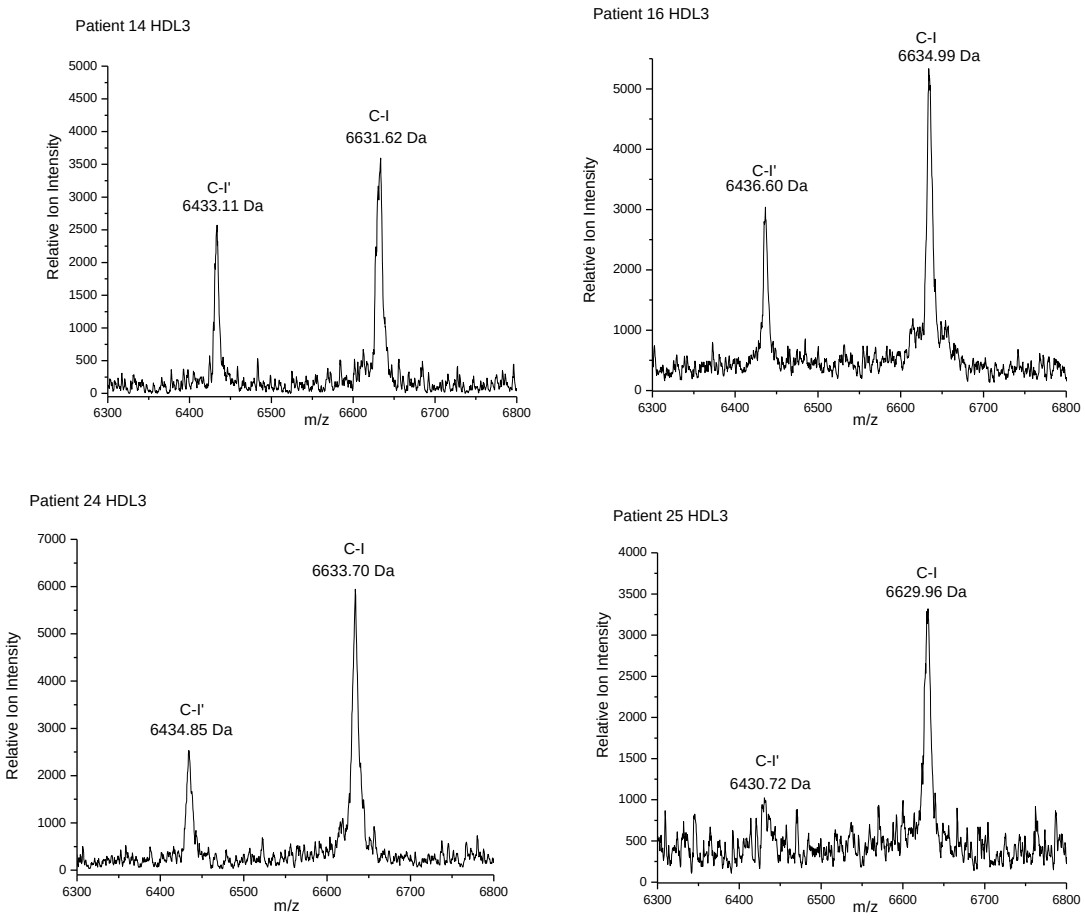

Figure 31. MALDI-MS HDL_3 apoC-I spectra from control cohort patients 14, 16, 24, and 25.

Table 8 reports the average mass values of the apoC-I' and apoC-I peaks in the control cohort, as well as their differences from the known mass values of these peaks. Tables 9 – 10 report the average masses of the apoC-I peaks in the HDL serum subfractions. Due to the accuracy and precision of the apoC-I values in the control cohort to the known masses of these proteins, apoC-I served also as an internal standard of the method.

Table 8. Total control cohort average apoC-I masses by MALDI.

	Control Cohort ApoC-I'	**Control Cohort ApoC-I**
Average Mass	6434.40 ± 0.93	6633.05 ± 1.08
Known Mass	6432.50	6630.60
Difference	1.90 ± 0.93	2.45 ± 1.08

Table 9. Control cohort HDL_2 fraction average apoC-I masses by MALDI.

	Control Cohort ApoC-I'	**Control Cohort ApoC-I**
Average Mass	6434.73 ± 1.36	6632.96 ± 1.61
Known Mass	6432.50	6630.60
Difference	2.23 ± 1.36	2.36 ± 1.61

Table 10. Control cohort HDL_3 fraction average apoC-I masses by MALDI.

	Control Cohort ApoC-I'	**Control Cohort ApoC-I**
Average Mass	6434.22 ± 2.04	6632.43 ± 1.92
Known Mass	6432.50	6630.60
Difference	1.72 ± 2.04	1.83 ± 1.92

In the CAD cohort, it was observed that the peaks which were assumed to be apoC-I and apoC-I' upon initial visual inspection, possessed a molecular weight greater than the known calculated mass of these proteins. Due to this significant shift in molecular weight, the peaks were designated apoC-I'_1 and apoC-I_1. Figures 32 and 32 show the HDL_2 and HDL_3 apoC-I spectra respectively, for the CAD cohort patients

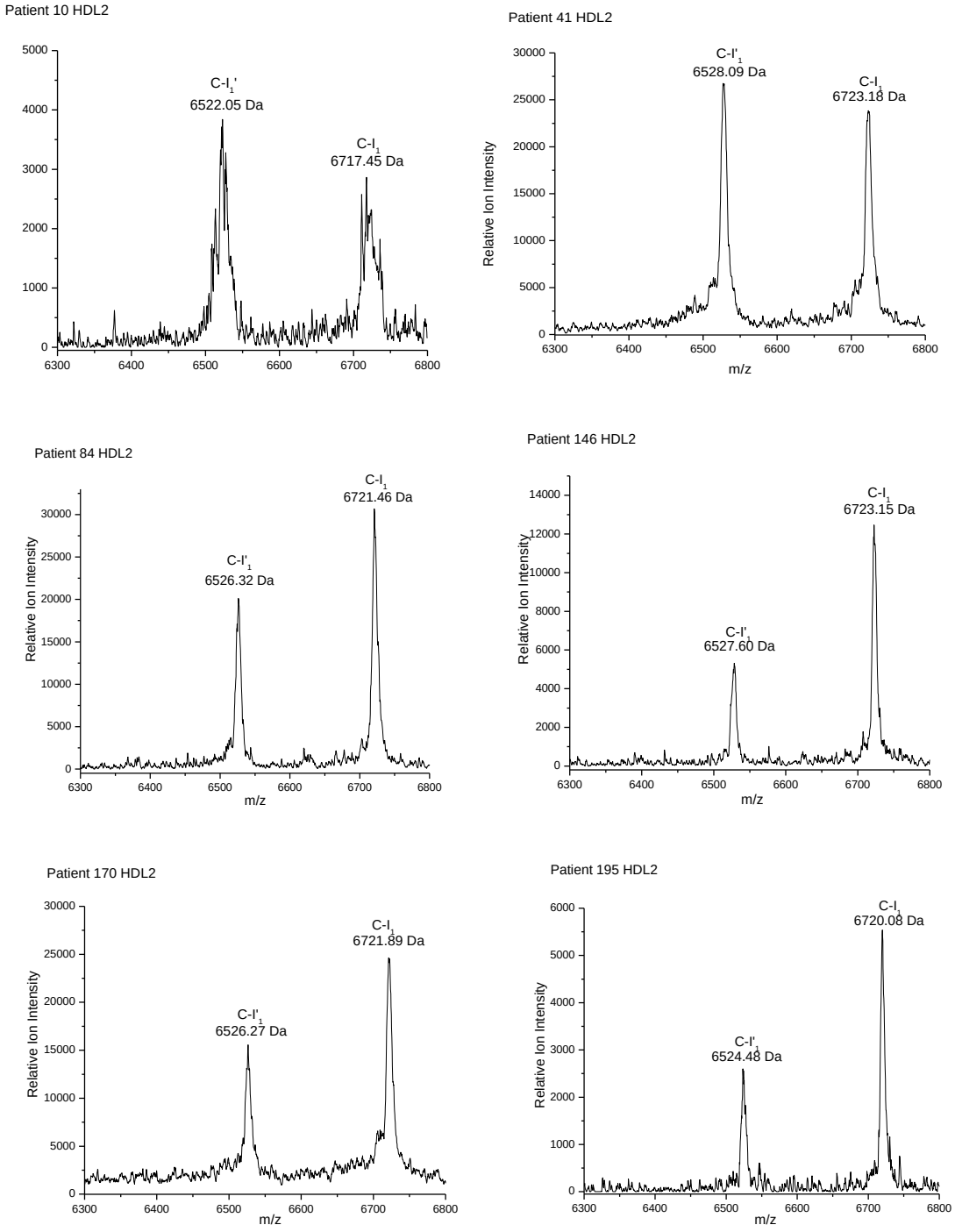

Figure 32. CAD cohort HDL_2 apoC-I MALDI-MS spectra.

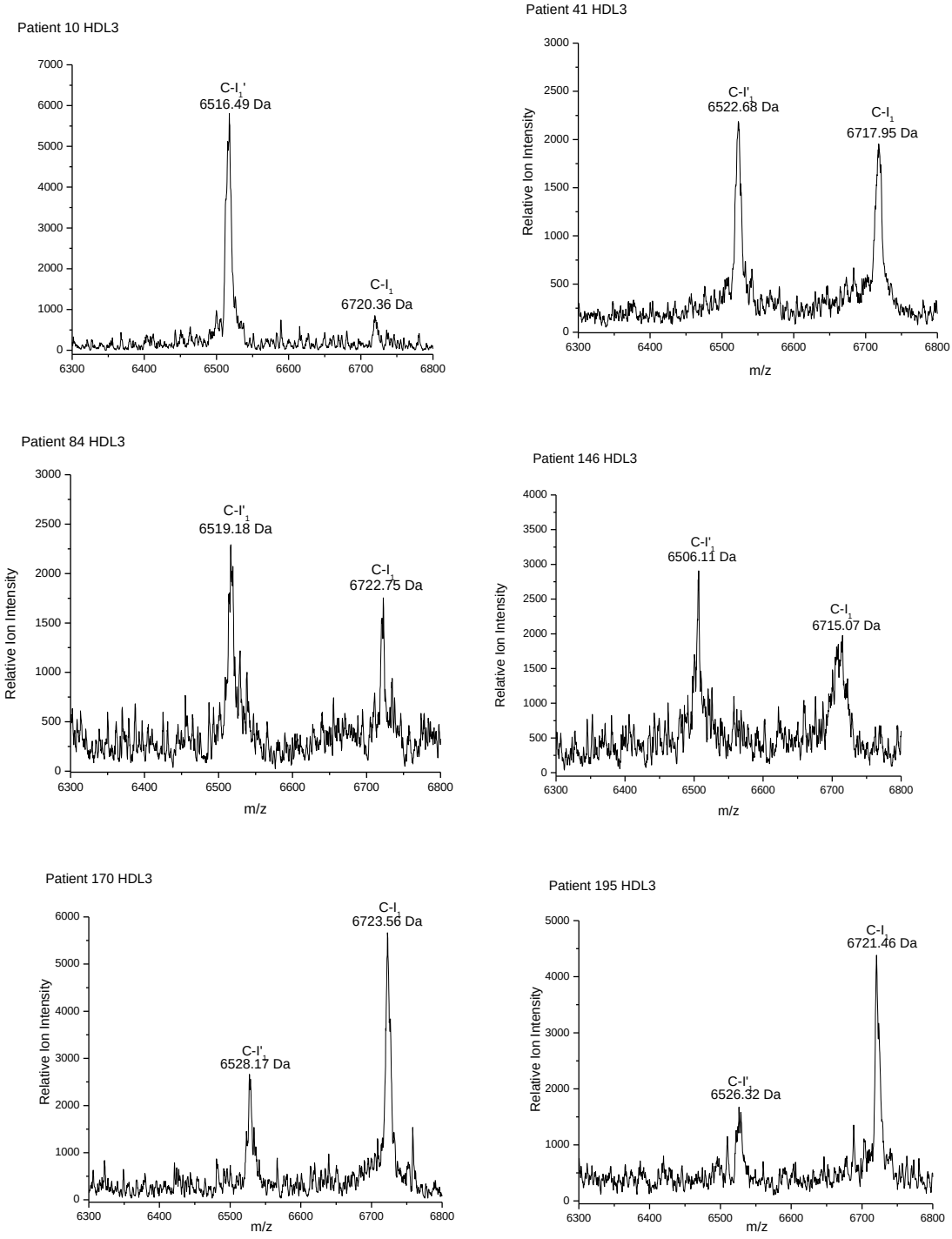

Figure 33. CAD cohort HDL_3 apoC-I MALDI-MS spectra.

In all samples of the CAD cohort it was observed that apoC-I contained peaks with greater masses than the known literature masses. Due to this significant shift in molecular weight, the peaks were designated apoC-I′$_1$ and apoC-I$_1$. Such a finding indicated post-translational modifications occurring in the CAD cohort which may be linked to CAD, as this diagnosis was the distinguishing difference between the two cohorts. This analysis of HDL serum fractions in the CAD cohort, also demonstrated further variability in the isoform pattern in some subjects within the CAD cohort. Figure 34 shows the doublets observed in the HDL subfractions from CAD patient 143. These further modified isoforms have been designated apoC-I$_2$' and apoC-I$_2$.

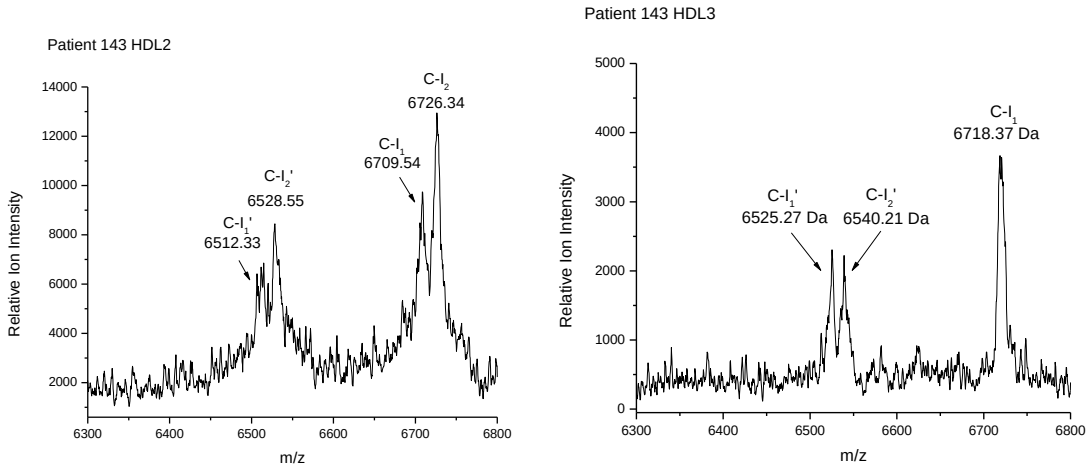

Figure 34. CAD cohort HDL subfractions from patient 143 showing further variability in apoC-I.

Due to this variability, it is apparent that there are factors controlling the post-translational modifications of apoC-I in the lipoprotein particles. In certain patient samples it was observed that the apoC-I$_1$ peak appeared to be nearly depleted. It is hypothesized that some mechanism or process is resulting in the depletion of native apoC-I. Perhaps the acceleration of CAD is resulting in the rapid transformation of apoC-I to apoC-I$_1$, decreased or even inhibited apoC-I synthesis, or rapid removal of the derivative apoC-I$_1$ from the body as a counter measure.

The differences between known apoC-I and apoC-I' masses and the observed apoC-I'$_1$ and apoC-I$_1$ masses were assessed to identify the variation between measurements. The CAD cohort apoC-I peaks were averaged, and the standard deviation was calculated at the 95% confidence level. Table 11 shows the average masses of the apoC-I'$_1$ and apoC-I$_1$ peaks in the CAD cohort. Tables 12 – 13 show the average masses of the apoC-I'$_1$ and apoC-I$_1$ peaks in each serum subfraction.

Table 11. Total CAD cohort average apoC-I masses by MALDI.

	CAD Cohort ApoC-I'$_1$	**CAD Cohort ApoC-I$_1$**
Average Mass	6522.47 ± 2.78	6720.47 ± 2.09
Known Mass	6432.50	6630.60
Difference	89.97 ± 2.78	89.87 ± 2.09

Table 12. Total CAD cohort HDL$_2$ fraction average apoC-I masses by MALDI.

	CAD Cohort ApoC-I'$_1$	**CAD Cohort ApoC-I$_1$**
Average Mass	6523.73 ± 4.54	6721.34 ± 4.08
Known Mass	6432.50	6630.60
Difference	91.23 ± 4.54	90.74 ± 4.08

Table 13. Total CAD cohort HDL$_3$ fraction average apoC-I masses by MALDI.

	CAD Cohort ApoC-I'$_1$	**CAD Cohort ApoC-I$_1$**
Average Mass	6520.79 ± 6.28	6719.79 ± 2.49
Known Mass	6432.50	6630.60
Difference	88.29 ± 6.28	89.19 ± 2.49

Additionally, one patient, patient 49, displayed MALDI-MS results in accordance with the CAD cohort despite not having a CAD diagnosis. Figure 35 shows the HDL spectra corresponding to apoC-I for this patient. This result suggests that this analysis may be an initial screening that could indicate the future development of CAD and serve as a biomarker for CAD in this individual, as its MALDI spectra showed characteristics as seen in the CAD cohort.

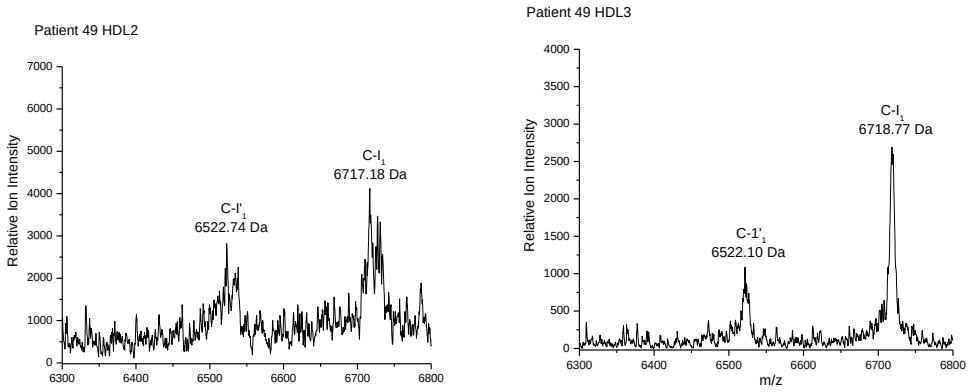

Figure 35. MALDI-MS apoC-I spectra from patient 49.

Patient history and lipoprotein density profiles are presented in this section for each of the 16 patients analyzed to correlate with each patient's full MALDI-MS spectra and CE results.

Control Cohort Analysis

Table 14. Control patient 1 medical information

Control Patient 1	
Age	48 years old
Height	66 inches
Weight	136 lbs.
Gender	Female
Race	Caucasian
Major Risk Factors	None
Current Medications	Beta Blocker

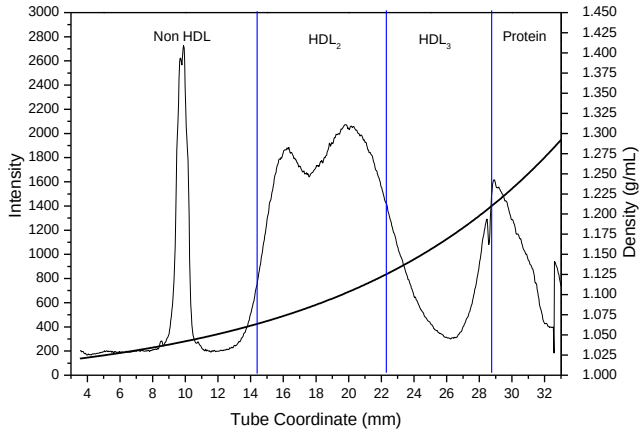

Figure 36. Lipoprotein density profile from control patient 1 in a 0.300M solution of Cs_2CdY, spun for 6 hours at 120,000RPM at 5°C after treatment with dextran sulfate.

Control Patient 1 Discussion

Control patient 1, whose medical history is presented in Table 14, is a 48 year old Caucasian female who does not have CAD and does not possess major risk factors. The

Cs_2CdY lipoprotein profile which expands the HDL region is shown in Figure 36 and shows a broad peak spanning both HDL subfractions, but primarily in the HDL_2 subclass.

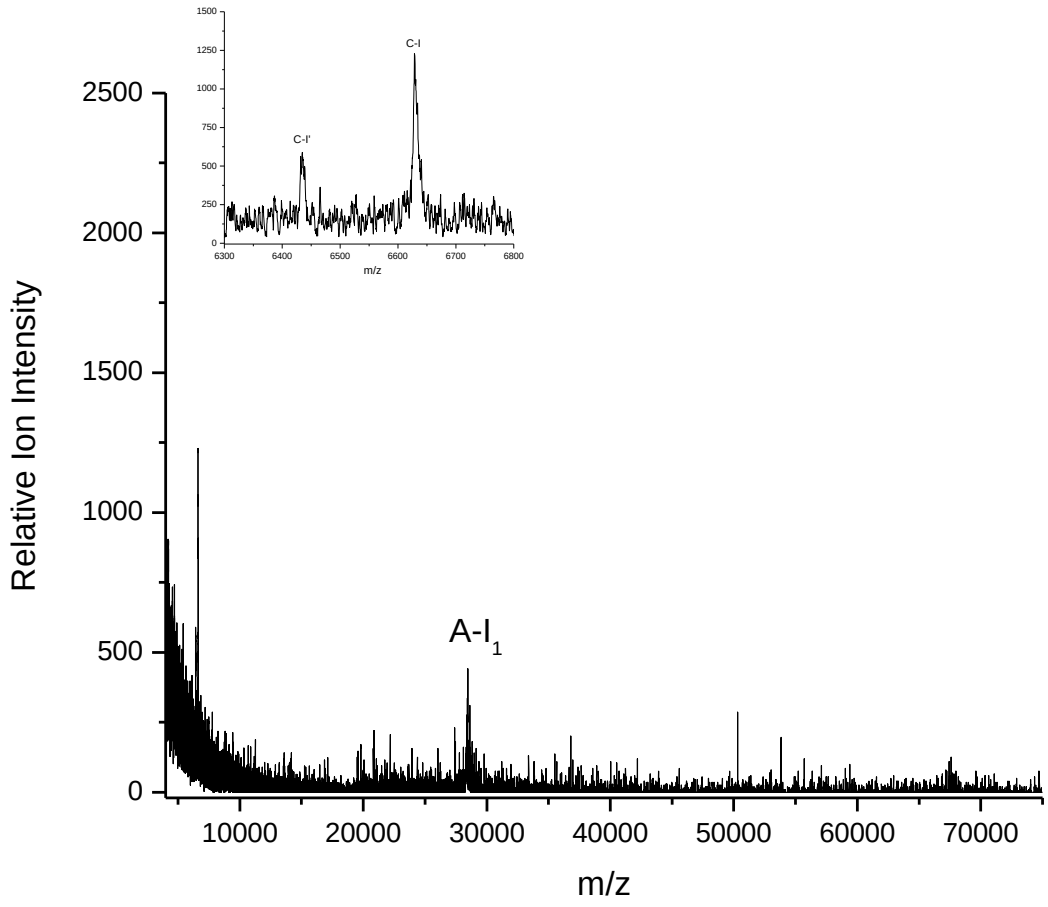

Figure 37. MALDI-MS non HDL spectra from control patient 1.

Table 15. Identification of apolipoproteins in the non HDL fraction from control patient 1.

Identification	Mass (Da)
ApoC-I'	6432.16
ApoC-I	6629.37
ApoA-I_1	28444.99

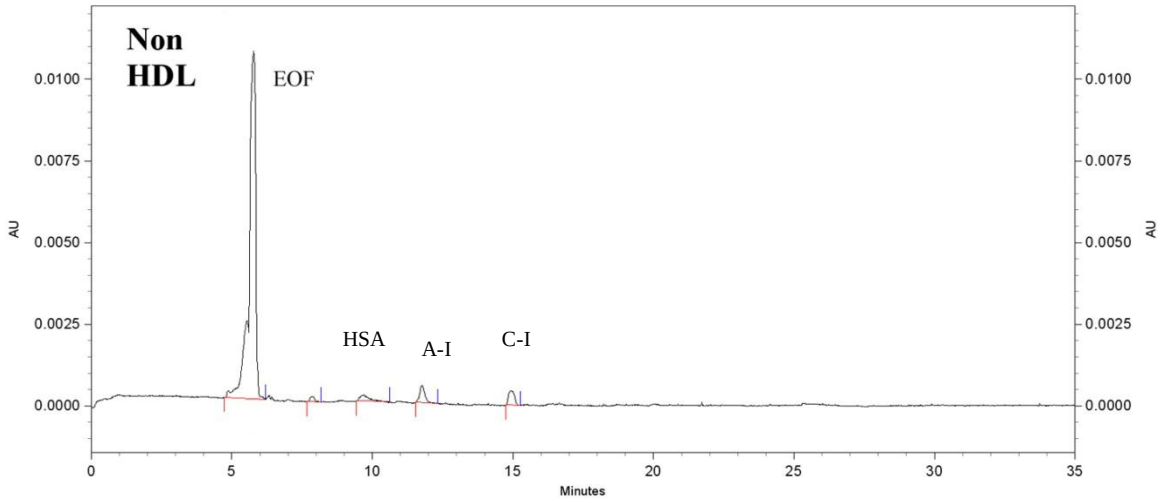

Figure 38. Electropherogram of the non HDL fraction from control patient 1.

Table 16. CE data for the non HDL fraction from a 200µL serum sample from control patient 1.

Protein	Elution Time (min)	Mobility (x $10^{-5}$$cm^2$/Vs)	CPA	Concentration (mg/dL)
HSA	9.7	-21.109	360	0.36
ApoA-I	11.8	-26.443	480	1.33
ApoC-I	14.9	-31.773	364	0.86

Figure 37 shows the MALDI spectra for the non HDL subfraction which contained apos C-I', C-I, A-I, and HSA. Table 15 shows the peak masses for this fraction. All proteins present in this most buoyant fraction were relatively low in intensity which suggests minimal concentration of these proteins in this fraction. The presence of proteins in this fraction indicated mixing with the neighboring HDL_2 fraction following excision. The proteins were identified through comparison with their known masses which are based on amino acid sequences in well validated databases such as the Swiss-Prot database (www.ebi.ac.uk/swissprot). Apolipoprotein A-I, however, was higher in mass than the

known value of this protein, further analysis of the remaining patients in the cohort would identify if this mass shifting would be unanimous or restricted to this particular patient. Due to this shifting, however, the protein was designated as A-I_1. Figure 38 shows the electropherogram from the CE analysis of the non HDL fraction. Low intensity peaks with mobilities matching albumin, apoA-I, and apoC-I were detected, which further indicated mixing from the neighboring HDL_2 fraction. Compared to the MALDI-MS results, all proteins were detected with the exception of albumin.

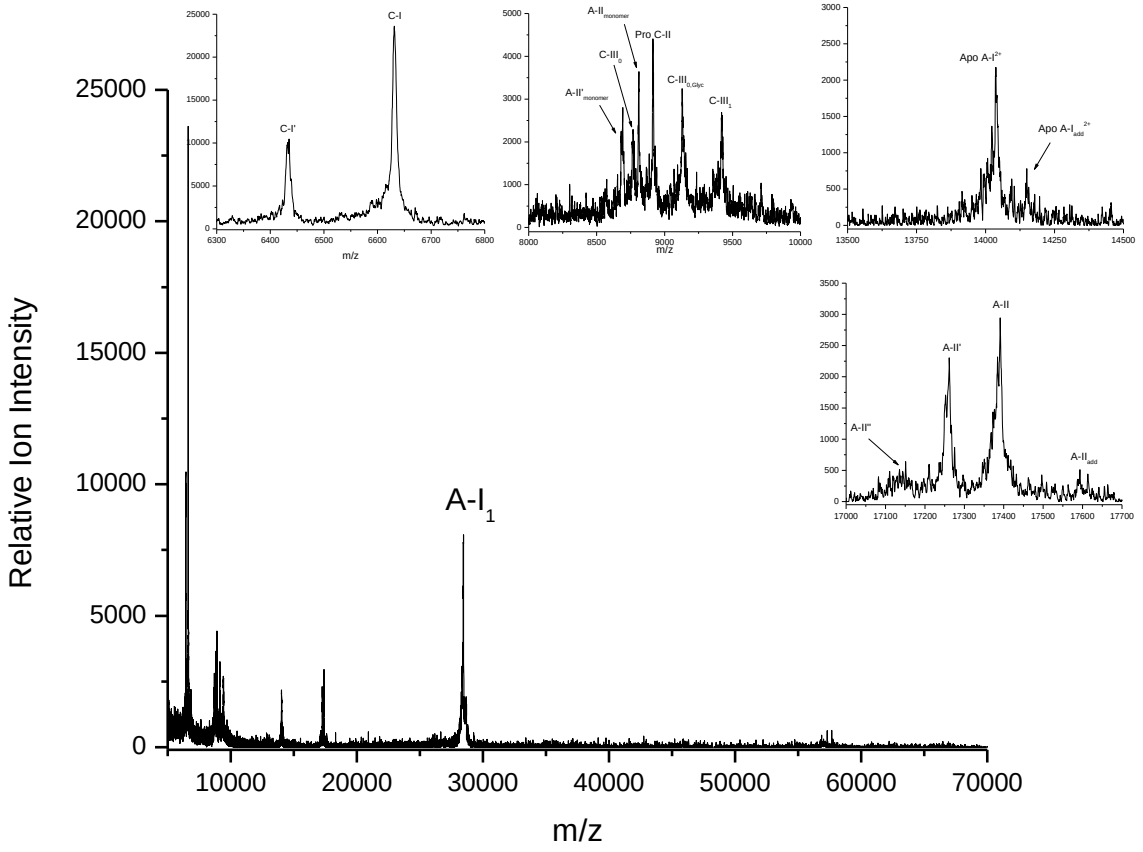

Figure 39. MALDI-MS HDL_2 spectra from control patient 1.

Table 17. Identification of apolipoproteins in the HDL_2 fraction from control patient 1.

Identification	Mass (Da)
ApoC-I'	6434.93
ApoC-I	6631.52
ApoA-II'_m	8692.76
ApoC-III_0	8768.46
ApoA-II_m	8809.81
Pro ApoC-II	8914.36
ApoC-$III_{0,glyc}$	9130.18
ApoC-III_1	9418.77
ApoA-I^{2+}	14037.06
ApoA-I^{2+}_{add}	14149.75
ApoA-II''	17146.11
ApoA-II'	17260.55
ApoA-II	17391.00
ApoA-II_{add}	17591.94
ApoA-I_1	28447.82

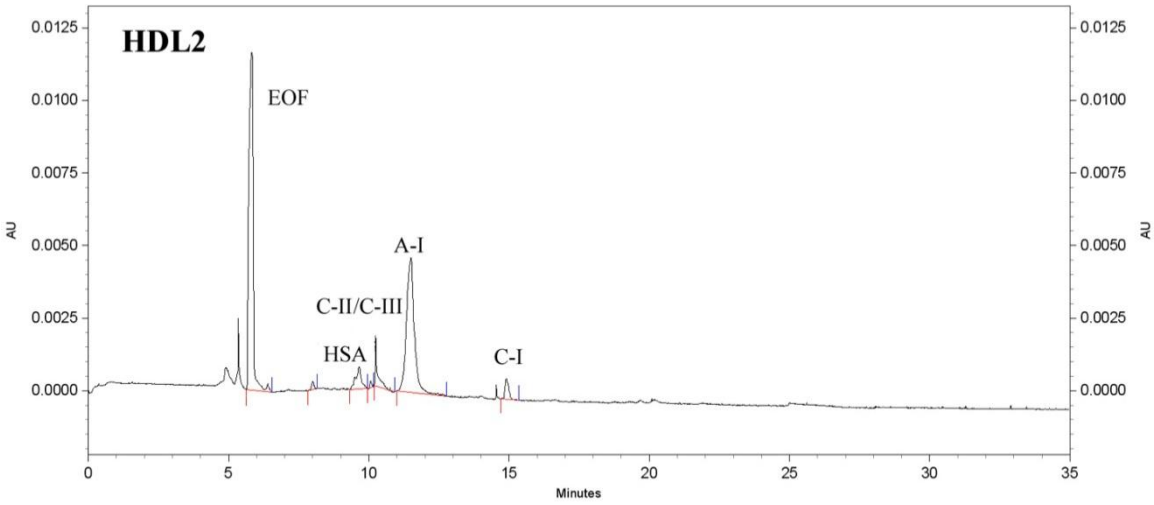

Figure 40. Electropherogram of the HDL_2 fraction from control patient 1.

Table 18. CE data for the HDL_2 fraction from a 200µL serum sample from control patient 1.

Protein	Elution Time (min)	Mobility (x $10^{-5}cm^2/Vs$)	CPA	Concentration (mg/dL)
HSA	9.7	-20.414	905	0.91
ApoC-II	10.1	-21.653	90	-------
ApoC-III	10.2	-22.182	729	-------
ApoA-I	11.5	-25.355	6582	18.26
ApoC-I	14.9	-31.213	366	0.86

The HDL_2 subfraction MALDI-MS spectra, shown in Figure 39, contained several proteins including apos C-I', C-I, A-$II_{monomer}$, C-III_0, Pro C-II, C-$III_{0,glyc}$, C-III_1, A-I^{2+}, A-II, and A-I_1. Table 17 shows the peak masses for this fraction The intensity and high resolution suggested an enrichment of these apolipoproteins in this buoyant HDL subfraction. This subfraction showed sharp peaks corresponding to apoC-I along with its truncated form apoC-I' which appeared at an intensity slightly lower than half of that seen by apoC-I. The mass region between *m/z* 8000 – 10000, showed many peaks corresponding to apos C-II and C-III with pro apoC-II having the highest peak intensity. Figure 40 shows the electropherogram following the CE analysis of the HDL_2 fraction. Albumin and apos C-II, C-III, A-I, and C-I were detected and identified based upon their electrophoretic mobilities. Though apoC-II, and apoC-III calibration curves were not constructed in this work, these apolipoproteins were identified by the mobilities presented in previous work.[79] ApoA-I was the strongest peak observed in this fraction, indicating that this protein had the highest concentration, followed by apoC-III, and apoC-I. Compared to the MALDI-MS results, albumin was detected by CE only, while apoA-II was detected by MALDI-MS only.

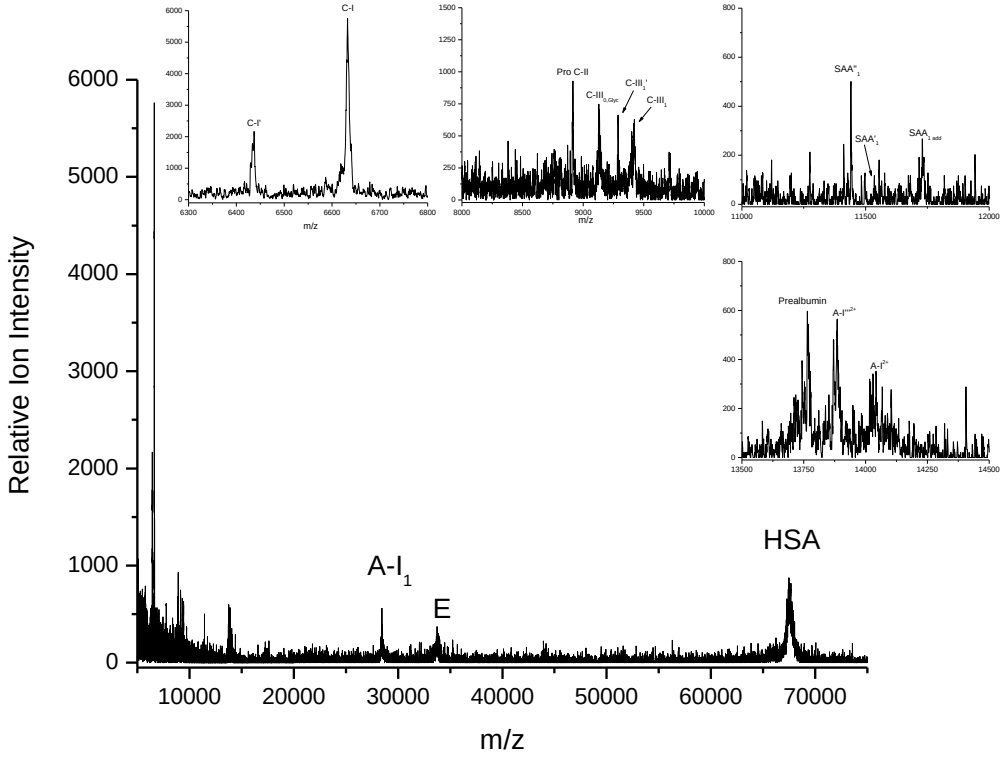

Figure 41. MALDI-MS HDL_3 spectra from control patient 1

.Table 19. Identification of apolipoproteins in the HDL_3 fraction from control patient 1.

Identification	Mass (Da)
ApoC-I'	6436.81
ApoC-I	6632.77
Pro ApoC-II	8915.57
$ApoC\text{-}III_{0,glyc}$	9129.22
$ApoC\text{-}III_1'$	9294.38
$ApoC\text{-}III_1$	9422.96
$SAA_1"$	11440.92
SAA_1'	11536.19
SAA_{1add}	11730.31
Prealbumin	13767.87
$ApoA\text{-}I'''^{2+}$	13885.53
$ApoA\text{-}I^{2+}$	14046.65

Table 19. (Continued)

Identification	Mass (Da)
ApoA-I_1	28444.81
ApoE	33738.66
HSA	67476.65

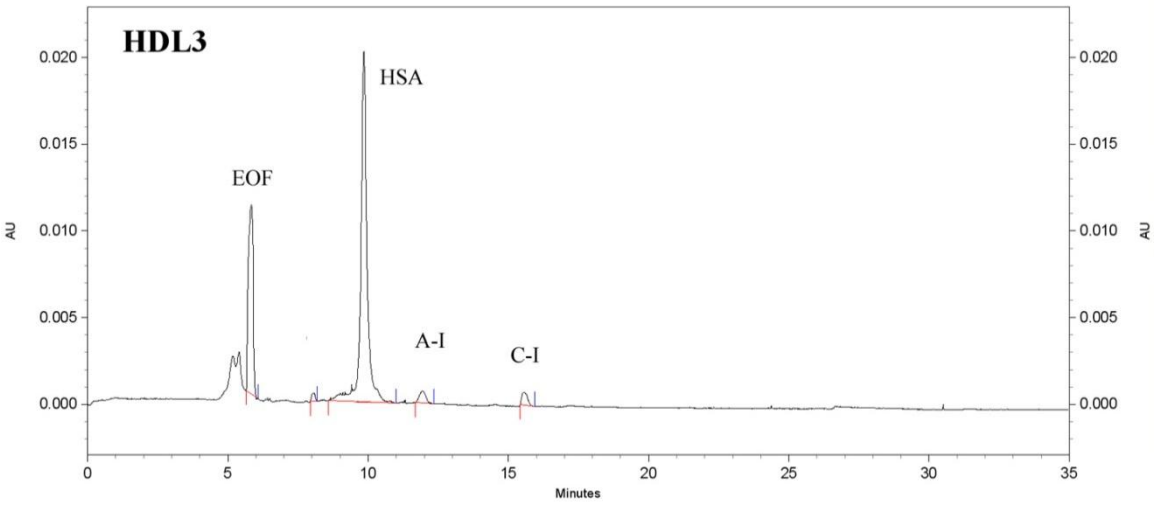

Figure 42. Electropherogram of the HDL_3 fraction from control patient 1.

Table 20. CE data for the HDL_3 fraction from a 200µL serum sample from control patient 1.

Protein	Elution Time (min)	Mobility (x $10^{-5}cm^2/Vs$)	CPA	Concentration (mg/dL)
HSA	9.8	-20.967	26687	26.87
ApoA-I	11.9	-26.241	778	2.16
ApoC-I	15.6	-32.025	555	1.31

Figure 41 shows the HDL_3 subfraction MALDI-MS spectra which contained apos C-I', C-I, Pro C-II, $C\text{-}III_{0glyc}$, $C\text{-}III_1$, SAA_1, SAA_4, A-I+, $A\text{-}I_1$, E, and HSA. Table 19 shows the peak masses for this fraction. The apoC-I peaks were sharp with apoC-I appearing at approximately 3 times higher relative ion intensity. The region spanning *m/z* 8000 – 10000 in this subfraction, did not show the abundance of proteins nor the resolution that were observed in the HDL_2 subfraction. Likewise, the apoA-II peaks were not present in this fraction. Interestingly, serum amyloid a (SAA) peaks were observed in the region between *m/z* 11000 – 12000. Serum amyloid a isoforms are expressed constitutively or in response to inflammatory stimuli. Patient 1 contained both SAA_1 and SAA_4, SAA_4 is a constitutive isoform of SAA, and, SAA_1 is an acute phase SAA protein (A-SAA). Although this patient was confirmed to not possess CAD, A-SAA proteins have been implicated in several chronic inflammatory diseases such as atherosclerosis. Figure 42 shows the electropherogram from the CE analysis of the HDL_3 fraction. A large and sharp peak corresponding to albumin was detected in addition to apoA-I and apoC-I. ApoA-I was detected in a much lower abundance than the HDL_3 fraction, while apoC-I was detected in a greater abundance. Compared to the MALDI-MS results from this subfraction, all protein peaks detected by CE were also detected by MALDI-MS. MALDI-MS also detected SAA peaks as well as apoE, apoC-II, and apoC-III peaks, all of which were low in relative ion intensity .

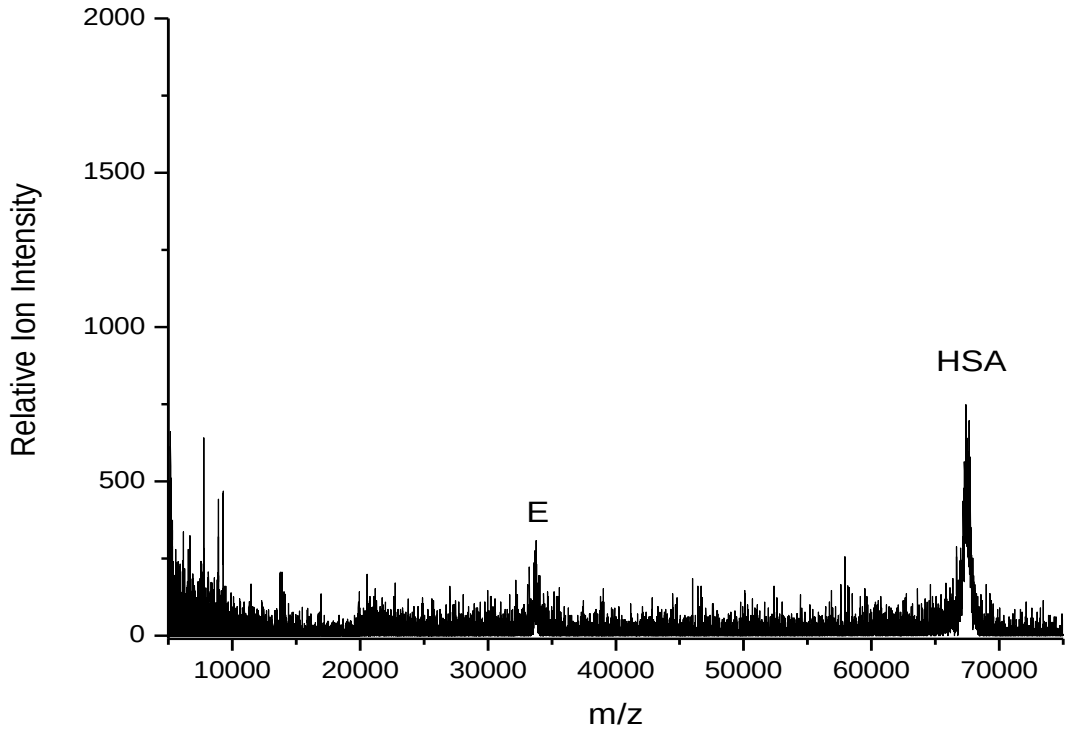

Figure 43. MALDI-MS protein spectra from control patient 1.

Table 21. Identification of apolipoproteins in the protein fraction from control patient 1.

Identification	Mass (Da)
ApoE	33782.86
HSA	67396.19

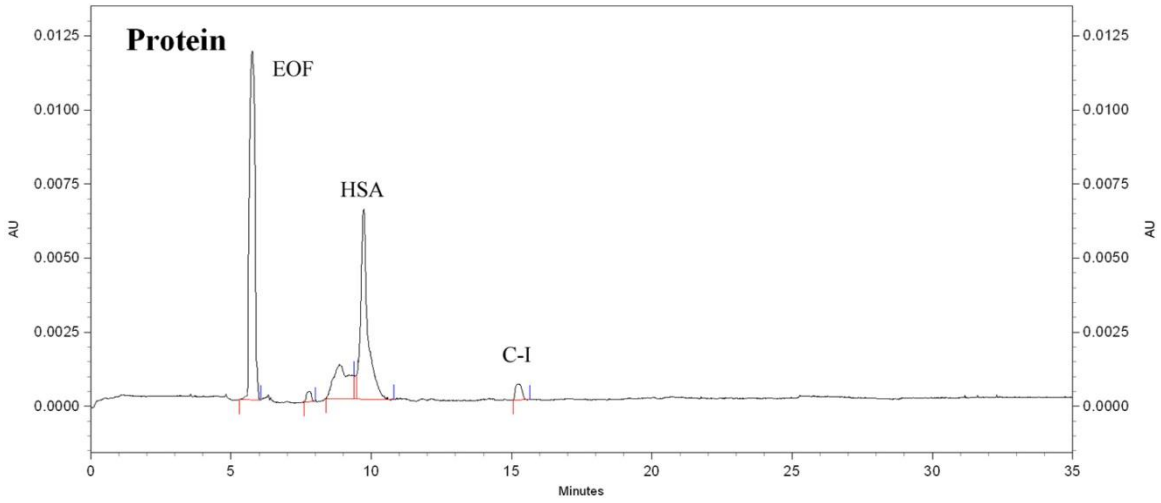

Figure 44. Electropherogram of the protein fraction from control patient 1.

Table 22. CE data for the protein fraction from a 200µL serum sample from control patient 1.

Protein	Elution Time (min)	Mobility (x $10^{-5}$$cm^2$/Vs)	CPA	Concentration (mg/dL)
HSA	9.7	-21.363	9640	9.71
ApoC-I	15.3	-32.392	471	1.11

The protein subfraction for patient 1 contained only apoE and human serum albumin as shown in the MALDI-MS spectrum in Figure 43. Table 21 shows the peak masses for this fraction. Albumin was present at approximately three times the intensity of apoE. The CE results following the analysis of this fraction are shown in Figure 44 and shows peaks corresponding to the mobility of albumin and apoC-I. The albumin peak contained a shoulder which may be due to its co-elution with another serum component. Compared to the MALDI-MS results from this subfraction, both methods detected albumin, while CE detected apoC-I and MALDI-MS detected apoE. It is possible that apoE has an

electrophoretic mobility which matches that of apoC-I, and that the apoC-I identified by CE is actually apoE.

Table 23. Control patient 3 medical information

Control Patient 3	
Age	77 years old
Height	61 inches
Weight	130 lbs.
Gender	Female
Race	Caucasian
Major Risk Factors	Family history of CAD

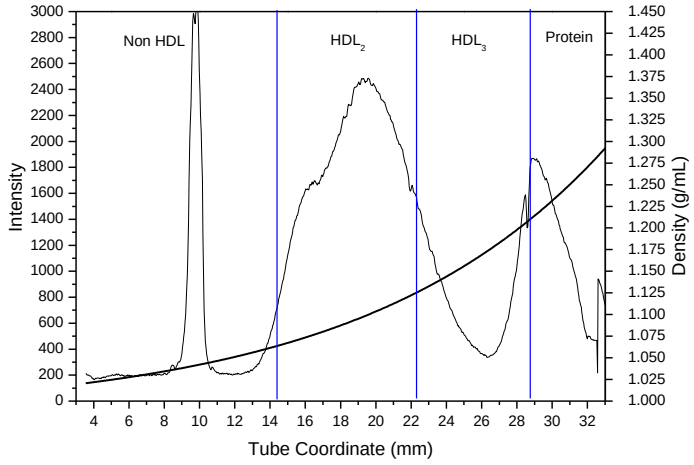

Figure 45. Lipoprotein density profile using a 200µL serum sample from control patient 3 in a 0.300M solution of Cs_2CdY, spun for 6 hours at 120,000rpm at 5°C after treatment with dextran sulfate.

Control Patient 3 Discussion

Control patient 3, whose medical history is presented in Table 23, is a 77 year old Caucasian female who does not have CAD however, does have a family history of the disease. Figure 51 shows the Cs_2CdY profile showing the expanded HDL region for this patient which contains one sharp peak with a small shoulder on its buoyant side.

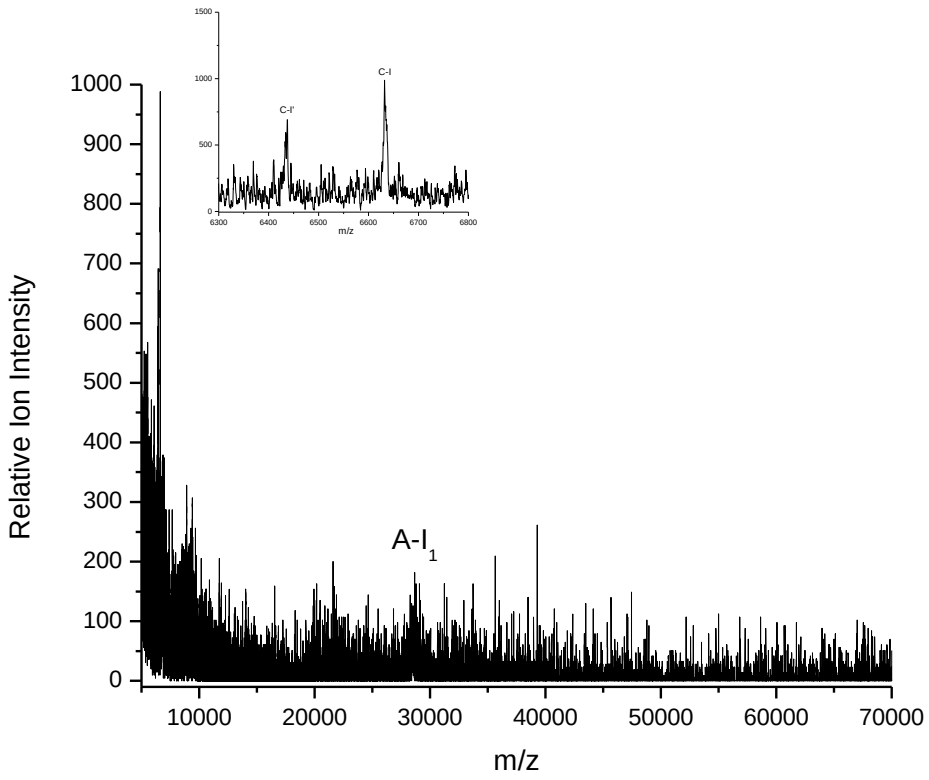

Figure 46. MALDI-MS non HDL spectra from control patient 3.

Table 24. Identification of apolipoproteins in the non HDL fraction from control patient 3.

Identification	Mass (Da)
ApoC-I'	6432.09
ApoC-I	6633.61
ApoA-I_1	28656.42

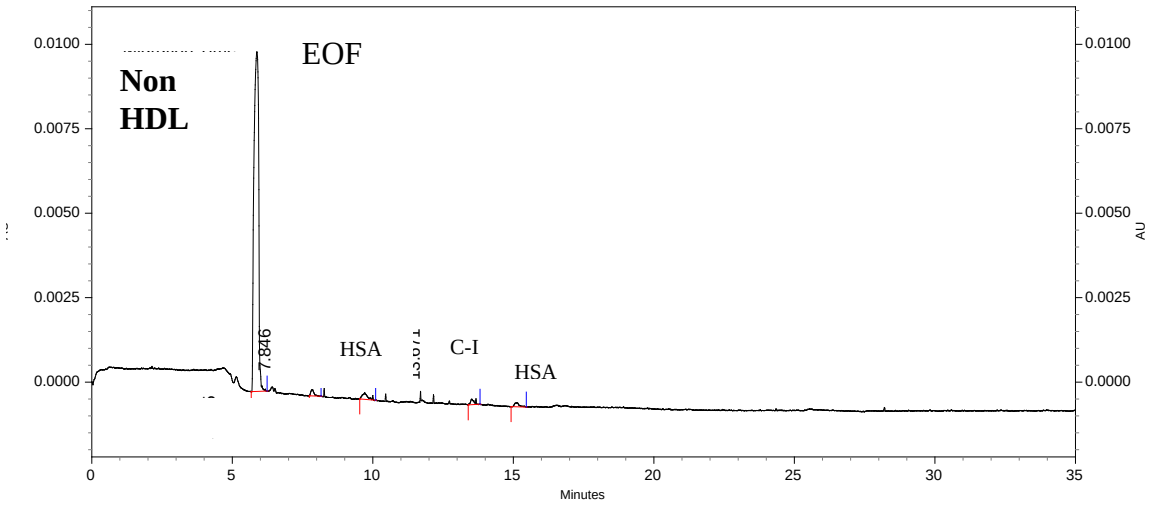

Figure 47. Electropherogram of the non HDL fraction from control patient 3.

Table 25. CE data for the non HDL fraction from a 200µL serum sample from control patient 3.

Protein	Elution Time (min)	Mobility (x $10^{-5}cm^2/Vs$)	CPA	Concentration (mg/dL)
HSA	9.7	-20.205	224	0.23
ApoA-I	13.7	-29.067	93	0.26
ApoC-I	15.1	-31.150	77	0.18

Figure 46 shows the MALDI spectra for the non HDL subfraction for this patient which contained apos C-I', C-I, and A-I_1. Table 24 shows the peak masses for this fraction. The apoC-I peaks were poorly resolved and were low in relative ion intensity. The CE results for this fraction are shown in Figure 47. Very low intensity peaks were observed with mobilities corresponding to albumin, apoA-I, and apoC-I demonstrating minimal mixing of HDL_2 with non HDL. In comparison to MALDI-MS analysis, apos A-I and C-I were detected by both methods. The CE results also detected a peak whose

mobility matched that of albumin, however, no albumin was detected in this fraction by MALDI-MS.

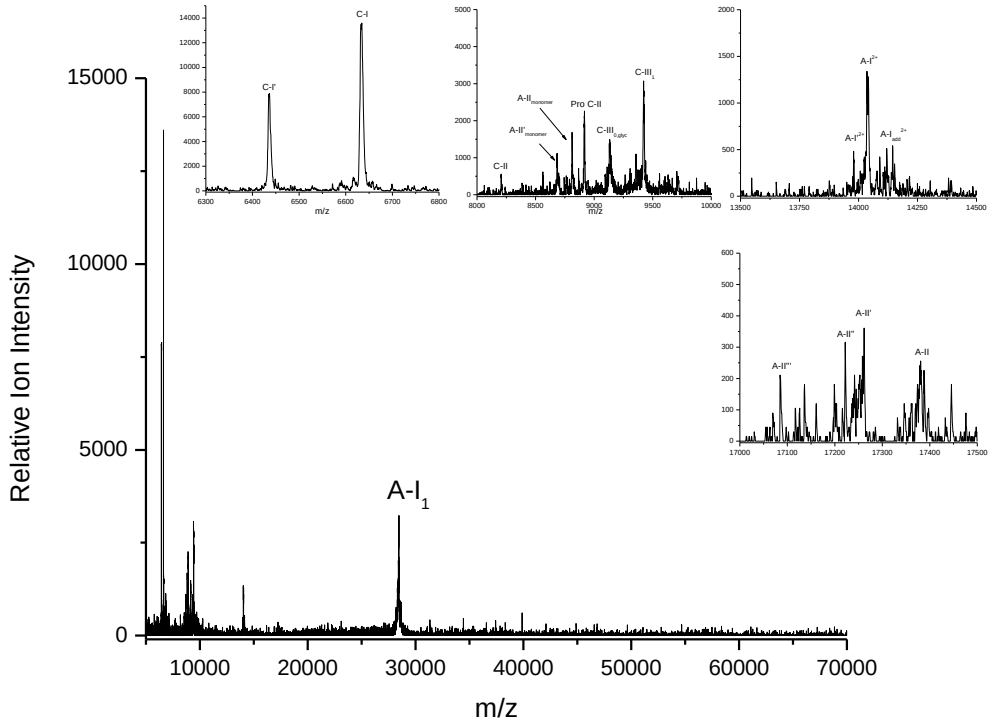

Figure 48. MALDI-MS HDL_2 spectra from control patient 3.

Table 26. Identification of apolipoproteins in the HDL_2 fraction from control patient 3.

Identification	Mass (Da)
ApoC-I'	6436.23
ApoC-I	6632.92
ApoC-II	8206.61
ApoA-II'$_m$	8683.24
ApoA-II$_m$	8812.34
Pro ApoC-II	8916.87
ApoC-III$_{0,glyc}$	9134.99
ApoC-III$_1$	9423.04
A-I'$^{2+}$	13980.43
ApoA-I^{2+}	14036.87

Table 26. (Continued)

Identification	Mass (Da)
ApoA-I^{2+}_{add}	14147.70
ApoA-II'''	17085.46
ApoA-II''	17135.98
ApoA-II'	17262.97
ApoA-II	17382.68
ApoA-I_1	28453.53

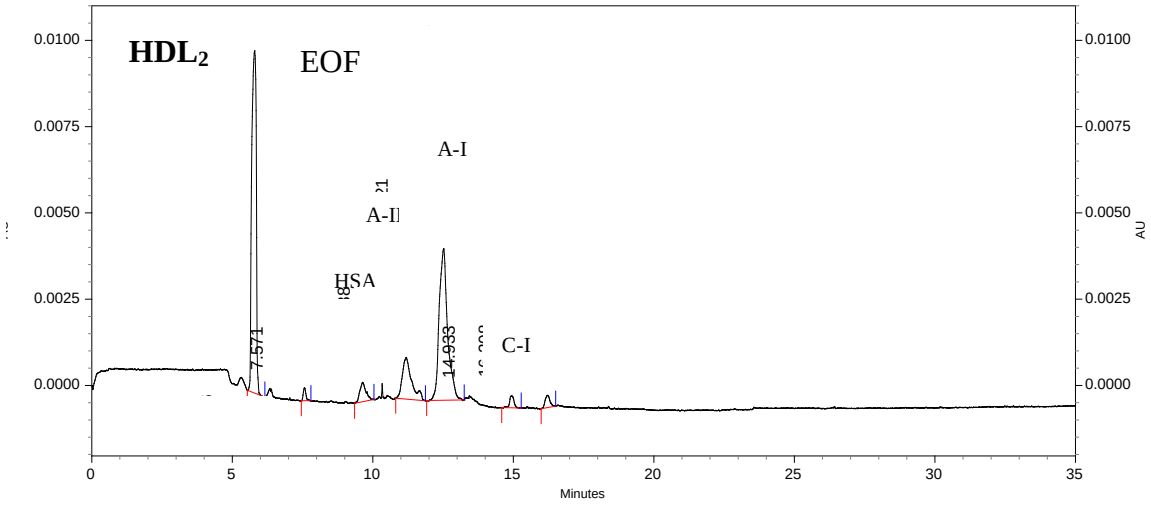

Figure 49. Electropherogram of the HDL_2 fraction from control patient 3.

Table 27. CE data for the HDL_2 fraction from a 200µL serum sample from control patient 3.

Protein	Elution Time (min)	Mobility (x $10^{-5}cm^2/Vs$)	CPA	Concentration (mg/dL)
HSA	9.6	-20.657	734	0.74
ApoA-II	11.2	-24.915	2076	-------
ApoA-I	12.5	-27.734	6110	16.95
ApoC-I	14.9	-31.151	214	0.51
Unidentified	16.2	-33.098	221	-------

Figure 48 shows the MALDI-MS spectra for the HDL_2 subfraction which detected peaks for apos C-I', C-I, Pro C-II, A-$II_{monomer}$, C-$III_{0,glyc}$, C-III_0, C-III_1, A-I^{2+}, A-II, and A-I_1. Table 26 shows the peak masses for this fraction. ApoC-I peaks were sharp and high in relative ion intensity. The region between *m/z* 8000 – 10000 was also abundant in proteins which appeared as sharp, highly resolved peaks. The strongest peak in this mass range was apoC-III_1. Two peaks were shown corresponding to the doubly protonated form of apoA-I as well as several peaks corresponding to apoA-II. Following apoC-I, the next strongest peak in intensity corresponded to apoA-I. No human serum albumin was present in this fraction. Figure 49, shows the CE results for this fraction which detected albumin, apoA-II, apoA-I, apoC-I, and an unidentified peak eluting after apoC-I. The largest peak detected corresponded to apoA-I, followed by apoA-II. ApoA-II also appeared with a small shoulder. Both methods detected apos A-I, C-I, and A-II. It is interesting to note that the apoA-II peak contained a shoulder in CE which may correspond to the isoforms observed in the MALDI spectra.

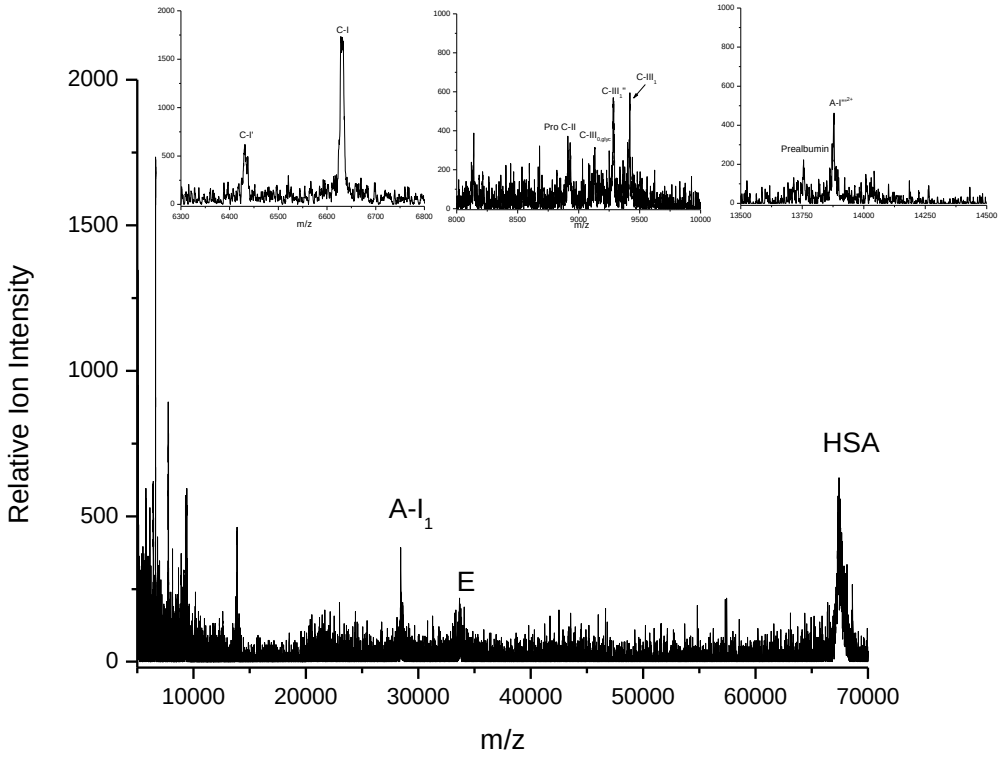

Figure 50. MALDI-MS HDL_3 spectra from control patient 3.

Table 28. Identification of apolipoproteins in the HDL_3 fraction from control patient 3.

Identification	**Mass (Da)**
ApoC-I'	6431.27
ApoC-I	6628.75
Pro ApoC-II	8912.14
$ApoC\text{-}III_{0,\ glyc}$	9133.93
$ApoC\text{-}III_1''$	9289.26
$ApoC\text{-}III_1$	9419.06
Prealbumin	13759.67
$ApoA\text{-}I''^{2+}$	13879.38
$ApoA\text{-}I_1$	28435.98
ApoE	33653.85
HSA	67421.95

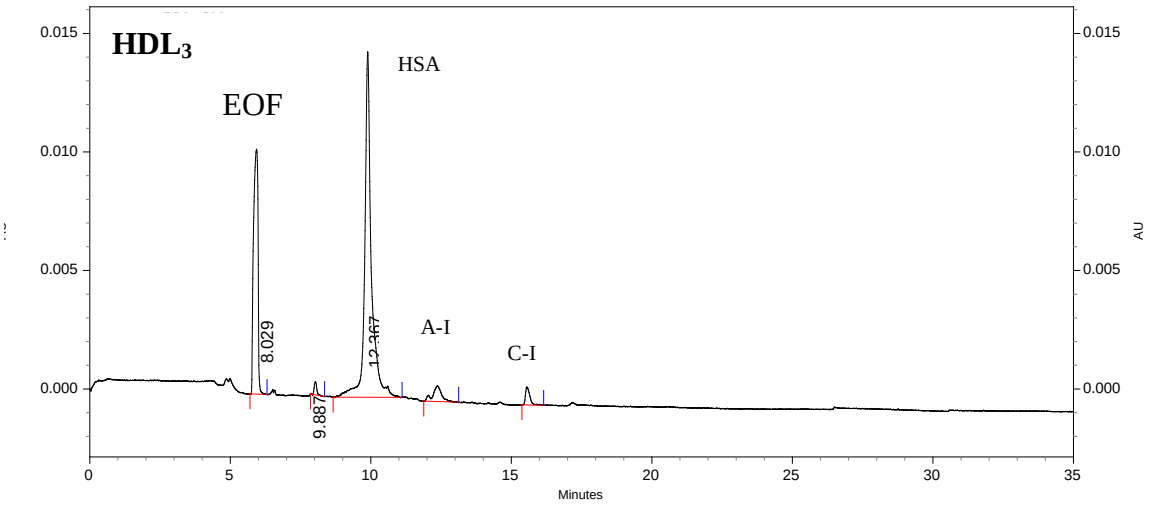

Figure 51. Electropherogram of the HDL_3 fraction from control patient 3.

Table 29. CE data for the HDL_3 fraction from a 200µL serum sample from control patient 3.

Protein	Elution Time (min)	Mobility (x $10^{-5}cm^2/Vs$)	CPA	Concentration (mg/dL)
HSA	9.9	-20.206	20,288	20.43
ApoA-I	12.4	-26.219	964	2.67
ApoC-I	15.6	-31.107	438	1.03

The HDL_3 subfraction MALDI-MS spectra is shown in Figure 50 and contained apos C-I', C-I, Pro C-II, C-$III_{0,glyc}$, C-III_1, A-I^{2+}, A-I_1, E, and HSA. Table 28 shows the peak masses for this fraction. As seen in the HDL_2 fraction, apoC-I was present along with its truncated form. The intensity of these two peaks however was lower in the HDL_3 subfraction than the HDL_2 fraction despite the lysine content of apoC-I which results in its strong basicity. The C-I' peak was also substantially lower in intensity in this fraction, the apoC-I peak was observed to be over 3 times as intense as C-I'. As also observed in the subfractions of patient 1, there were not as many apoC peaks in this fraction compared to the more buoyant HDL_2 fraction for patient 3. The relative intensity and resolution of these peaks were also lower than the more buoyant fraction.

The doubly charged ion of apoA-I was detected however, without any related isoforms and with a lower relative ion intensity than that the HDL_2 fraction. Figure 51 shows the CE results for this subfraction which detected albumin, apoA-I and apoC-I. The apoA-I and apoC-I peaks were substantially lower than the albumin peak, and the apoA-I peak also contained a small shoulder. All peaks detected by CE were also identified by MALDI-MS; MALDI-MS further identified apoE and apoC-III isoforms.

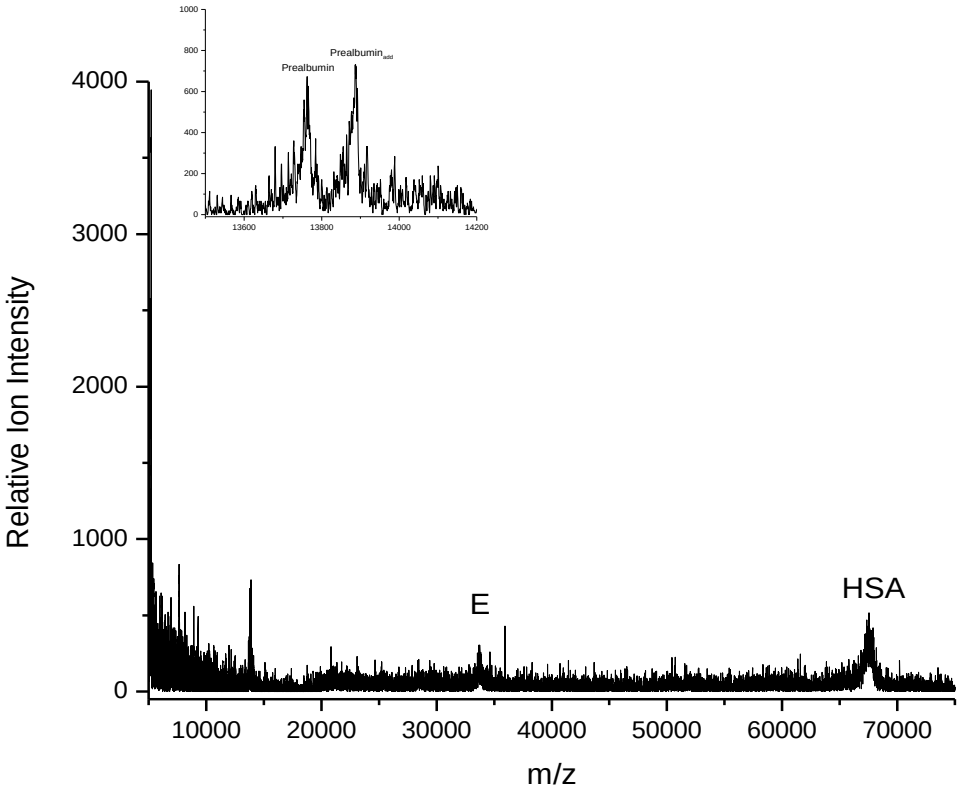

Figure 52. MALDI-MS protein spectra from control patient 3.

Table 30. Identification of apolipoproteins in the protein fraction from control patient 3.

Identification	Mass (Da)
Prealbumin	13765.90
$Prealbumin_{add}$	13885.77
ApoE	35934.86

Table 30. (Continued)

Identification	Mass (Da)
HSA	67687.42

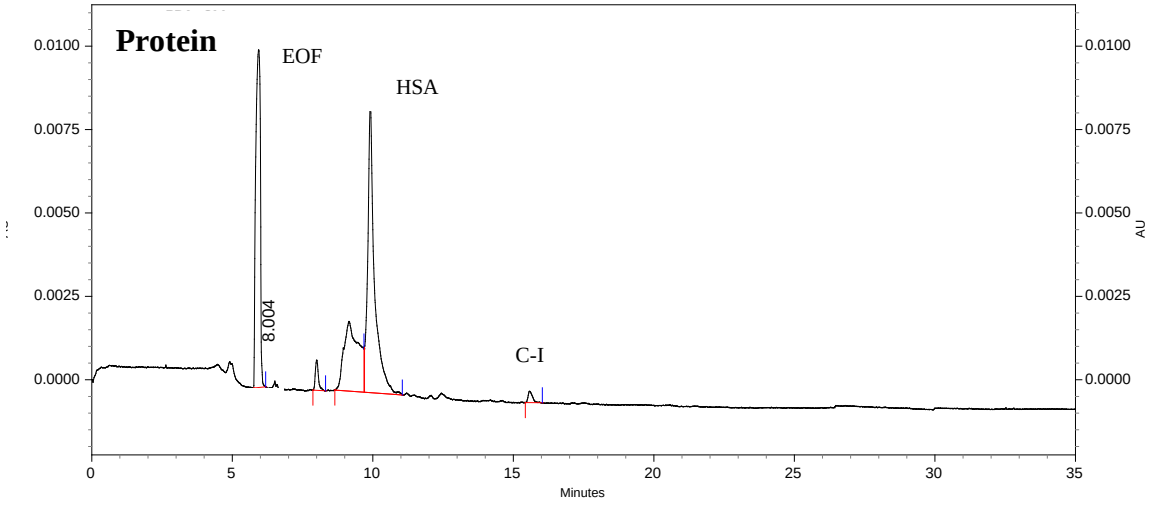

Figure 53. Electropherogram of the protein fraction from control patient 3.

Table 31. CE data for the protein fraction from a 200µL serum sample from control patient 3.

Protein	Elution Time (min)	Mobility (x $10^{-5}$$cm^2$/Vs)	CPA	Concentration (mg/dL)
HSA	9.9	-20.289	12198	12.28
ApoC-I	15.6	-31.154	197	0.47

In the protein subfraction, shown in Figure 52, there were peaks corresponding to human serum albumin, and low relative ion intensity peaks corresponding to prealbumin and apoE. Table 30 shows the peak masses for this fraction. The CE results for this fraction, shown in Figure 53, detected albumin and apoC-I. The albumin peak was large indicating an enrichment of the protein in this fraction. In comparison to the MALDI-MS spectra for this fraction, human serum and albumin were detected by both methods, neither of which detected apoA-I.

Table 32. Control patient 7 medical information

Control Patient 7	
Age	44 years old
Height	66.5 inches
Weight	185 lbs.
Gender	Female
Race	Caucasian
Major Risk Factors	Family history of CAD

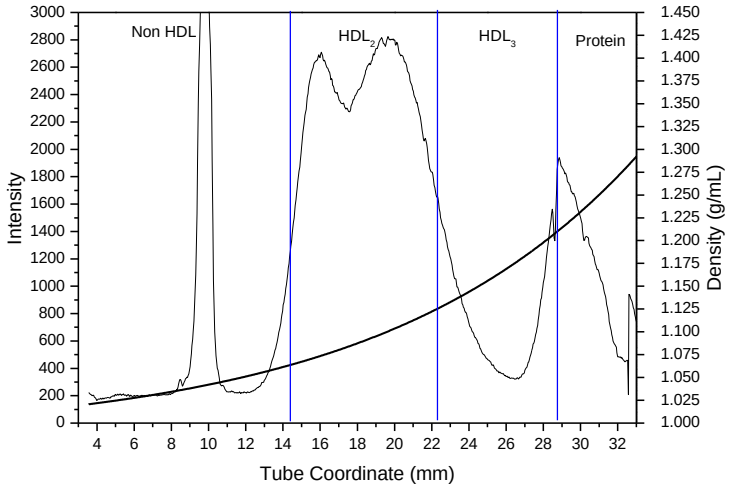

Figure 54. Lipoprotein density profile from control patient 7 in a 0.300M solution of Cs_2CdY, spun for 6 hours at 120,000RPM at 5°C after treatment with dextran sulfate.

Control Patient 7 Discussion

Control patient 7, whose medical history is presented in Table 32, is a 44 year old Caucasian female who does not have CAD, however, does have a family history of the disease. Figure 54 shows the Cs_2CdY lipoprotein profile for this patient which contains a split peak with high intensity.

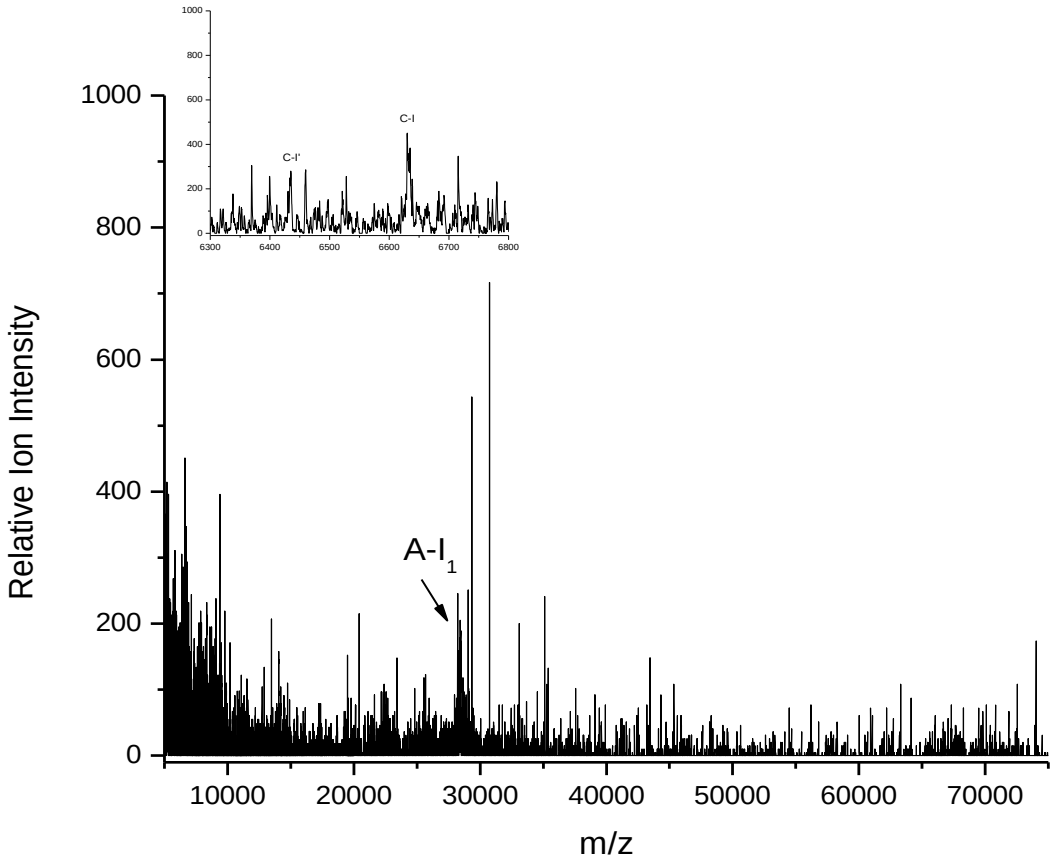

Figure 55. MALDI-MS non HDL spectra from control patient 7.

Table 33. Identification of apolipoproteins in the non HDL fraction from control patient 7.

Identification	Mass (Da)
ApoC-I'	6399.72
ApoC-I	6630.61
ApoA-I_1	28297.62

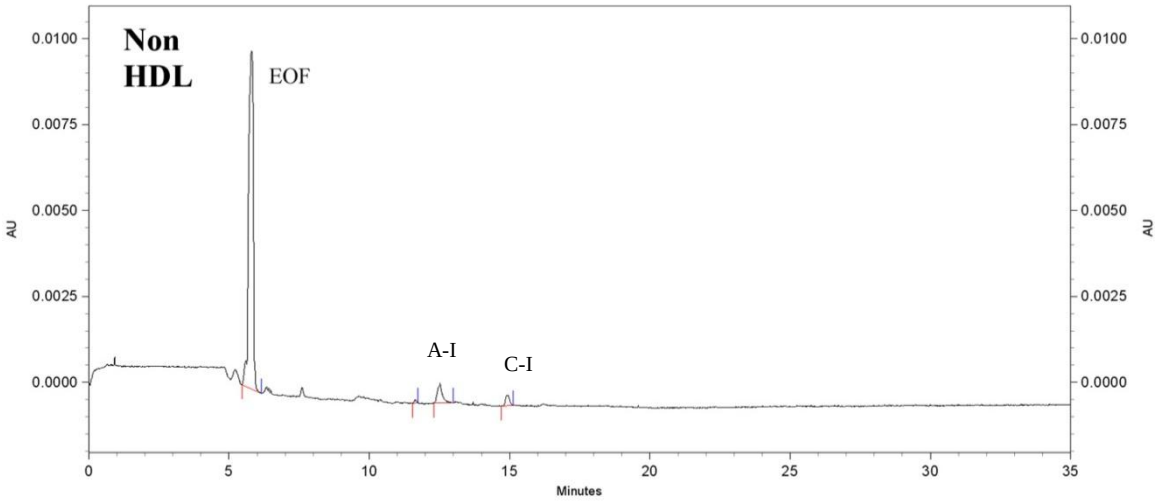

Figure 56. Electropherogram of the non HDL fraction from control patient 7.

Table 34. CE data for the non HDL fraction from a 200µL serum sample from control patient 7.

Protein	Elution Time (min)	Mobility (x $10^{-5}$$cm^2$/Vs)	CPA	Concentration (mg/dL)
ApoA-I	12.5	-27.628	437	1.21
ApoC-I	14.9	-31.455	168	0.40

Figures 55 shows the MALDI-MS spectra for the non HDL subfraction which contained low intensity and low resolution peaks corresponding to apoC-I and C-I', and a low intensity peak corresponding to apoA-I_1. Table 33 shows the peak masses for this fraction. The C-I' peak was hardly visible and the C-I peak was only slightly higher in relative ion intensity. The CE analysis of this fraction detected only apoA-I and apoC-I as shown in Figure 56. Both methods detected apoA-I and apoC-I at very low intensities, indicating minimal contamination of HDL_2.

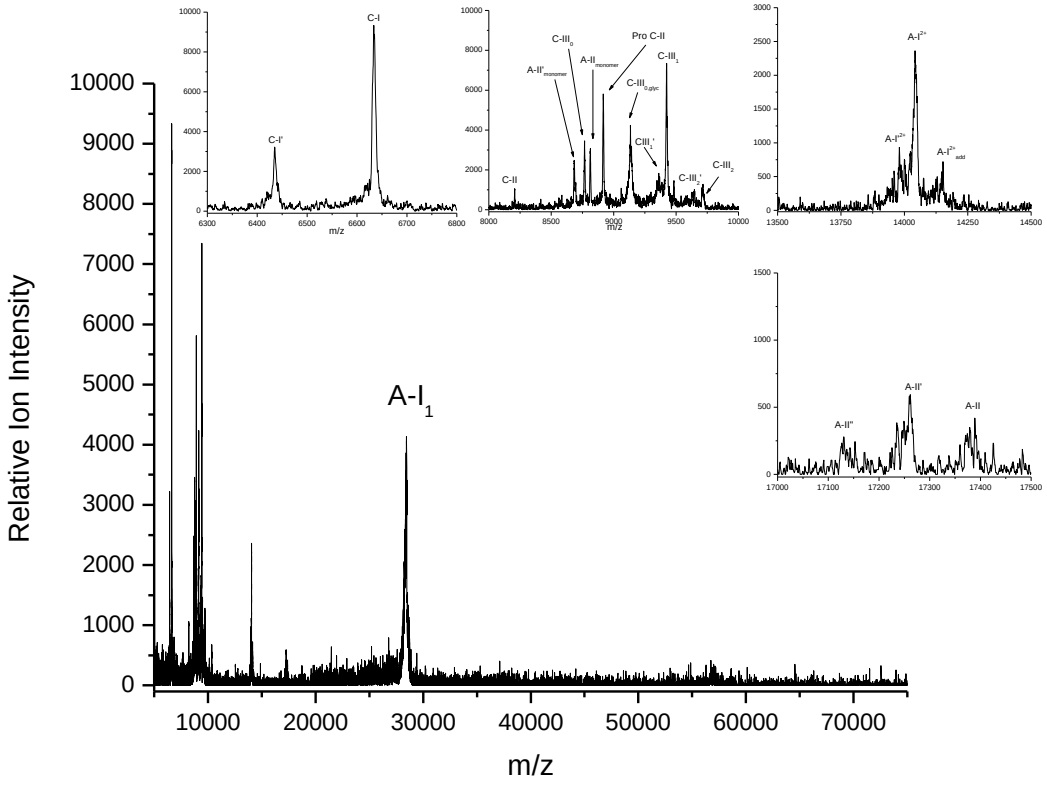

Figure 57. MALDI-MS HDL_2 spectra from control patient 7.

Table 35. Identification of apolipoproteins in the HDL_2 fraction from control patient 7.

Identification	Mass (Da)
ApoC-I'	6435.40
ApoC-I	6633.97
ApoC-II	8210.33
ApoA-II'$_m$	8684.24
ApoC-III$_0$	8767.09
ApoA-II$_m$	8812.73
Pro ApoC-II	8917.12
ApoC-III$_{0,glyc}$	9133.92
ApoC-III'$_1$	9361.55
ApoC-III$_1$	9424.38
ApoC-III$_2$'	9647.17

Table 35. (Continued)

Identification	Mass (Da)
ApoC-III_2	9717.28
ApoA-I'^{2+}	13980.76
ApoA-I^{2+}	14044.54
ApoA-I^{2+}_{add}	14152.17
ApoA-II"	17132.03
ApoA-II'	17261.50
ApoA-II	17388.00
ApoA-I_1	28456.30

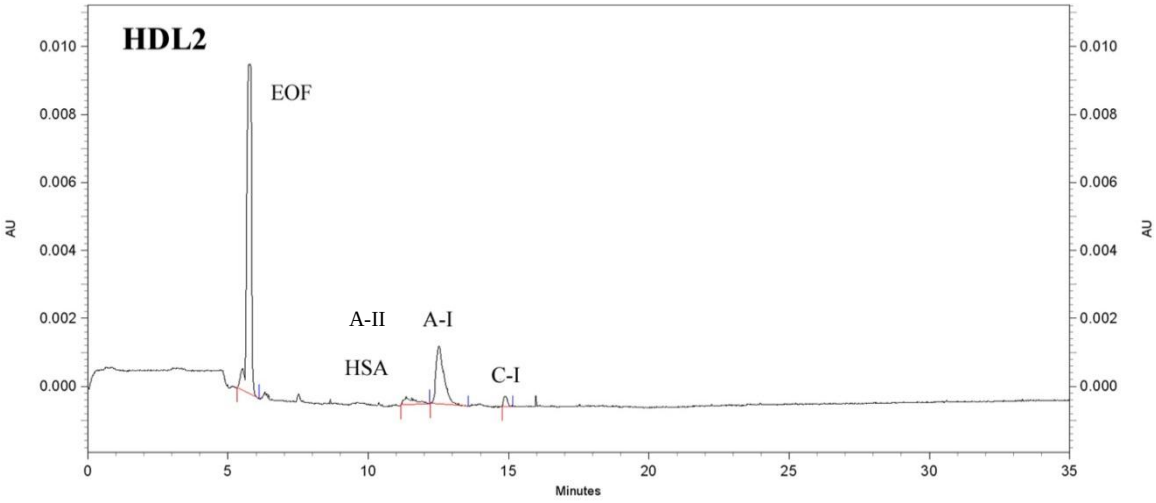

Figure 58. Electropherogram of the HDL_2 fraction from control patient 7.

Table 36. CE data for the HDL_2 fraction from a 200µL serum sample from control patient 7.

Protein	Elution Time (min)	Mobility (x $10^{-5}cm^2/Vs$)	CPA	Concentration (mg/dL)
ApoA-II	11.3	-25.540	438	-------
ApoA-I	12.5	-27.994	2232	6.19
ApoC-I	14.9	-31.750	169	0.40

Figure 57 shows the MALDI-MS spectra corresponding to the HDL_2 subfraction which contained apos C-I', C-I, C-II, A-$II_{monomer}$, C-III_0, Pro C-II, C-$III_{0,glyc}$, C-III_1, A-I^{2+}, A-II, and A-I_1. Table 35 shows the peak masses for this fraction. The apoC-I peaks were sharp with C-I having a relative ion intensity greater than twice the intensity of C-I'. As observed in the HDL_2 subfractions of other patients, there was an abundance of proteins in the region between *m/z* 8000 – 10000 with the highest peak detected from ApoC-III_1. With the exception of the apoA-II peaks, the peaks in this subfraction were highly resolved. Figure 58 shows the CE results following the analysis of this subfraction and detected apoA-II, apoA-I, and apoC-I. Both MALDI-MS and CE detected the same apos with MALDI-MS additionally detecting apoA-II, and apoC-III isoforms, neither method detected albumin in this fraction.

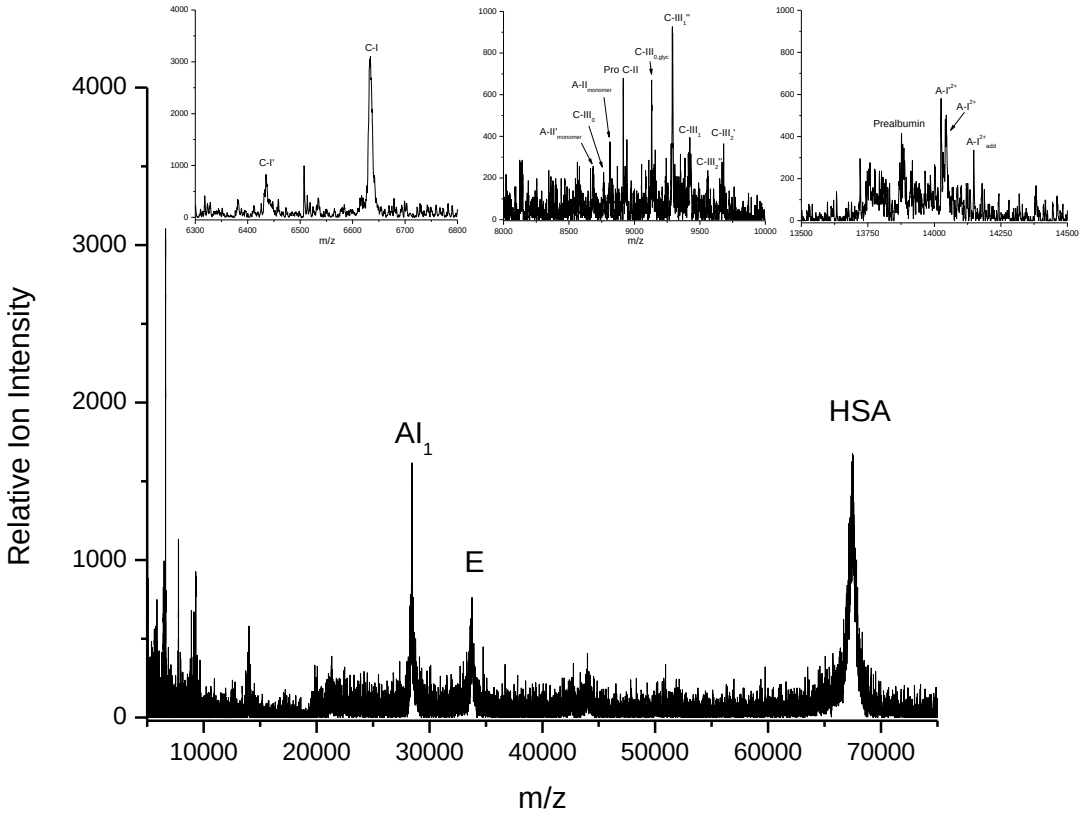

Figure 59. MALDI-MS HDL_3 spectra from control patient 7.

Table 37. Identification of apolipoproteins in the HDL_3 fraction from control patient 7.

Identification	Mass (Da)
ApoC-I'	6435.43
ApoC-I	6633.90
ApoA-II'$_m$	8685.18
ApoC-III$_0$	8763.49
ApoA-II$_m$	8813.11
Pro ApoC-II	8914.86
ApoC-III$_{0,glyc}$	9130.89
ApoC-III'$_1$	9291.11
ApoC-III$_1$	9419.99
ApoC-III$_2$''	9564.72
ApoC-III$_2$'	9681.73
Prealbumin	13877.65

Table 37. (Continued)

Identification	Mass (Da)
ApoA-I^{2+}	14047.01
ApoA-I^{2+}_{add}	14150.13
ApoA-I_1	28444.91
ApoE	33761.59
HSA	67496.18

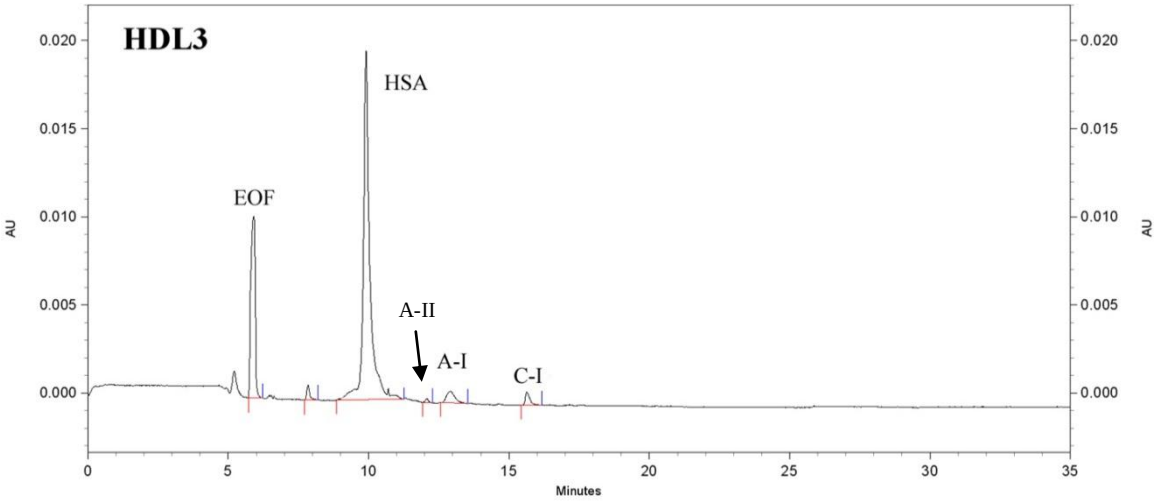

Figure 60. Electropherogram of the HDL_3 fraction from control patient 7.

Table 38. CE data for the HDL_3 fraction from a 200µL serum sample from control patient 7.

Protein	Elution Time (min)	Mobility (x $10^{-5}cm^2/Vs$)	CPA	Concentration (mg/dL)
HSA	9.9	-20.578	26598	26.78
ApoA-II	12.1	-25.954	114	-------
ApoA-I	12.9	-27.559	877	2.43
ApoC-I	15.6	-31.519	439	1.04

The HDL_3 subfraction contained apos C-I', C-I, C-II, C-III, A-II, A-I^{2+}, A-I_1, E, and HSA as shown in Figure 59. Table 37 shows the peak masses for this fraction. Overall, the HDL_3 peaks were less intense than those observed in the HDL_2 subfraction for patient 7. The apoC-I' peak was barely visible with less than three times the relative ion intensity of apoC-I. The albumin peak was also as intense as the apoA-I_1 peak in this region. The CE results for this fraction, shown in Figure 60 detected albumin, apoA-II, apoA-I, and apoC-I.

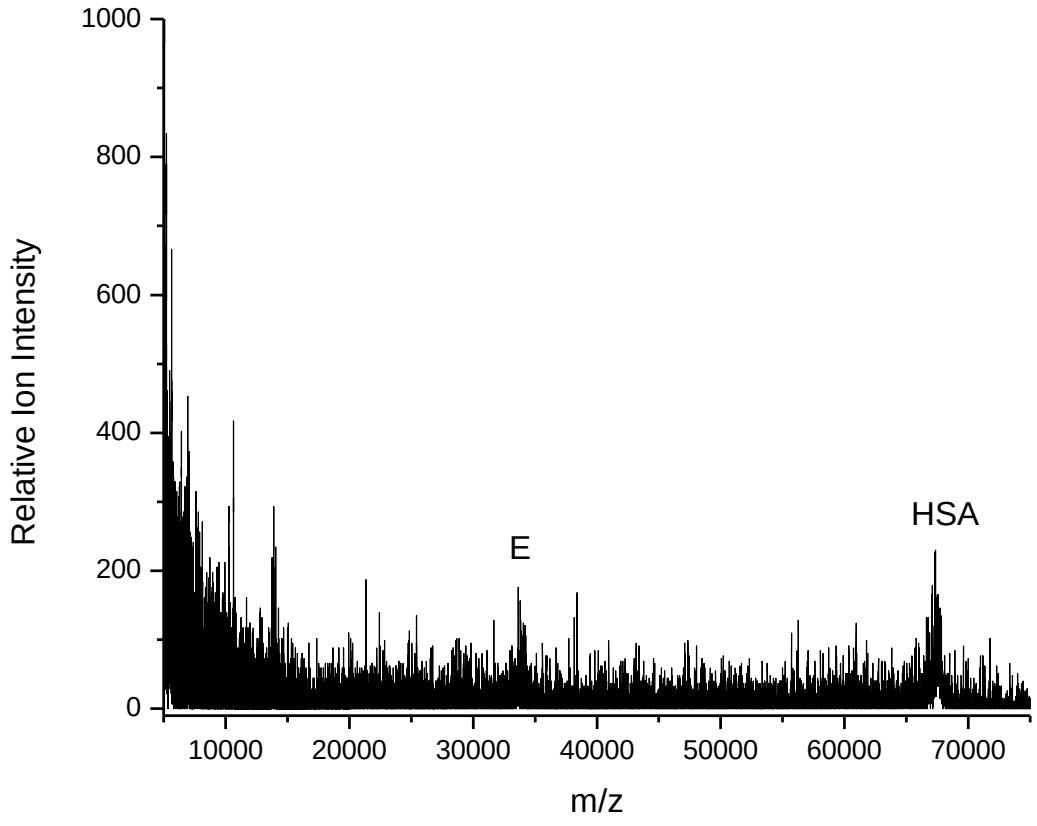

Figure 61. MALDI-MS protein spectra from control patient 7.

Table 39. Identification of apolipoproteins in the protein fraction from control patient 7.

Identification	Mass (Da)
ApoE	33644.00
HSA	67087.75

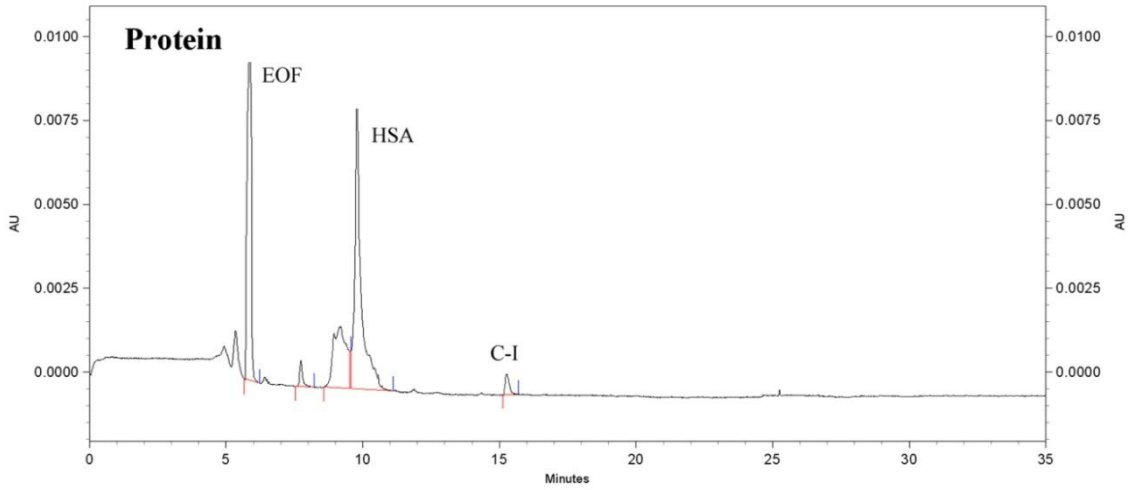

Figure 62. Electropherogram of the protein fraction from control patient 7.

Table 40. CE data for the protein fraction from a 200µL serum sample from control patient73.

Protein	Elution Time (min)	Mobility (x $10^{-5}$$cm^2$/Vs)	CPA	Concentration (mg/dL)
HSA	9.8	-20.521	12083	12.17
ApoC-I	15.3	-31.370	351	0.83

The MALDI-MS spectrum for the protein subfraction, shown in Figure 61, contained apoE, and HSA at low relative ion intensities. Table 39 shows the peak masses for this fraction. The CE results for this subfraction, shown in Figure 62, detected albumin and apoC-I. As also observed in previously reported protein subfractions, albumin contained a shoulder which may be due to its co-migration with another analyte. As also

previously observed, the MALDI-MS spectrum detected apoE along with albumin while the CE results detected apoC-I along with albumin.

Table 41. Control patient 13 medical information

Control Patient 13	
Age	66 years old
Height	60 inches
Weight	98 lbs.
Gender	Female
Race	Hispanic
Major Risk Factors	Hypertension

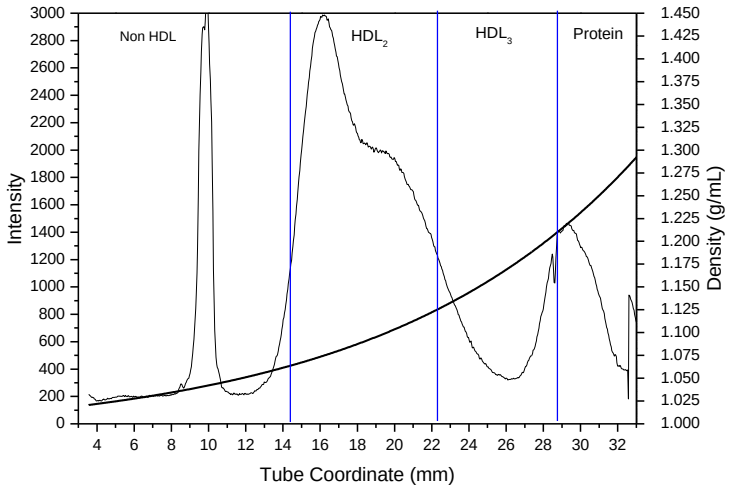

Figure 63. Lipoprotein density profile from control patient 13 in a 0.300M solution of Cs_2CdY, spun for 6 hours at 120,000RPM at 5°C after treatment with dextran sulfate.

Control Patient 13 Discussion

Control patient 13, whose medical history is presented in Table 41, is a 66 year old Hispanic female who does not have CAD, but suffers from hypertension. Figure 63

shows the Cs_2CdY profile for this subject which contains a sharp peak with high intensity that is shifted toward the non HDL region and has a shoulder on its denser side.

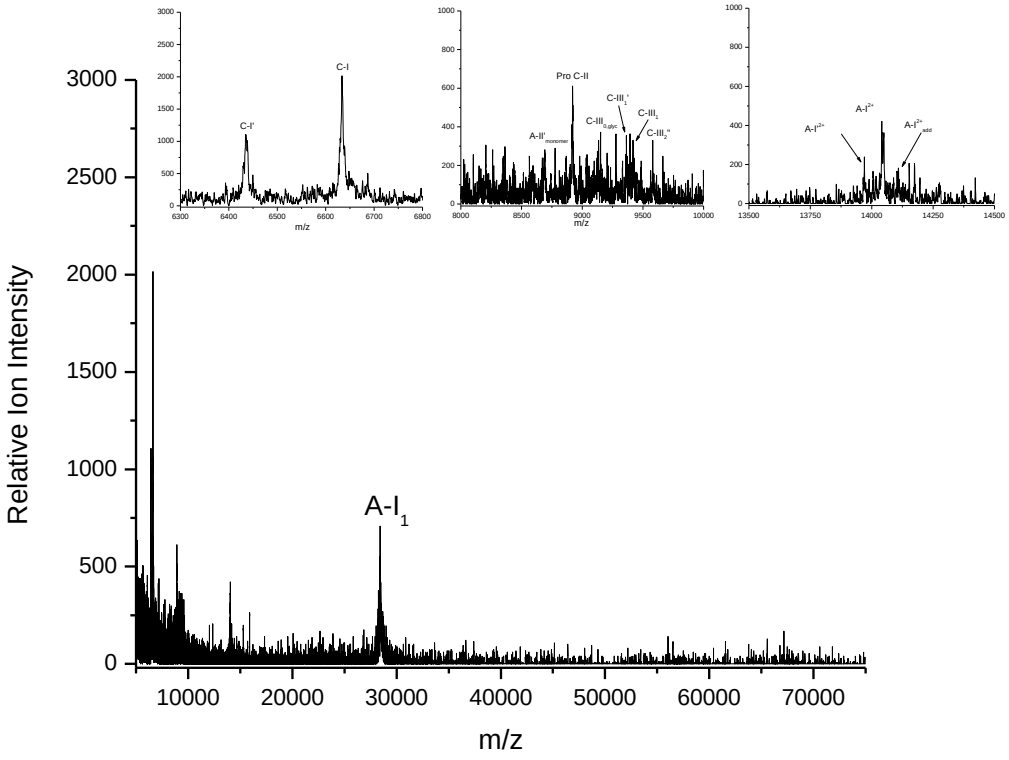

Figure 64. MALDI-MS non HDL spectra from control patient 13.

Table 42. Identification of apolipoproteins in the non HDL fraction from control patient 13.

Identification	Mass (Da)
ApoC-I'	6436.18
ApoC-I	6633.76
$ApoA\text{-}II'_m$	8689.28
Pro ApoC-II	8921.29
$ApoC\text{-}III_{0,glyc}$	9151.57
$ApoC\text{-}III_1'$	9366.26
$ApoC\text{-}III_1$	9419.98
$ApoC\text{-}III_2''$	9589.35

Table 42. (Continued)

Identification	Mass (Da)
A-I'^{2+}	13968.47
A-I^{2+}	14041.73
A-I^{2+}_{add}	14104.83
ApoA-I_1	28409.59

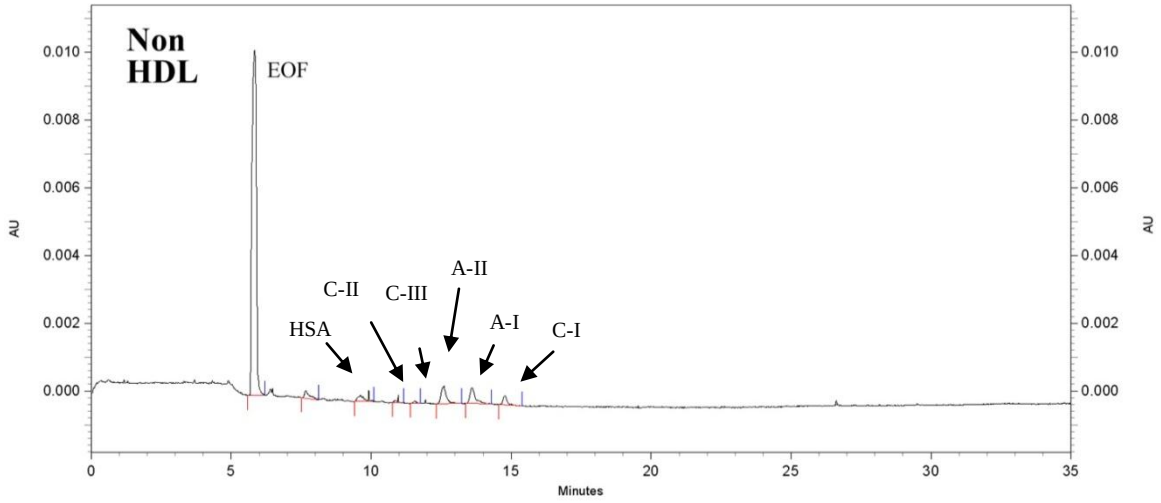

Figure 65. Electropherogram of the non HDL fraction from control patient 13.

Table 43. CE data for the non HDL fraction from a 200µL serum sample from control patient 13.

Protein	Elution Time (min)	Mobility (x $10^{-5}cm^2/Vs$)	CPA	Concentration (mg/dL)
HSA	9.9	-21.171	276	0.28
ApoC-II	11.0	-24.045	59	-------
ApoC-III	12.6	-25.395	30	-------
ApoA-II	13.6	-27.562	427	-------
ApoA-I	14.8	-29.289	396	1.10
ApoC-I	14.8	-31.011	170	0.40

Figure 64 show the MALDI spectra for the non HDL subfraction which contained apos C-'I, C-I, A-$II_{monomer}$, Pro C-II, C-$III_{0,glyc}$, C-III_1, C-III_2, A-I^{2+}, and A-I_1. Table 42 shows the peak masses for this fraction. It appears as though this individual has more buoyant HDL_2 compared to other patients due to the greater quantity of proteins in the non HDL subfraction, though the intensity of these proteins was low. The CE results from the analysis of this fraction are shown in Figure 65, and also showed an abundance of very small protein peaks corresponding to apos C-II, C-III, A-II, A-I, and C-I. Both methods detected similar apos all of which were low in intensity suggesting very minimal mixing of the HDL_2 subfraction.

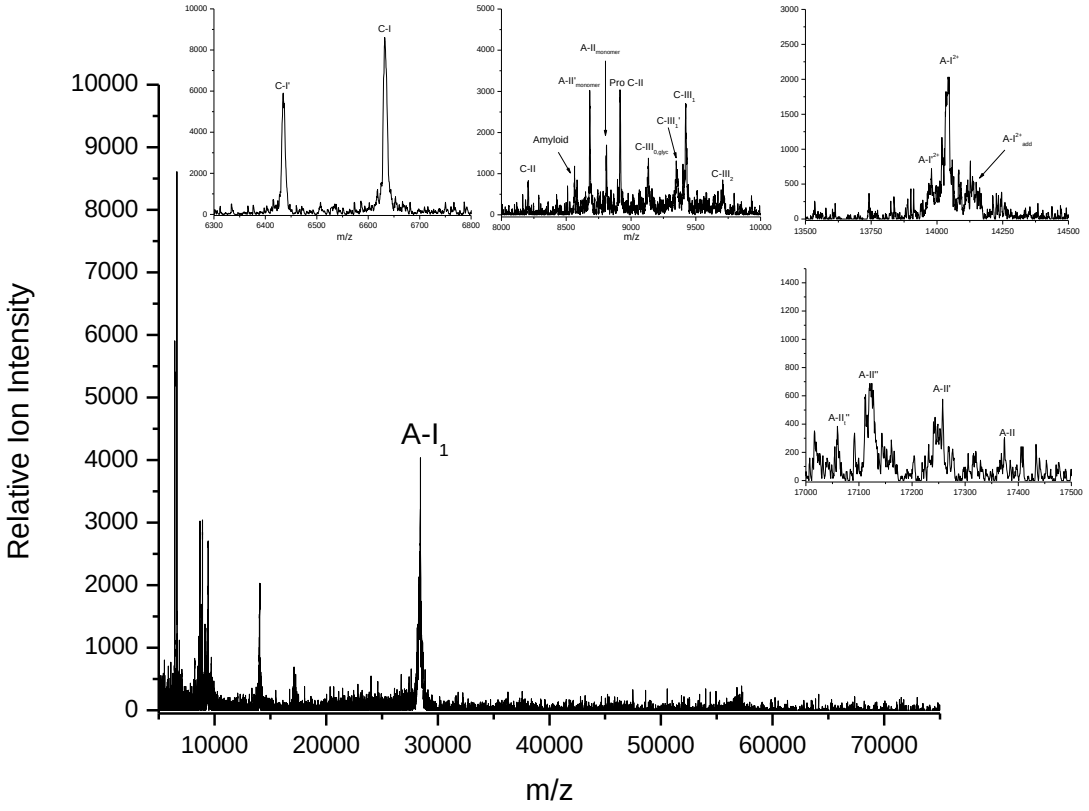

Figure 66. MALDI-MS HDL_2 spectra from control patient 13.

Table 44. Identification of apolipoproteins in the HDL_2 fraction from control patient 13.

Identification	Mass (Da)
ApoC-I'	6435.10
ApoC-I	6632.82
ApoC-II	8207.62
Amyloid	8563.95
ApoA-II_m	8685.18
ApoA-II_m	8811.14
Pro ApoC-II	8916.41
ApoC-$III_{0,glyc}$	9133.77
ApoC-III_1'	9353.21
ApoC-III_1	9422.45
ApoC-III_2	9707.24
ApoA-I'^{2+}	13974.62
ApoA-I^{2+}	14046.19
ApoA-I^{2+}_{add}	14133.74
ApoA-II_t''	17061.80
ApoA-II''	17123.09
ApoA-II'	17259.05
ApoA-II	17375.71
ApoA-I_1	28451.60

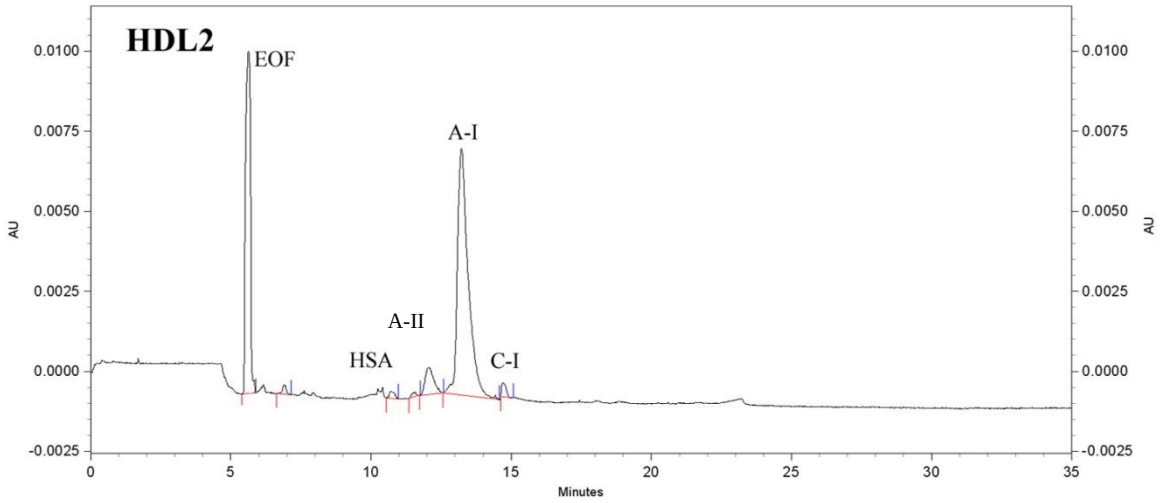

Figure 67. Electropherogram of the HDL_2 fraction from control patient 13.

Table 45. CE data for the HDL_2 fraction from a 200µL serum sample from control patient 13.

Protein	Elution Time (min)	Mobility (x $10^{-5}cm^2/Vs$)	CPA	Concentration (mg/dL)
HSA	9.7	-20.198	543	0.55
ApoA-II	11.2	-24.387	2028	-------
ApoA-I	12.4	-26.896	8902	24.70
ApoC-I	14.9	-30.927	369	0.87

The MALDI-MS spectra from the HDL_2 subfraction, shown in Figure 66, contained apos C-I', C-I, C-II, amyloid, A-$II_{monomer}$, Pro C-II, C-$III_{0,glyc}$, C-III_1, C-III_2, A-I^{2+}, A-II, and A-I_1. Table 44 shows the peak masses for this fraction. These protein peaks were highly resolved and higher in intensity than any other subfraction for this patient. This subfraction contained amyloid, a protein involved in many diseases including atherosclerosis. The CE analysis shown in Figure 67, contained peaks corresponding to albumin, apoA-II, apoA-I, and apoC-I. ApoA-I was the greatest peak in this subfraction. Both methods reported comparable results with MALDI-MS detecting the presence of apoC-III isoforms that were not detected by CE.

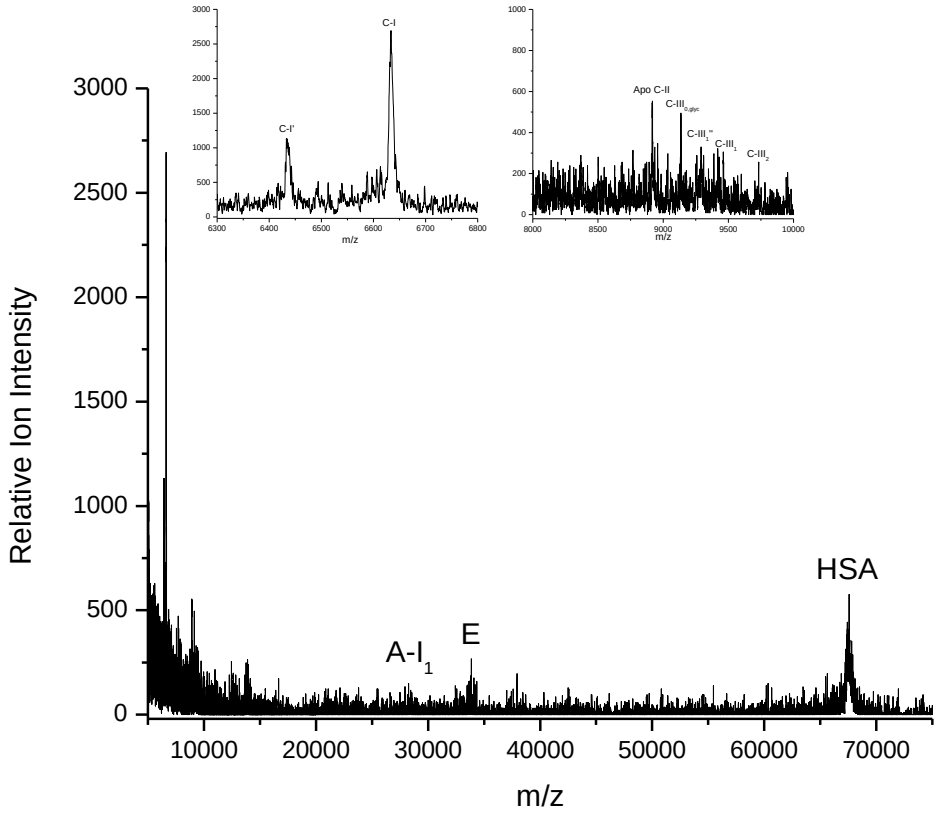

Figure 68. MALDI-MS HDL_3 spectra from control patient 13.

Table 46. Identification of apolipoproteins in the HDL_3 fraction from control patient 13.

Identification	Mass (Da)
ApoC-I'	6434.93
ApoC-I	6633.72
Pro ApoC-II	8917.01
$ApoC\text{-}III_{0,glyc}$	9134.99
$ApoC\text{-}III_1$	9428.18
$ApoC\text{-}III_1$'	9316.64
$ApoC\text{-}III_2$	9729.57
$ApoA\text{-}I_1$	28306.78
ApoE	33858.07
HSA	67576.77

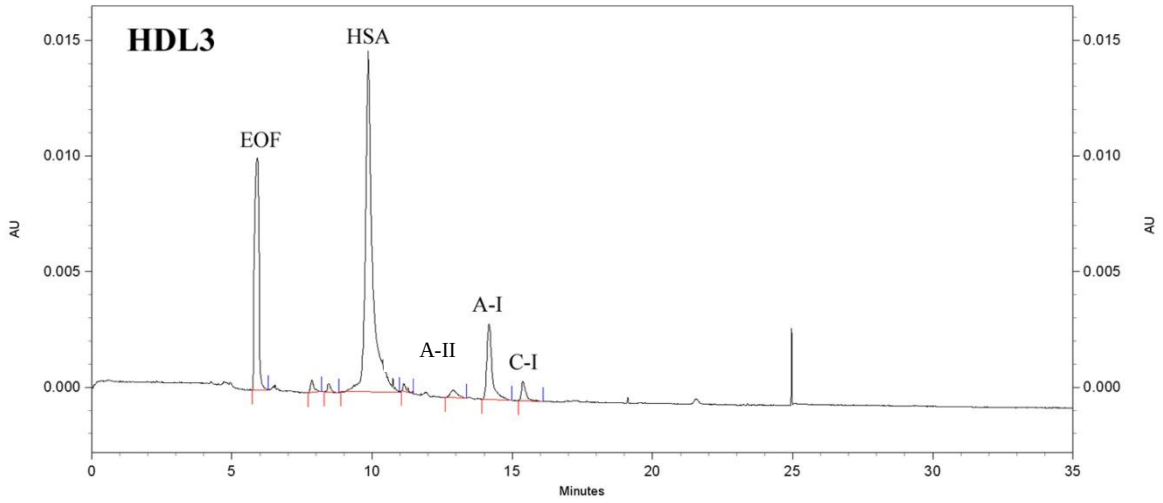

Figure 69. Electropherogram of the HDL_3 fraction from control patient 13.

Table 47. CE data for the HDL_3 fraction from a 200µL serum sample from control patient 13.

Protein	Elution Time (min)	Mobility (x $10^{-5}cm^2/Vs$)	CPA	Concentration (mg/dL)
HSA	9.9	-20.381	21940	22.09
ApoA-II	12.9	-27.461	381	-------
ApoA-I	14.2	-29.536	2535	7.03
ApoC-I	15.4	-31.115	499	1.18

Figure 68 shows the HDL_3 subfraction MALDI-MS spectra, which contained apos C-I', C-I, C-II, $C\text{-}III_{0,glyc}$, $C\text{-}III_1$, $A\text{-}I_1$, E, and HSA. Table 46 shows the peak masses for this fraction. The relative ion intensity of the peaks in the region spanning *m/z* 8000 – 10000 were overall low and the HSA peak had higher relative ion intensity than the apoA-I peak, indicating a predominance of HSA. Figure 69 shows the CE results for this subfraction which detected albumin, apoA-II, apoA-I and apoC-I. The

largest peak detected was from albumin followed by apoA-I, which corresponded to the albumin enrichment observed by MALDI-MS.

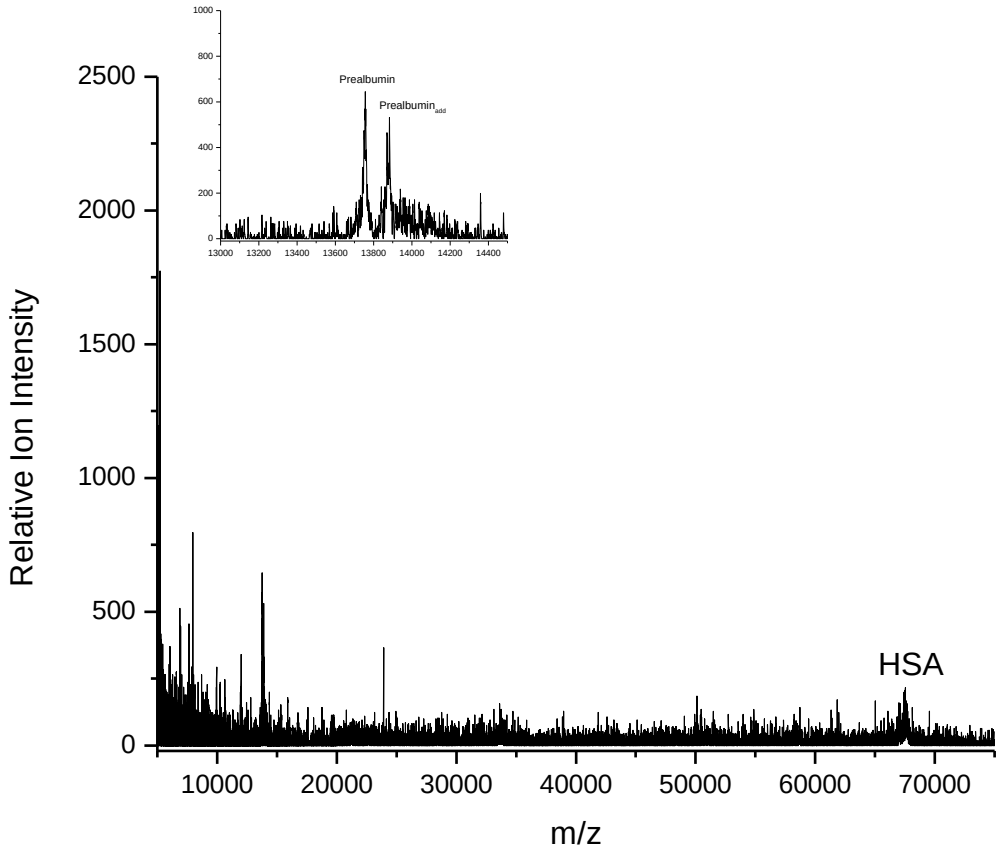

Figure 70. MALDI-MS protein spectra from control patient 13.

Table 48. Identification of apolipoproteins in the protein fraction from control patient 13.

Identification	Mass (Da)
Prealbumin	13756.91
Prealbumin$_{add}$	13883.16
HSA	67671.83

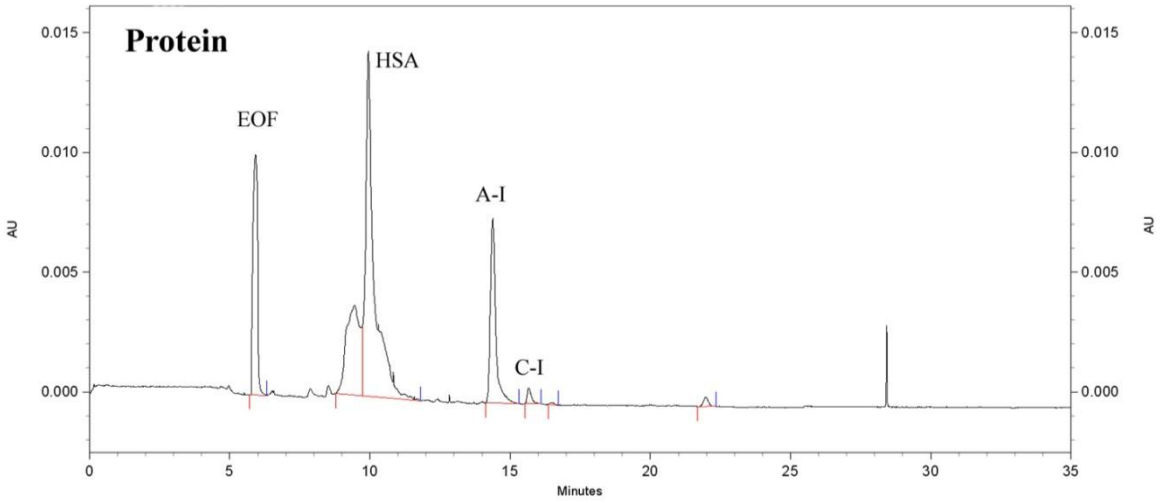

Figure 71. Electropherogram of the protein fraction from control patient 13**.**

Table 49. CE data for the protein fraction from a 200µL serum sample from control patient 13.

Protein	Elution Time (min)	Mobility (x $10^{-5}$$cm^2$/Vs)	CPA	Concentration (mg/dL)
HSA	9.9	-20.497	25763	25.95
ApoA-I	14.4	-29.696	6009	16.67
ApoC-I	15.7	-31.367	356	0.84
Unidentified	21.9	-36.771	186	-------

The MALDI-MS protein subfraction spectra contained prealbumin and HSA as shown in Figure 70. Table 48 shows the peak masses for this fraction. The CE results in Figure 71 detected an enrichment of albumin, in addition to apoA-I, apoC-I, and an unidentified peak. The albumin peak also contained a large shoulder. It is possible that prealbumin and apoA-I have comparable electrophoretic mobilities since apoA-I was not detected by MALDI-MS.

Table 50. Control patient 14 medical information

Control Patient 14	
Age	75 years old
Height	64 inches
Weight	145 lbs.
Gender	Female
Race	Caucasian
Major Risk Factors	Family history of CAD

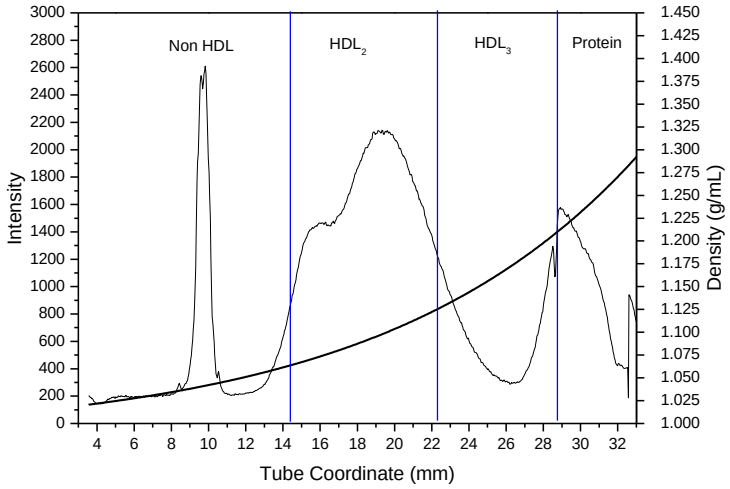

Figure 72. Lipoprotein density profile from control patient 14 in a 0.300M solution of Cs_2CdY, spun for 6 hours at 120,000RPM at 5°C after treatment with dextran sulfate.

Control Patient 14 Discussion

Control patient 14, whose medical history is presented in Table 50, is a 76 year old Caucasian female who does not have CAD, however, does have a family history of the disease. Figure 72 shows the Cs_2CdY profile for this subject which contains a broad peak with a shoulder on the buoyant side of the peak.

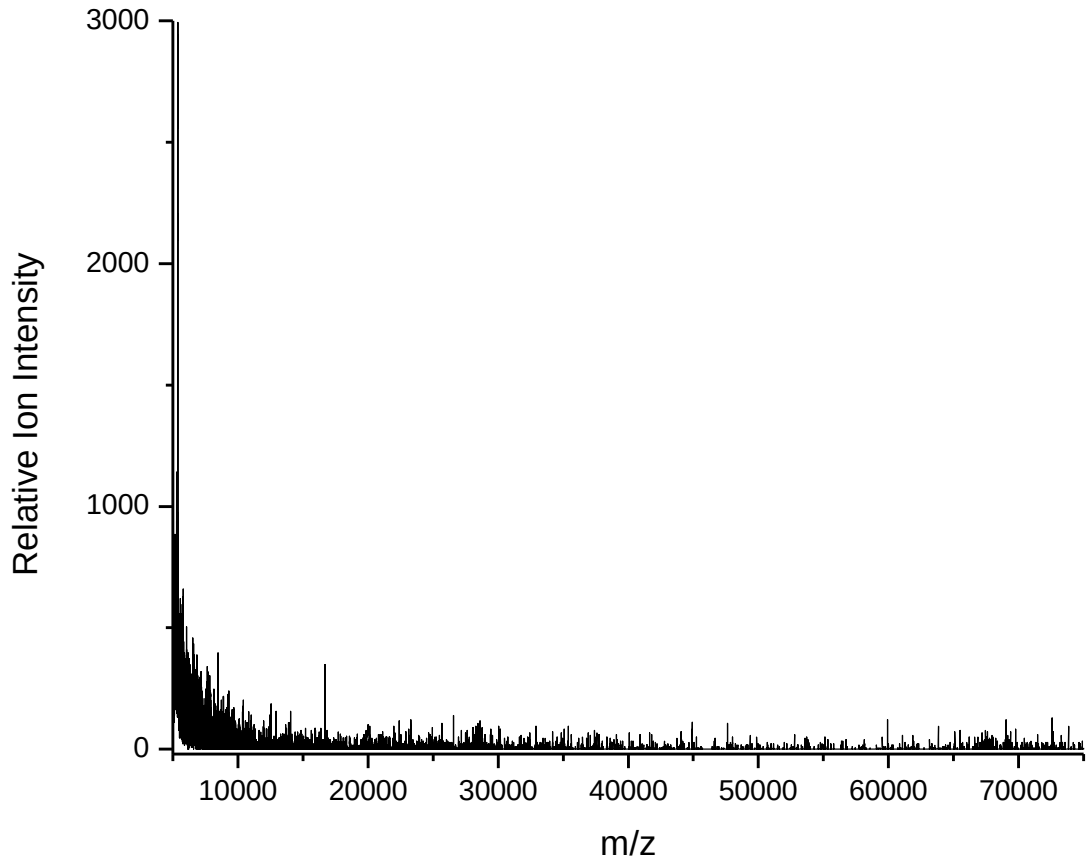

Figure 73. MALDI-MS non HDL spectra from control patient 14.

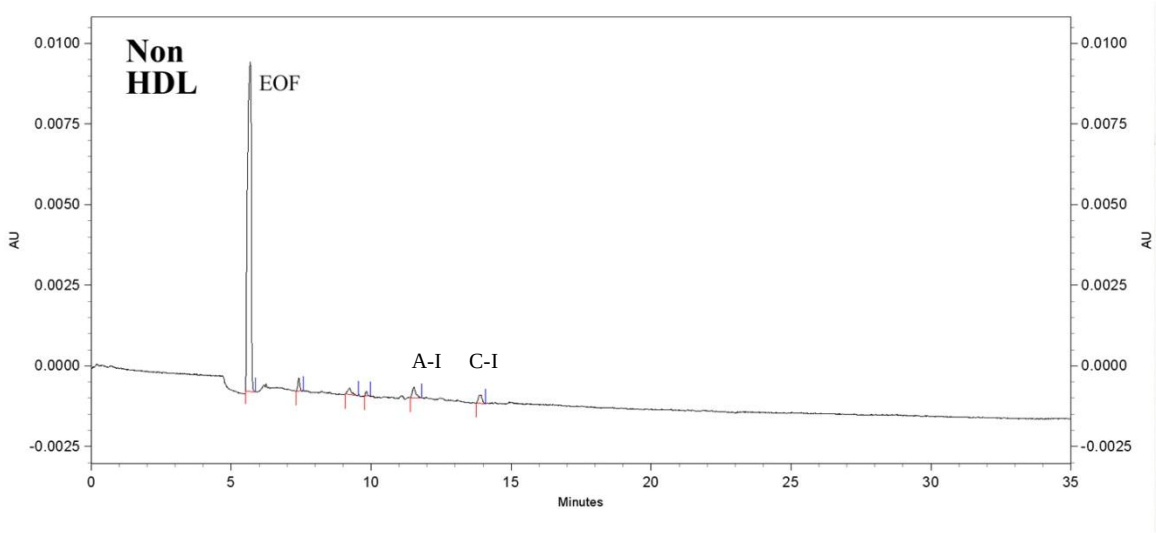

Figure 74. Electropherogram of the non HDL fraction from control patient 14.

Table 51. CE data for the non HDL fraction from a 200µL serum sample from control patient 14.

Protein	Elution Time (min)	Mobility (x $10^{-5}$$cm^2$/Vs)	CPA	Concentration (mg/dL)
ApoA-I	11.5	-26.804	210	0.58
ApoC-I	13.9	-31.225	141	0.33

Figure 73 shows the MALDI spectrum for the non HDL subfraction for this patient which did not contain any apolipoproteins. The CE analysis detected small peaks which corresponded to the electrophoretic mobilities of apoA-I and apoC-I, shown in Figure 74. Due to the sensitivity of the MALDI-MS technique, it is possible that the peaks detected by CE were artifacts or impurities.

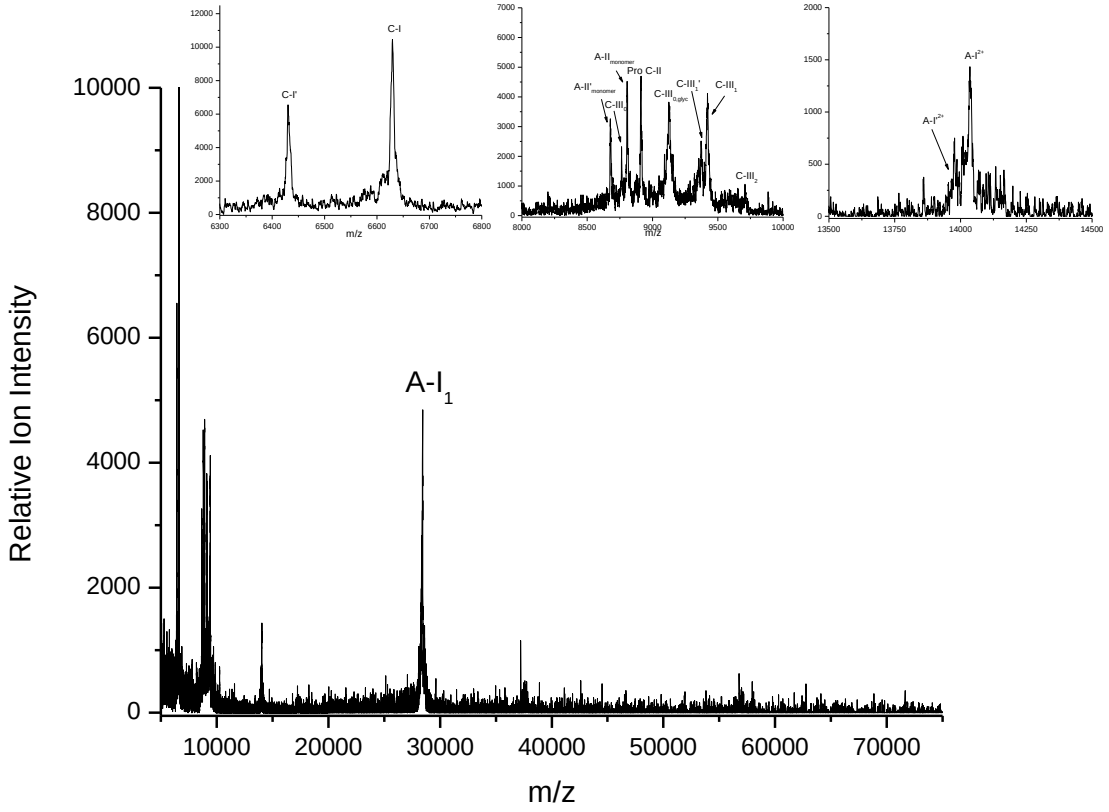

Figure 75. MALDI-MS HDL_2 spectra from control patient 14.

Table 52. Identification of apolipoproteins in the HDL_2 fraction from control patient 14.

Identification	Mass (Da)
ApoC-I'	6431.60
ApoC-I	6629.29
ApoA-II'$_m$	8678.25
ApoA-II$_m$	8809.01
ApoC-III$_0$	8763.49
Pro ApoC-II	8912.07
C-III$_{0,glyc}$	9125.06
C-III$_1$'	9372.32
C-III$_1$	9421.80
C-III$_2$	9709.08

Table 52. (Continued)

Identification	Mass (Da)
ApoA-I'$^{2+}$	13978.72
ApoA-I^{2+}	14036.83
ApoA-I_1	28439.96

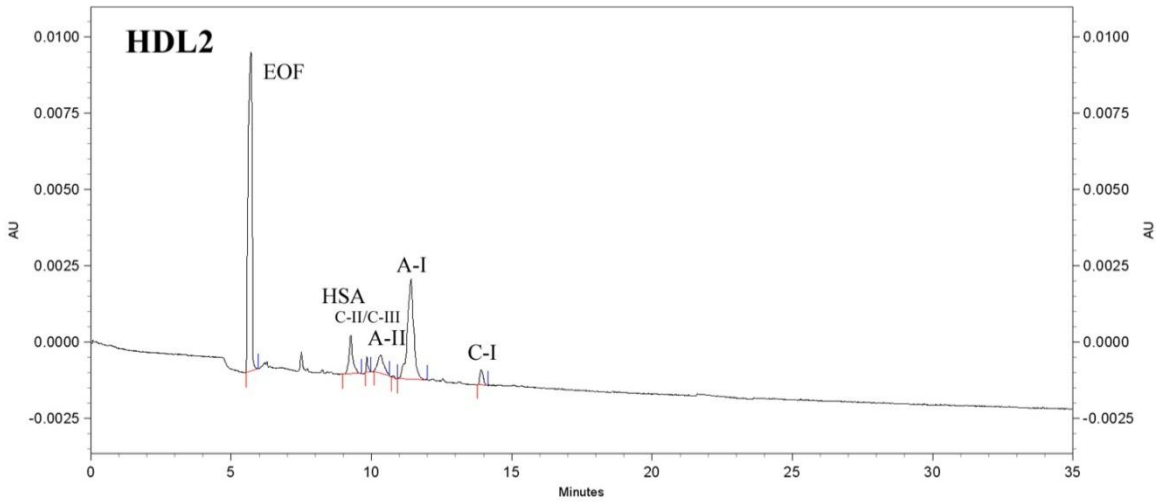

Figure 76. Electropherogram of the HDL_2 fraction from control patient 14.

Table 53. CE data for the HDL_2 fraction from a 200µL serum sample from control patient 14.

Protein	Elution Time (min)	Mobility (x $10^{-5}cm^2/Vs$)	CPA	Concentration (mg/dL)
HSA	9.3	-20.221	1050	1.06
ApoC-II	9.8	-22.071	152	-------
ApoC-III	10.3	-23.521	717	-------
ApoA-II	10.7	-24.720	26	-------
ApoA-I	11.4	-26.246	3779	10.49
ApoC-I	13.9	-30.888	241	0.57

Figure 75 shows the MALDI-MS spectra corresponding to the HDL_2 subfraction which contained apos C-I', C-I, A-$II_{monomer}$, C-III_0, Pro C-II, C-$III_{0,glyc}$, C-III_1, A-I^{2+}, and A-I_1. Table 52 shows the peak masses for this fraction. The apoC-I peaks were sharp with what appeared to be a shoulder. The region spanning *m/z* 8000 – 10000 was abundant in proteins which were overall slightly less intense than apoC-I'. Figure 76 shows the CE results from this fraction which detected albumin, and apos C-II, C-III, A-II, A-I, and C-I. Apo A-I was the largest peak in this fraction. Both methods reported comparable results.

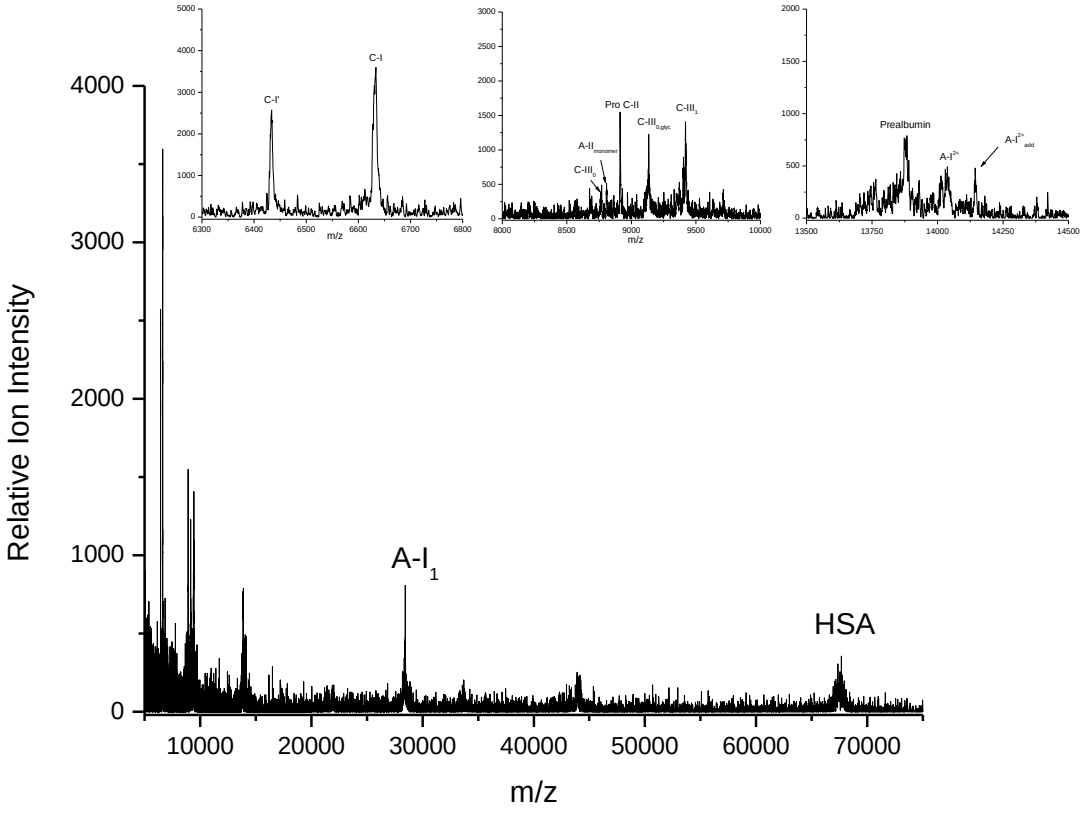

Figure 77. MALDI-MS HDL_3 spectra from control patient 14.

Table 54. Identification of apolipoproteins in the HDL_3 fraction from control patient 14.

Identification	Mass (Da)
ApoC-I'	6433.11
ApoC-I	6631.62
ApoC-III_0	8767.58
ApoA-II_m	8808.72
Pro ApoC-II	8913.38
ApoC-$III_{0,glyc}$	9134.75
ApoC-III_1	9419.93
Prealbumin	13883.19
ApoA-I^{2+}	14038.58
ApoA-$I^{2+}{}_{add}$	14141.93
ApoA-I_1	28443.19
HSA	67674.20

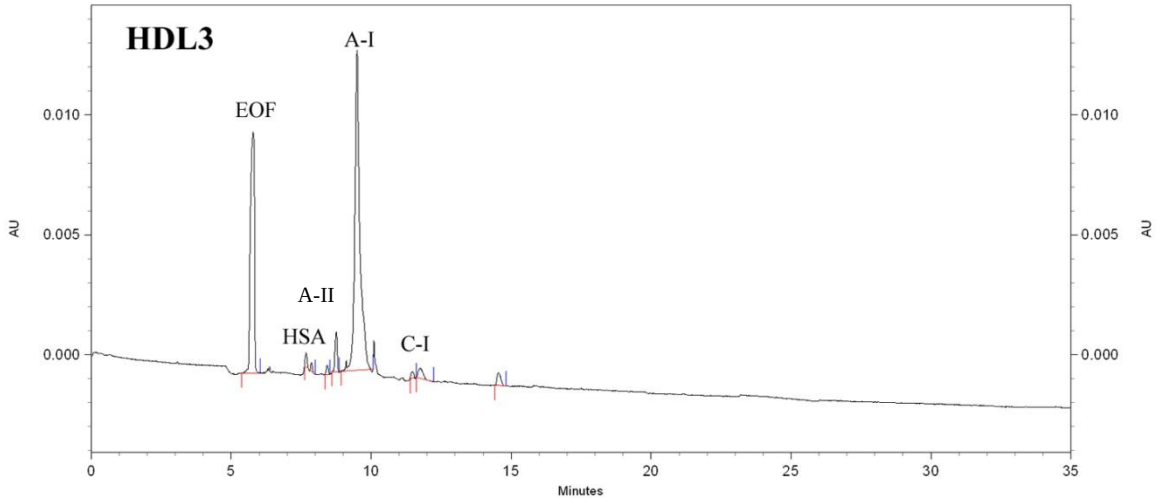

Figure 78. Electropherogram of the HDL_3 fraction from control patient 14.

Table 55. CE data for the HDL_3 fraction from a 200µL serum sample from control patient 14.

Protein	Elution Time (min)	Mobility (x $10^{-5}cm^2/Vs$)	CPA	Concentration (mg/dL)
HSA	9.5	-20.323	14643	14.74

Table 55. (Continued)

Protein	Elution Time (min)	Mobility (x $10^{-5}cm^2/Vs$)	CPA	Concentration (mg/dL)
ApoA-II	11.5	-25.698	124	-------
ApoA-I	11.7	-26.303	361	1.00
ApoC-I	14.6	-31.162	284	0.67

The HDL_3 subfraction MALDI-MS spectra contained apos C-I', C-I, C-III_0, A-$II_{monomer}$, Pro C-II, C-$III_{0,glyc}$, C-III_1, prealbumin, A-I^{2+}, A-I_1, and HSA as shown in Figure 77. Table 54 shows the peak masses for this fraction. The apoC-I peaks were approximately equal in relative ion intensity. The relative ion intensities were lower in this fraction compared to HDL_2 as was the abundance of proteins in the 8000 – 10000 *m/z* region. The CE results, shown in Figure 78, were comparable to MALDI-MS and detected albumin, and apos A-II, A-I, and C-I.

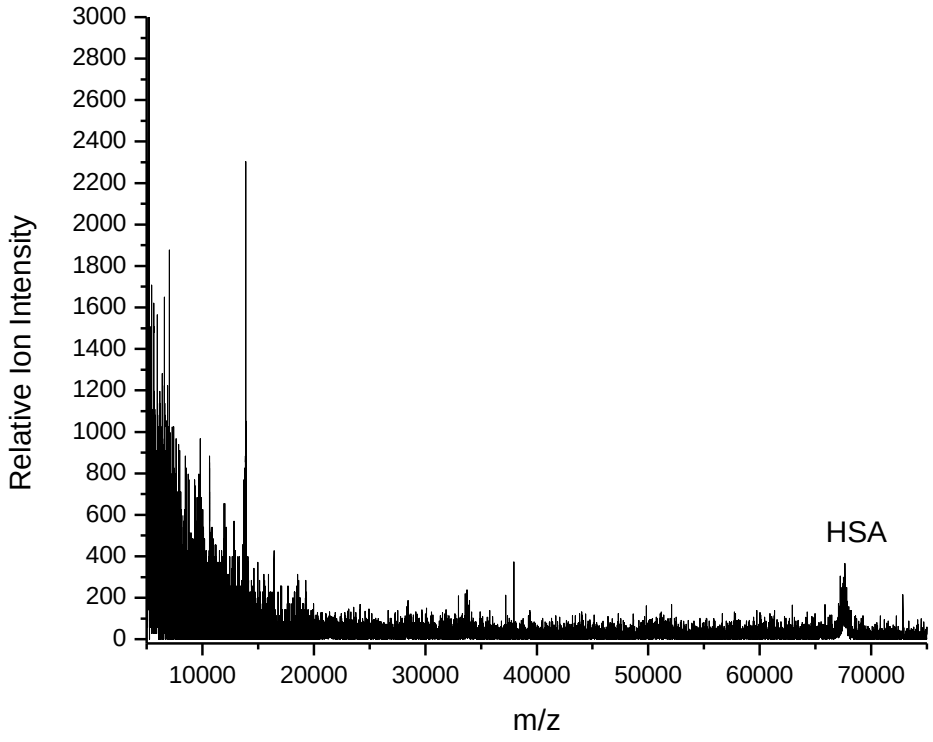

Figure 79. MALDI-MS protein spectra from control patient 14.

Table 56. Identification of apolipoproteins in the protein fraction from control patient 14.

Identification	Mass (Da)
HSA	67644.32

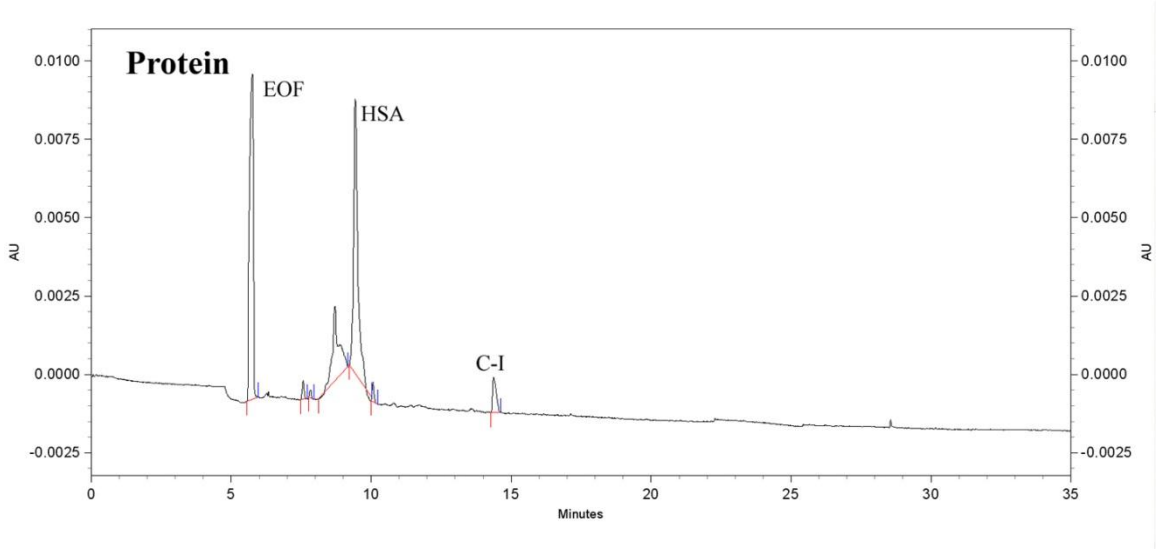

Figure 80. Electropherogram of the protein fraction from control patient 14.

Table 57. CE data for the protein fraction from a 200µL serum sample from control patient 14.

Protein	Elution Time (min)	Mobility (x $10^{-5}cm^2/Vs$)	CPA	Concentration (mg/dL)
HSA	9.4	-20.411	8010	8.07
ApoC-I	14.4	-31.279	587	1.39

The protein subfraction contained only HSA in the MALDI-MS spectrum shown in Figure 79. Table 56 shows the peak masses for this fraction. The CE results detected peaks corresponding to albumin and apoC-I in Figure 80.

Table 58. Control patient 16 medical information

Control Patient 16	
Age	73 years old
Height	58 inches
Weight	92 lbs.
Gender	Female
Race	Caucasian
Major Risk Factors	None

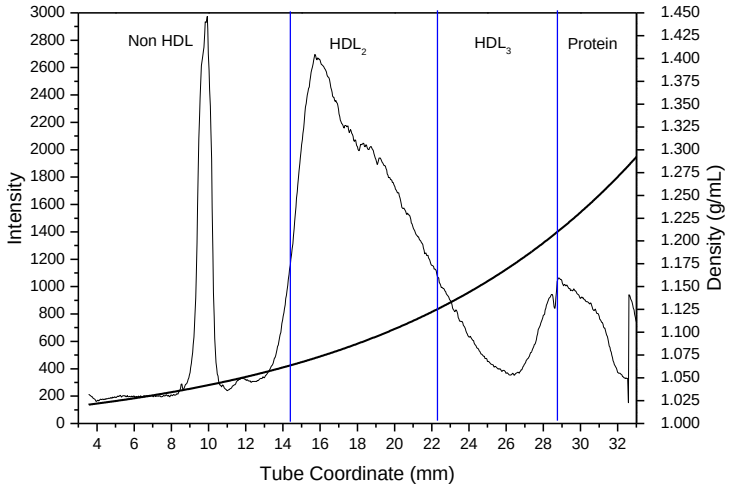

Figure 81. Lipoprotein density profile from control patient 16 in a 0.300M solution of Cs_2CdY, spun for 6 hours at 120,000RPM at 5°C after treatment with dextran sulfate.

Control Patient 16 Discussion

Control patient 16, whose medical history is presented in Table 58, is a 73 year old Caucasian female who does not have CAD and does not possess any risk factors. Figure 81 shows the Cs_2CdY profile for this subject which contains a sharp peak with a poorly resolved shoulder on its denser side.

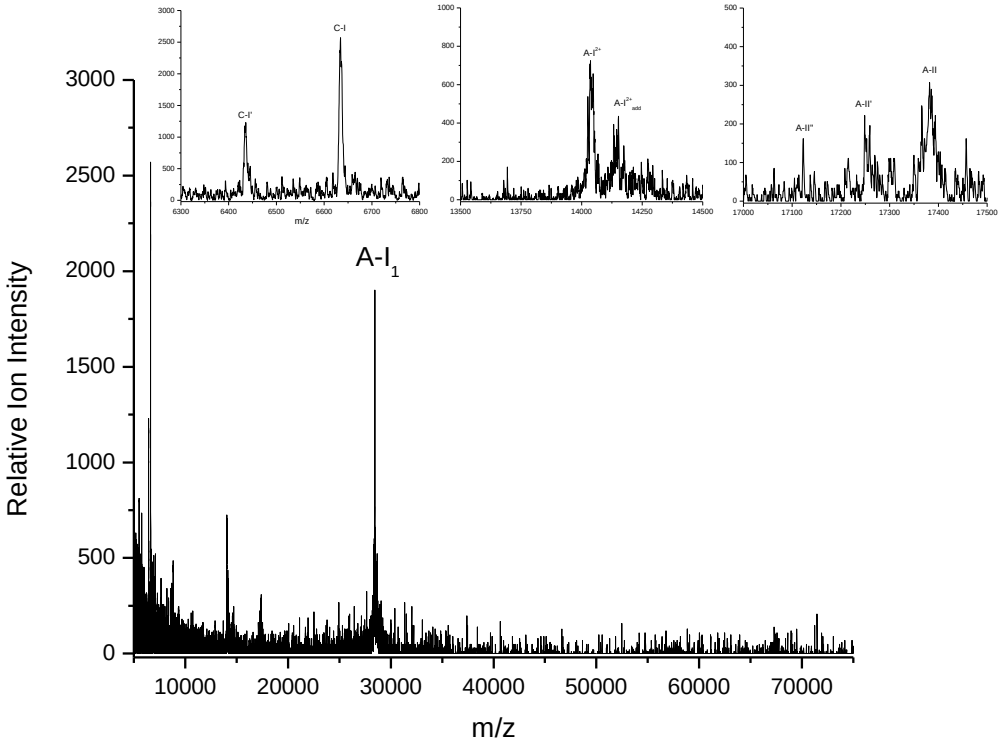

Figure 82. MALDI-MS non HDL spectra from control patient 16.

Table 59. Identification of apolipoproteins in the non HDL fraction from control patient 16.

Identification	Mass (Da)
ApoC-I'	6436.00
ApoC-I	6634.51
ApoA-I^{2+}	14037.34
ApoA-I^{2+}_{add}	14152.24
ApoA-II''	17122.55
ApoA-II'	17250.57
ApoA-II	17384.11
ApoA-I_1	28450.03
HSA	67644.32

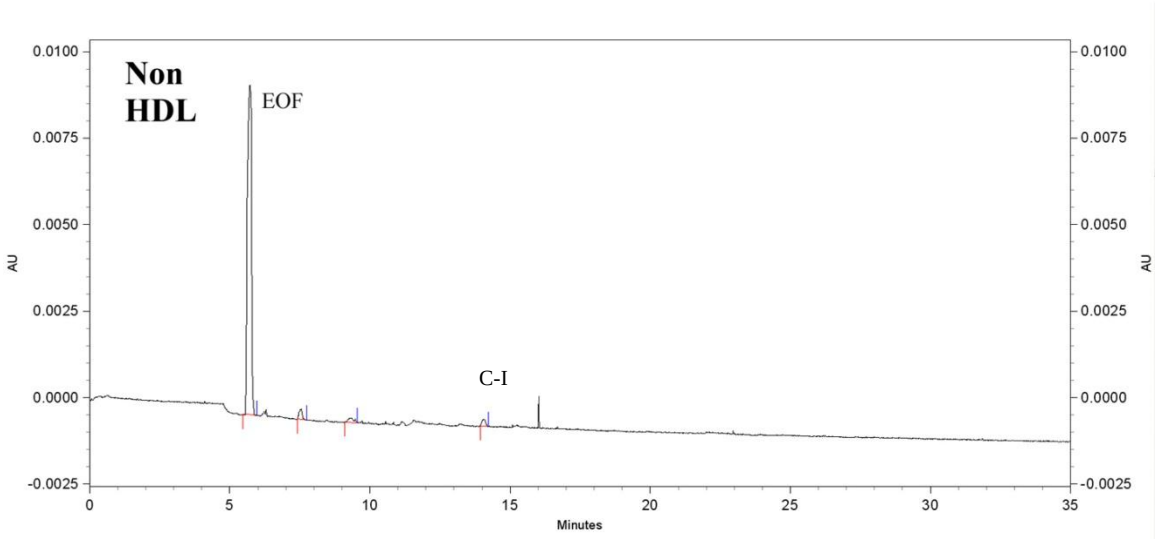

Figure 83. Electropherogram of the non HDL fraction from control patient 16.

Table 60. CE data for the non HDL fraction from a 200µL serum sample from control patient 16.

Protein	Elution Time (min)	Mobility (x $10^{-5}cm^2/Vs$)	CPA	Concentration (mg/dL)
ApoC-I	14.1	-31.033	105	0.25

Figure 82 shows the MALDI spectra for the non HDL subfraction which contained several proteins including apos C-I', C-I, A-I^{2+}, A-II and A-I_1. Table 59 shows the peak masses for this fraction. The abundance of protein suggests an overlap of HDL_2 into this neighboring region, although the overlap is assumed to be minimal due to the relative ion intensity of the peaks. The CE results from this fraction, shown in Figure 83, detected a small peak corresponding to the mobility of apoC-I.

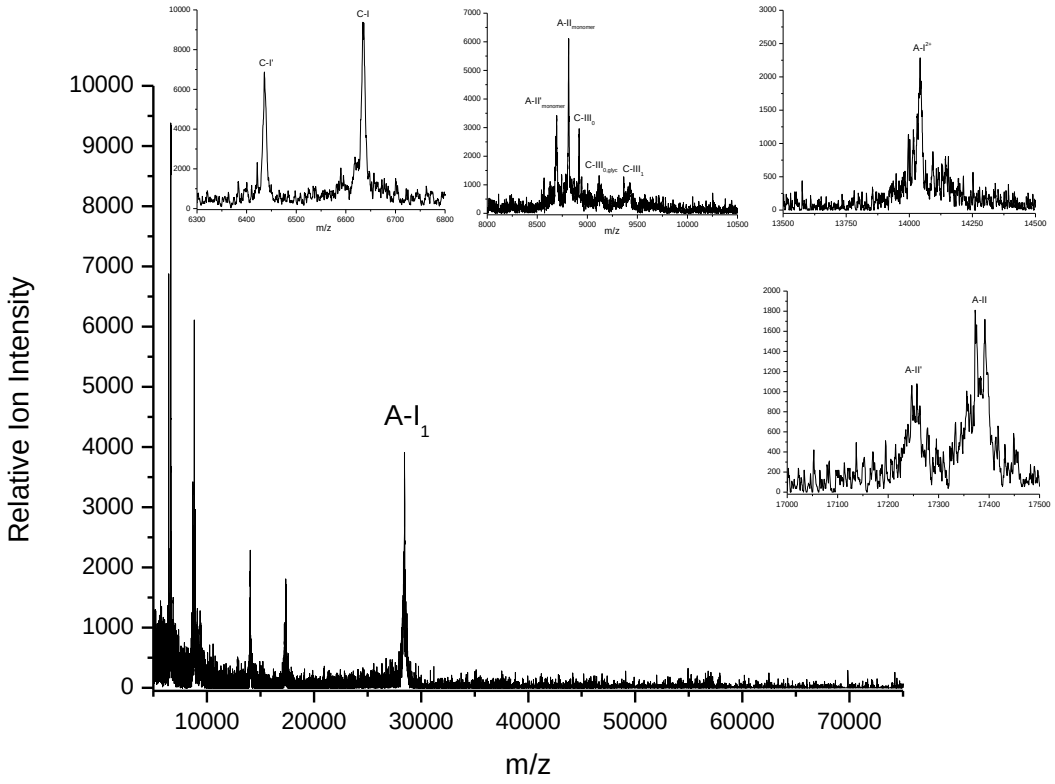

Figure 84. MALDI-MS HDL_2 spectra from control patient 16.

Table 61. Identification of apolipoproteins in the HDL_2 fraction from control patient 16.

Identification	Mass (Da)
ApoC-I'	6436.33
ApoC-I	6635.31
ApoA-II'$_m$	8693.06
ApoA-II$_m$	8813.00
Pro ApoC-II	8917.72
ApoC-III$_{0,glyc}$	9145.57
ApoC-III$_1$	9428.98
ApoA-I^{2+}	14042.58
ApoA-II'	17247.49
ApoA-II	17374.24
ApoA-I$_1$	28453.02
HSA	67644.32

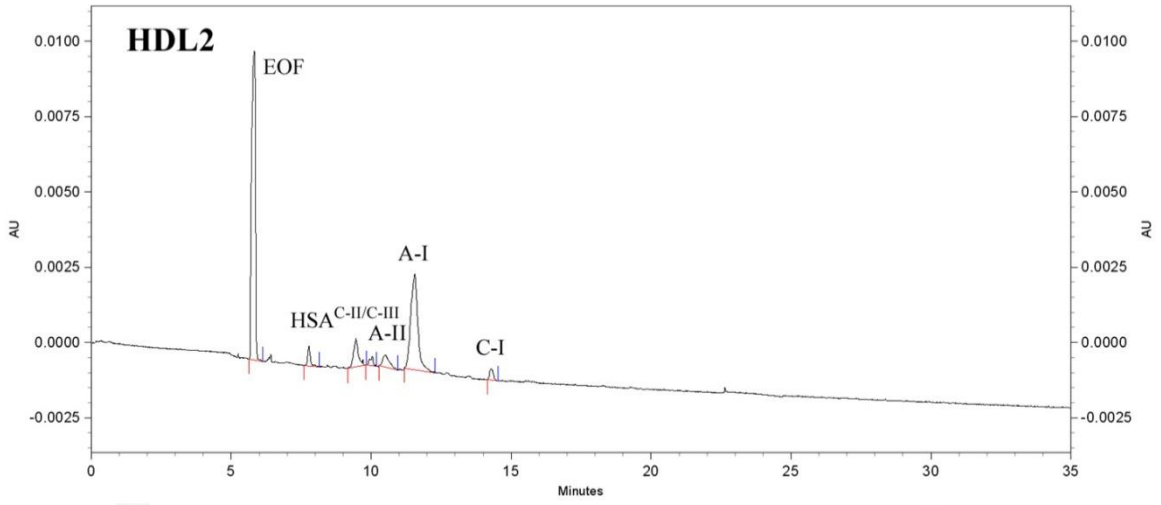

Figure 85. Electropherogram of the HDL_2 fraction from control patient 16.

Table 62. CE data for the HDL_2 fraction from a 200µL serum sample from control patient 16.

Protein	Elution Time (min)	Mobility (x $10^{-5}cm^2/Vs$)	CPA	Concentration (mg/dL)
HSA	9.5	-19.792	982	0.989
ApoC-II	10.0	-21.646	219	-------
ApoC-III	10.5	-22.948	544	-------
ApoA-I	11.6	-25.504	4020	11.15
ApoC-I	14.3	-30.402	200	0.47

Figure 84 shows the MALDI-MS spectra corresponding to the HDL_2 subfraction which contained apos C-I', C-I, A-$II_{monomer}$, C-III_0, C-$III_{0,glyc}$, C-III_1, A-I^{2+}, A-II and A-I_1. Table 61 shows the peak masses for this fraction. The peaks in this subfraction were higher in intensity that those observed in the non HDL fraction. The apoC-I peaks were sharp and nearly equal in intensity and apoC-I contained a small shoulder on the lower mass side of the peak. ApoA-II peaks consisted of doublets which may indicate

oxidative processes. The CE results for this fraction, shown in Figure 85, detected albumin, and apos C-II, C-III, A-II, A-I, and C-I. The greatest peak corresponded to apoA-I followed by apoC-III. Both MALDI-MS and CE detected the same apolipoproteins with MALDI-MS detecting further isoforms of these proteins.

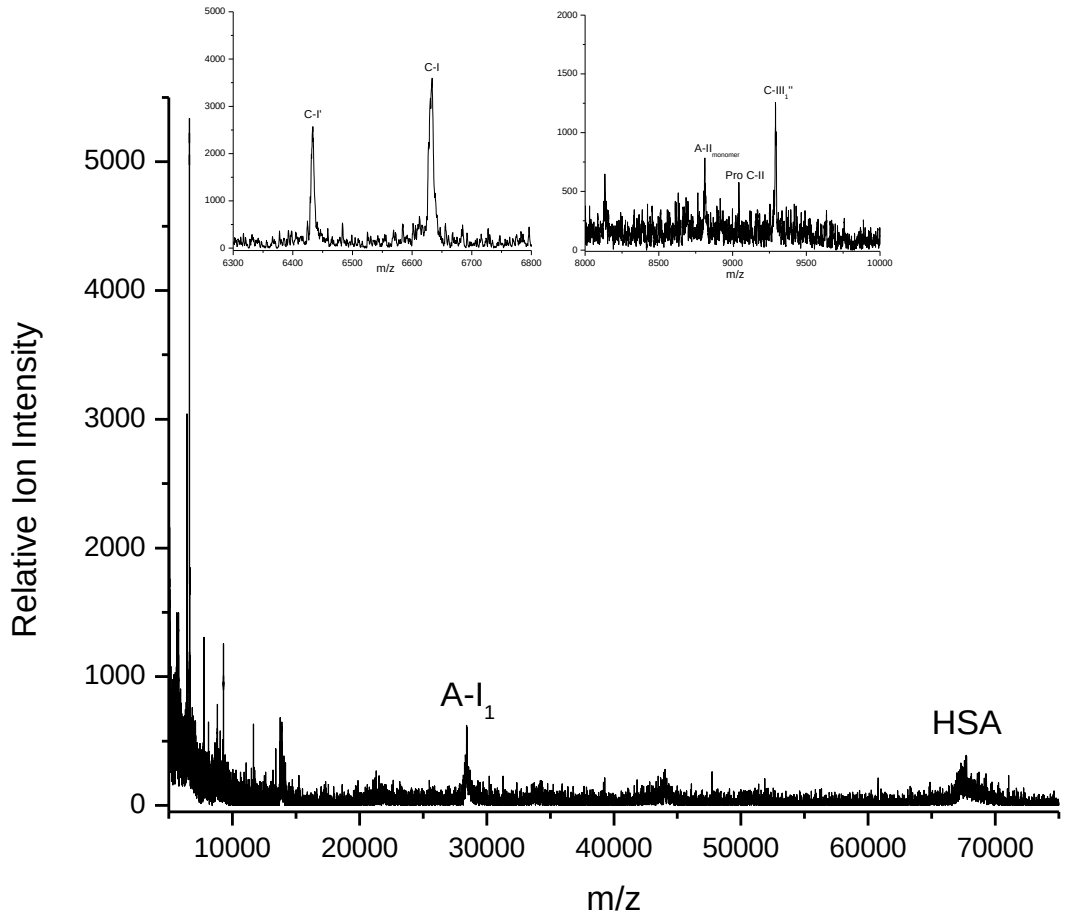

Figure 86. MALDI-MS HDL_3 spectra from control patient 16.

Table 63. Identification of apolipoproteins in the HDL_3 fraction from control patient 16.

Identification	Mass (Da)
ApoC-I'	6436.60
ApoC-I	6634.99

Table 63. (Continued)

Identification	Mass (Da)
ApoA-II_m	8809.01
Pro ApoC-II	9040.29
ApoC-III_1"	9292.71
ApoA-I_1	28421.80
HSA	67713.86

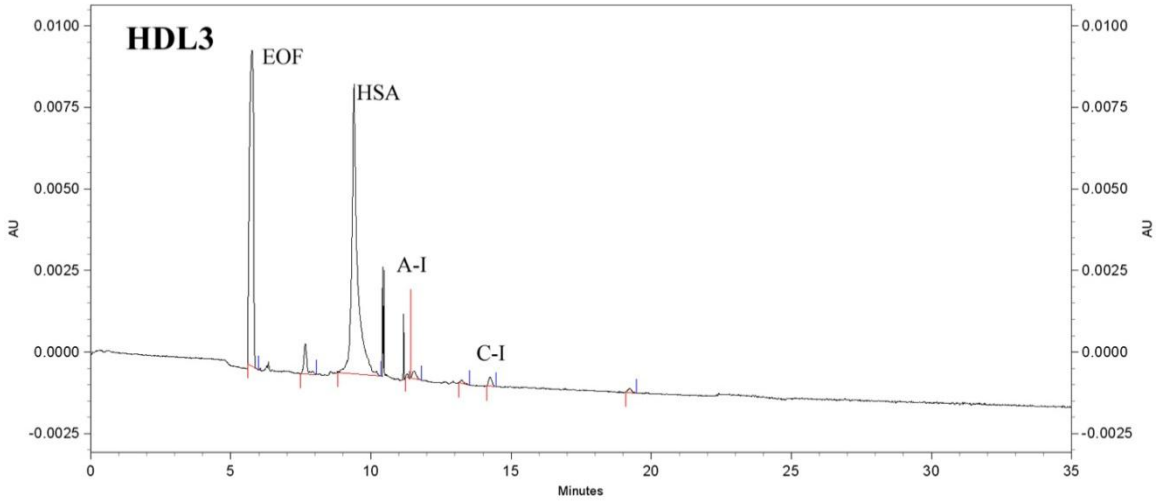

Figure 87. Electropherogram of the HDL_3 fraction from control patient 16.

Table 64. CE data for the HDL_3 fraction from a 200µL serum sample from control patient 16.

Protein	Elution Time (min)	Mobility (x $10^{-5}cm^2/Vs$)	CPA	Concentration (mg/dL)
HSA	9.7	-20.795	13916	14.01
ApoA-I	11.8	-26.269	101	0.28
ApoC-I	14.9	-31.578	180	0.43

Figure 86 shows the MALDI-MS spectra for the HDL_3 subfraction which contained apos C-I', C-I, A-$II_{monomer}$, Pro C-II, C-III_1, A-I_1, and HSA. Table 63 shows the peak masses for this fraction. The apoC-I peaks were sharp with apoC-I being only slightly higher in relative ion intensity than apoC-I'. Figure 87, shows the CE results which detected albumin, apoA-I and apoC-I.

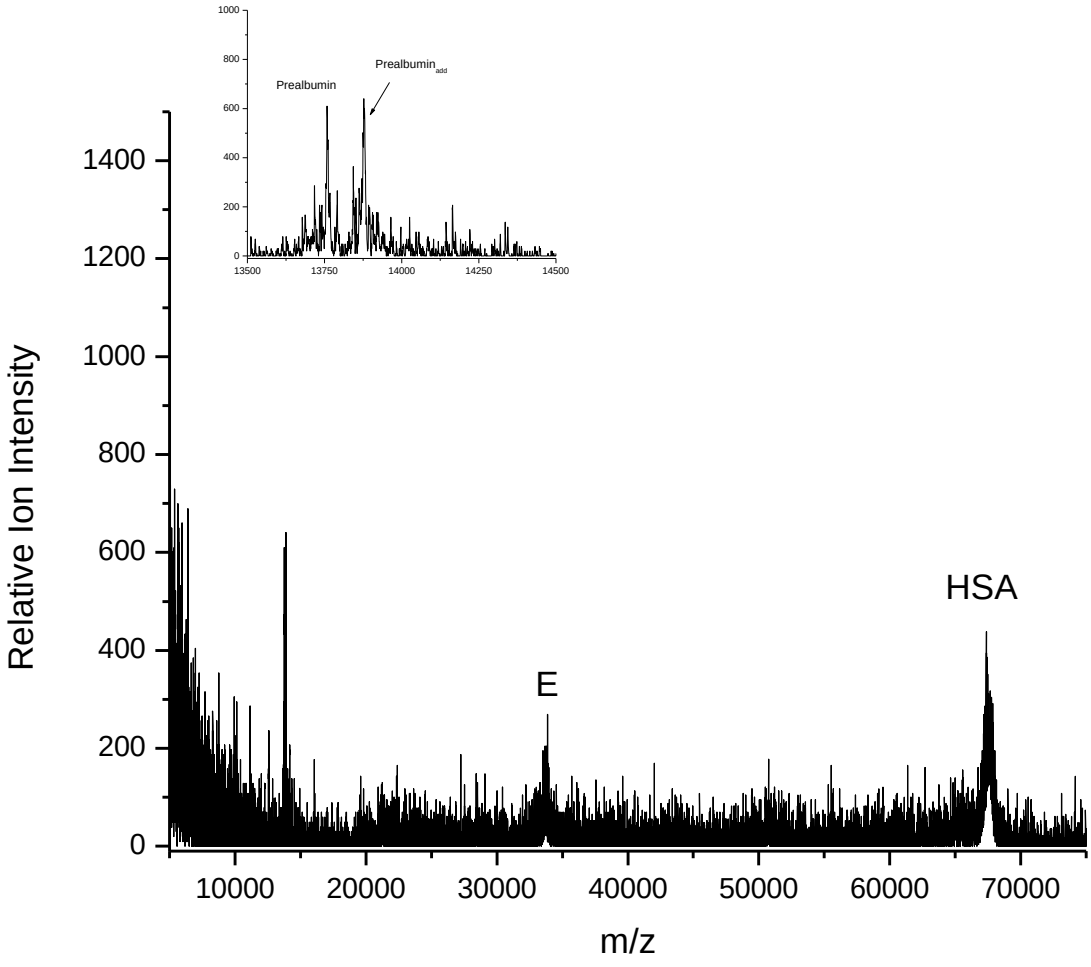

Figure 88. MALDI-MS protein spectra from control patient 16.

Table 65. Identification of apolipoproteins in the protein fraction from control patient 16.

Identification	Mass (Da)
Prealbumin	13788.75
$Prealbumin_{add}$	13843.35
ApoE	33869.45
HSA	67382.43

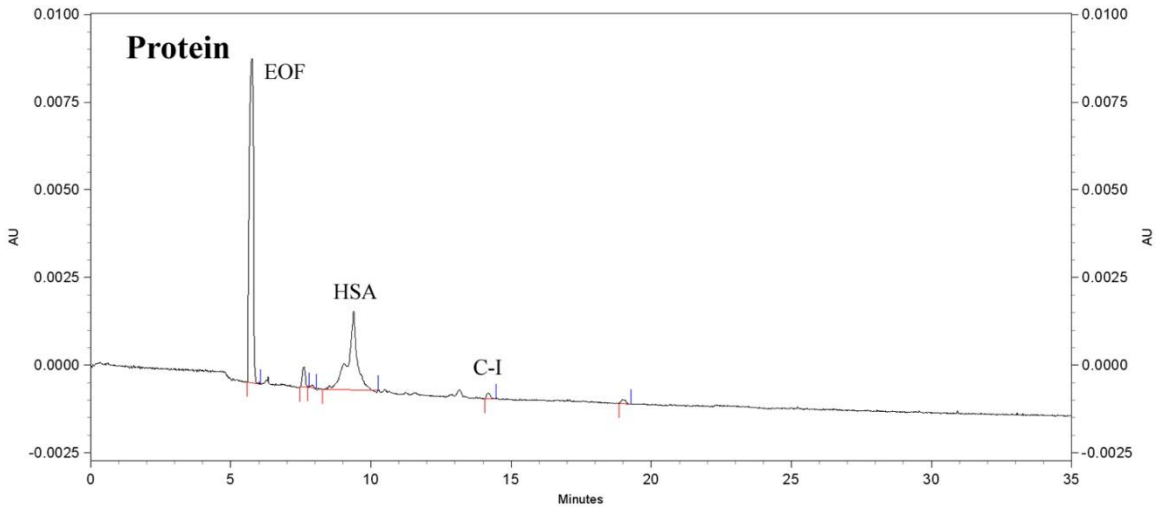

Figure 89. Electropherogram of the protein fraction from control patient 16.

Table 66. CE data for the protein fraction from a 200µL serum sample from control patient 16.

Protein	Elution Time (min)	Mobility (x $10^{-5}cm^2/Vs$)	CPA	Concentration (mg/dL)
HSA	9.4	-20.213	4552	4.58
ApoC-I	14.1	-30.898	87	0.21
Unidentified	19.0	-36.177	53	-------

Figure 88 shows the MALDI-MS spectra corresponding to the protein fraction which contained prealbumin, apoE, and HSA. Table 65 shows the peak masses for this fraction. The CE results shown in Figure 89, detected albumin and apoC-I. Albumin contained a shoulder, however, both the shoulder and overall peak was smaller than those previously observed in other control patient protein subfractions.

Table 67. Control patient 24 medical information

Control Patient 24	
Age	68 years old
Height	63 inches
Weight	176 lbs.
Gender	Female
Race	Caucasian
Major Risk Factors	Family history of CAD Hypertension

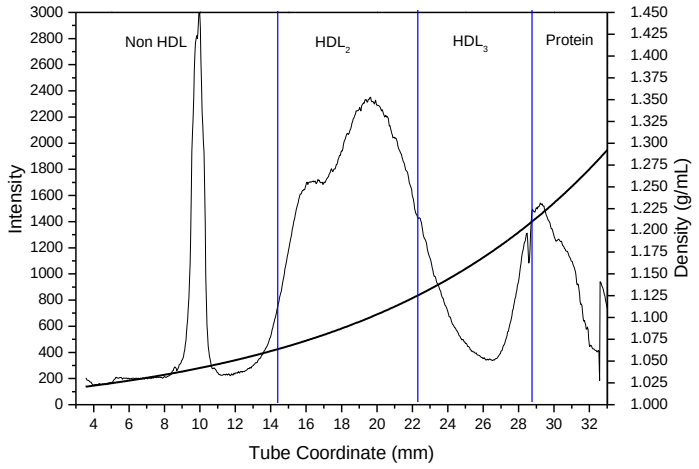

Figure 90. Lipoprotein density profile from control patient 24 in a 0.300M solution of Cs_2CdY, spun for 6 hours at 120,000RPM at 5°C after treatment with dextran sulfate.

Control Patient 24 Discussion

Control patient 24, whose medical history is presented in Table 67, is a 68 year old Caucasian female who does not have CAD, however, does have a family history of the disease and suffers from hypertension. Figure 90 shows the Cs_2CdY profile for this subject which contains a broad peak with a shoulder on its buoyant side.

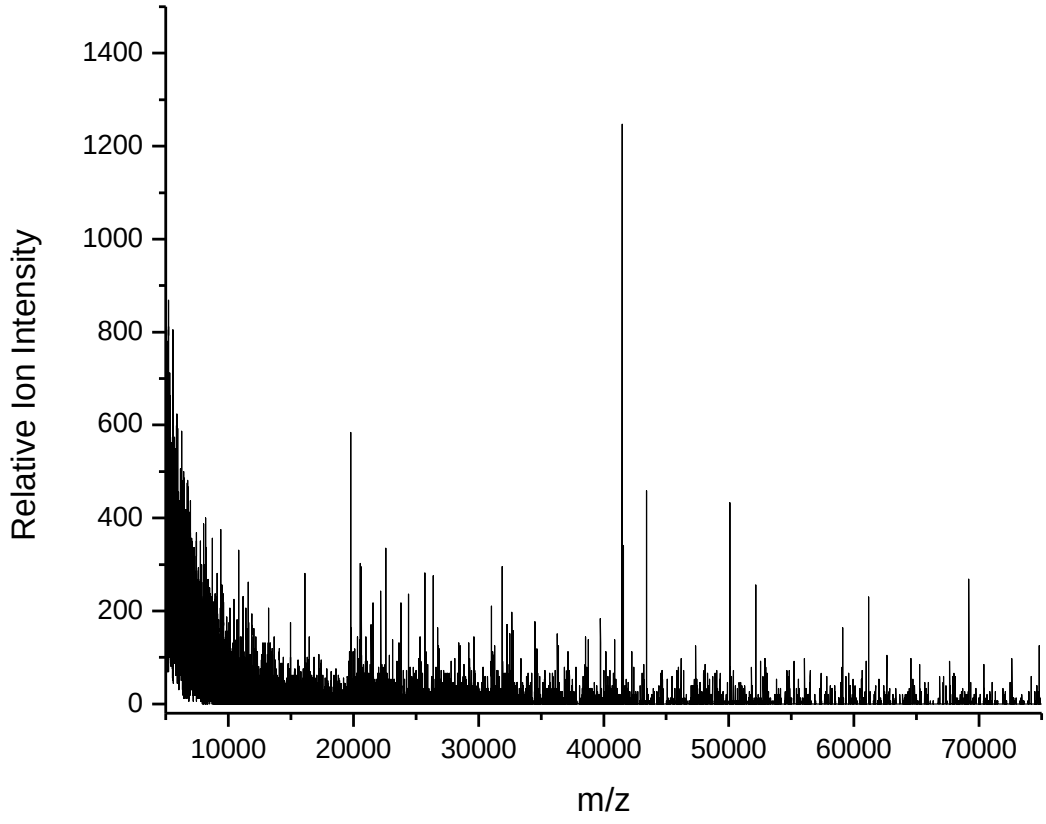

Figure 91. MALDI-MS non HDL spectra from control patient 24.

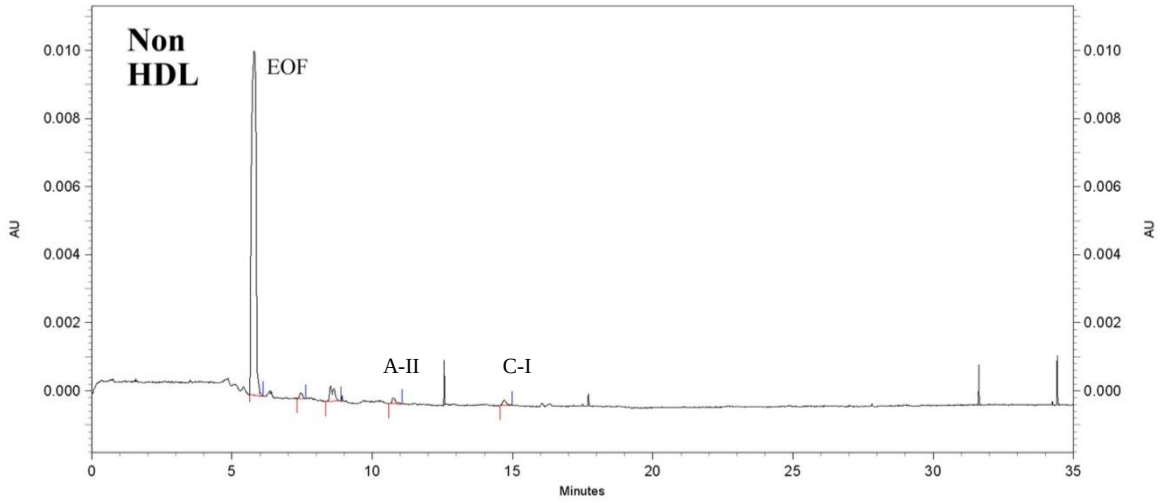

Figure 92. Electropherogram of the non HDL fraction from control patient 24.

Table 68. CE data for the non HDL fraction from a 200µL serum sample from control patient 24.

Protein	Elution Time (min)	Mobility (x $10^{-5}$$cm^2$/Vs)	CPA	Concentration (mg/dL)
ApoA-II	10.8	-23.933	118	-------
ApoC-I	14.7	-31.272	80	0.19

Figure 91 shows the MALDI-MS spectra for the serum subfractions for this patient. The non HDL subfraction did not contain any proteins as also observed in the non HDL fraction of patient 16. The CE results for this fraction contained barely visible peaks with mobilities matching apoA-II and apoC-I as shown in Figure 92.

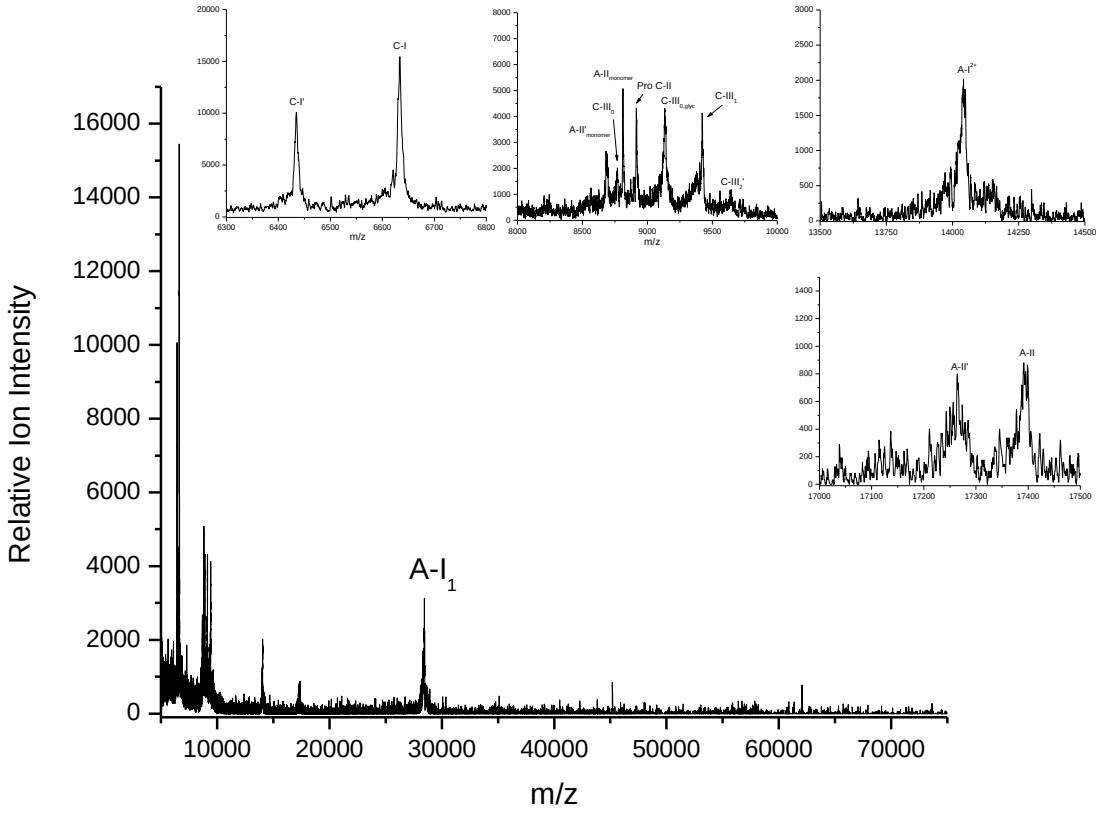

Figure 93. MALDI-MS HDL_2 spectra from control patient 24.

Table 69. Identification of apolipoproteins in the HDL_2 fraction from control patient 24.

Identification	**Mass (Da)**
ApoC-I'	6434.50
ApoC-I	6633.07
ApoA-II'$_m$	8681.69
ApoC-III$_0$	8771.05
ApoA-II$_m$	8811.94
Pro ApoC-II	8919.89
ApoC-III$_{0,glyc}$	9134.05
ApoC-III$_1$	9427.40
ApoC-III$_2$'	9646.34
ApoA-I^{2+}	14040.37
A-II'	17265.01
A-II	17396.11

Table 69. (Continued)

Identification	Mass (Da)
ApoA-I_1	28448.99

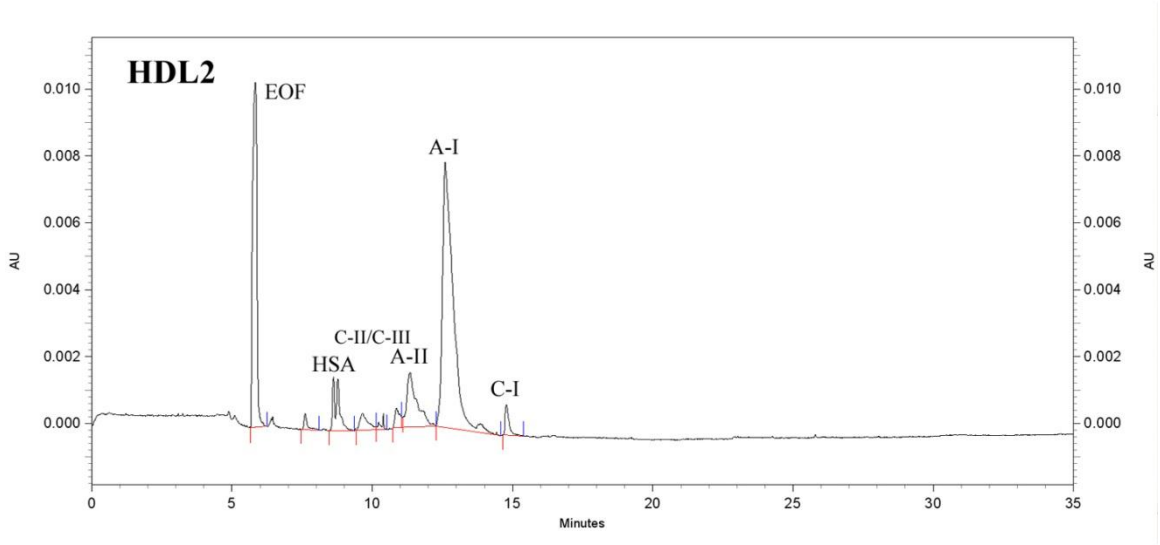

Figure 94. Electropherogram of the HDL_2 fraction from control patient 24.

Table 70. CE data for the HDL_2 fraction from a 200µL serum sample from control patient 24.

Protein	Elution Time (min)	Mobility (x $10^{-5}cm^2/Vs$)	CPA	Concentration (mg/dL)
HSA	9.7	-20.398	842	0.85
ApoC-II	10.4	-22.598	201	-------
ApoC-III	10.9	-23.848	536	-------
ApoA-II	11.4	-24.991	3044	-------
ApoA-I	12.6	-27.585	13967	38.75
ApoC-I	14.8	-31.041	495	1.17

The HDL_2 subfraction contained apos C-I', C-I, A-$II_{monomer}$, C-III_0, Pro C-II, C-$III_{0,glyc}$, C-III_1, C-III_2, A-I^{2+}, A-II, and A-I_1 as shown in Figure 93. Table 69 shows the peak masses for this fraction. The apoC-I peaks were highly resolved with what appeared to be a small shoulder on apoC-I. The doubly protonated apoA-I peak appeared as a single peak and apoA-II appeared as two poorly resolved peaks. The CE results for this fraction, shown in Figure 94, detected albumin, and apos C-II, C-III, A-II, A-I, and C-I. The predominant peak in this fraction was apoA-I. Both methods had comparable results.

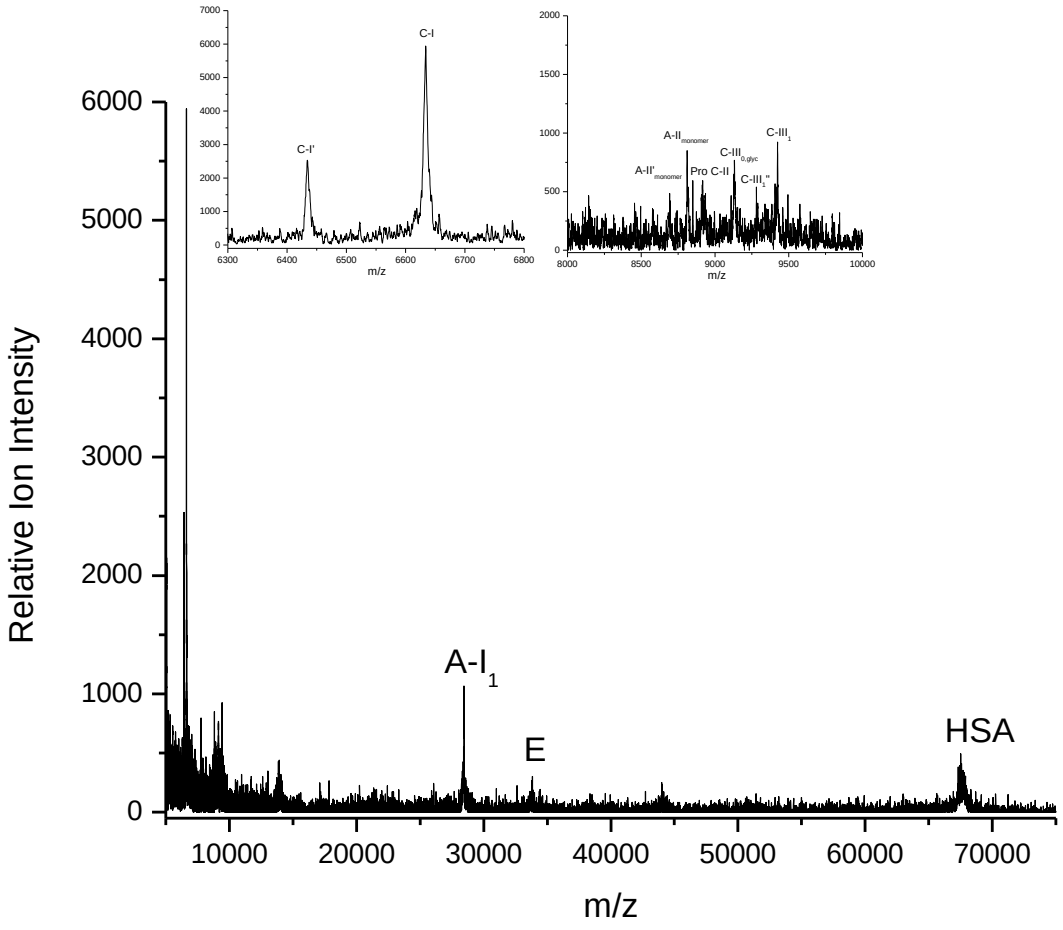

Figure 95. MALDI-MS HDL_3 spectra from control patient 24.

Table 71. Identification of apolipoproteins in the HDL_3 fraction from control patient 24.

Identification	Mass (Da)
ApoC-I'	6434.85
ApoC-I	6633.70
ApoA-II'_m	8696.86
ApoA-II_m	8812.47
Pro ApoC-II	8923.99
ApoC-$III_{0,glyc}$	9134.27
ApoC-III_1"	9279.01
ApoC-III_1	9431.49
ApoA-I_1	28455.00
ApoE	33845.75
HSA	67594.72

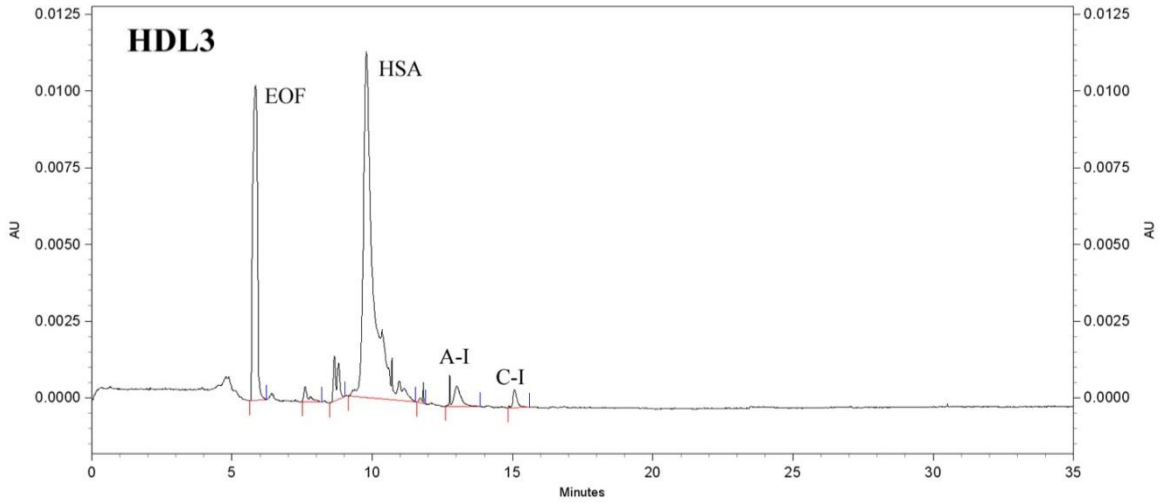

Figure 96. Electropherogram of the HDL_3 fraction from control patient 24.

Table 72. CE data for the HDL_3 fraction from a 200µL serum sample from control patient 24.

Protein	Elution Time (min)	Mobility (x $10^{-5}cm^2/Vs$)	CPA	Concentration (mg/dL)
HSA	9.8	-20.715	23356	23.52
ApoA-I	12.8	-27.797	841	2.33

Table 72. (Continued)

Protein	Elution Time (min)	Mobility (x $10^{-5}$$cm^2$/Vs)	CPA	Concentration (mg/dL)
ApoC-I	15.1	-31.338	332	0.78

The HDL_3 subfraction MALDI-MS spectra, shown in Figure 95, contained apos C-I', C-I, A-$II_{monomer}$, Pro C-II, C-$III_{0,glyc}$, C-III_1, A-I_1, E, and HSA. Table 71 shows the peak masses for this fraction. The apoC-I peak was approximately three times higher in relative ion intensity than apoC-I' and apoC-III peaks were low in relative ion intensity. The CE results shown in Figure 96, detected albumin, and apos A-I and C-I.

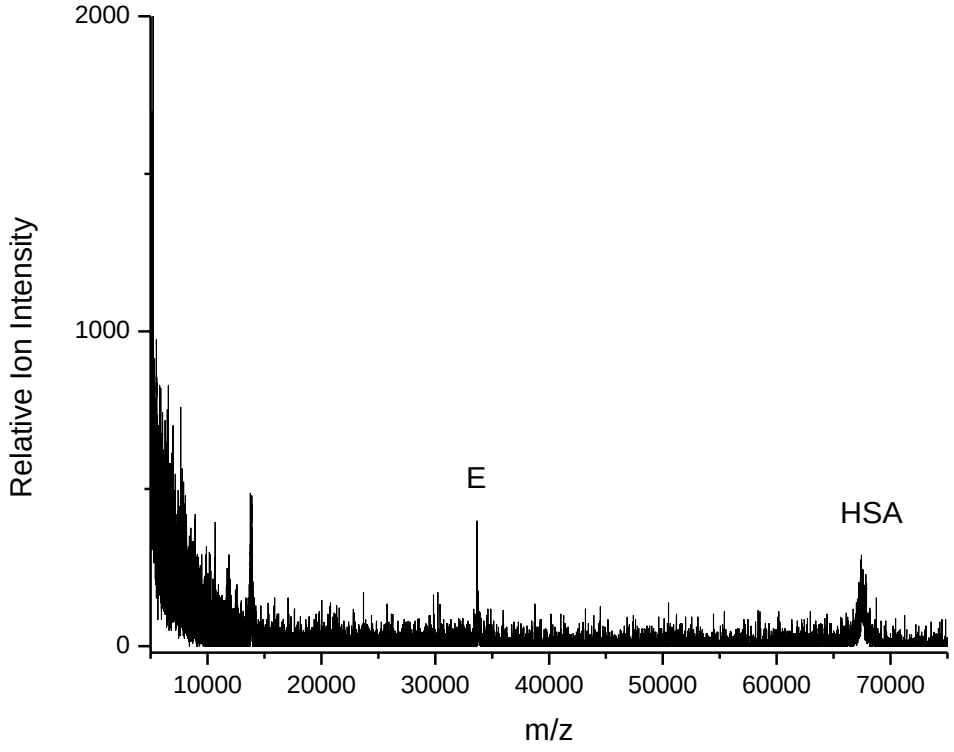

Figure 97. MALDI-MS protein spectra from control patient 24.

Table 73. Identification of apolipoproteins in the HDL_2 fraction from control patient 24.

Identification	Mass (Da)
ApoE	33685.00
HSA	67414.29

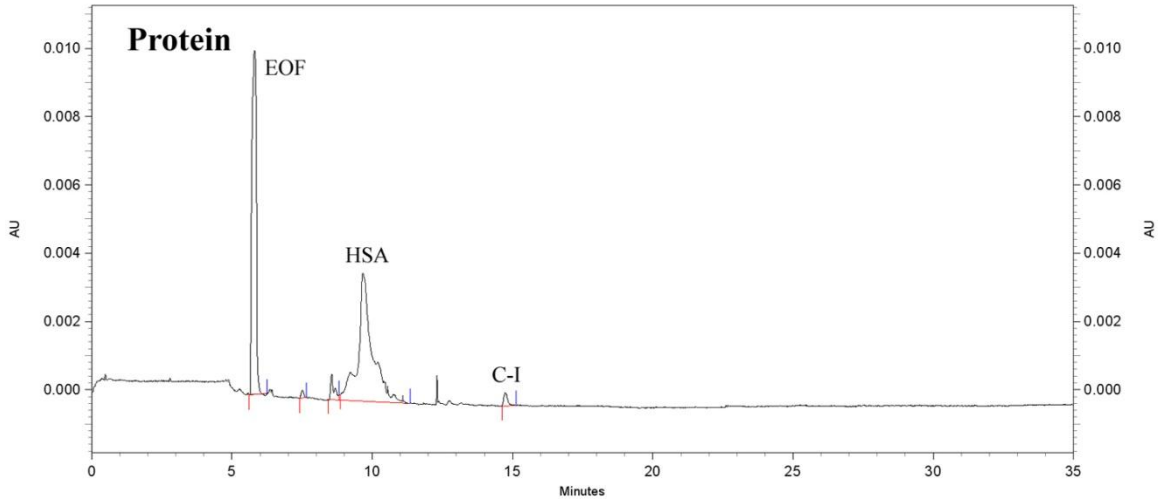

Figure 98. Electropherogram of the protein fraction from control patient 24.

Table 74. CE data for the protein fraction from a 200µL serum sample from control patient 24.

Protein	Elution Time (min)	Mobility (x $10^{-5}$$cm^2$/Vs)	CPA	Concentration (mg/dL)
HSA	9.7	-20.459	11307	11.39
ApoC-I	14.8	-31.000	208	0.49

Figure 97 shows the MALDI-MS spectrum corresponding to the protein subfraction which contained apo E and HSA at relatively low intensity. Table 73 shows the peak masses for this fraction. The CE results detected albumin and apoC-I as shown in Figure 98. The albumin peak contained a broad base in addition to shoulders.

Table 75. Control patient 25 medical information

Control Patient 25	
Age	50 years old
Height	71 inches
Weight	181 lbs.
Gender	Male
Race	African-American
Major Risk Factors	Hypertension

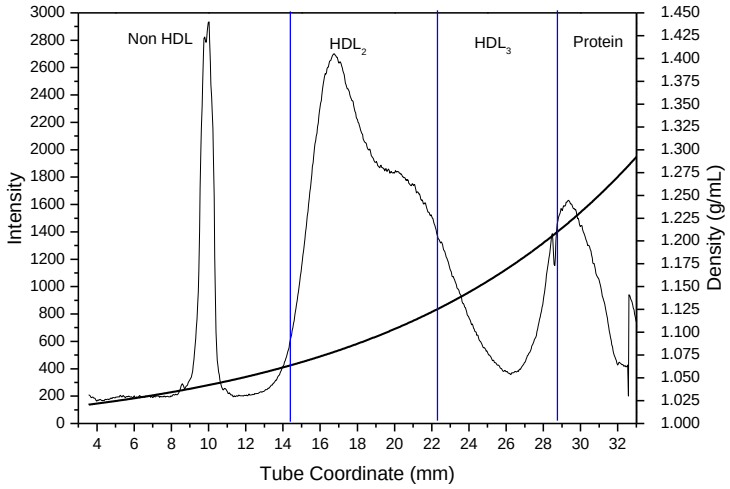

Figure 99. Lipoprotein density profile from control patient 25 in a 0.300M solution of Cs_2CdY, spun for 6 hours at 120,000RPM at 5°C after treatment with dextran sulfate.

Patient 25 Discussion

Control patient 25, whose medical history is presented in Table 75, is a 50 year old African-American male who does not have CAD, however, does have a family history of the disease and suffers from hypertension. Figure 99 shows the Cs_2CdY profile for this subject which contains a sharp peak with a shoulder on its denser side.

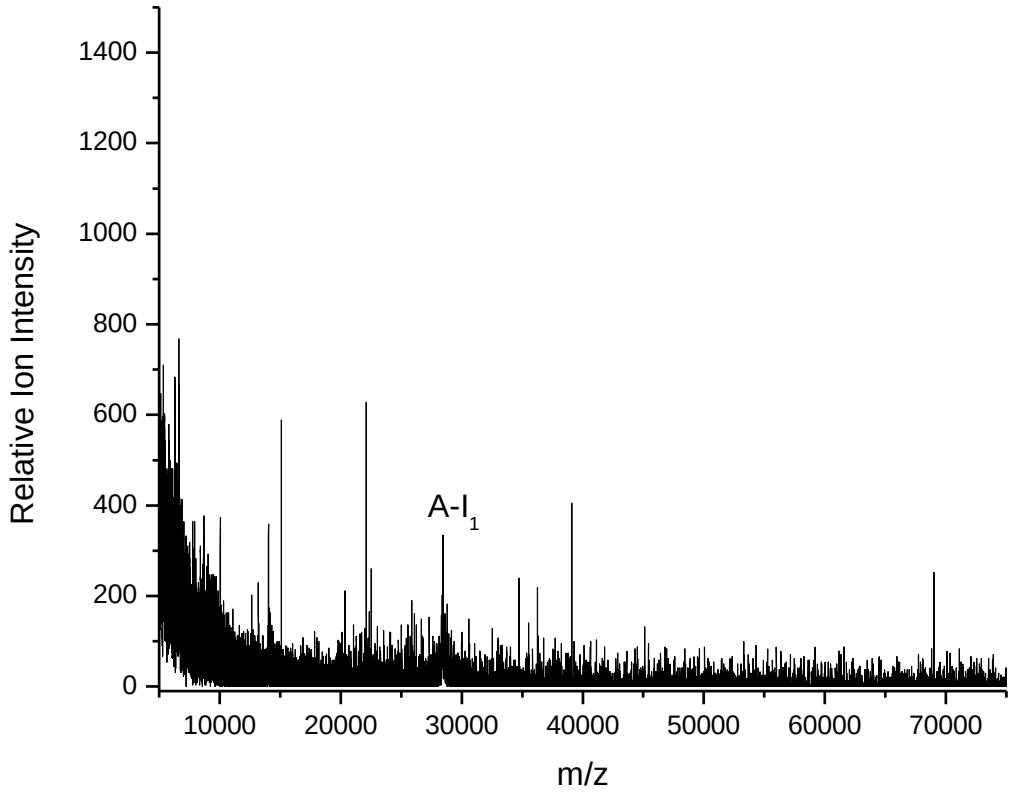

Figure 100. MALDI-MS non HDL spectra from control patient 25.

Table 76. Identification of apolipoproteins in the non HDL fraction from control patient 25.

Identification	Mass (Da)
ApoA-I_1	28450.76

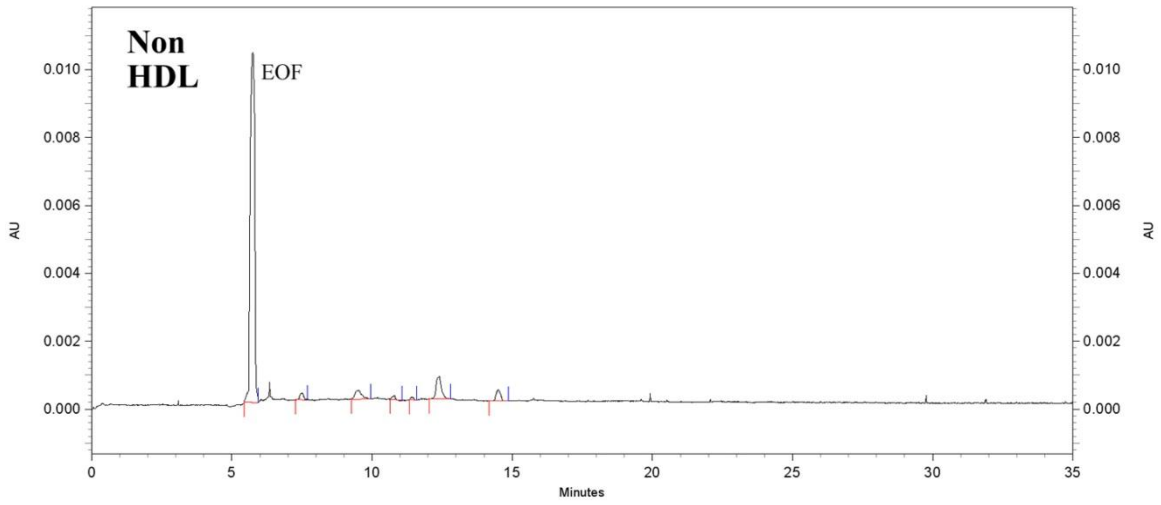

Figure 101. Electropherogram of the non HDL fraction from control patient 25

.

Table 77. CE data for the non HDL fraction from a 200µL serum sample from control patient 25.

Protein	Elution Time (min)	Mobility (x $10^{-5}$$cm^2$/Vs)	CPA
Unidentified	12.4	-15.678	578
Unidentified	14.5	-19.142	209

Figure 100 shows the MALDI spectrum for the non HDL fraction which contained a poorly resolved A-I_1 peak. Table 76 shows the peak mass for this fraction. Figure 101 shows the CE results for this fraction, low intensity unidentified peaks were detected with elution times similar to apoA-I and C-I though the mobilities did not match those of these two proteins.

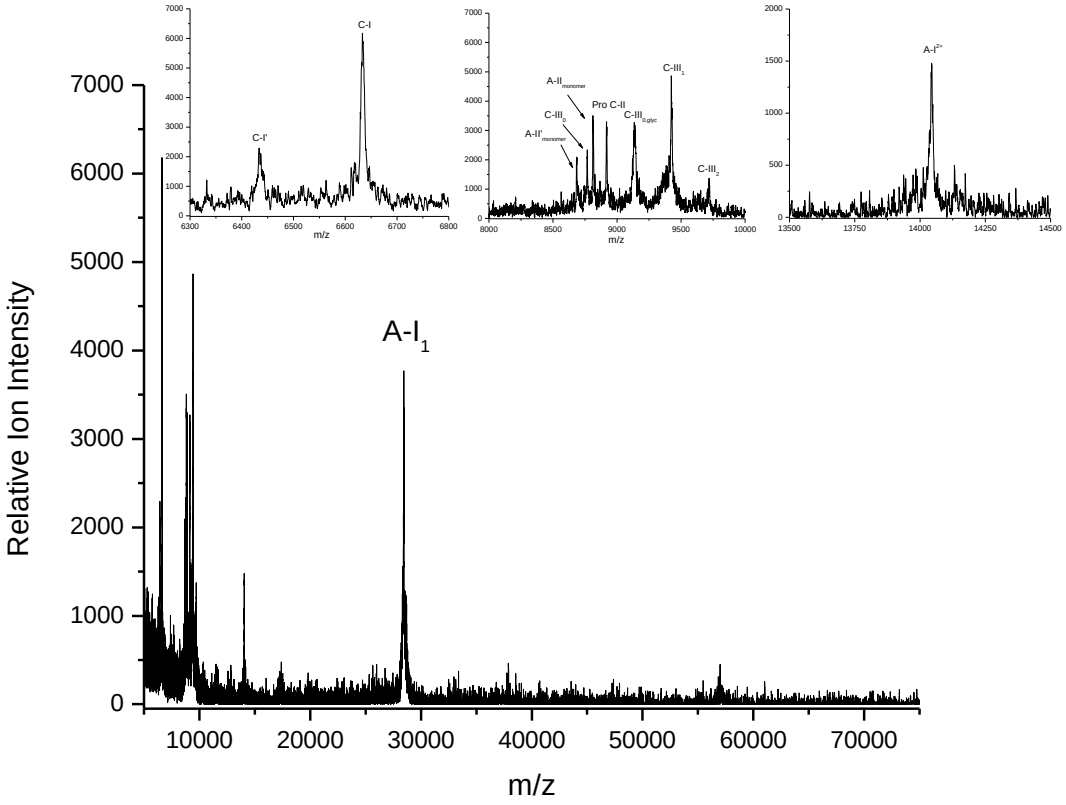

Figure 102. MALDI-MS HDL_2 spectra from control patient 25.

Table 78. Identification of apolipoproteins in the HDL_2 fraction from control patient 25.

Identification	Mass (Da)
ApoC-I'	6433.71
ApoC-I	6633.80
ApoA-II'$_m$	8688.67
ApoC-III$_0$	8767.23
ApoA-II$_m$	8813.17
Pro ApoC-II	8918.80
ApoC-III$_{0,glyc}$	9143.45
ApoC-III$_1$	9424.67
ApoC-III$_2$	9720.53
ApoA-I^{2+}	14044.78
ApoA-I$_1$	28457.12

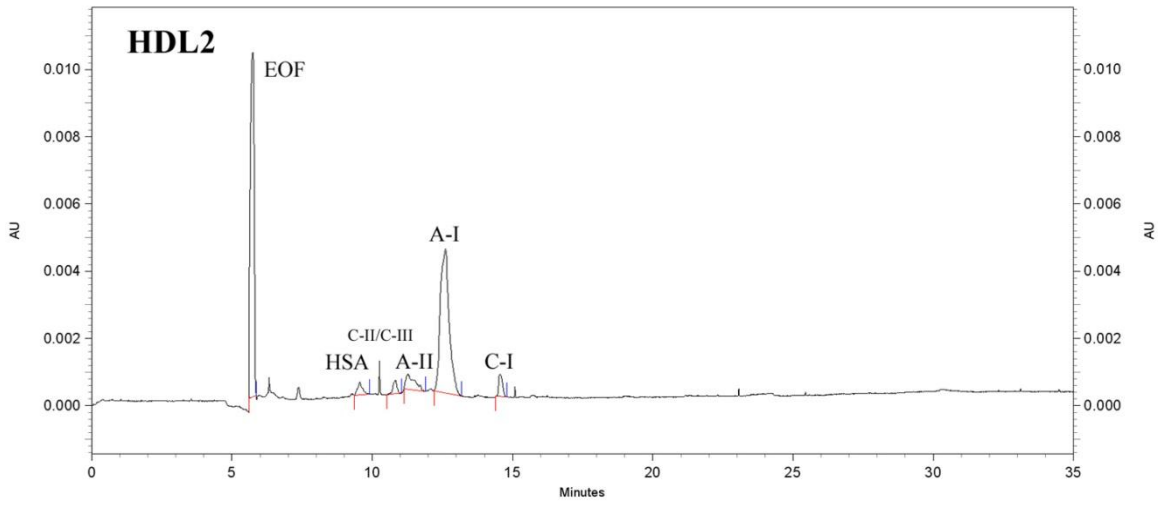

Figure 103. Electropherogram of the HDL_2 fraction from control patient 25.

Table 79. CE data for the HDL_2 fraction from a 200µL serum sample from control patient 25.

Protein	Elution Time (min)	Mobility (x $10^{-5}cm^2/Vs$)	CPA	Concentration (mg/dL)
HSA	9.6	-20.929	388	0.39
ApoC-III	10.8	-24.589	306	-------
ApoA-II	11.3	-25.643	734	--------
ApoA-I	12.6	-28.449	6206	17.22
ApoC-I	14.6	-31.575	365	0.80

Figure 102 shows the HDL_2 subfraction which contained apos C-I', C-I, A-$II_{monomer}$, C-III_0, Pro C-II, C-$III_{0,glyc}$, C-III_1, C-III_2, A-I^{2+}, and A-I_1. Table 78 shows the peak masses for this fraction. The apoC-I peaks were poorly resolved and C-I' was very low in relative ion intensity. One sharp peak corresponding to apoA-I^{2+} was detected and several peaks relating to apoC-III. The CE results are shown in Figure 103 for this

subfraction and contained albumin, and apos C-II, C-III, A-II, A-I, and C-I. The predominant peak was apoA-I. Both methods showed comparable results.

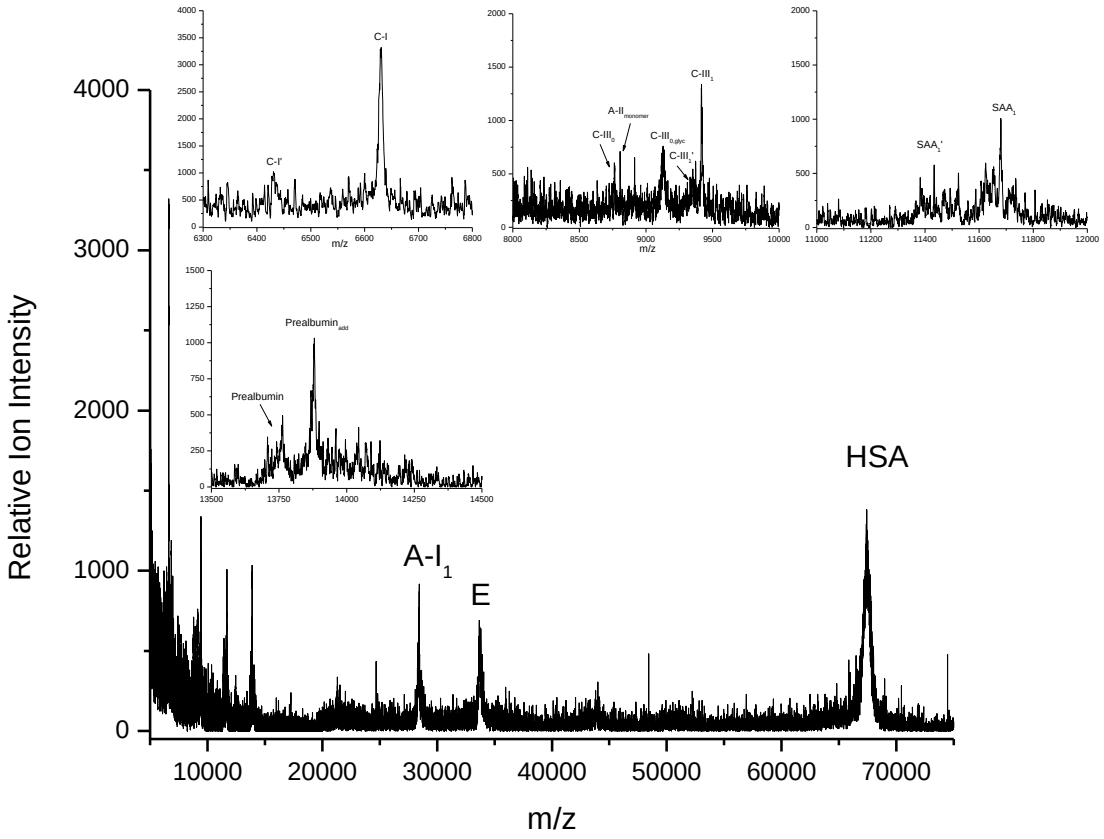

Figure 104. MALDI-MS HDL_3 spectra from control patient 25.

Table 80. Identification of apolipoproteins in the HDL_3 fraction from control patient 25.

Identification	Mass (Da)
ApoC-I'	6430.72
ApoC-I	6629.96
ApoC-III_0	8762.86
ApoA-II_m	8806.04
ApoC-$III_{0,glyc}$	9134.27
ApoC-III_1'	9361.40
ApoC-III_1	9416.74
SAA_1'	11433.75

Table 80. (Continued)

Identification	Mass (Da)
SAA_1	11679.68
Prealbumin	13761.72
$Prealbumin_{add}$	13881.43
$ApoA\text{-}I_1$	28430.86
ApoE	33654.23
HSA	67396.47

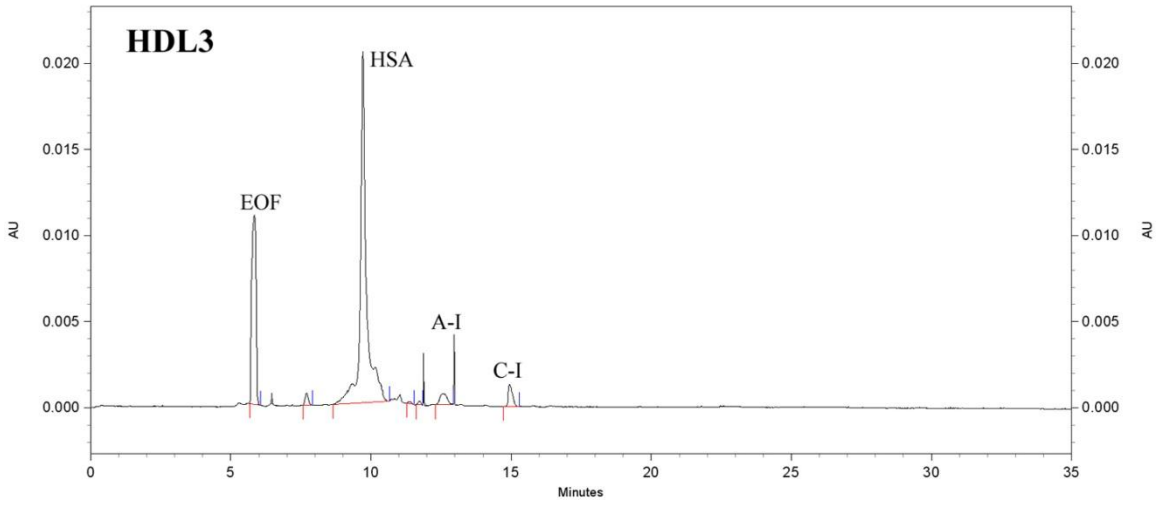

Figure 105. Electropherogram of the HDL_3 fraction from control patient 25.

Table 81. CE data for the HDL_3 fraction from a 200µL serum sample from control patient 25.

Protein	Elution Time (min)	Mobility (x $10^{-5}cm^2/Vs$)	CPA	Concentration (mg/dL)
HSA	9.7	-20.472	26225	26.41
ApoC-III	11.4	-24.960	74	-------
ApoA-II	11.7	-25.728	98	-------
ApoA-I	12.6	-27.410	746	2.07
ApoC-I	14.9	-31.146	725	1.71

The HDL_3 subfraction MALDI-MS spectra contained apos C-I', C-I, $C\text{-}III_0$, $A\text{-}II_{monomer}$, $C\text{-}III_{0,glyc}$, $C\text{-}III_1$, SAA_1, prealbumin, $A\text{-}I_1$, E, and HSA as shown in Figure 104. Table 80 shows the peak masses for this fraction. ApoC-I' was barely visible. The acute inflammatory response protein SAA_1 was also present in this fraction. The CE results for this fraction, shown in Figure 105 detected albumin, which was the predominant peak, as well as apos A-I and C-I.

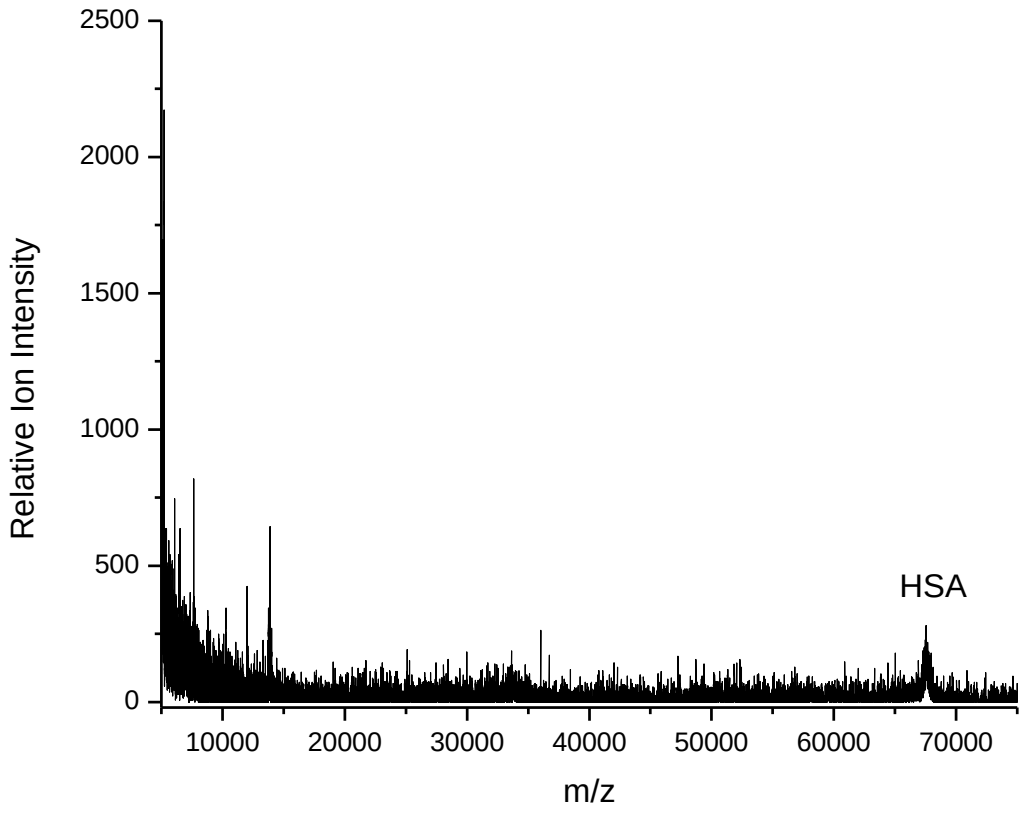

Figure 106. MALDI-MS protein spectra from control patient 25.

Table 82. Identification of apolipoproteins in the protein fraction from control patient 25.

Identification	Mass (Da)
HSA	67541.51

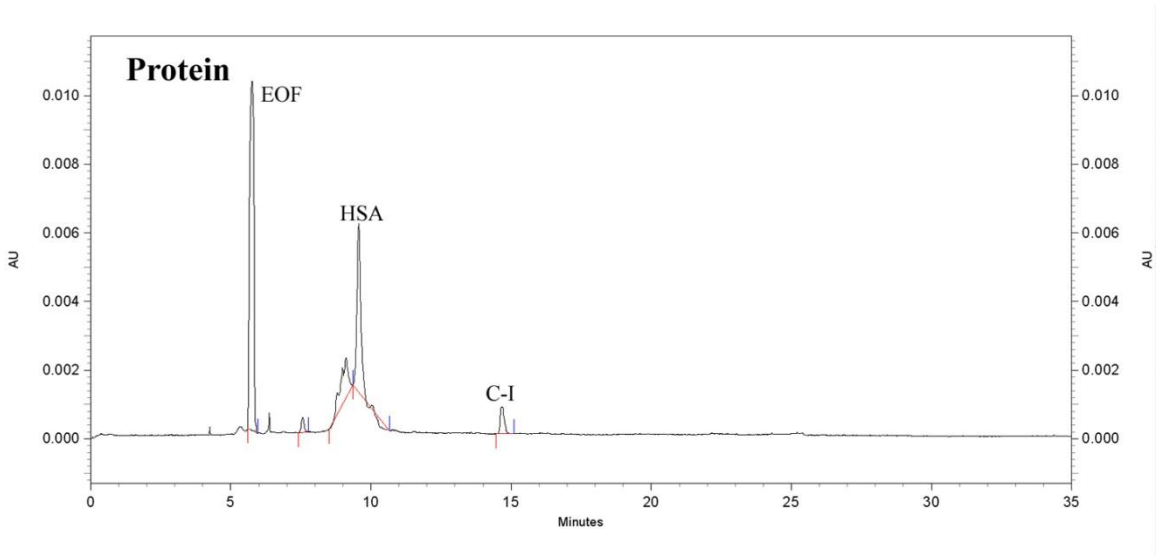

Figure 107. Electropherogram of the protein fraction from control patient 25.

Table 83. CE data for the protein fraction from a 200µL serum sample from control patient 25.

Protein	Elution Time (min)	Mobility (x $10^{-5}$$cm^2$/Vs)	CPA	Concentration (mg/dL)
HSA	9.6	-20.764	3846	3.87
ApoC-I	14.7	-31.584	448	1.06

The protein subfraction contained HSA only as shown in the MALDI-MS spectrum in Figure 106. Table 82 shows the peak masses for this fraction. The CE results, shown in Figure 107, detected albumin and apoC-I. Albumin contained a large shoulder.

Control Cohort MALDI-MS Overview Discussion

In analyzing the control cohort MALDI-MS spectra, the major apolipoprotein peaks seen in the non HDL fraction were apos: C-I', C-I, C-II, C-III, A-II, A-I^{2+}, A-I_1 and HSA. All patient non HDL fractions with the exception of patients 14 and 24 showed apolipoprotein peaks. In patients 3 and 7, apoC-I was very poorly resolved while patient 16 contained sharp apoC-I peaks. Most patients containing apoC-I peaks had a ratio of relative ion intensity that was approximately 1:2 for apoC-I' and apoC-I. The presence of these proteins in this fraction was due to minimal overlap from the HDL_2 region.

The HDL_2 subfractions from the control cohort showed an abundance of apolipoproteins. The major apolipoprotein peaks in the HDL_2 subfractions of the control samples were apos: C-I', C-I, C-II, C-III, A-II, SAA_4, amyloid, A-I^{2+}, A-I_1 and D. It was observed that none of the control patient HDL_2 samples contained human serum albumin. Across the cohort, the HDL_2 fractions contained the highest abundance of proteins and highest relative ion intensities, indicating protein enrichment in this fraction. Sharp apoC-I peaks were present in the HDL_2 spectra for all patients; though all C-I peaks were more intense than C-I' peaks, the ratio varied. Patient 7 however, had an apoC-I' peak that was substantially low in intensity. Patient 1 also displayed slight splitting of the C-I' peak which may suggest early signs of oxidative processes. The apoC-II/C-III region was highly populated in most patients with isoforms of apos C-II and C-III which possessed high mass accuracy. ApoA-II appeared in all patients with the exception of patients 14 and 25 and was poorly resolved with splitting. ApoA-I_1 intensity was overall consistent with slightly lower intensity in patients 3 and 24.

The HDL_3 subfractions from the control cohort showed major apolipoprotein peaks for: C-I', C-I, C-II, C-III, A-I_1, E, SAA_1, SAA_4, prealbumin, and human serum albumin. ApoC-I peaks had overall lower relative ion intensity and poorer resolution in this fraction. There was also greater variation in the intensity ratio between C-I' and C-I in this subfraction. Patients 3, 7, 13, and 25 had hardly visible C-I' peaks. The protein SAA_1 was also present in patients 1 and 25 which indicates an acute inflammatory

response. Human serum albumin was present in all patients which may be due to mixing between the protein and HDL_3 fractions as shown in re-ultracentrifugation studies.

The protein subfractions from the control cohort showed peaks corresponding to human serum albumin, prealbumin, SAA_1, and apoE primarily. None of the patients contained peaks corresponding to apoA-I in this fraction, which strongly demonstrated that there was minimal if any HDL contamination in this protein fraction. The HSA peak intensity was relatively high with apo E intensities ranging from 40% to 75% of HSA peak intensity. The acute inflammatory response protein SAA_1 was also observed in this fraction for patient 7 which was likely due to its dissociation from an HDL particle.

Control Cohort ApoA-I_1 MALDI-MS Discussion

The apoA-I peaks were observed in detail in the mass range spanning 27,000 – 30,000m/z where this protein was expected to be found. In the control cohort, upon closer inspection it was observed that the peak in this region was shifted. Due to this shift, this apolipoprotein peak was designated as apoA-I_1. Such mass shifting may be due to biological processes. To evaluate the differences between the known mass of apoA-I and the observed mass of $apoA_1$ in the control cohort, the mathematical differences between these values were calculated for the cohort. The mass accuracy of the apoA-I_1 peaks was determined by averaging the masses of each peak from the control cohort, and calculating the standard deviation at the 95% confidence level. The apoA-I_1 peaks for the total cohort had an average mass of 28440.96 ± 29.36Da, which indicated a shifted mass of approximately 362Da. The apoA-I_1 peaks for the non HDL fractions had an average mass of 28451.57 ± 116.17 Da, which was 373Da higher than the known mass of this protein. ApoA-I_1 peaks in the HDL_2 subfraction had an average mass of 28451.04 ± 4.92 Da with a mass difference of 372Da between this experimental value and the known mass value of the protein. Likewise, the HDL_3 subfraction had an average apoA-I_1 mass of 28422.92 ± 42.89, which corresponded to a difference of approximately 344Da.

Apolipoprotein A-I is composed of 243 amino acids and has a calculated molecular weight of 28,079 Da. ApoA-I post-translational modifications can have a large impact on its function and is a prominent factor that can lead to HDL dysfunction. Copper mediated oxidation of HDL results in altered HDL migration on an agarose gel, apoA-I proteolysis, and decreased ability of HDL to unload cholesteryl esters from cholesterol-loaded macrophages.[183] HDL from diabetic subjects has evidence of glycated apoA-I, this glycated apoA-I has altered structure and lipid binding activity.[184] Myeloperoxidase (MPO) is an enzyme that uses hydrogen peroxide to generate chlorinating and nitrating oxidants. These reactive species can also modify host proteins and lipids. Myeloperoxidase is enriched in human atheroma and its presence may promote lesion progression, by increasing LDL oxidation, and block plaque regression by modifications of apoA-I/HDL that impair reverse cholesterol transport.[185] ApoA-I has also been shown to exhibit increased molecular weight when modified by carbonyls. Intact protein analysis by MALDI demonstrated a steadily increased molecular weight of apoA-I after exposure to malondialdehyde (MDA) of approximately 350 Da. This result indicates that MDA covalently modifies apoA-I and progressively increases the proteins molecular weight.[165]

Overall, the apoA-I peaks were not as resolved as other spectral peaks such as apoC-I and showed the appearance of multiple adducts and truncations. In the control cohort, it is highly probable that the post-translational modification resulting in this adduct, if atherogenic, are prevented from causing atherogenic effects due to other HDL atheroprotective functions and proteins. Additionally, the sample preparation and purification techniques could account for the addition of mass of this protein as it was seen consistently in all samples from this cohort.

Control Cohort CE Analysis Discussion

In the control cohort, A-I was most abundant in the HDL_2 subfraction, apoC-I was most abundant in the HDL_3 subfraction and human serum albumin was most abundant in the HDL_3 subfractions. The ratio of apoA-I to apoC-I was observed to be

higher in the HDL_2 subfraction and similarly, this subfraction had a larger quantity of serum proteins. It is worth noting that the CPA values obtained by CE were relatively low compared to the known concentrations of these apolipoproteins in human serum. This decrease in calculated concentrations from these fractions may be attributed to sample loss from primary and secondary methods of analysis, sample preparation, and purification techniques including dextran sulfate precipitation, ultracentrifugation, fraction excision, solid phase extraction, and evaporation.

In reference to the electrophoretic mobilities, the apoA-I mobility was highest in the non HDL and HDL_3 subfractions and lower in the HDL_2 subfractions, though all average mobilities were higher than that observed from the commercial apoA-I standard. The apoC-I mobility was more constant and highest in the protein fraction while lowest in the HDL_2 fraction, though all values were quite comparable to that observed from the commercial apoC-I standard. The human serum albumin mobility was also fairly constant and was highest in the non HDL fraction and lowest in the HDL_2 fraction though all values were also comparable to that observed from the commercial bovine serum albumin standard. Throughout the cohort, mobility values were consistently lower in the HDL_2 fraction. This abundance of proteins in this fraction may have attributed to the rate at which each protein migrated through the capillary. The average electrophoretic mobility values for each fraction are shown in Table 84 for the control cohort.

Table 84. Average electrophoretic mobilities for the non HDL, HDL_2, HDL_3, and protein fractions from 200µL serum samples from the control cohort.

Serum Fraction	Average ApoA-I Mobility (x $10^{-5}cm^2/Vs$)	Average ApoC-I Mobility (x $10^{-5}cm^2/Vs$)	Average HSA Mobility (x $10^{-5}cm^2/Vs$)
Non HDL	-27.469 ± 1.163	-31.244 ± 0.278	-20.721 ± 0.491
HDL_2	-26.824 ± 1.175	-31.085 ± 0.409	-20.373 ± 0.404
HDL_3	-27.258 ± 1.192	-31.359 ± 0.337	-20.551 ± 0.279
Protein	----------	-31.377 ± 0.498	-20.571 ± 0.406
Overall Average	-27.271 ± 1.254	-31.267 ± 0.389	-20.533 ± 0.366

In the control cohort, the non HDL fraction contained homogeneous electropherograms. For this subfraction, there were very small peaks with mobilities corresponding to albumin, apoA-I, and apoC-I in most patients. These results correlated well with MALDI-MS results from this subfraction. In the HDL_2 subfraction, there were peaks corresponding to apoA-II, apoC-II, apoC-III, apoA-I, apoC-I and albumin. Patient 7 did not show peaks corresponding to apoC-II and apoC-III in this fraction. Patient 13 contained a sharp apoA-I peak, and patient 14 contained an apoA-I peak with a shoulder. Patient 24 showed an apoA-II peak containing a shoulder as well as a split human serum albumin peak. ApoA-I was the predominant peak in this fraction and these results correlated well with MALDI-MS results. Although CE detected albumin in these subfractions, MALDI-MS did not detect this protein. It is probable that albumin identified by CE was actually another serum protein with a comparable electrophoretic mobility. In the HDL_3 subfraction, across the cohort, there was an enrichment of albumin which was seen in the large albumin peaks in this fraction, which mostly contained very broad bases. Patients 24 and 25 contained albumin peaks with shoulders. Patient 13 contained many unidentified peaks eluting before and after the albumin peak which may have been contaminants or serum proteins. Patient 14 contained a very sharp apoA-I peak and also contained many small unidentified peaks eluting before the apoA-I peak. The results from this fraction correlated well with MALDI-MS which also showed the albumin enrichment. In the protein fraction, it was observed that none of the patients contained apoA-I. This fraction was also enriched with human serum albumin, which appeared as a doublet. ApoC-I was consistently observed in this fraction, though MALDI-MS did not detect apoC-I in most spectra, apoE was consistently observed. It is possible that apoE has a mobility that is comparable to apoC-I, which may have resulted in its misidentification by CE.

In several patients, a small peak was observed eluting after apoC-I. This peak's mobility and elution time indicated that it was smaller and more highly charged than apoC-I. It was hypothesized that this small peak corresponded to the truncated form of apoC-I, apoC-I′.

CAD Cohort Analysis

Table 85. CAD patient 10 medical information

CAD Patient 10	
Age	75 years old
Height	65 inches
Weight	163 lbs.
Gender	Female
Race	Caucasian
Family History of Premature CAD/CAD/PVD	First Degree – Yes Second Degree - No
Major Risk Factors	Family history of CAD
Prior or Current History Of:	Angina, MI, Angioplasty or Stent
Current Medications	Statin, Estrogen, Beta Blocker, Thiazide
Highest LDL	130-160mg/dL
Highest TG	> 200mg/dL
Any Prior HDL <35	No
Any Prior Homocysteine >14	No

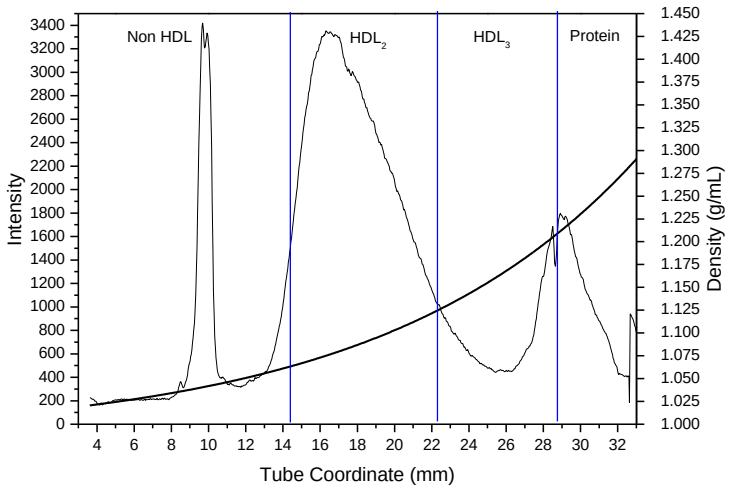

Figure 108. Lipoprotein density profile using a 200µL serum sample from CAD patient 10 in a 0.300M solution of Cs_2CdY, spun for 6 hours at 120,000rpm at 5°C after treatment with dextran sulfate.

CAD Patient 10 Discussion

CAD patient 10 whose medical history is presented in Table 85, is a 75 year old Caucasian female who has been diagnosed with CAD, and has a family history of premature first degree CAD. Patient 10 has prior and/or current history of angina, myocardial infarction, angioplasty and/or stent, and is currently prescribed and taking a statin, beta blocker, thiazide, and estrogen therapy. Their highest LDL level was 130 – 160 mg/dL and their highest triglyceride level was greater than 200 mg/dL. There are no prior levels of HDL below 35 mg/dL or homocysteine above 14 mg/dL. Figure 108 shows the Cs_2CdY profile for this subject which contains a sharp peak overlapping into the non HDL fraction.

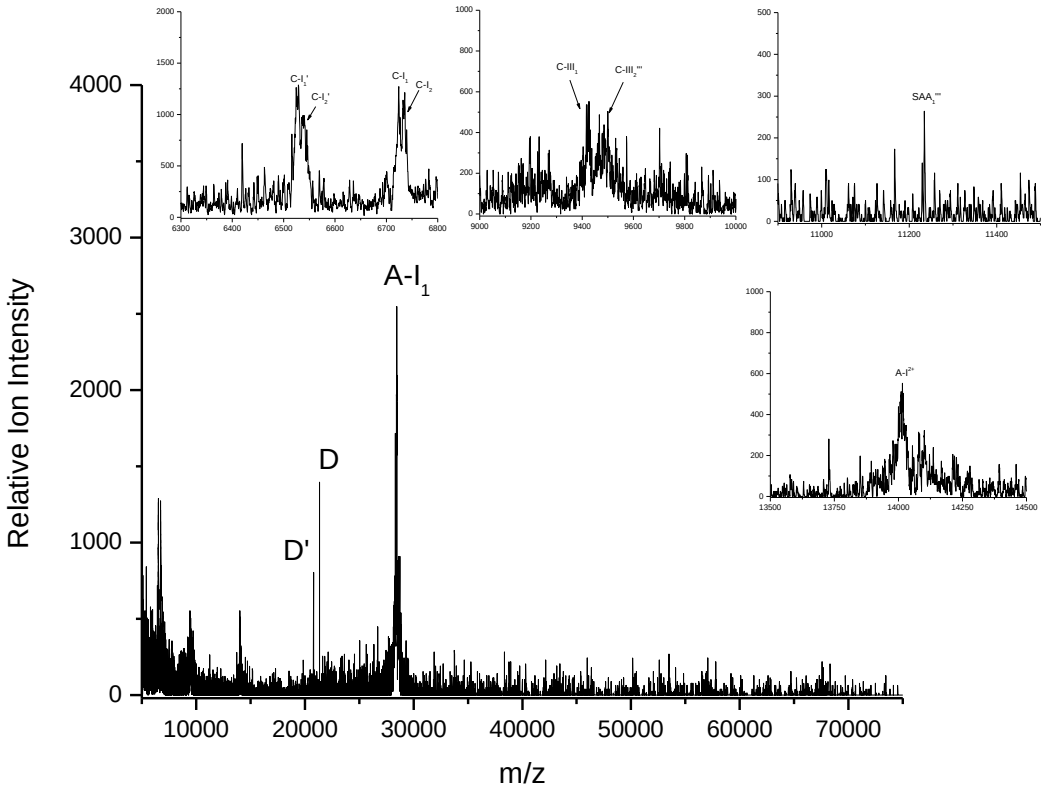

Figure 109. MALDI-MS non HDL spectra from CAD Patient 10

Table 86. Identification of apolipoproteins in the non HDL fraction from CAD patient 10.

Identification	Mass (Da)
ApoC-I_1'	6528.95
ApoC-I_2'	6538.05
ApoC-I_1	6724.13
ApoC-I_2	6734.91
ApoC-III_1	9427.02
ApoC-III_2'''	9467.59
SAA_1'''	11234.79
ApoA-I^{2+}	14016.95
ApoD'	20778.80
ApoD	21343.17
ApoA-I_1	28447.30

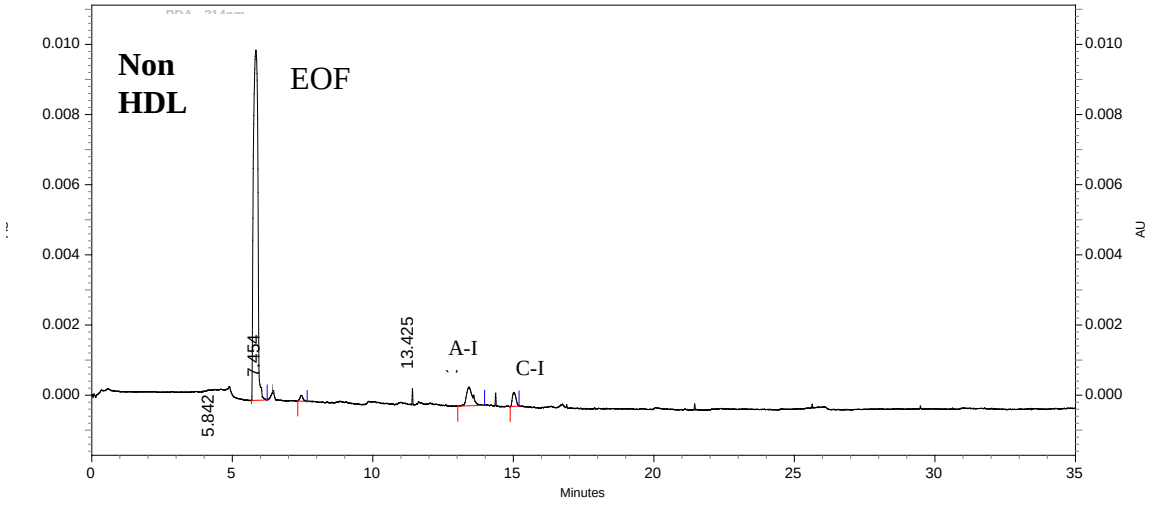

Figure 110. Electropherogram of the non HDL fraction from CAD patient 10.

Table 87. CE data for the non HDL fraction from a 200µL serum sample from CAD patient 10.

Protein	Elution Time (min)	Mobility (x $10^{-5}cm^2/Vs$)	CPA	Concentration (mg/dL)
ApoA-I	13.4	-28.936	509	1.41
ApoC-I	15.0	-31.273	198	0.47

Figure 109 shows the MALDI-MS spectra for the non HDL subfraction which contained apos C-I_1', C-I_2' C-I_1, C-I_2, C-III_1, C-III_2, SAA_1, D', D, and A-I_1. Table 86 shows the peak masses for this fraction. ApoC-I peaks, were observed in this fraction at relatively equal intensities and at a higher mass than the known value of these proteins and as a result, were designated C-I_1' and C-I_1. In addition to the mass shift, apoC-I peaks also showed splitting, these additional peaks were designated C-I_2' and C-I_2. The acute inflammatory response marker SAA_1 was observed as well as two peaks which corresponded to the mass of apoD, one of which was a truncated form of this protein. Lastly, a high relative ion intensity peak corresponding to apoA-I_1 was observed. The CE results for this fraction are shown in Figure 110. Very small peaks corresponding to apos A-I and C-I were detected in this subfraction. In comparison to the MALDI-MS results, apos A-I and C-I were detected by both methods, however the human serum albumin detected by CE was not observed in the MALDI spectrum.

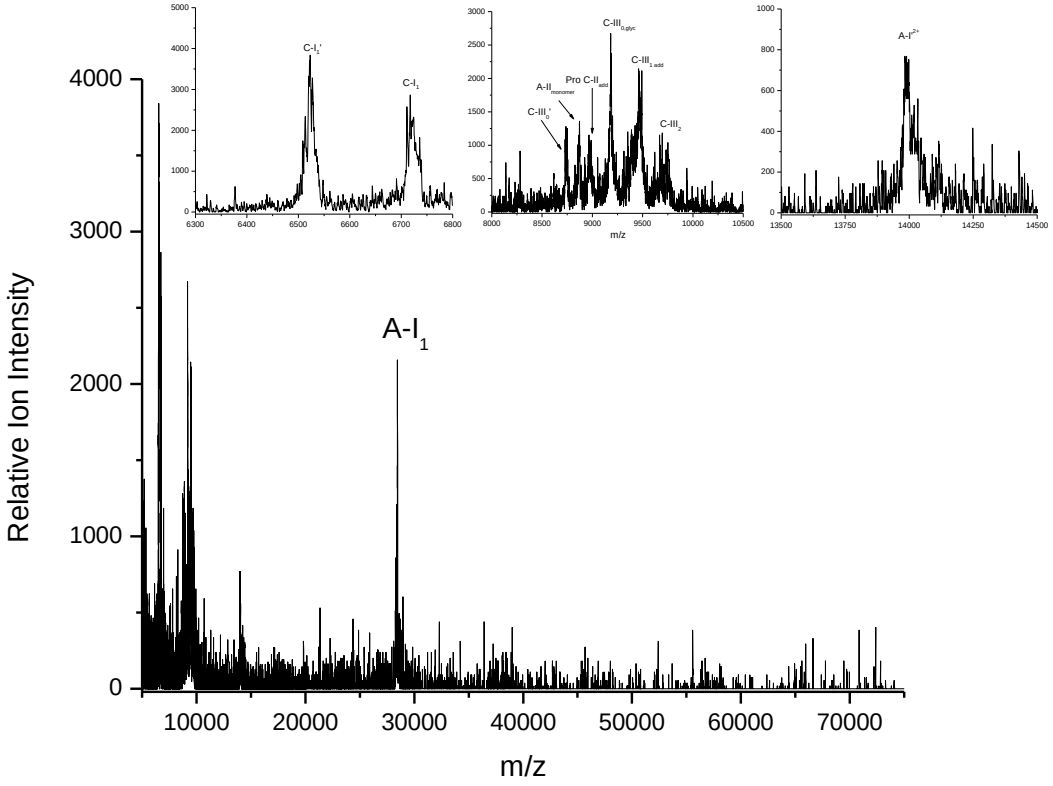

Figure 111. MALDI-MS HDL_2 spectra from CAD Patient 10

Table 88. Identification of apolipoproteins in the HDL_2 fraction from CAD patient 10.

Identification	**Mass (Da)**
ApoC-I_1'	6522.06
ApoC-I_1	6717.45
ApoC-III_0'	8737.59
ApoA-II_m	8817.07
Apo Pro C-II_{add}	8974.18
ApoC-$III_{0,glyc\ add}$	9181.99
ApoC-$III_{1\ add}$	9459.69
ApoC-III_2	9694.74
ApoA-I'^{2+}	13990.89
ApoA-I_1	28459.01

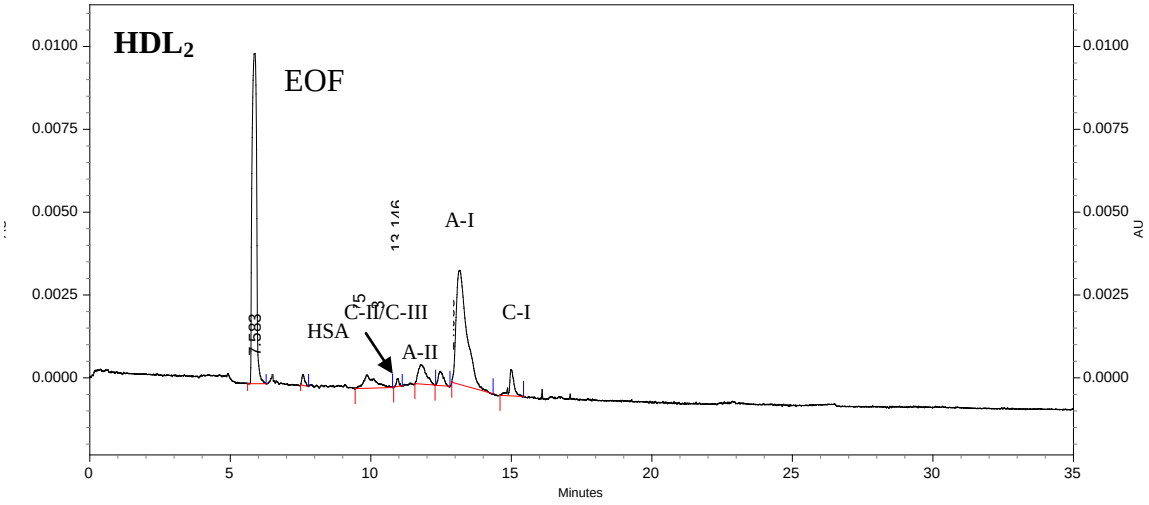

Figure 112. Electropherogram of the HDL_2 fraction from CAD patient 10.

Table 89. CE data for the HDL_2 fraction from a 200µL serum sample from CAD patient 10.

Protein	Elution Time (min)	Mobility (x $10^{-5}cm^2/Vs$)	CPA	Concentration (mg/dL)
HSA	9.8	-20.771	986	0.99
ApoC-II	10.9	-23.738	113	-------
ApoC-III	11.8	-25.658	841	-------
ApoA-II	12.5	-27.047	372	-------
ApoA-I	13.2	-28.282	5706	15.83
ApoC-I	15.0	-31.045	514	1.21

The HDL_2 subfraction contained apos C-I_1', C-I_1, C-III_0, A-$II_{monomer}$, Pro C-II, C-$III_{0,glyc}$, C-III_1, C-III_2, A-I^{2+}, and A-I as shown in the MALDI-MS spectra shown in Figure 111. Table 88 shows the peak masses for this fraction. The shapes of the apoC-I peaks were not as sharp as those seen in the control patient samples. It appeared that the two major apoC-I peaks contained shoulders as well. This HDL_2 subfraction also contained several peaks in the 8000 – 10000 *m/z* region as seen in the HDL_2 subfractions

from control patients. There was no human serum albumin detected in this fraction as also observed in the control cohort HDL_2 subfractions. The CE results from this subfraction, shown in Figure 112, detected albumin, and apos C-II, C-III, A-II, A-I, and C-I. All CE peaks were also detected by MALDI-MS with the exception of albumin.

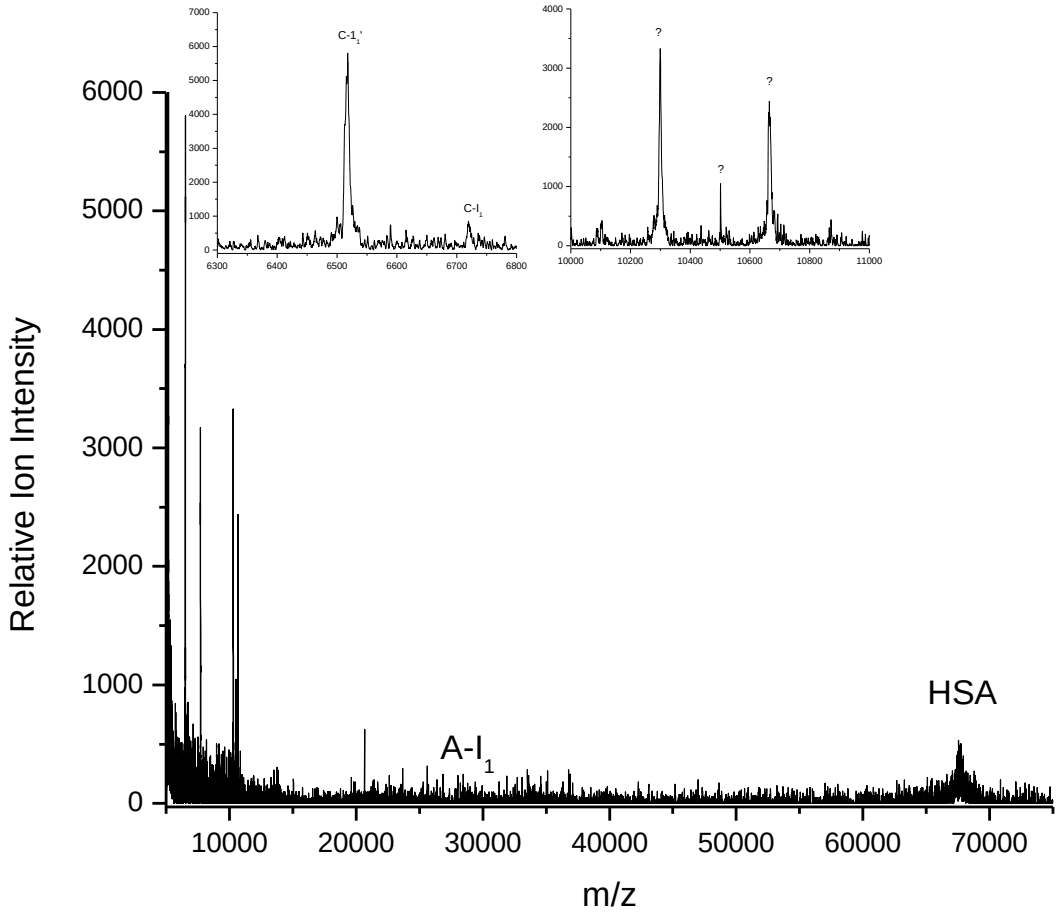

Figure 113. MALDI-MS HDL_3 spectra from CAD Patient 10

Table 90. Identification of apolipoproteins in the HDL_3 fraction from CAD patient 10.

Identification	Mass (Da)
ApoC-I_1'	6516.49
ApoC-I_1	6720.36
Unidentified Peak 1	10299.49

Table 90. (Continued)

Identification	Mass (Da)
Unidentified Peak 2	10501.76
Unidentified Peak 3	10665.79
ApoA-I_1	28513.88
HSA	67550.63

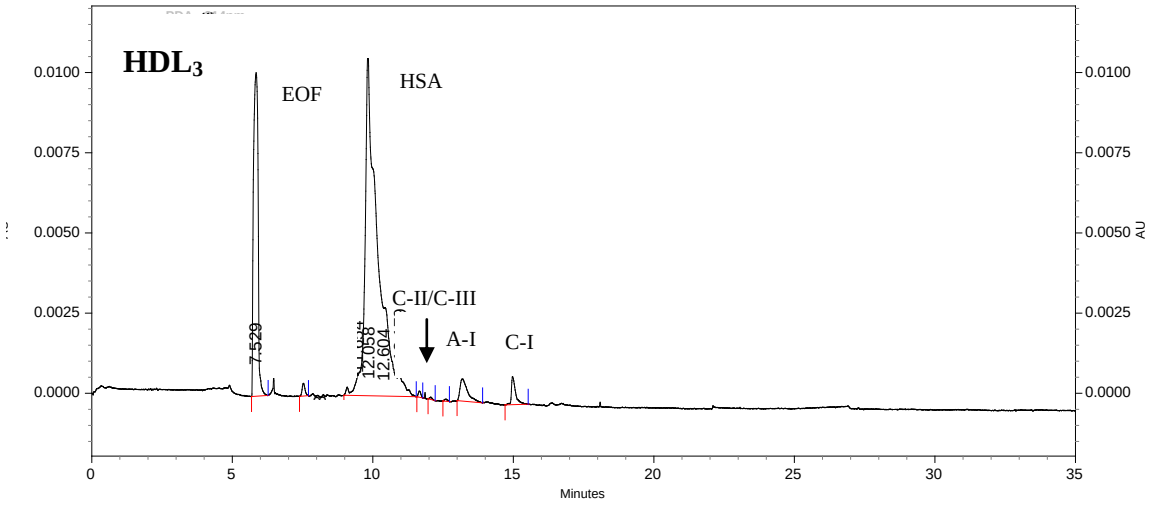

Figure 114. Electropherogram of the HDL_3 fraction from CAD patient 10.

Table 91. CE data for the HDL_3 fraction from a 200µL serum sample from CAD patient 10.

Protein	Elution Time (min)	Mobility (x $10^{-5}cm^2/Vs$)	CPA	Concentration (mg/dL)
HSA	9.8	-20.821	28140	28.33
ApoC-II	11.7	-25.539	85	-------
ApoC-III	12.1	-26.391	30	-------
ApoA-II	12.6	-27.455	32	-------
ApoA-I	13.2	-28.478	816	2.26
ApoC-I	15.0	-31.160	503	1.19

Figure 113 shows the MALDI-MS spectra for the HDL_3 subfraction which contained apos C-I_1', C-I_1, A-I_1, and HSA in addition to several unidentified proteins.

Table 90 shows the peak masses for this fraction. There was an aberration from the normal appearance of apoC-I in this sample in that there was only one high intensity peak with a subsequent low intensity peak corresponding to apoC-I_1, instead of two high intensity peaks corresponding to the truncated and full form of the protein. Another interesting finding in this sample was the observation of several unidentified peaks in the 10kDa mass range. It is hypothesized that these unidentified peaks correspond to an inflammatory marker such as a modified form of serum amyloid a. It is also highly probable that these unidentified proteins are related to CAD since they were not detected in the control cohort. There was a peak corresponding to HSA in this fraction as also observed in the control cohort HDL_3 fractions. The CE results for this subfraction are shown in Figure 114. The CE analysis detected albumin, and apos C-II, C-III, A-II, A-I, and C-I.

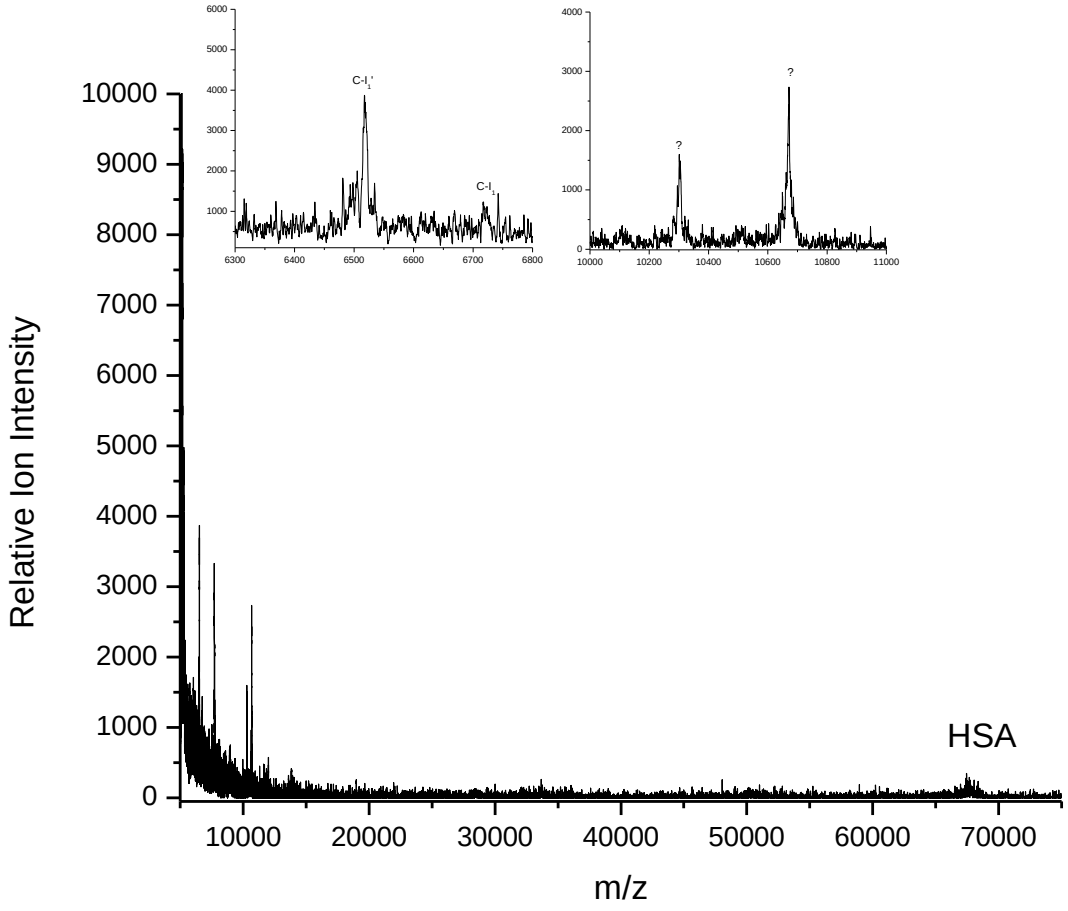

Figure 115. MALDI-MS protein spectra from CAD Patient 10.

Table 92. Identification of apolipoproteins in the protein fraction from CAD patient 10.

Identification	**Mass (Da)**
ApoC-I_1'	6518.61
ApoC-I_1	6719.89
Unidentified Peak 1	10305.46
Unidentified Peak 2	10670.82
HSA	67459.81

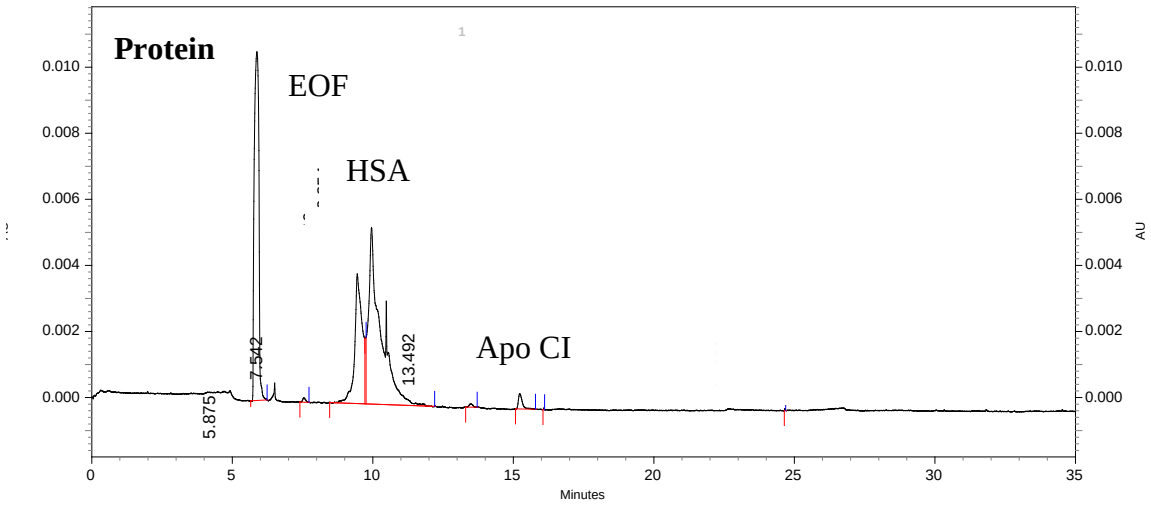

Figure 116. Electropherogram of the protein fraction from CAD patient 10.

Table 93. CE data for the protein fraction from a 200µL serum sample from CAD patient 10.

Protein	Elution Time (min)	Mobility (x $10^{-5}$$cm^2$/Vs)	CPA	Concentration (mg/dL)
HSA	9.9	-20.922	13734	13.83
ApoA-I	13.5	-28.730	54	0.15
ApoC-I	15.2	-31.226	246	0.58

The protein subfraction contained apos C-I_1', C-I_1, HSA and two unidentified peaks as shown in the MALDI-MS spectra in Figure 115. Table 92 shows the peak masses for this fraction. ApoC-I peaks were poorly resolved with C-I_1' having substantial splitting and C-I_1 being hardly visible. The CE results are shown in Figure 116 and contained a poorly resolved albumin peak and a peak corresponding to apoC-I. In comparison to the MALDI-MS results for the protein fraction both methods identified apoC-I and albumin in this fraction.

Table 94. CAD patient 41 medical information

CAD Patient 41	
Age	72 years old
Height	66 inches
Weight	163 lbs.
Gender	Female
Race	Caucasian
Family History of Premature CAD/CAD/PVD	First Degree – Yes Second Degree – Yes
Major Risk Factors	Family history of CAD Hypertension
Prior or Current History Of:	Angina, MI, Angioplasty or Stent, CABG, Tobacco use
Current Medications	Statin, Beta Blocker
Highest LDL	>160mg/dL
Highest TG	150 – 200mg/dL
Any Prior HDL <35	No
Any Prior Homocysteine >14	Yes

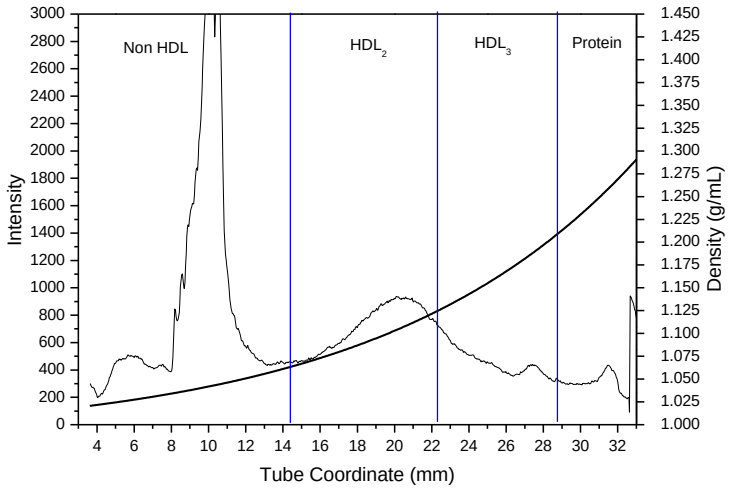

Figure 117. Lipoprotein density profile from CAD patient 41 in a 0.300M solution of Cs_2CdY, spun for 6 hours at 120,000RPM at 5°C after treatment with dextran sulfate.

CAD Patient 41 Discussion

CAD patient 41 whose medical history is presented in Table 94, is a 72 year old Caucasian female who has been diagnosed with CAD, has a family history of premature first and second degree CAD, and suffers from hypertension. Patient 41 has prior and/or current history of angina, myocardial infarction, angioplasty and/or stent, coronary artery bypass graft (CABG) surgery and tobacco use. Patient 41 is currently prescribed and taking a statin and beta blocker. Their highest LDL was above 160 mg/dL and their highest triglyceride level was between 150 - 200 mg/dL. There are no prior levels of HDL below 35 mg/dL however there are prior homocysteine levels above 14 mg/dL. Figure 117 shows the Cs_2CdY profile for this subject which contains a low intensity peak in the HDL_2 region.

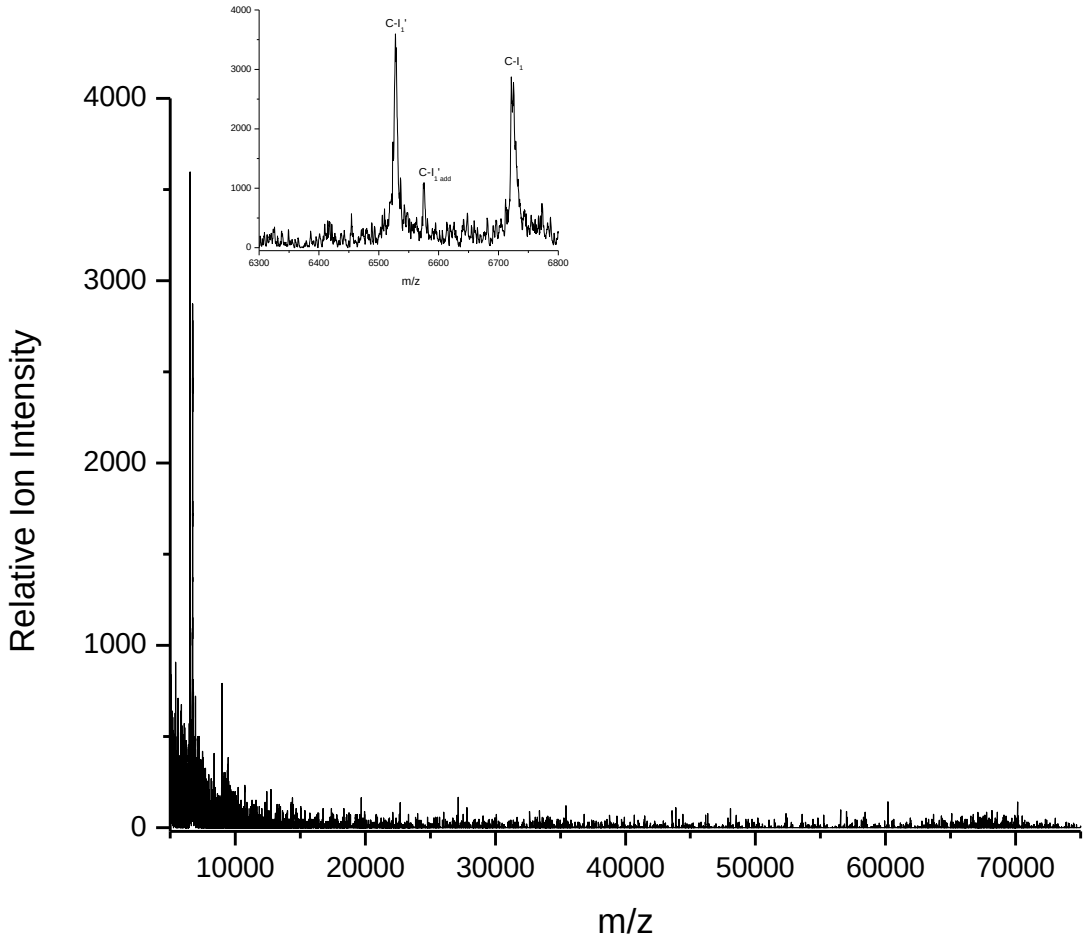

Figure 118. MALDI-MS non HDL spectra from CAD patient 41**.**

Table 95. Identification of apolipoproteins in the non HDL fraction from CAD patient 41.

Identification	**Mass (Da)**
ApoC-I_1'	6528.28
ApoC-$I_1'_{add}$	6576.29
ApoC-I_1	6721.97

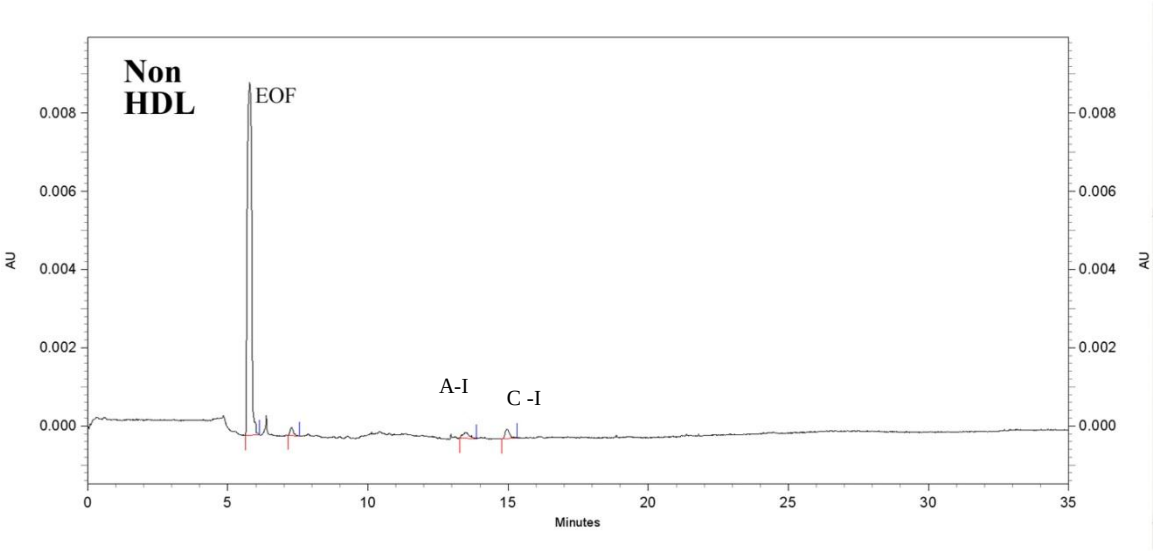

Figure 119. Electropherogram of the non HDL fraction from CAD patient 41**.**

Table 96. CE data for the non HDL fraction from a 200µL serum sample from CAD patient 41.

Protein	Elution Time (min)	Mobility (x $10^{-5}$$cm^2$/Vs)	CPA	Concentration (mg/dL)
ApoA-I	13.5	-29.582	156	0.43
ApoC-I	15.0	-31.792	147	0.35

Figure 118 shows the MALDI-MS spectra for the non HDL subfraction which only contained apoC-I peaks. Table 95 shows the peak masses for this fraction. The truncated form of the protein had a higher relative ion intensity than the full protein and also contained a small adduct peak. The CE analysis results are shown in Figure 119 and contain barely visible peaks corresponding to apos A-I and C-I.

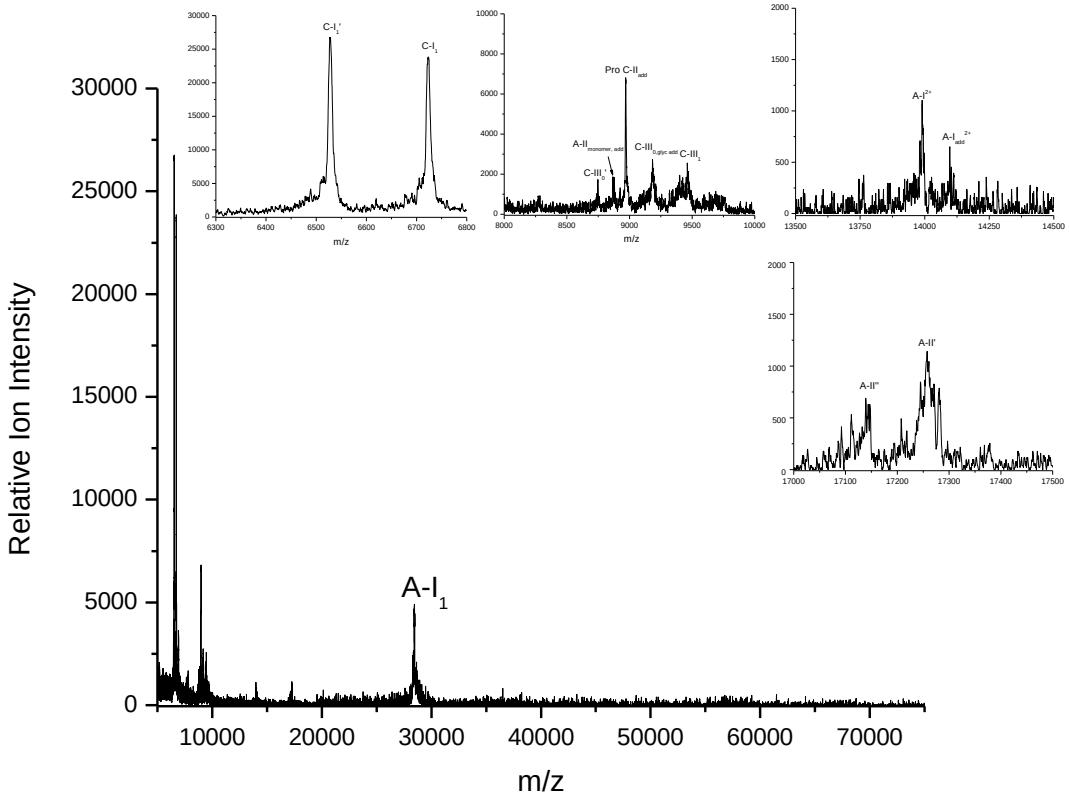

Figure 120. MALDI-MS HDL_2 spectra from CAD patient 41.

Table 97. Identification of apolipoproteins in the HDL_2 fraction from CAD patient 41.

Identification	Mass (Da)
ApoC-I_1'	6528.09
ApoC-I_1	6723.18
ApoC-III_0'	8746.47
ApoA-$II_{m\ add}$	8878.47
Pro ApoC-$II_{\ add}$	8969.05
ApoC-$III_{0,glyc\ add}$	9183.89
ApoC-III_1	9431.49
ApoA-I^{2+}	13991.40
ApoA-$I^{2+}{}_{add}$	14098.09
ApoA-II'''	17143.26
ApoA-II''	17258.11

Table 97. (Continued)

Identification	Mass (Da)
ApoA-I_1	28468.82

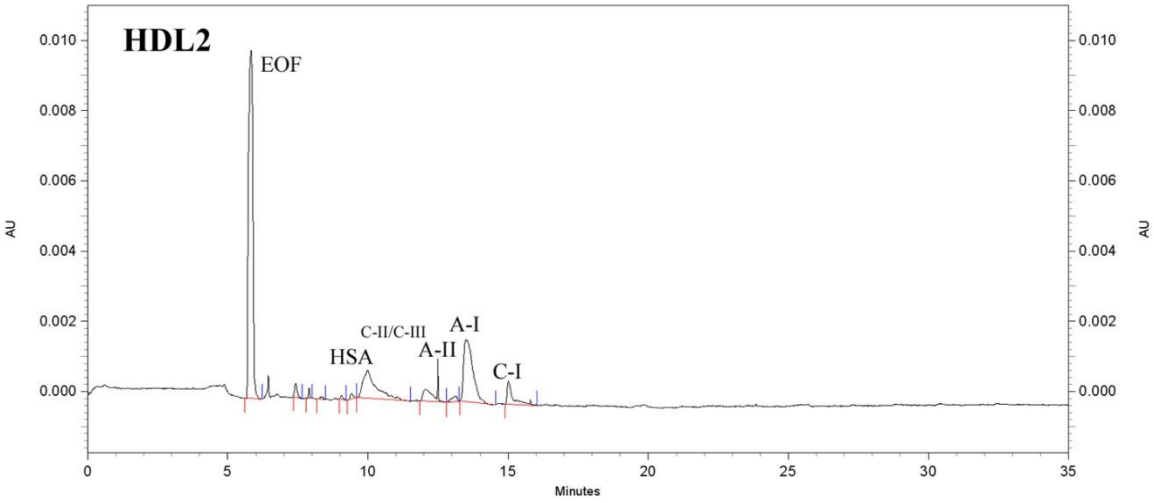

Figure 121. Electropherogram of the HDL_2 fraction from CAD patient 41.

Table 98. CE data for the HDL_2 fraction from a 200µL serum sample from CAD patient 41.

Protein	Elution Time (min)	Mobility (x $10^{-5}cm^2/Vs$)	CPA	Concentration (mg/dL)
HSA	9.9	-21.545	2225	2.24
ApoC-III	12.5	-27.405	614	-------
ApoA-II	13.1	-28.519	130	-------
ApoA-I	13.5	-29.166	2500	6.94
ApoC-I	15.0	-31.364	520	1.23

The HDL_2 subfraction MALDI-MS spectra contained apos C-I_1', C-I_1, C-III_0, A-$II_{monomer}$, Pro C-II, C-$III_{0,glyc}$, C-III_1, A-I^{2+}, A-II and A-I_1 as shown in Figure 120. Table

97 shows the peak masses for this fraction. The apoC-I' peak had a slightly higher relative ion intensity in the truncated form and both peaks were highly resolved. ApoA-I^{2+} was poorly resolved and apoA-II peaks had substantial splitting. The CE results are shown in Figure 121 and contain peaks corresponding to albumin, and apos C-III, A-II, A-I, and C-I.

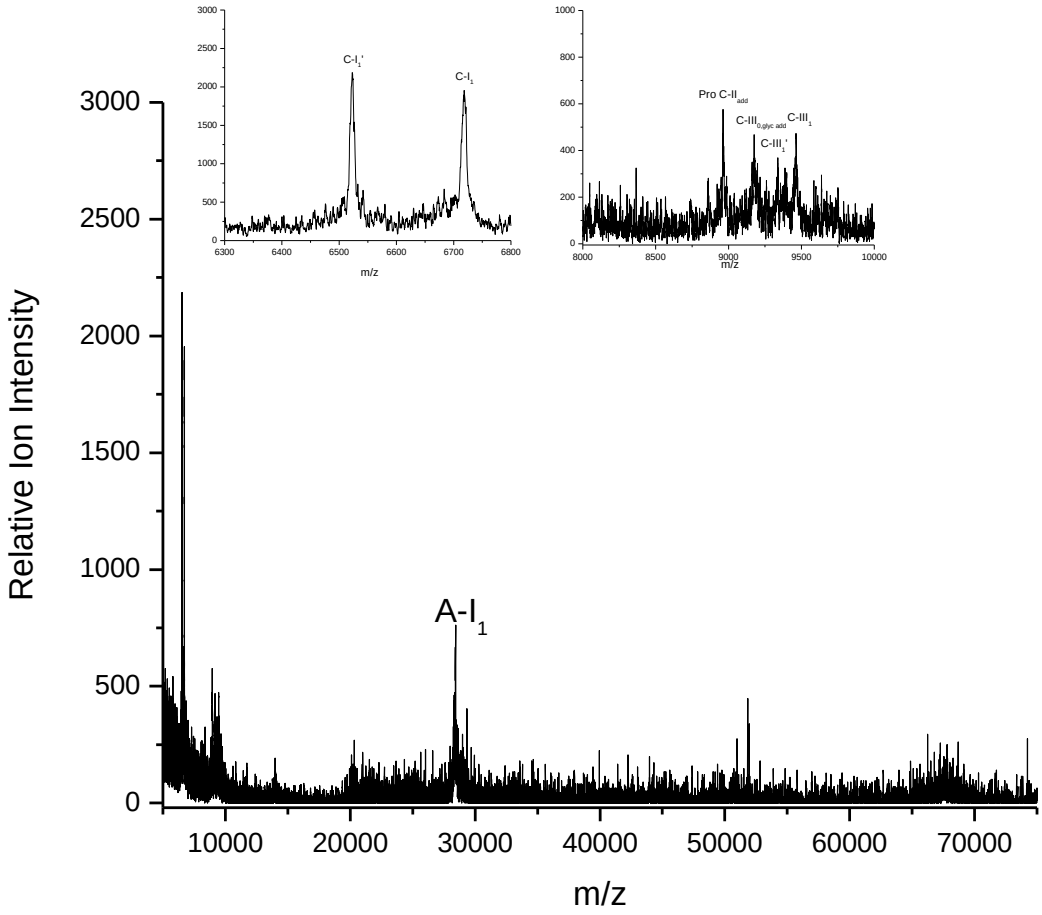

Figure 122. MALDI-MS HDL_3 spectra from CAD patient 41.

Table 99. Identification of apolipoproteins in the HDL_3 fraction from CAD patient 41.

Identification	Mass (Da)
ApoC-I_1'	6522.68

Table 99. (Continued)

Identification	Mass (Da)
ApoC-I_1	6717.95
Pro ApoC-II $_{add}$	8961.49
ApoC-$III_{0,glyc\ add}$	9175.15
ApoC-III_1'	9340.46
ApoC-III_1	9459.38
ApoA-I_1	28446.90

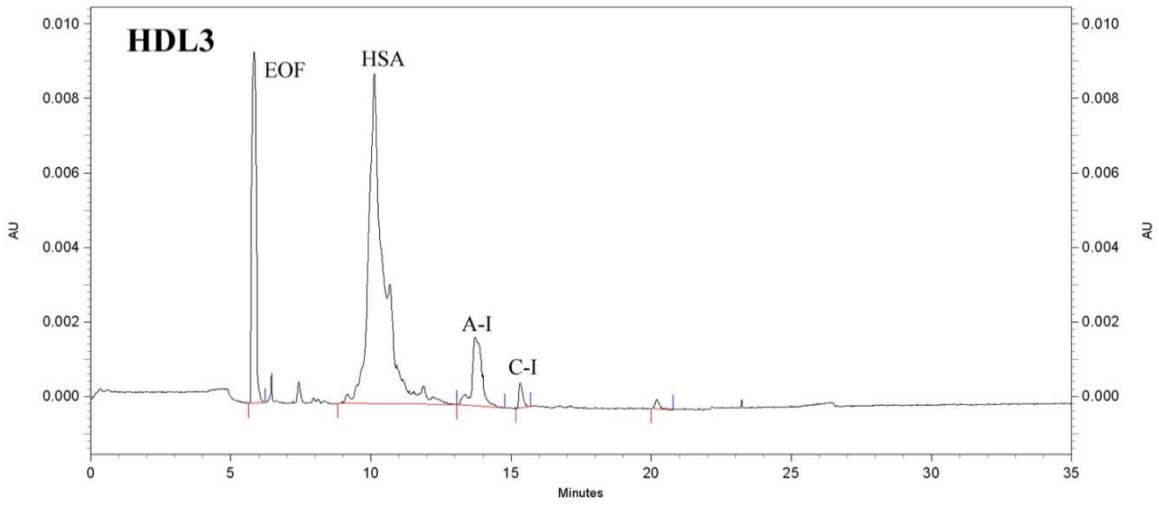

Figure 123. Electropherogram of the HDL_3 fraction from CAD patient 41.

Table 100. CE data for the HDL_3 fraction from a 200µL serum sample from CAD patient 41.

Protein	Elution Time (min)	Mobility (x $10^{-5}cm^2/Vs$)	CPA	Concentration (mg/dL)
HSA	10.1	-21.809	27847	28.04
ApoA-I	13.7	-29.477	2778	7.71
ApoC-I	15.3	-31.739	361	0.85
Unidentified	20.2	-36.383	115	-------

The HDL_3 subfraction MALDI-MS spectra, shown in Figure 122 contained apos C-I_1', C-I_1, Pro C-II, C-$III_{0,glyc}$, C-III_1, and A-I_1. Table 99 shows the peak masses for this fraction. In this fraction, the apoC-I peaks had high resolution, C-I_1' was slightly higher in intensity than C-I_1. Additionally, the peaks in the 8000 – 10000 *m/z* region had lower relative ion intensity than those in the HDL_3 fraction, which is indicative of much lower concentration in this fraction. The CE results, shown in Figure 123, contained albumin, apoA-I, and apoC-I. The albumin peak contained a small shoulder and was the predominant peak.

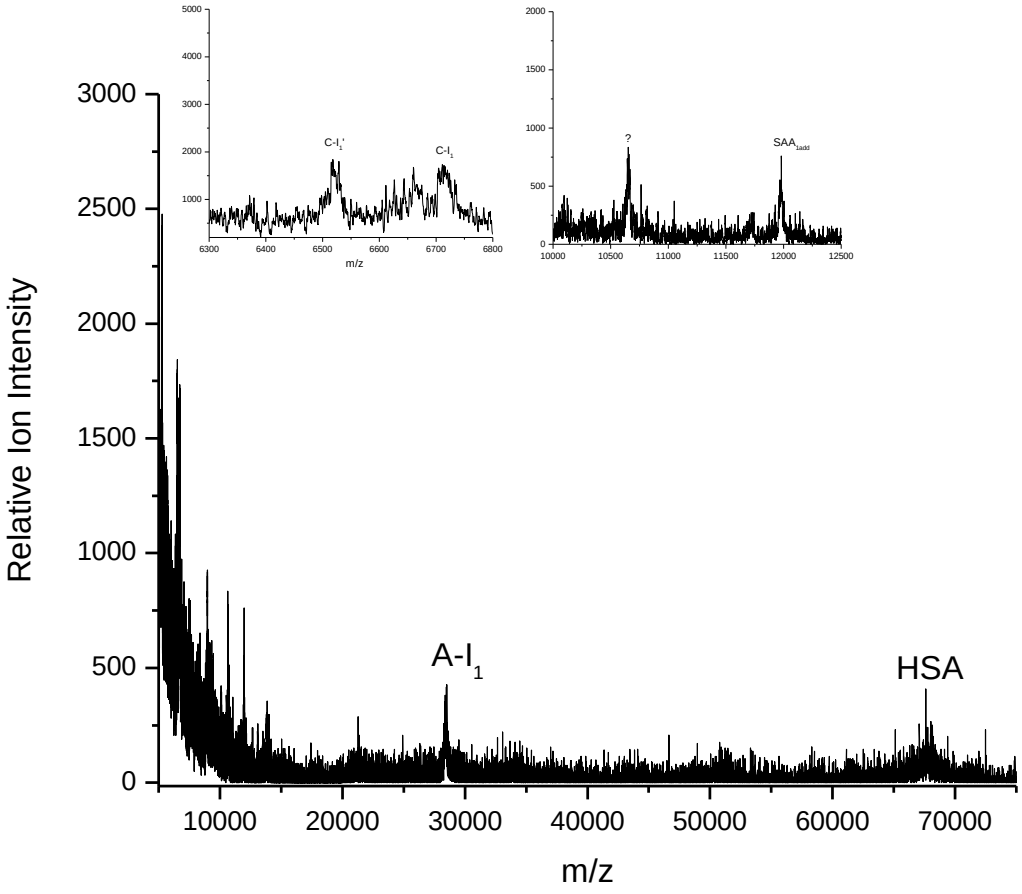

Figure 124. MALDI-MS protein spectra from CAD patient 41.

Table 101. Identification of apolipoproteins in the protein fraction from CAD patient 41.

Identification	Mass (Da)
ApoC-I_1'	6515.64
ApoC-I_1	6733.33
Unidentified Peak	10652.81
SAA_{1add}	11981.23
ApoA-I_1	28368.13
HSA	67614.33

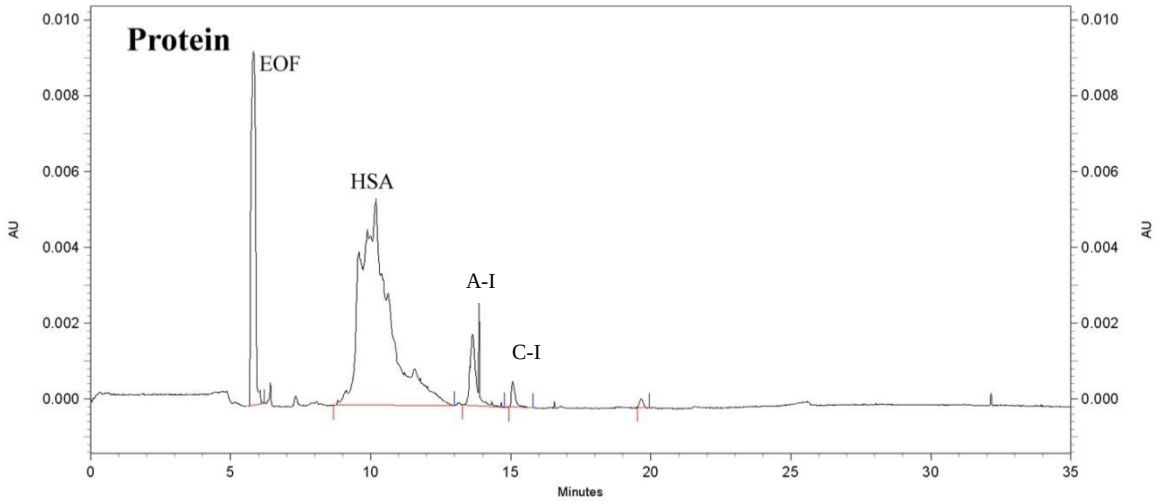

Figure 125. Electropherogram of the protein fraction from CAD patient 41.

Table 102. CE data for the protein fraction from a 200µL serum sample from CAD patient 41.

Protein	Elution Time (min)	Mobility (x $10^{-5}cm^2/Vs$)	CPA	Concentration (mg/dL)
HSA	10.6	-23.767	25463	25.64
ApoA-I	13.5	-29.700	1848	5.13
ApoC-I	15.0	-31.896	346	0.82
Unidentified	19.0	-36.029	94	--------

Figure 124 shows the protein subfraction which contained apos C-I_1', C-I_1, SAA_1, A-I_1, HSA, and an unidentified peak. Table 101 shows the peak masses for this fraction. The apoC-I peaks were hardly visible with low relative ion intensity and low resolution, and the C-I_1' and C-I_1 peaks were of equal intensity. Figure 125 shows the CE results which detected albumin and apoC-I. The albumin peak was poorly resolved, contained a shoulder, and was the predominant peak.

Table 103. Patient 49 medical information

Patient 49	
Age	56 years old
Height	64 inches
Weight	162 lbs.
Gender	Female
Race	Caucasian
Family History of Premature CAD/CAD/PVD	First Degree – Yes Second Degree – Yes
Major Risk Factors	Family history of CAD
Current Medications	Estrogen
Highest LDL	100 – 129mg/dL
Highest TG	150 – 200mg/dL
Any Prior HDL <35	No
Any Prior Homocysteine >14	No

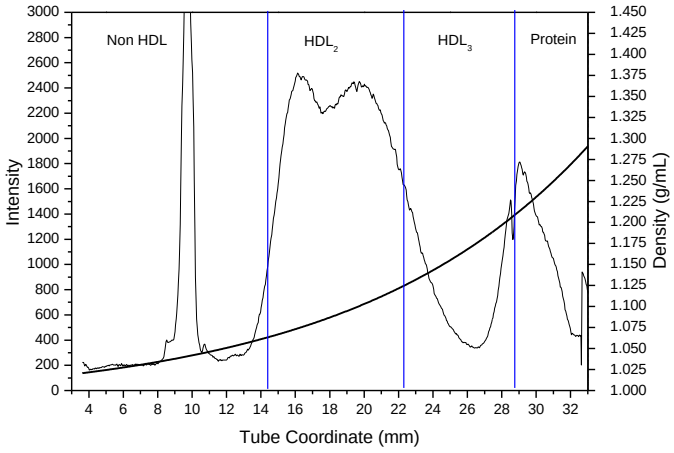

Figure 126. Lipoprotein density profile from patient 49 in a 0.300M solution of Cs_2CdY, spun for 6 hours at 120,000RPM at 5°C after treatment with dextran sulfate.

Patient 49 Discussion

Patient 49 whose medical history is presented in Table 103, is a 56 year old Caucasian female who has not had coronary angiography and has not been diagnosed with CAD. This patient has a family history of premature first and second degree CAD and is currently taking estrogen therapy. Their highest LDL was between 100 – 129 mg/dL and their highest triglyceride level was between 150 - 200 mg/dL. There are no prior levels of HDL below 35 mg/dL or homocysteine levels above 14 mg/dL. Figure 126 shows the Cs_2CdY profile for this subject which contains a broad split peak.

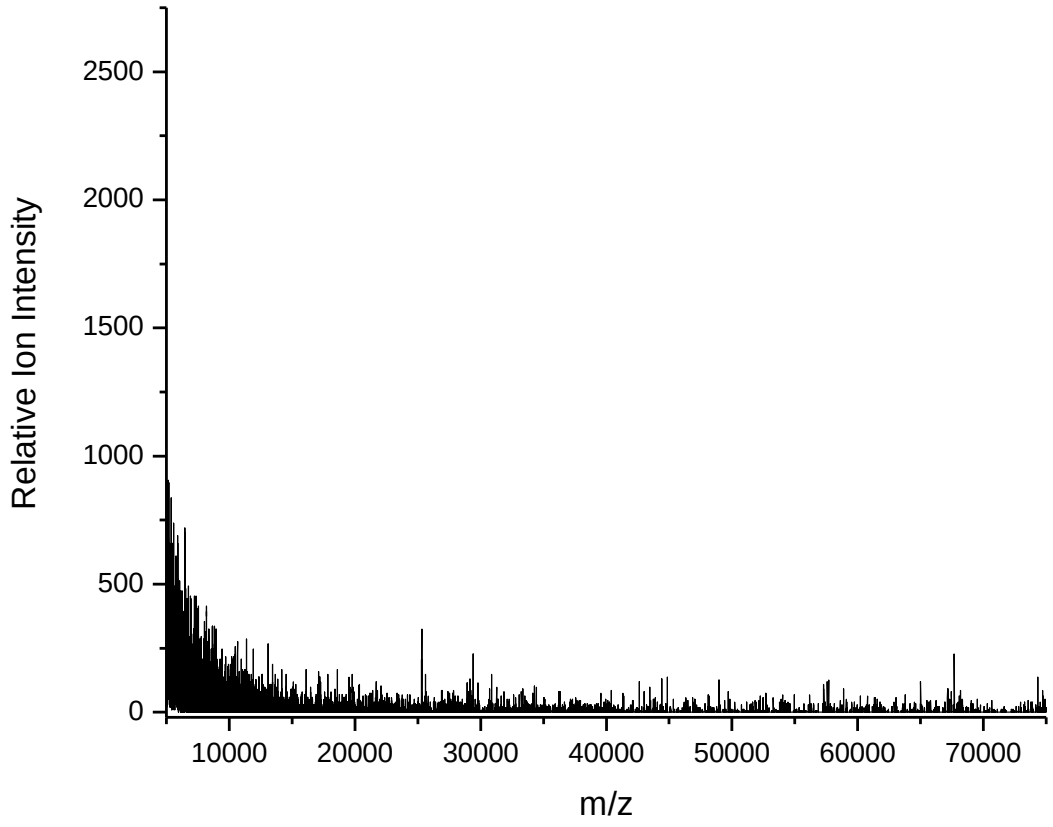

Figure 127. MALDI-MS non HDL spectra from patient 49.

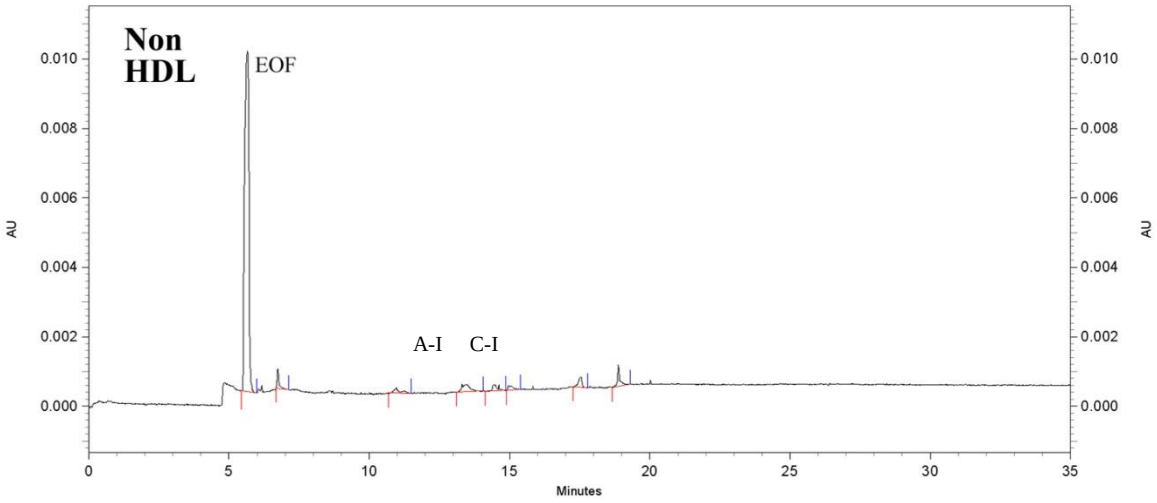

Figure 128. Electropherogram of the non HDL fraction from patient 49.

Table 104. CE data for the non HDL fraction from a 200µL serum sample from patient 49.

Protein	Elution Time (min)	Mobility (x $10^{-5}$$cm^2$/Vs)	CPA	Concentration (mg/dL)
ApoA-I	10.9	-25.717	152	0.42
ApoC-I	13.3	-30.482	254	0.60

Figure 127 shows the MALDI-MS spectra for the non HDL subfraction which did not contain any proteins. Figure 128 shows the CE results for this fraction which detected small peaks with mobilities matching apos A-I and C-I.

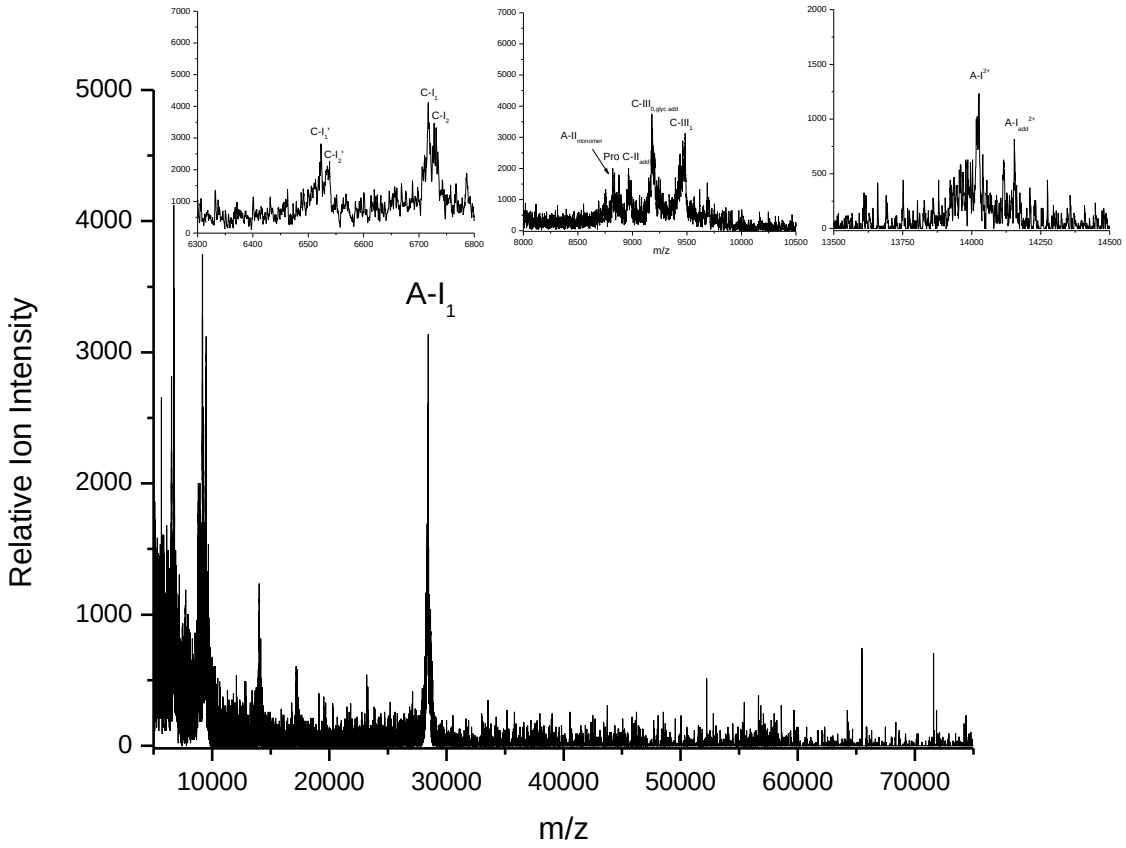

Figure 129. MALDI-MS HDL_2 spectra from patient 49.

Table 105. Identification of apolipoproteins in the HDL_2 fraction from patient 49.

Identification	**Mass (Da)**
ApoC-I_1'	6522.74
ApoC-I_2'	6536.12
ApoC-I_1	6717.18
ApoC-I_2	6730.02
ApoA-II_m	8814.18
Pro ApoC-II_{add}	8964.63
ApoC-$III_{0,glyc\ add}$	9178.25
ApoC-III_1	9459.38
ApoA-I^{2+}	14025.85

Table 105. (Continued)

Identification	Mass (Da)
ApoA-I^{2+}_{add}	14155.43
ApoA-I_1	28437.96

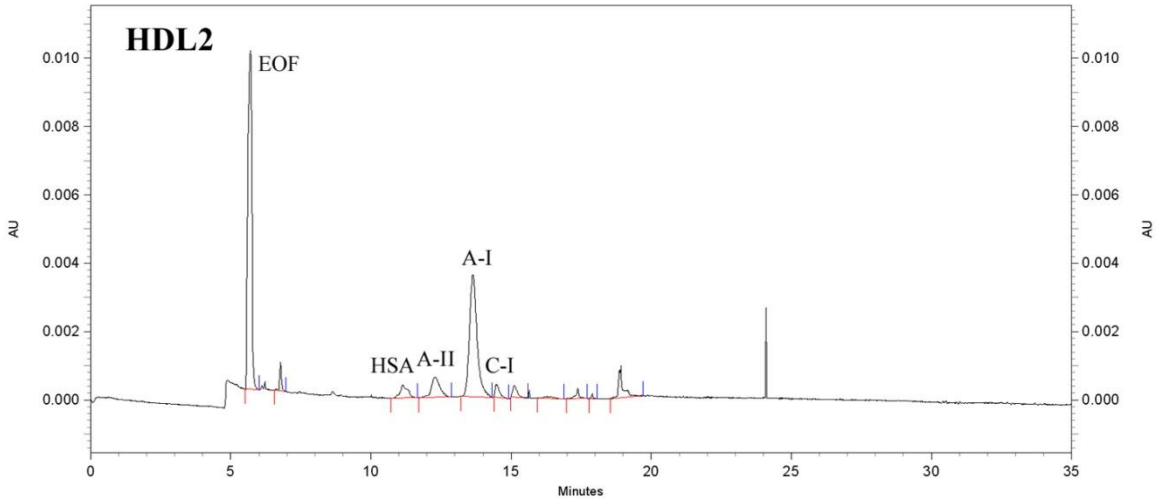

Figure 130. Electropherogram of the HDL_2 fraction from patient 49.

Table 106. CE data for the HDL_2 fraction from a 200µL serum sample from patient 49.

Protein	Elution Time (min)	Mobility (x $10^{-5}cm^2/Vs$)	CPA	Concentration (mg/dL)
HSA	13.6	-25.669	4122	4.15
ApoA-II	14.5	-28.139	250	-------
ApoA-I	15.1	-30.556	207	0.57
ApoC-I	17.4	-31.798	109	0.26
Unidentified	18.9	-35.212	435	-------

The HDL_2 subfraction contained apos C-I_1', C-I_2', C-I_1, C-I_2, A-$II_{monomer}$, Pro C-II, C-$III_{0,glyc}$,C-III_0, A-I^{2+}, and A-I_1, as shown in Figure 129. Table 105 shows the peak

masses for this fraction. The apoC-I peaks were poorly resolved and showed splitting in addition to the mass shifting. Figure 130 shows the CE results for this fraction, which detected albumin and apos A-II, A-I, C-I and an unidentified peak.

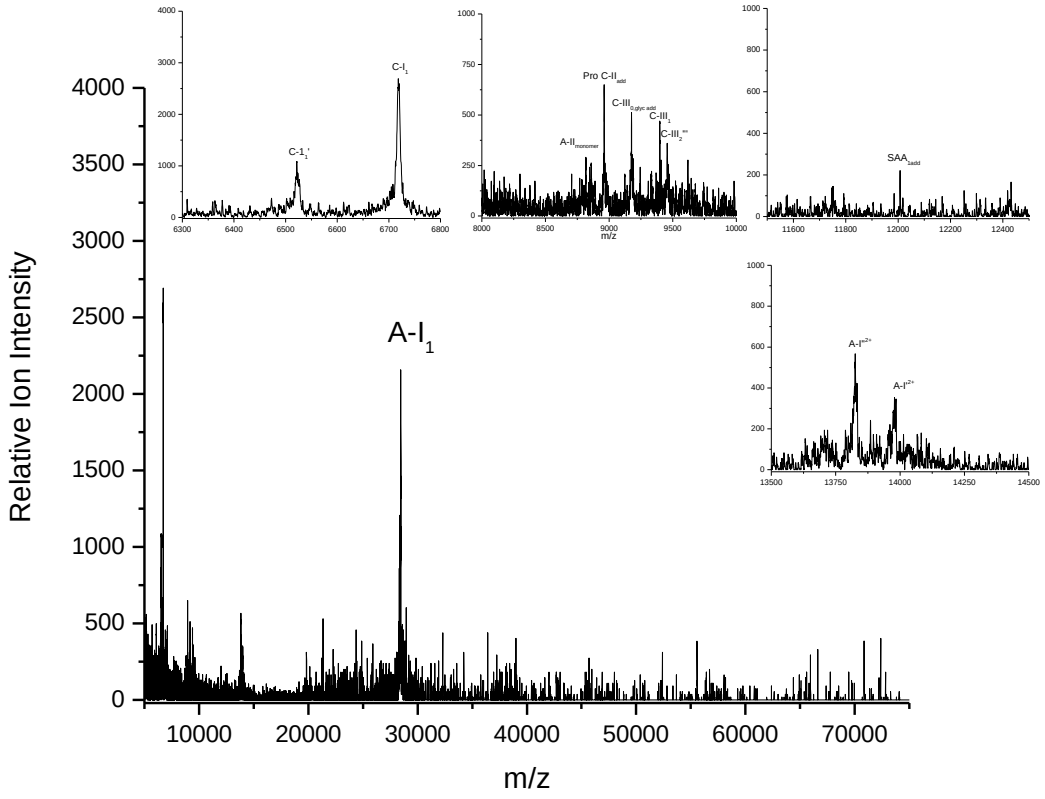

Figure 131. MALDI-MS HDL_3 spectra from patient 49.

Table 107. Identification of apolipoproteins in the HDL_3 fraction from patient 49.

Identification	Mass (Da)
ApoC-I_1'	6522.10
ApoC-I_1	6718.77
ApoA-II_m	8817.46
Pro ApoC-II $_{add}$	8961.35
ApoC-$III_{0,glyc\ add}$	9176.12
ApoC-III_1	9402.48

Table 107. (Continued)

Identification	Mass (Da)
ApoC-III_2'''	9464.49
SAA_{1add}	12007.23
ApoA-I''$^{2+}$	13826.32
ApoA-I'$^{2+}$	13978.30
ApoA-I_1	28523.29

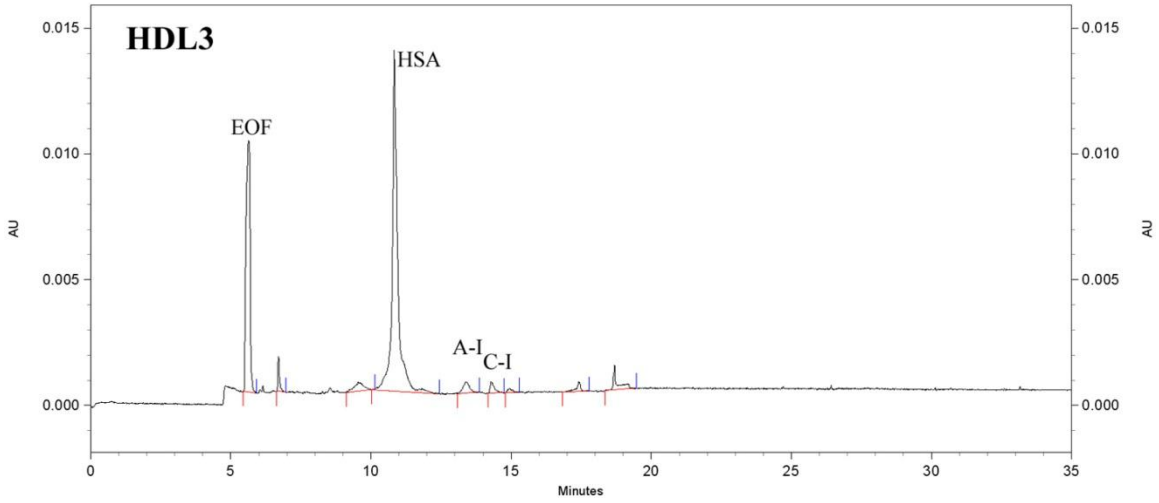

Figure 132. Electropherogram of the HDL_3 fraction from patient 49.

Table 108. CE data for the HDL_3 fraction from a 200µL serum sample from patient 49.

Protein	Elution Time (min)	Mobility (x $10^{-5}cm^2/Vs$)	CPA	Concentration (mg/dL)
HSA	10.8	-25.537	13889	13.99
ApoA-I	13.7	-30.802	422	1.17
ApoC-I	14.3	-32.151	279	0.66
Unidentified	17.4	-35.852	184	-------

Figure 131 shows the HDL_3 subfraction MALDI-MS spectra which contained apos C-I_1', C-I_1, A-$II_{monomer}$, Pro C-II, C-$III_{0,glyc}$, C-III_1, C-III_2, SAA_1, A-I^{2+}, and A-I_1. Table 107 shows the peak masses for this fraction. The C-I_1' peak was low in relative ion intensity, with the C-I_1 peak having approximately three times the intensity of C-I_1'. The inflammatory marker SAA_1 was also present in this fraction. The CE results, shown in Figure 132, detected albumin, apos A-I and C-I, and an unidentified peak.

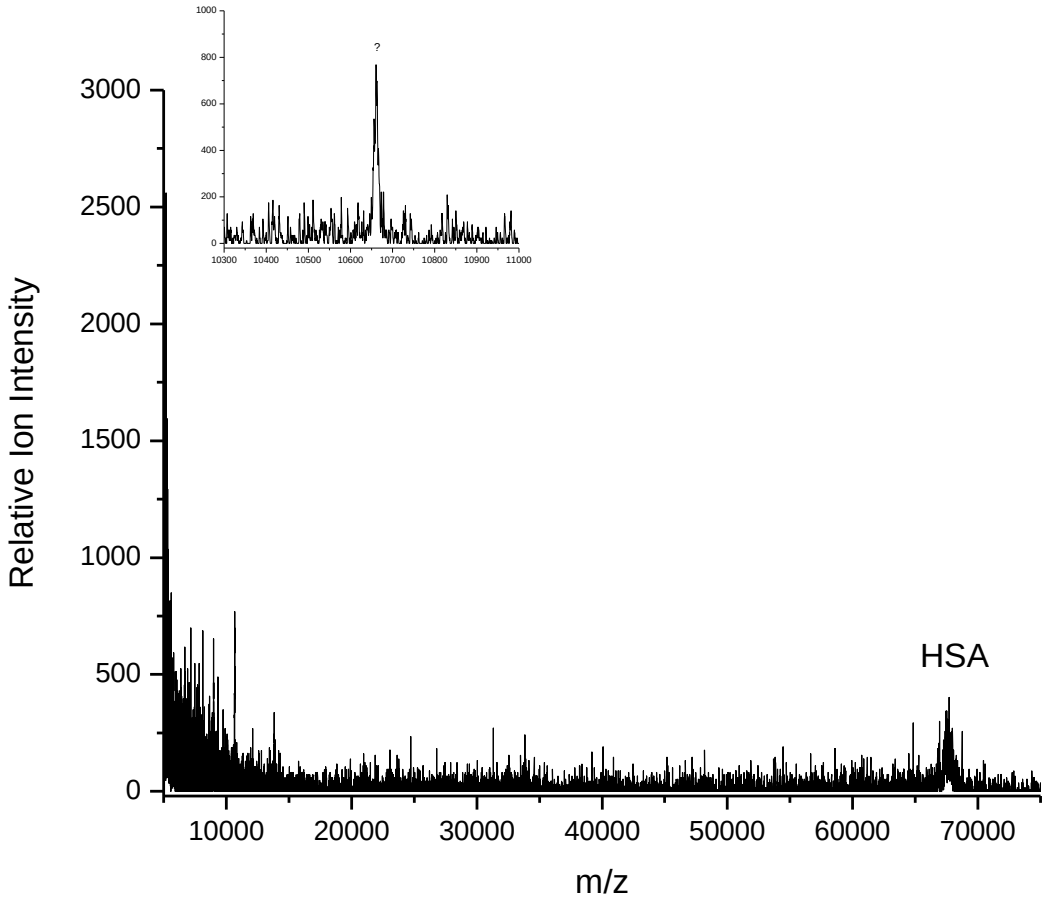

Figure 133. MALDI-MS protein spectra from patient 49.

Table 109. Identification of apolipoproteins in the protein fraction from patient 49.

Identification	Mass (Da)
Unidentified Peak	10661.77
HSA	67712.50

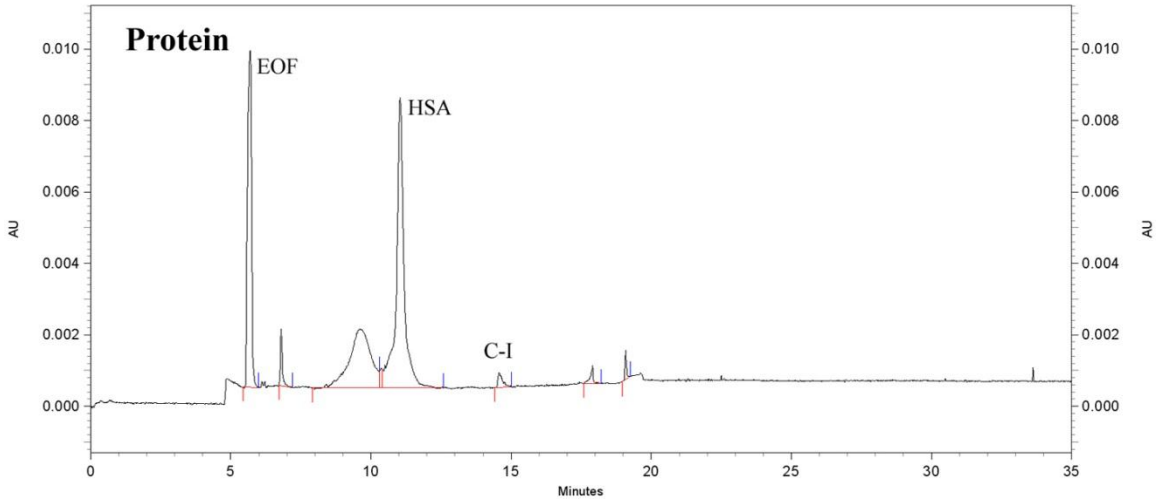

Figure 134. Electropherogram of the protein fraction from patient 49.

Table 110. CE data for the protein fraction from a 200µL serum sample from patient 49.

Protein	Elution Time (min)	Mobility (x $10^{-5}$$cm^2$/Vs)	CPA	Concentration (mg/dL)
HSA	11.0	-25.567	11765	11.85
ApoC-I	14.6	-32.064	261	0.62
Unidentified	17.9	-35.835	167	-------

The protein fraction contained HSA and an unidentified peak as shown in the MALDI-MS spectra in Figure 133. Table 109 shows the peak masses for this fraction. The CE results, shown in Figure 134, contained albumin and apoC-I. The albumin peak co-eluted with an unidentified peak.

Table 111. CAD patient 84 medical information

CAD Patient 84	
Age	37 years old
Height	61 inches
Weight	172 lbs.
Gender	Female
Race	Caucasian
Family History of Premature CAD/CAD/PVD	First Degree – Yes Second Degree – Yes
Major Risk Factors	Hypertension, DM, Tobacco use, Family history of CAD, HDL <35mg/dl
Prior or Current History Of:	Angina, Angioplasty or Stent, CHF (EF <50%), PVD, Tobacco use
Current Medications	Statin, Beta Blocker, Thiazide
Highest LDL	> 160mg/dL
Highest TG	150 – 200mg/dL
Any Prior HDL <35	Yes
Any Prior Homocysteine >14	No

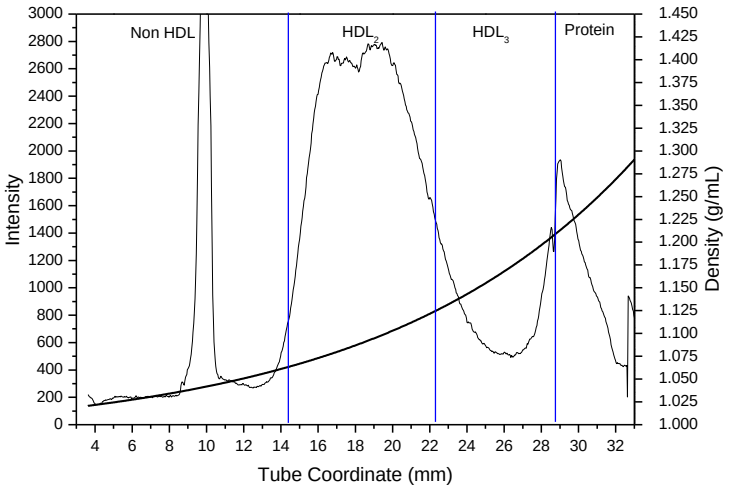

Figure 135. Lipoprotein density profile from CAD patient 84 in a 0.300M solution of Cs_2CdY, spun for 6 hours at 120,000RPM at 5°C after treatment with dextran sulfate.

CAD Patient 84 Discussion

CAD patient 84 whose medical history is presented in Table 111, is a 75 year old Caucasian female who has been diagnosed with CAD, and has a family history of premature first and second degree CAD. Patient 84 has major risk factors including hypertension, diabetes mellitus, tobacco use, and HDL levels below 35mg/dL. Patient 84 also has prior and/or current history of angina, angioplasty and/or stent, congestive heart failure, and peripheral vascular disease, and is currently prescribed and taking a statin, beta blocker, and thiazide. Their highest LDL was above 160 mg/dL and their highest triglyceride level was between 150 - 200 mg/dL. There are no prior levels of homocysteine above 14 mg/dL. Figure 135 shows the Cs_2CdY profile for this subject which contains a slightly split peak with high intensity.

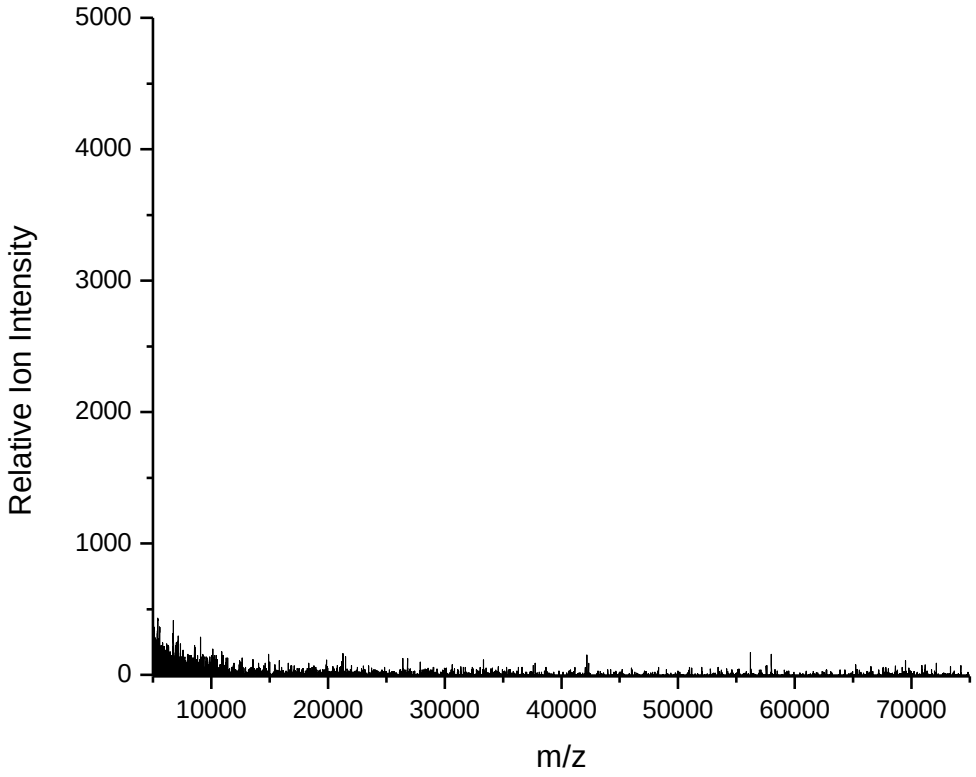

Figure 136. MALDI-MS non HDL spectra from CAD patient 84.

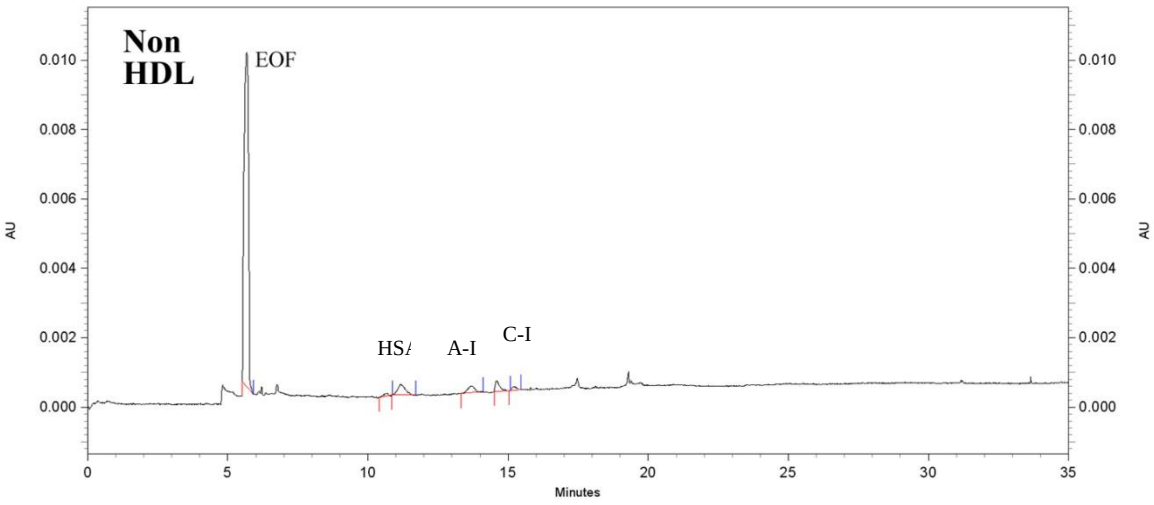

Figure 137. Electropherogram of the non HDL fraction from CAD patient 84.

Table 112. CE data for the non HDL fraction from a 200µL serum sample from CAD patient 84.

Protein	Elution Time (min)	Mobility (x $10^{-5}$$cm^2$/Vs)	CPA	Concentration (mg/dL)
HSA	11.2	-25.990	437	0.44
ApoA-I	13.7	-30.877	202	0.56
ApoC-I	15.2	-32.309	179	0.42

Figure 136 shows the MALDI-MS spectra for the non HDL subfraction and did not contain any proteins. The CE results for this fraction, shown in Figure 137, detected small peaks with mobilities corresponding to albumin, and apos A-I and C-I.

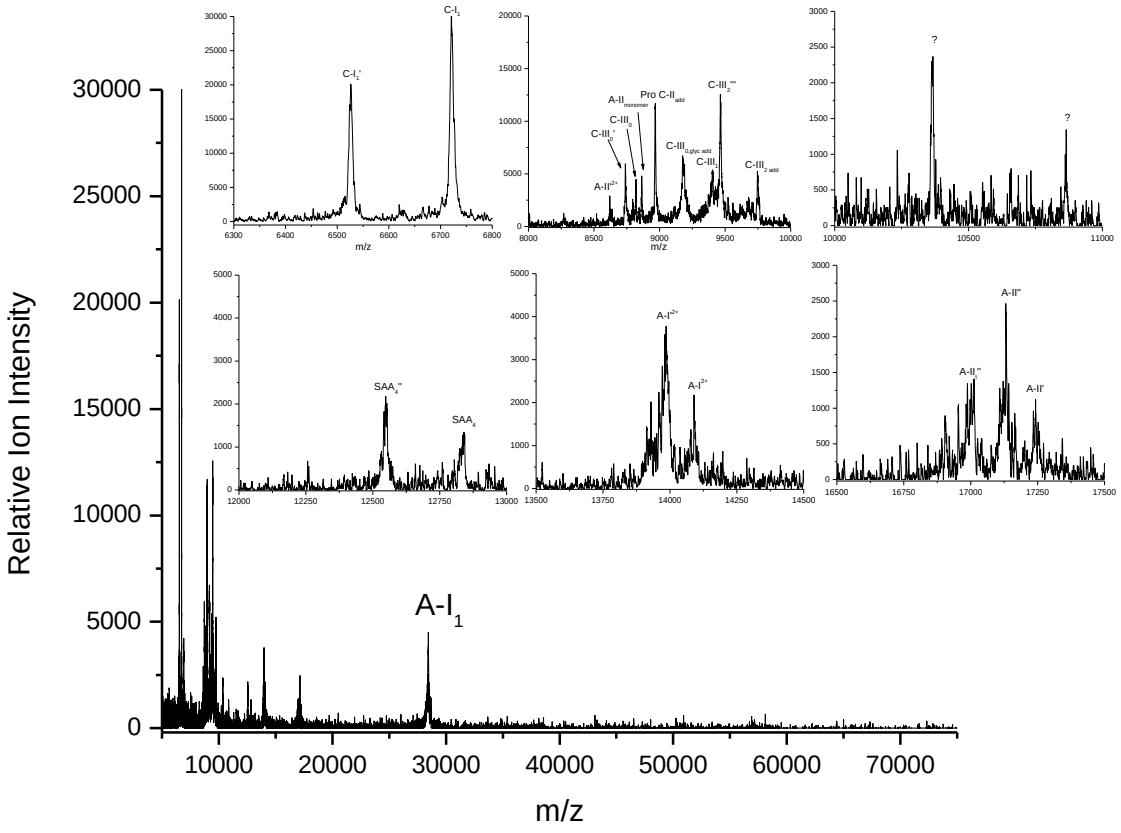

Figure 138. MALDI-MS HDL_2 spectra from CAD patient 84.

Table 113. Identification of apolipoproteins in the HDL_2 fraction from CAD patient 84.

Identification	Mass (Da)
ApoC-I_1'	6526.32
ApoC-I_1	6721.46
ApoA-II'^{2+}	8626.16
ApoC-III_0'	8746.47
ApoC-III_0	8791.53
ApoA-II_m	8820.66
ApoA-$II_{m\ add}$	8866.18
Pro ApoC-$II_{\ add}$	8964.95
ApoC-$III_{0,glyc\ add}$	9183.88

Table 113. (Continued)

Identification	Mass (Da)
$ApoC\text{-}III_1$	9402.82
$ApoC\text{-}III_2'''$	9472.92
$ApoC\text{-}III_{2\ add}$	9753.76
Unidentified Peak 1	10366.87
Unidentified Peak 2	10864.3
SAA_4''	12547.94
SAA_4	12839.65
$ApoA\text{-}I'^{2+}$	13986.13
$ApoA\text{-}I^{2+}$	14091.94
$ApoA\text{-}II_t''$	17009.33
ApoA-II''	17132.13
ApoA-II'	17248.97
$ApoA\text{-}I_1$	28448.96

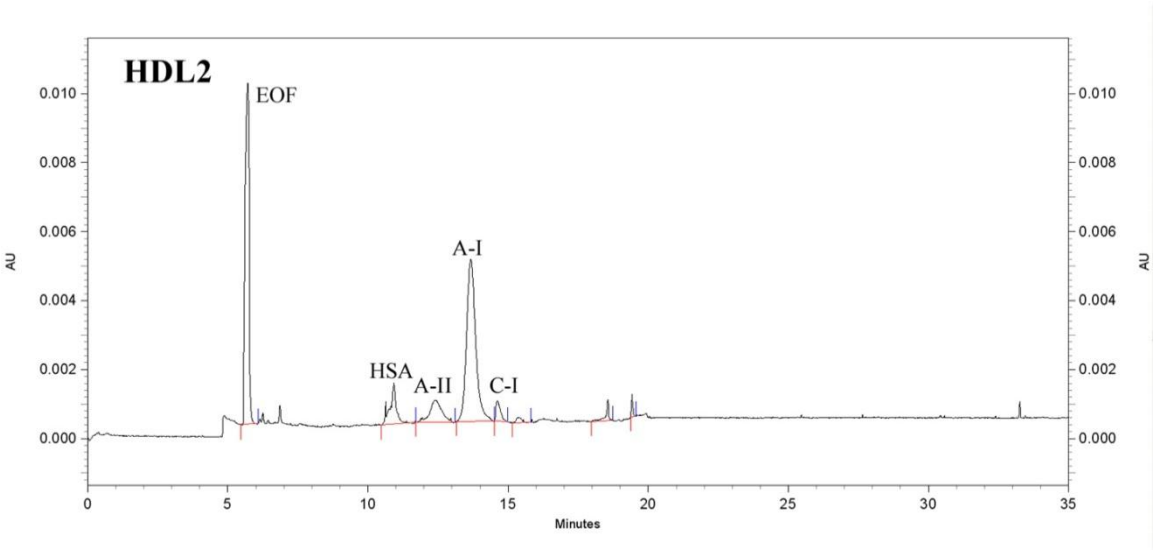

Figure 139. Electropherogram of the HDL_2 fraction from CAD patient 84.

Table 114. CE data for the HDL_2 fraction from a 200µL serum sample from CAD patient 84.

Protein	Elution Time (min)	Mobility (x $10^{-5}cm^2/Vs$)	CPA	Concentration (mg/dL)
HSA	10.9	-25.044	1325	1.33
ApoA-II	12.4	-28.330	1255	-------
ApoA-I	13.7	-30.486	6512	18.07
ApoC-I	14.6	-31.880	382	0.90
Unidentified	15.3	-32.877	109	-------
Unidentified	18.5	-36.178	179	-------
Unidentified	19.4	-36.878	91	-------

Figure 138 shows the HDL_2 subfraction MALDI-MS spectra which contained apos C-I_1', C-I_1, A-II^{2+}, C-III_0, A-$II_{monomer}$, Pro C-II, C-$III_{0.glyc}$, C-III_1, C-III_2, SAA_4, A-I^{2+}, A-II, A-I_1 and two unidentified proteins. Table 113 shows the peak masses for this fraction. The apoC-I peaks were highly resolved and there was an abundance of proteins in the range between 8000 – 10000 *m/z*. Two peaks were observed corresponding to the constitutive isomer SAA_4. Figure 139 shows the CE results for this fraction which contained albumin, apoA-II, A-I, C-I, and several unidentified peaks eluting after apoC-I.

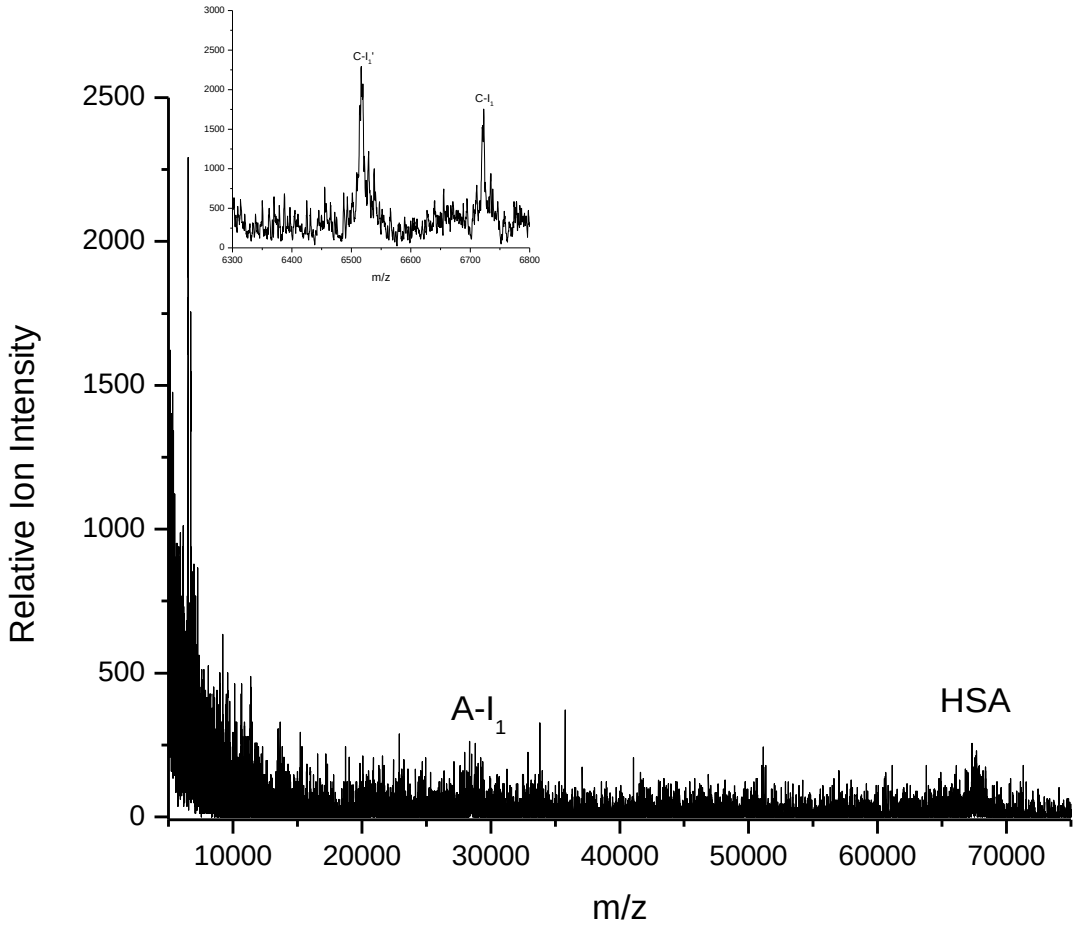

Figure 140. MALDI-MS HDL_3 spectra from CAD patient 84.

Table 115. Identification of apolipoproteins in the HDL_3 fraction from CAD patient 84.

Identification	Mass (Da)
ApoC-I_1'	6519.18
ApoC-I_1	6722.75
ApoA-I_1	28682.86
HSA	67568.87

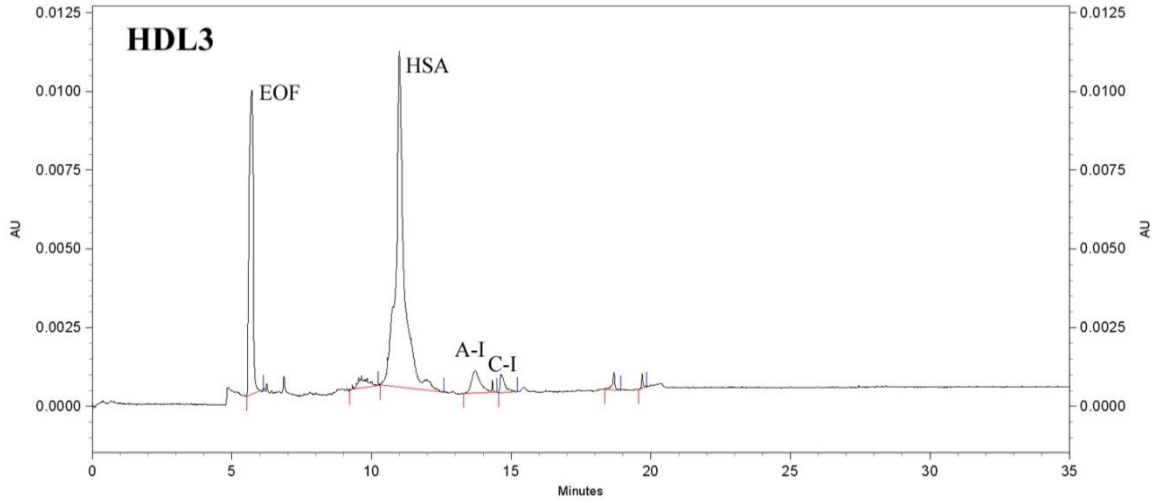

Figure 141. Electropherogram of the HDL_3 fraction from CAD patient 84.

Table 116. CE data for the HDL_3 fraction from a 200µL serum sample from CAD patient 84.

Protein	Elution Time (min)	Mobility (x $10^{-5}cm^2/Vs$)	CPA	Concentration (mg/dL)
HSA	10.9	-25.241	16589	16.70
ApoA-I	13.7	-30.571	985	2.73
ApoC-I	14.6	-31.933	383	0.90
Unidentified	18.7	-36.301	147	-------
Unidentified	19.7	-37.106	67	-------

The HDL_3 subfraction contained apos C-I_1', C-I_1, A-I_1 and HSA, shown in Figure 140. Table 115 shows the peak masses for this fraction. The apoC-I peaks were poorly resolved and C-I_1' had a higher relative ion intensity than C-I_1. The apoC-I peaks were overall lower in relative ion intensity in this fraction. The apoA-I_1 peak was also poorly resolved with low intensity. The CE results, shown in Figure 141 detected albumin, apoA-I, apoC-I, and unidentified peaks.

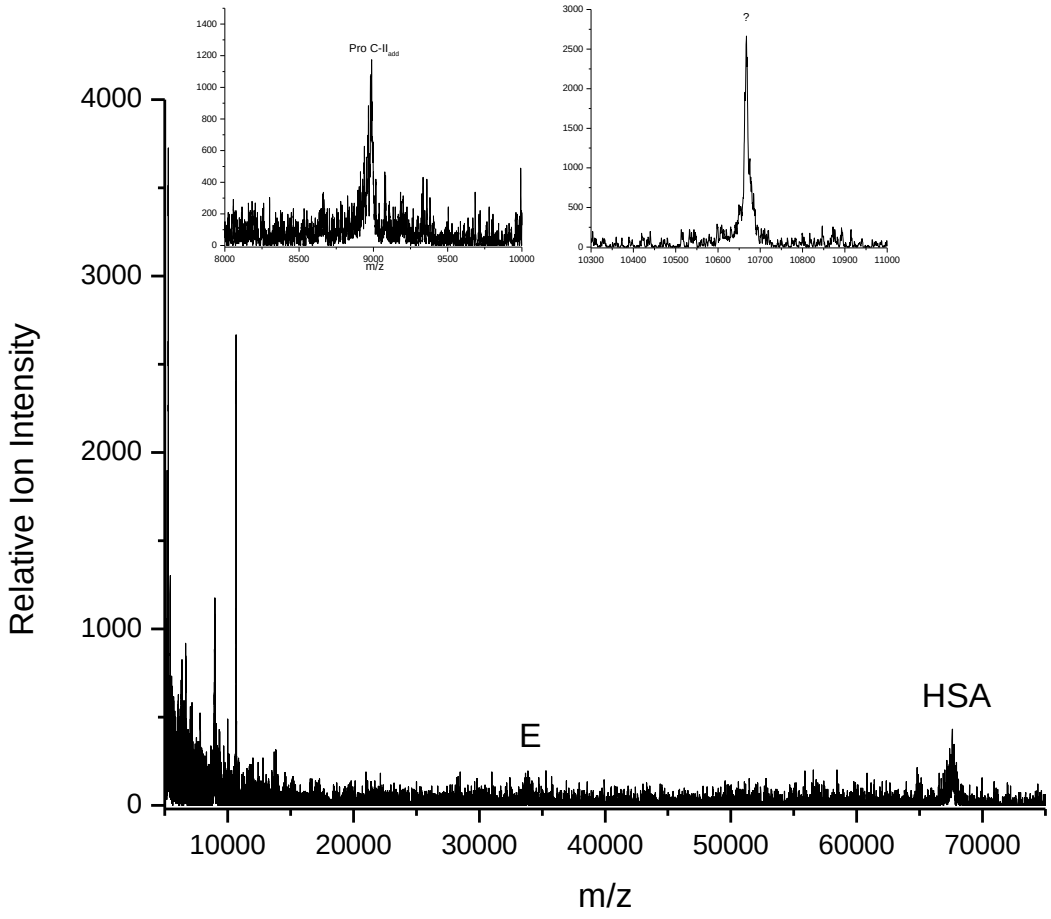

Figure 142. MALDI-MS protein spectra from CAD patient 84.

Table 117. Identification of apolipoproteins in the protein fraction from CAD patient 84.

Identification	**Mass (Da)**
Pro ApoC-II_{add}	8987.91
Unidentified Peak 1	10667.70
ApoE	33769.10
HSA	67594.14

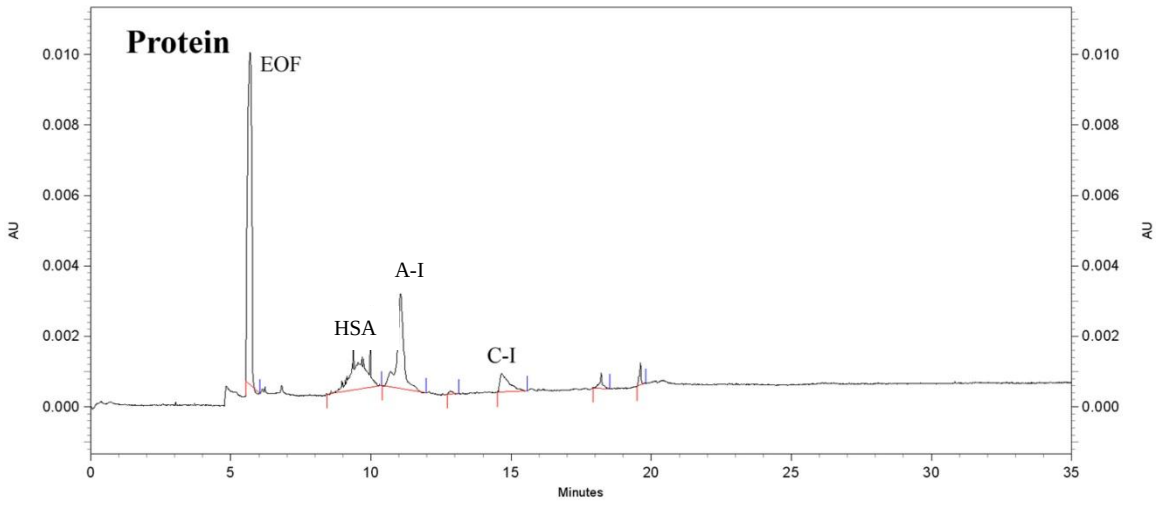

Figure 143. Electropherogram of the protein fraction from CAD patient 84.

Table 118. CE data for the protein fraction from a 200µL serum sample from CAD patient 84.

Protein	Elution Time (min)	Mobility (x $10^{-5}$$cm^2$/Vs)	CPA	Concentration (mg/dL)
HSA	9.9	-22.723	3181	3.20
ApoA-I	11.1	-25.619	3424	9.50
ApoC-I	14.7	-32.210	671	1.59
Unidentified	18.2	-36.131	135	-------
Unidentified	19.6	-37.286	104	-------

The protein subfraction contained apos Pro C-II, E, HSA and a sharp unidentified protein peak shown in the MALDI-MS spectra in Figure 142. Table 117 shows the peak masses for this fraction. Figure 143, shows the CE results for this fraction which detected albumin, apoA-I, apoC-I and two unidentified peaks.

Table 119. CAD patient 143 medical information

CAD Patient 143	
Age	54 years old
Height	68 inches
Weight	168 lbs.
Gender	Male
Race	Caucasian
Major Risk Factors	Family history of CAD, Hypertension
Prior or Current History Of:	MI, Beta Blockers
Current Medications	Statin

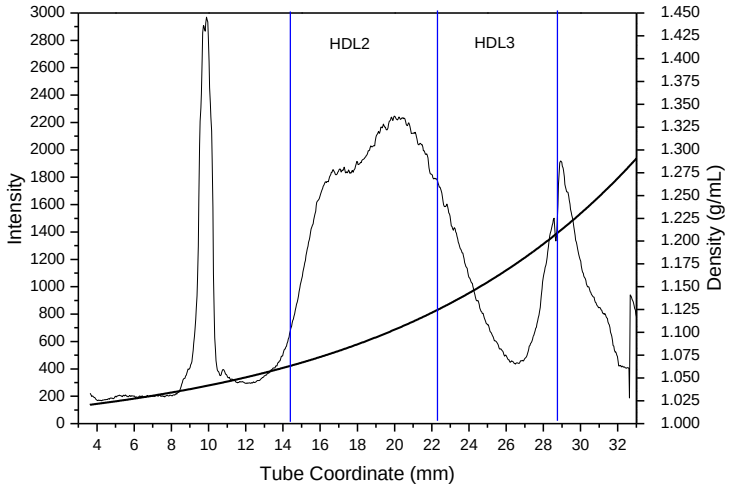

Figure 144. Lipoprotein density profile from CAD patient 143 in a 0.300M solution of Cs_2CdY, spun for 6 hours at 120,000RPM at 5°C after treatment with dextran sulfate.

CAD Patient 143 Discussion

CAD patient 143 whose medical history is presented in Table 119, is a 54 year old Caucasian male who has been diagnosed with CAD, has a family history of premature CAD, and suffers from hypertension. Patient 143 also has prior history of myocardial infarction (MI) and is currently prescribed and taking a statin and beta blocker, though no LDL lowering has resulted from statin therapy. Despite, having

elevated HDL levels this patient has CAD, having an HDL level of 67mg/dL at the time of MI. Figure 144 shows the Cs_2CdY profile for this subject which contains a broad peak spanning both HDL subclasses with a shoulder on its buoyant side.

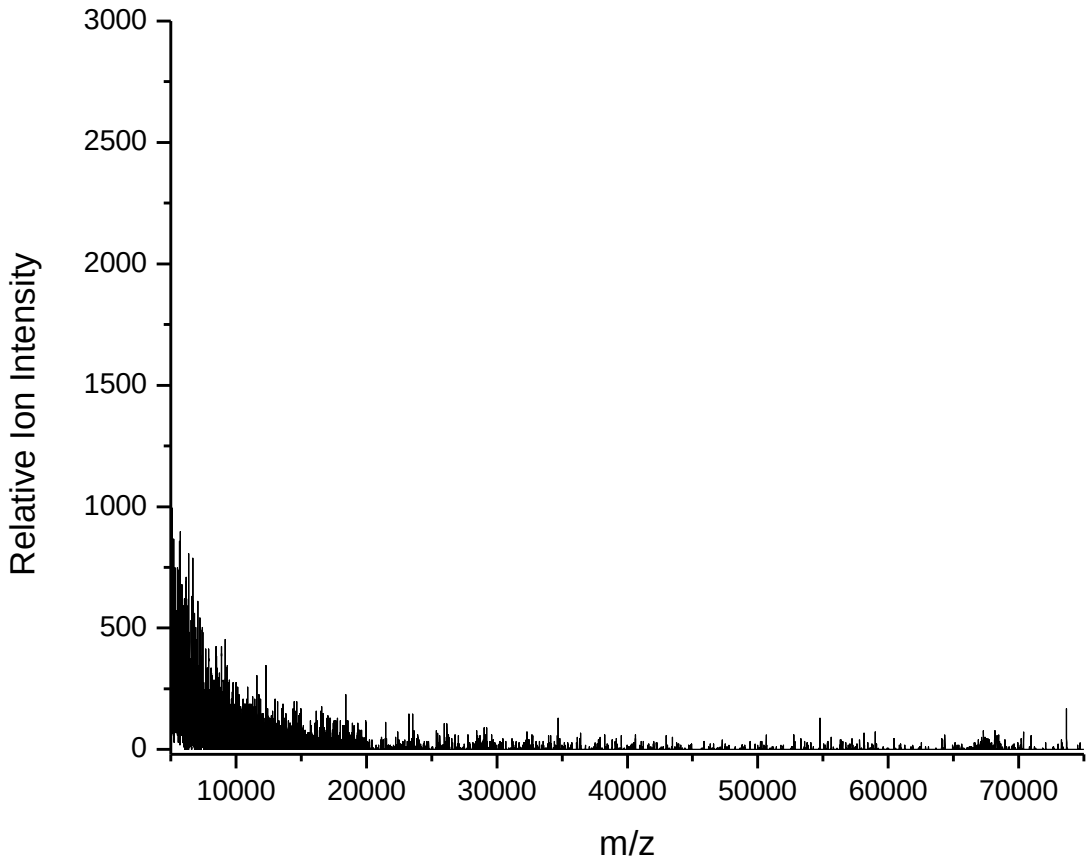

Figure 145. MALDI-MS non HDL spectra from CAD patient 143.

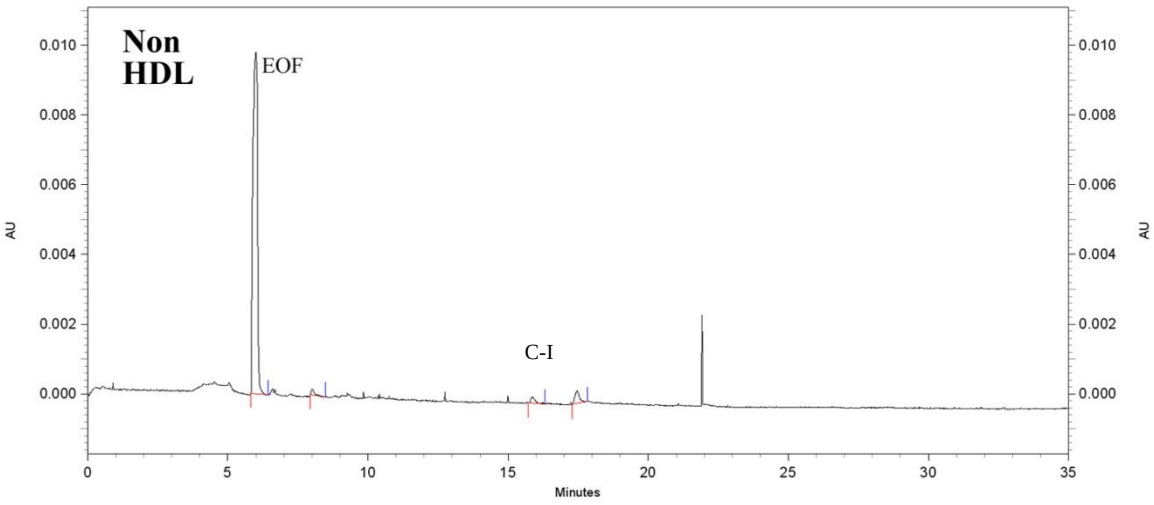

Figure 146. Electropherogram of the non HDL fraction from CAD patient 143.

Table 120. CE data for the non HDL fraction from a 200µL serum sample from CAD patient 143.

Protein	Elution Time (min)	Mobility (x $10^{-5}$$cm^2$/Vs)	CPA	Concentration (mg/dL)
ApoC-I	15.9	-30.973	101	0.24
Unidentified	17.5	-32.667	195	-------

Figure 145 shows the MALDI-MS spectra for the non HDL subfraction which did not contain any proteins. The CE results are shown in Figure 146, and contained barely visible peaks with mobilities corresponding to apoC-I and an unidentified peak.

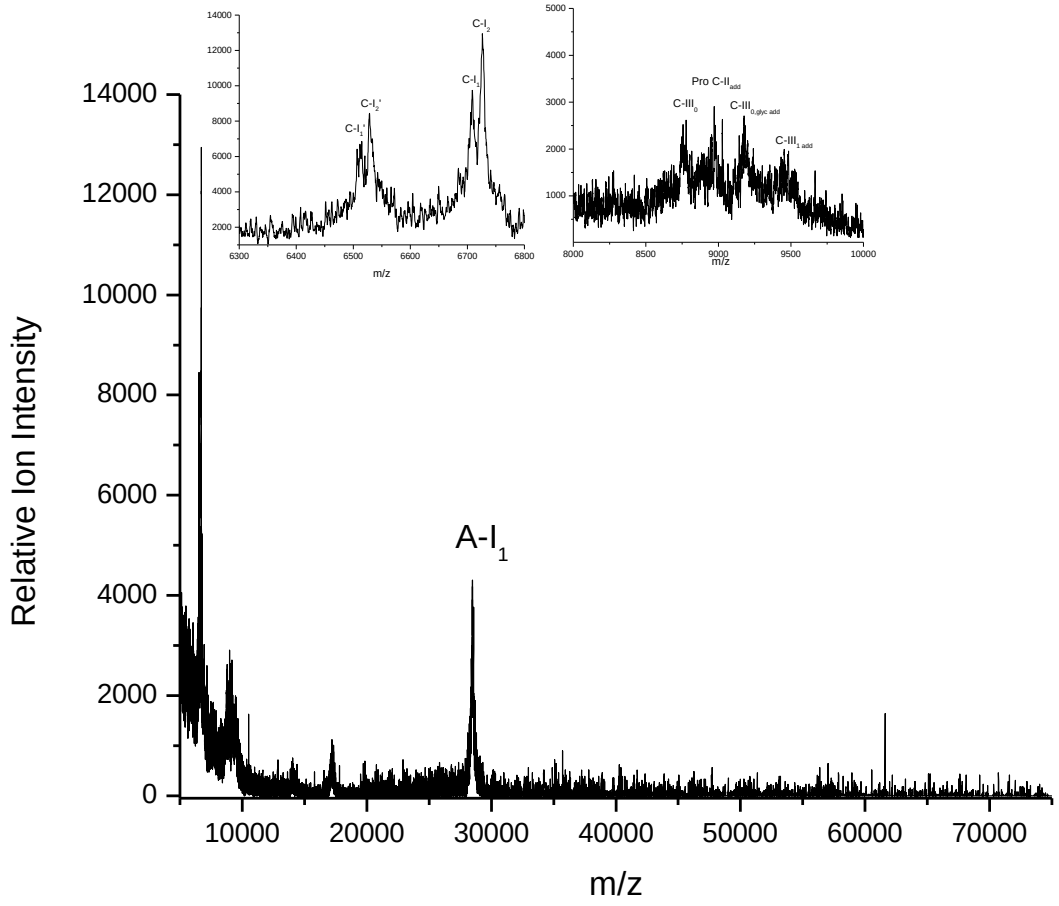

Figure 147. MALDI-MS HDL_2 spectra from CAD patient 143.

Table 121. Identification of apolipoproteins in the HDL_2 fraction from CAD patient 143.

Identification	Mass (Da)
ApoC-I_1'	6512.33
ApoC-I_2'	6528.55
ApoC-I_1	6709.54
ApoC-I_2	6726.34
ApoC-III_0'	8754.67
Pro ApoC-II $_{add}$	8977.69
ApoC-$III_{0,glyc\ add}$	9187.98

Table 121. (Continued)

Identification	Mass (Da)
ApoC-$III_{1\ add}$	9456.53
ApoA-I_1	28523.70

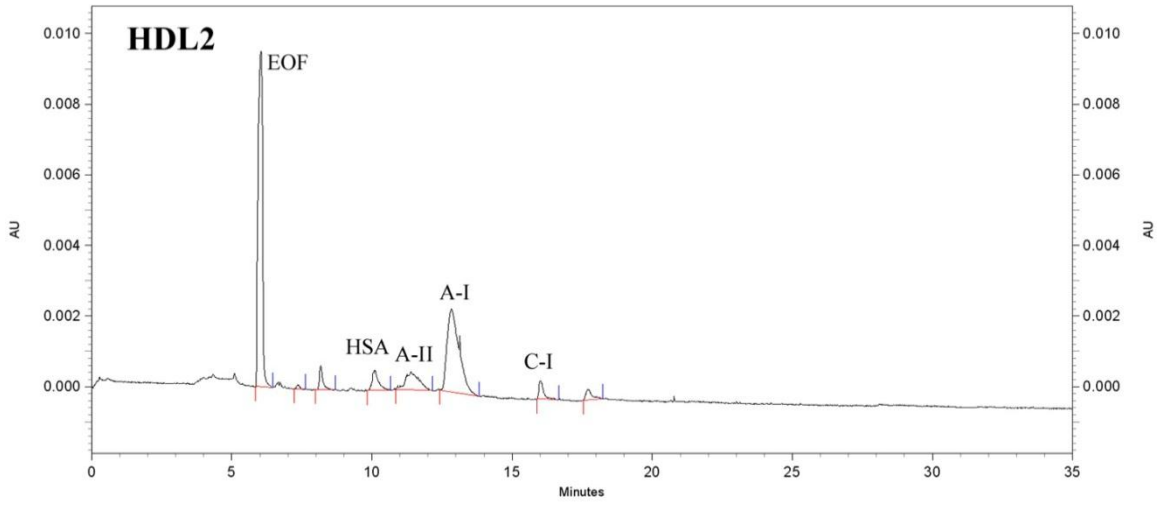

Figure 148. Electropherogram of the HDL_2 fraction from CAD patient 143.

Table 122. CE data for the HDL_2 fraction from a 200µL serum sample from CAD patient 143.

Protein	Elution Time (min)	Mobility (x $10^{-5}cm^2/Vs$)	CPA	Concentration (mg/dL)
HSA	10.1	-19.998	742	0.75
ApoA-II	11.4	-23.334	1252	-------
ApoA-I	12.8	-26.257	4599	12.76
ApoC-I	16.0	-30.892	320	0.76
Unidentified	17.7	-32.600	211	-------

The MALDI-MS spectra for the HDL_2 subfraction are shown in Figure 147, and contained apos C-I_1', C-I_2' C-I_2, C-III_0, Pro C-II, C-$III_{0,glyc}$, C-III_1, A-I_1, and an unidentified protein. Table 121 shows the peak masses for this fraction. The apoC-I peaks consisted of doublets, had low relative ion intensities and broad bases. The CE results are shown in Figure 148 and contained peaks corresponding to albumin, apos A-II, A-I, C-I and an unidentified peak.

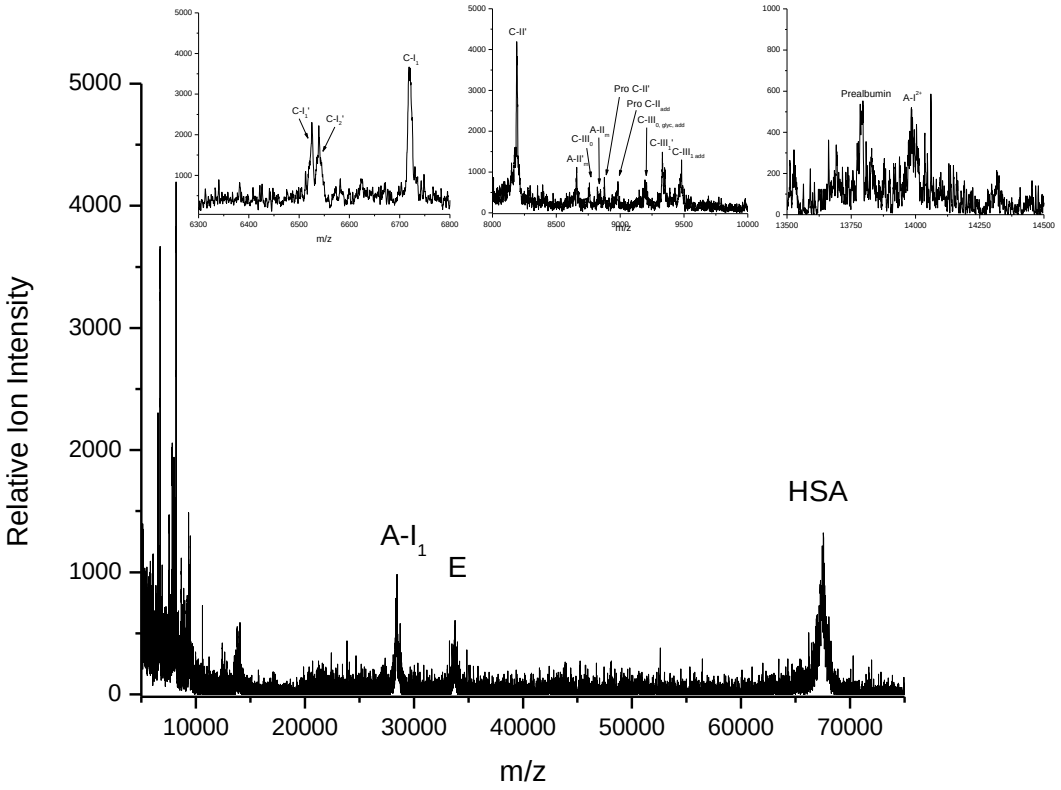

Figure 149. MALDI-MS HDL_3 spectra from CAD patient 143.

Table 123. Identification of apolipoproteins in the HDL_3 fraction from CAD patient 143.

Identification	Mass (Da)
ApoC-I_1'	6525.27
ApoC-I_2'	6540.21

Table 123. (Continued)

Identification	Mass (Da)
ApoC-I_1	6718.37
ApoC-II'	8188.89
ApoA-II'_m	8659.53
ApoC-III_0	8758.76
ApoA-II_m	8822.76
Pro ApoC-II'	8878.47
Pro ApoC-II_{add}	8981.79
ApoC-$III_{0,glyc\ add}$	9213.01
ApoC-III_1'	9332.73
ApoC-$III_{1\ add}$	9481.11
Prealbumin	13790.62
ApoA-I^{2+}	14060.50
ApoA-I_1	28315.85
ApoE	33731.90
HSA	67559.85

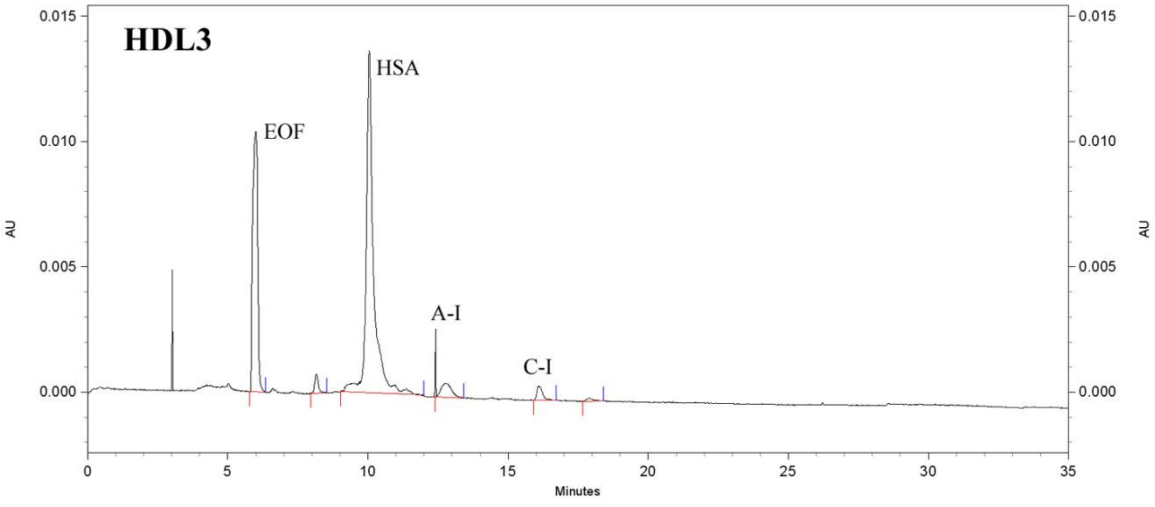

Figure 150. Electropherogram of the HDL_3 fraction from CAD patient 143.

Table 124. CE data for the HDL_3 fraction from a 200µL serum sample from CAD patient 143.

Protein	Elution Time (min)	Mobility (x $10^{-5}cm^2/Vs$)	CPA	Concentration (mg/dL)
HSA	10.1	-20.211	20696	20.84
ApoA-I	12.4	-25.836	1226	3.40
ApoC-I	16.1	-31.290	403	0.95
Unidentified	17.9	-33.126	92	-------

The HDL_3 subfraction MALDI-MS spectra contained apos C-I_1', C-I_2', C-I_1, C-II, A-$II_{monomer}$, C-III_0, Pro C-II, C-$III_{0,glyc}$, C-III_1, prealbumin, A-I_1, E, and HSA, as shown in Figure 149. Table 123 shows the peak masses for this fraction. The apoC-I peaks were lower in intensity than the HDL_2 fraction and the truncated form consisted of doublet peaks, while C-I_1 appeared as a singlet. The 8000 – 10000 *m/z* region consisted of an abundance of peaks with high resolution. The CE results, shown in Figure 150, contained peaks corresponding to albumin, apos A-I and C-I, and an unidentified peak.

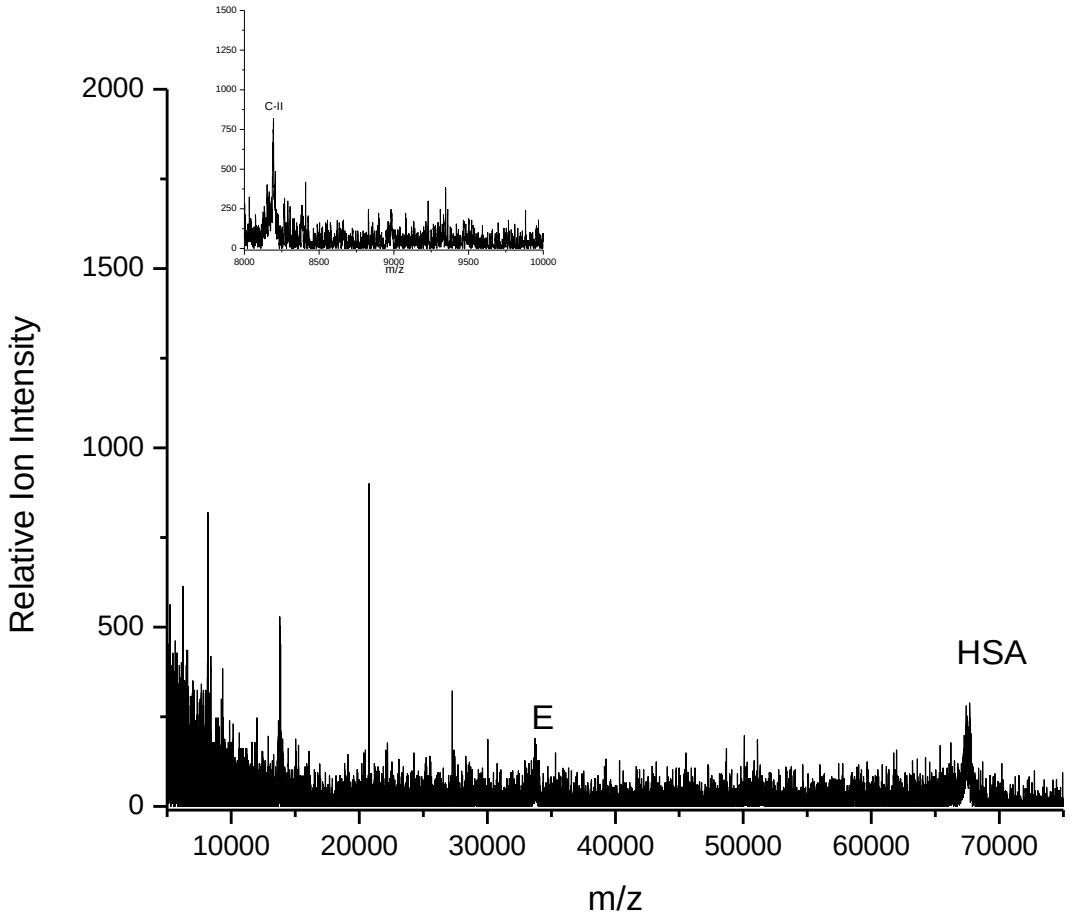

Figure 151. MALDI-MS protein spectra from CAD patient 143.

Table 125. Identification of apolipoproteins in the protein fraction from CAD patient 143.

Identification	Mass (Da)
ApoC-II'	8193.68
ApoE	33528.40
HSA	67423.67

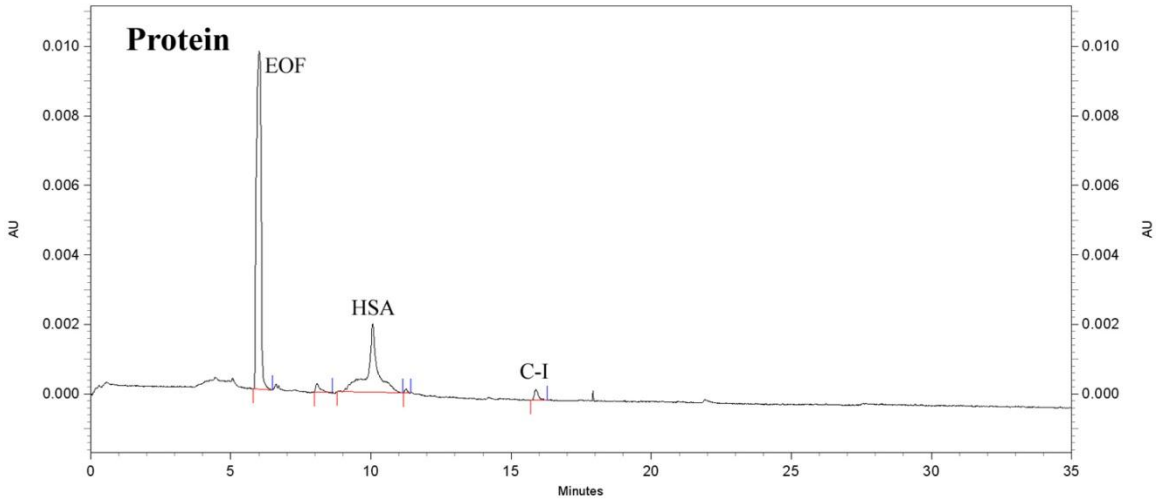

Figure 152. Electropherogram of the protein fraction from CAD patient 143.

Table 126. CE data for the protein fraction from a 200µL serum sample from CAD patient 143.

Protein	Elution Time (min)	Mobility (x $10^{-5}$$cm^2$/Vs)	CPA	Concentration (mg/dL)
HSA	11.2	-23.182	4181	4.21
ApoC-I	15.9	-30.860	155	0.37

The protein subfraction contained apos C-II, E, and HSA peaks as shown in the MALDI-MS spectra in Figure 151. Table 125 shows the peak masses for this fraction. The CE results from this fraction contained peaks corresponding to albumin and apoC-I, as shown in Figure 152.

Table 127. CAD patient 146 medical information

CAD Patient 146	
Age	77 years old
Height	61 inches
Weight	110 lbs.
Gender	Female
Race	Caucasian
Family History of Premature CAD/CAD/PVD	First Degree – No Second Degree – No
Major Risk Factors	Hypertension
Prior or Current History Of:	CABG – 3V
Current Medications	Statin, Beta Blockers, Estrogen
Highest LDL	160mg/dL

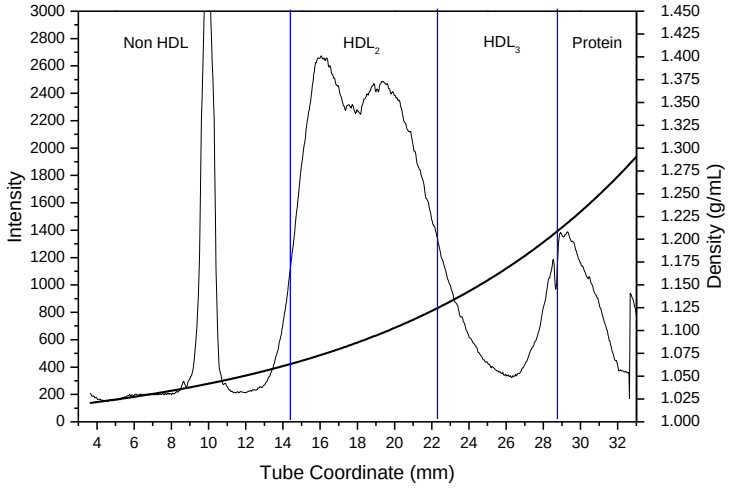

Figure 153. Lipoprotein density profile from CAD patient 146 in a 0.300M solution of Cs_2CdY, spun for 6 hours at 120,000RPM at 5°C after treatment with dextran sulfate.

CAD Patient 146 Discussion

CAD patient 146 whose medical history is presented in Table 127, is a 77 year old Caucasian female who has been diagnosed with CAD, has a family history of premature first and second degree CAD, and suffers from hypertension. Patient 146 also

has prior and/or current history of coronary artery bypass graft (CABG) surgery, and is currently prescribed and taking a statin, beta blocker, and estrogen therapy. Their highest LDL was above 160 mg/dL however, this patient has responded well to statin therapy. Patient 146 also has CAD despite elevated HDL levels. Figure 153 shows the Cs_2CdY profile for this subject which contains a slightly split peak with high intensity.

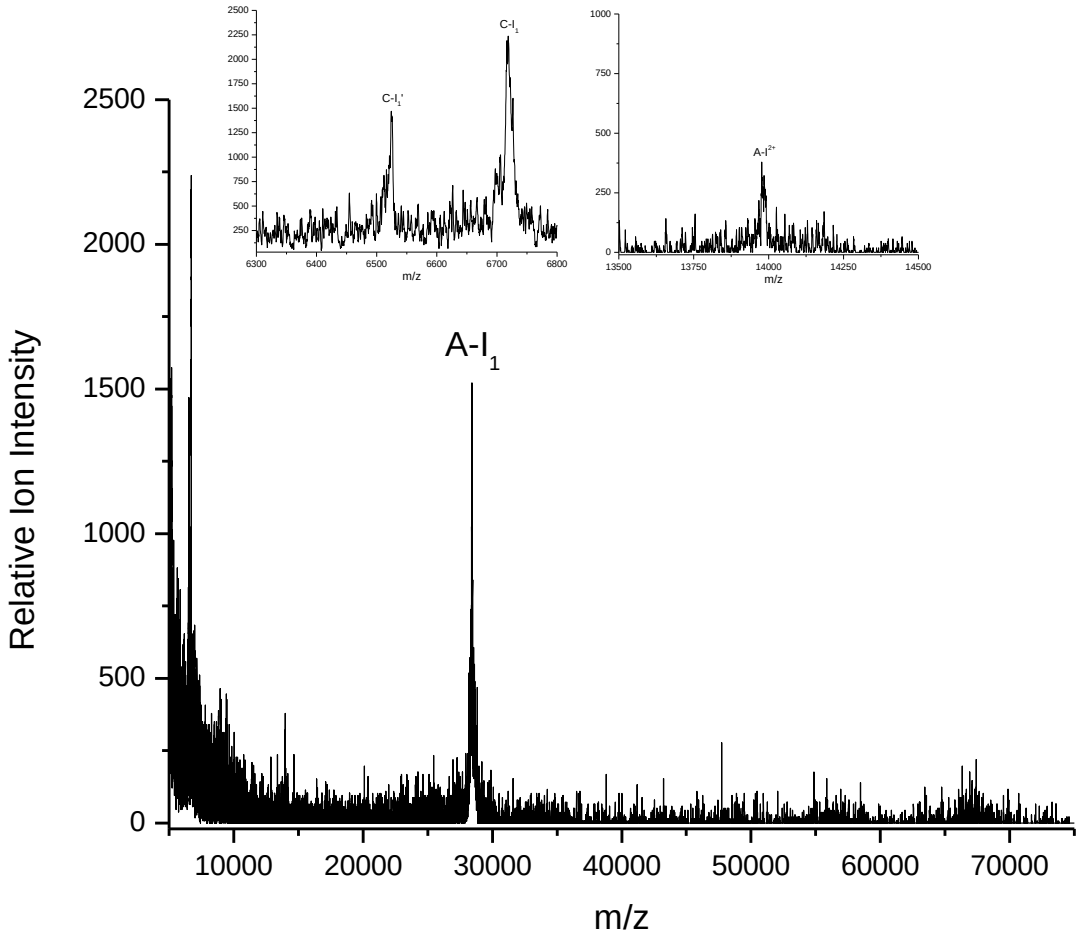

Figure 154. MALDI-MS non HDL Spectra from CAD patient 146.

Table 128. Identification of apolipoproteins in the non HDL fraction from CAD patient 146.

Identification	Mass (Da)
ApoC-I_1'	6524.31
ApoC-I_1	6718.87
ApoA-I^{2+}	13988.54
ApoA-I_1	28430.44

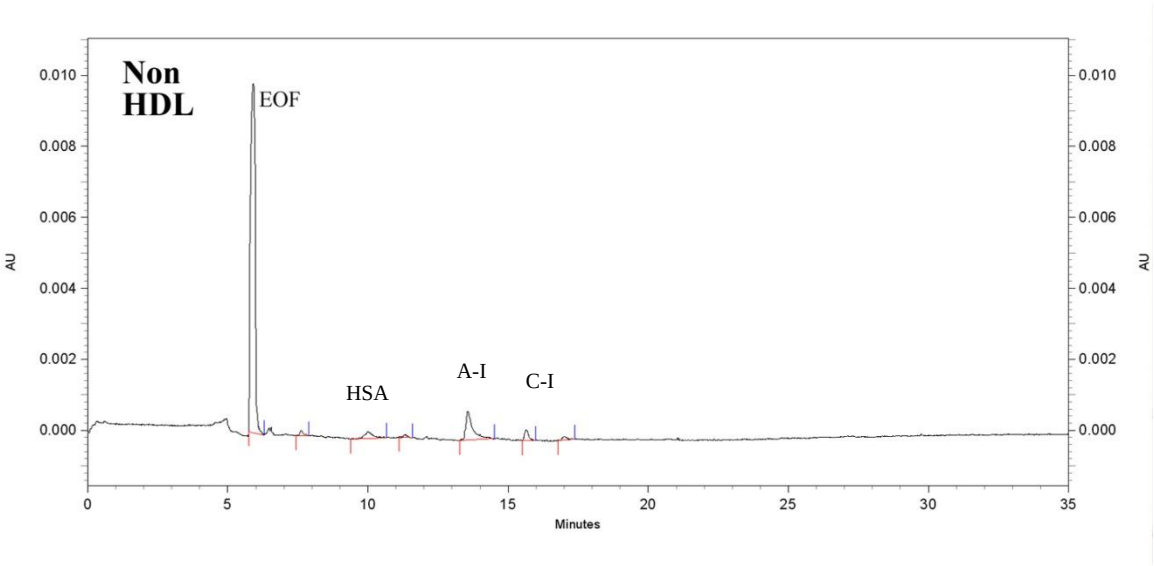

Figure 155. Electropherogram of the non HDL fraction from CAD patient 146.

Table 129. CE data for the non HDL fraction from a 200µL serum sample from CAD patient 146.

Protein	Elution Time (min)	Mobility (x $10^{-5}cm^2/Vs$)	CPA	Concentration (mg/dL)
HSA	10.0	-20.517	409	0.41
ApoA-I	13.5	-28.089	746	2.07
ApoC-I	15.7	-31.251	204	0.48

Figure 154 shows the MALDI-MS spectra for the non HDL subfraction which contained apos C-I_1', C-I_1, A-I^{2+}, and A-I_1. Table 128 shows the peak masses for this fraction. The apoC-I peaks were sharp with splitting near the base. The apoA-I_1 peak was sharp and had strong relative ion intensity. Figure 155 shows the CE results for this fraction which contained peaks corresponding to albumin, and apos A-I and C-I.

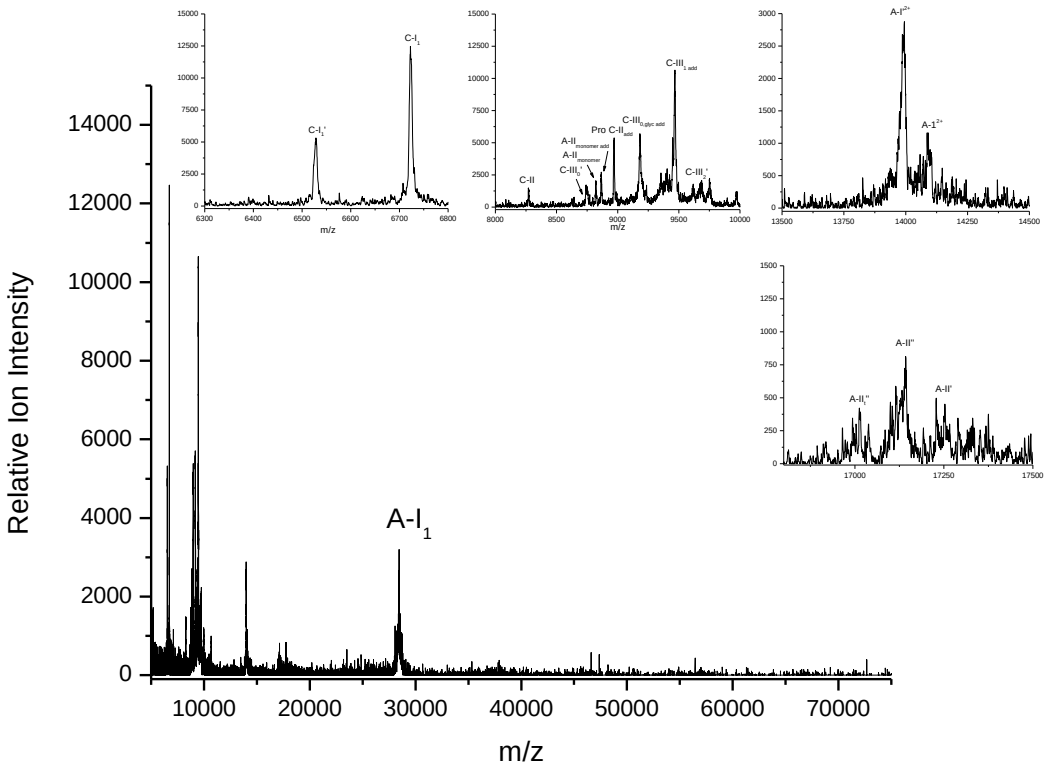

Figure 156. MALDI-MS HDL_2 spectra from CAD patient 146.

Table 130. Identification of apolipoproteins in the HDL_2 fraction from CAD patient 146.

Identification	Mass (Da)
ApoC-I_1'	6527.60
ApoC-I_1	6723.15
ApoC-II_{add}	8272.53

Table 130. (Continued)

Identification	Mass (Da)
ApoC-III_0'	8741.92
ApoA-II_m	8824.42
ApoA-$II_{m\ add}$	8865.95
Pro ApoC-II_{add}	8968.93
ApoC-$III_{0,\ glyc\ add}$	9180.59
ApoC-$III_{1\ add}$	9469.62
ApoC-III_2'	9679.53
ApoA-I'^{2+}	13994.75
ApoA-I^{2+}	14087.03
ApoA-II_t"	17013.47
ApoA-II"	17142.19
ApoA-II'	17251.95
ApoA-I_1	28455.20

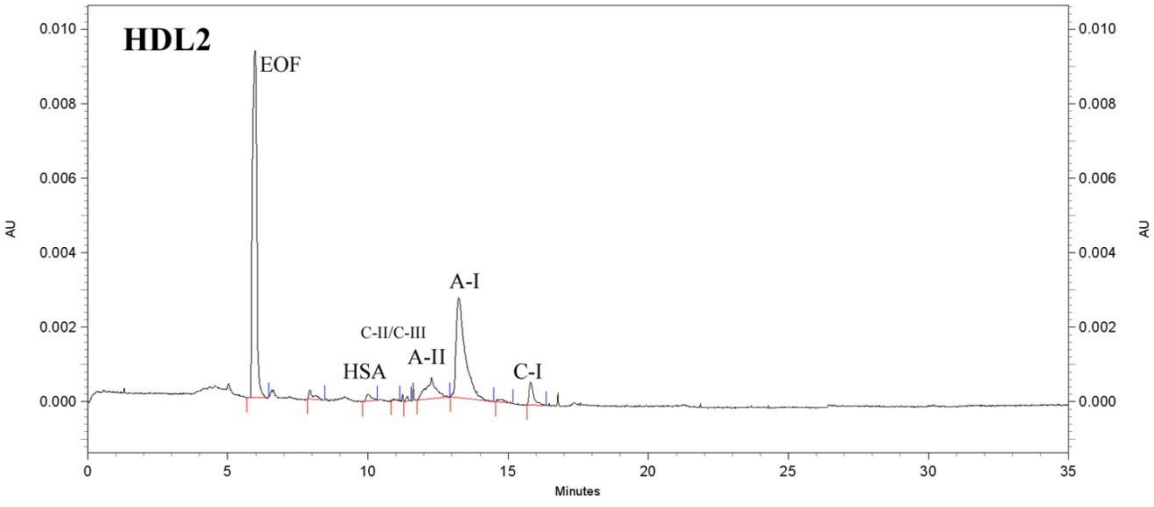

Figure 157. Electropherogram of the HDL_2 fraction from CAD patient 146.

Table 131. CE data for the HDL_2 fraction from a 200µL serum sample from CAD patient 146.

Protein	Elution Time (min)	Mobility (x $10^{-5}cm^2/Vs$)	CPA	Concentration (mg/dL)
ApoA-II	12.3	-25.773	949	0.96
ApoA-I	13.2	-27.535	3825	10.61
ApoC-I	15.8	-31.149	374	0.88

The HDL_2 subfraction MALDI-MS spectra contained apos C-I_1', C-I_1, C-II, C-III_0, A-II_m, Pro C-II, C-$III_{0,glyc}$, C-III_1, A-I^{2+}, A-II, and A-I_1, as shown in Figure 156. Table 130 shows the peak masses for this fraction. The apoC-I peaks were highly resolved and C-I_1 had a relative ion intensity that was approximately twice the intensity of C-I_1'. The CE results in Figure 157 detected peaks corresponding to apoA-II, apoA-I, and apoC-I.

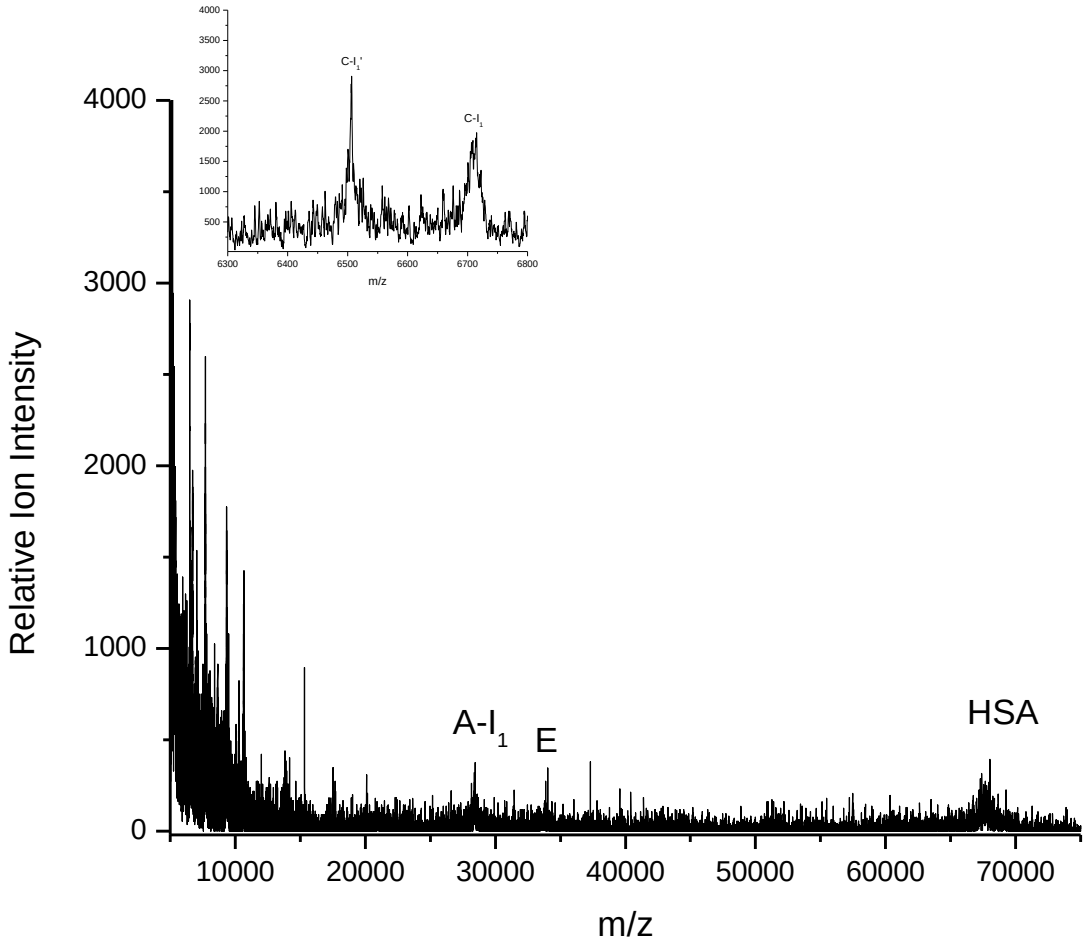

Figure 158. MALDI-MS HDL_3 spectra from CAD patient 146.

Table 132. Identification of apolipoproteins in the HDL_3 fraction from CAD patient 146.

Identification	Mass (Da)
ApoC-I_1'	6506.11
ApoC-I_1	6715.07
ApoA-I_1	28438.95
ApoE	34010.38
HSA	68033.10

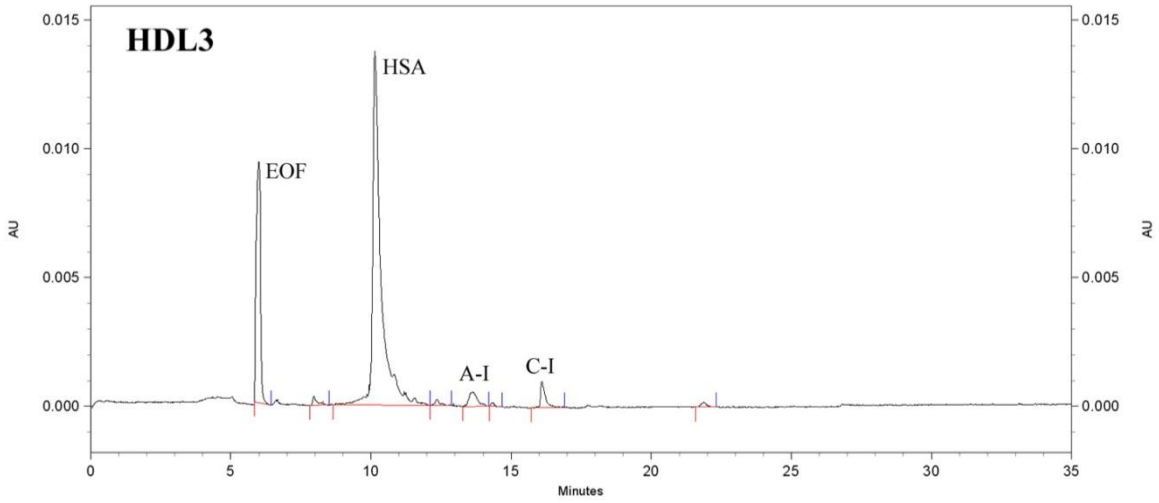

Figure 159. Electropherogram of the HDL_3 fraction from CAD patient 146.

Table 133. CE data for the HDL_3 fraction from a 200µL serum sample from CAD patient 146.

Protein	Elution Time (min)	Mobility (x $10^{-5}cm^2/Vs$)	CPA	Concentration (mg/dL)
HSA	10.1	-20.454	23333	23.49
ApoA-I	13.6	-27.895	721	2.00
ApoC-I	16.1	-31.248	605	1.43
Unidentified	21.9	-36.070	91	-------

The HDL_3 subfraction MALDI-MS spectra contained C-I_1', C-I_1, apoA-I_1, E, and HSA which are shown in Figure 158. Table 132 shows the peak masses for this fraction. The C-I peaks were much lower in intensity than HDL_2 and poorly resolved, C-I_1 appeared to have splitting to form the earliest appearance of a doublet and was less intense than C-I_1'. Figure 159 shows the CE results from this fraction which contained a sharp albumin peak and small peaks corresponding to apos A-I and C-I.

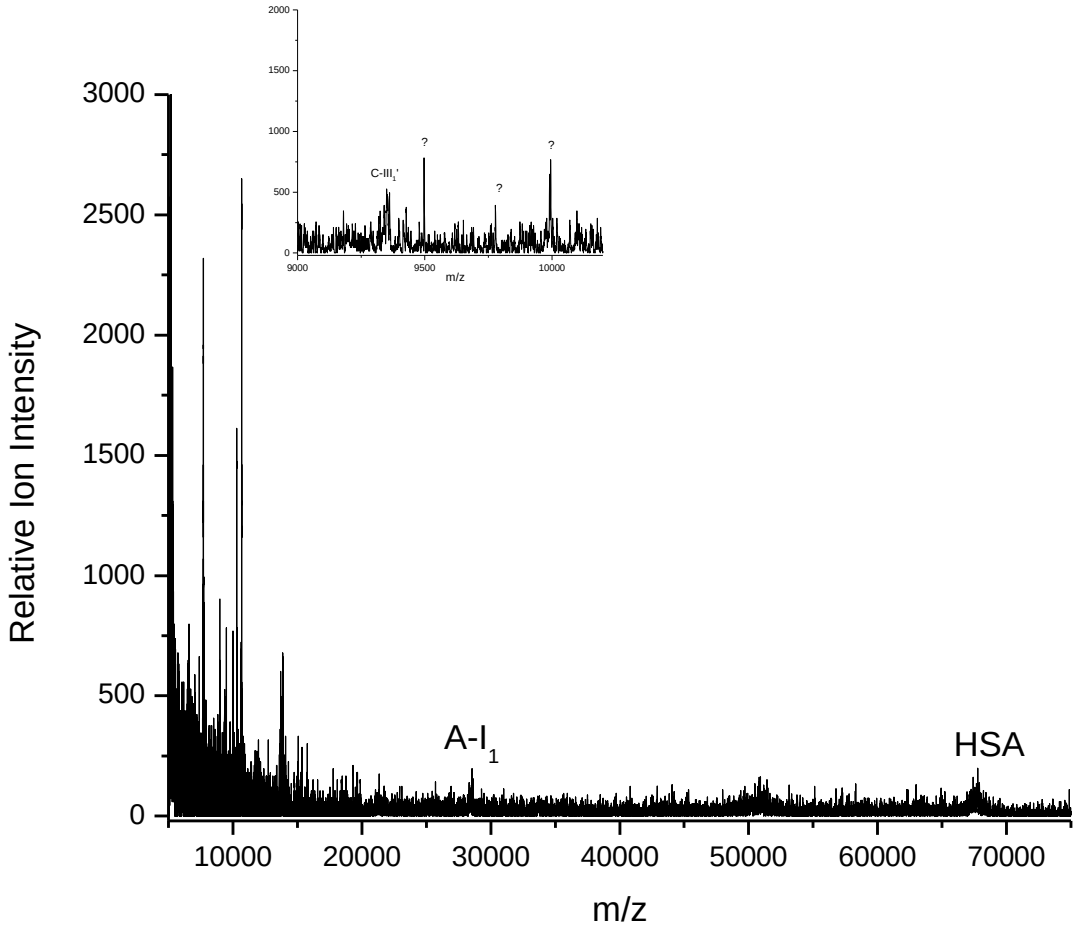

Figure 160. MALDI-MS protein spectra from CAD patient 146.

Table 134. Identification of apolipoproteins in the protein fraction from CAD patient 146.

Identification	Mass (Da)
ApoC-III_1'	9354.02
Unidentified Peak 1	9994.69
Unidentified Peak 2	10300.16
Unidentified Peak 3	10667.42
ApoA-I_1	28582.37
HSA	67575.75

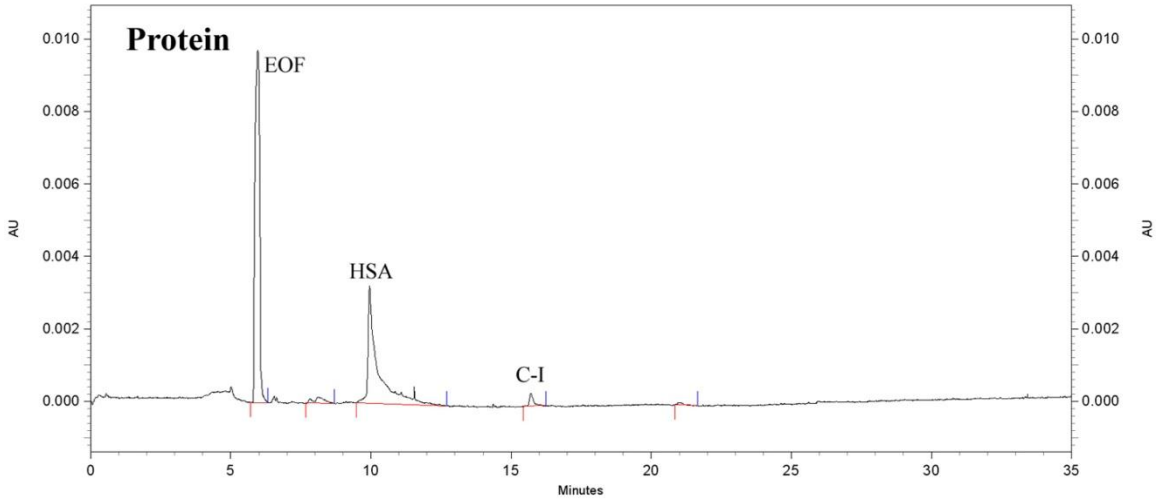

Figure 161. Electropherogram of the protein fraction from control patient 146.

Table 135. CE data for the protein fraction from a 200µL serum sample from control patient 146.

Protein	Elution Time (min)	Mobility (x $10^{-5}$$cm^2$/Vs)	CPA	Concentration (mg/dL)
HSA	10.9	-20.171	6508	6.55
ApoC-I	15.7	-31.056	187	0.44
Unidentified	21.1	-35.818	43	-------

The protein subfraction MALDI-MS spectra, shown in Figure 160 contained A-I_1, HSA and three unidentified proteins. Table 134 shows the peak masses for this fraction. The three unidentified proteins were sharp with strong relative ion intensity, while A-I_1 and HSA were poorly resolved and hardly visible. The CE results shown in Figure 161 contained albumin, apoC-I, and an unidentified peak.

Table 136. CAD patient 170 medical information

CAD Patient 170	
Age	75 years old
Gender	Male
Race	Caucasian
Major Risk Factors	Family history of CAD, Hypertension, Tobacco use
Current Medications	Statin, Niacin

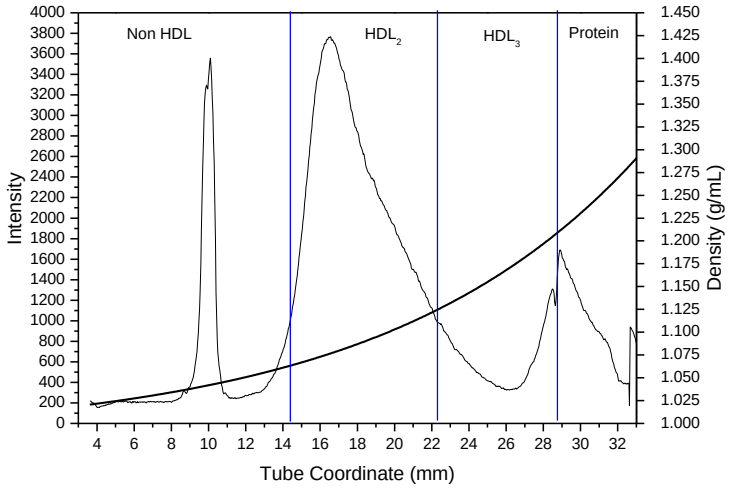

Figure 162. Lipoprotein density profile from CAD patient 170 in a 0.300M solution of Cs_2CdY, spun for 6 hours at 120,000RPM at 5°C after treatment with dextran sulfate.

CAD Patient 170 Discussion

CAD patient 170 whose medical history is presented in Table 136, is a 75 year old Caucasian male who has been diagnosed with CAD, has a family history of CAD, uses tobacco products, and suffers from hypertension. Patient 170 is currently prescribed and taking niacin and a statin. Figure 162 shows the Cs_2CdY profile for this patient which contains a sharp peak shifted towards the non HDL fraction.

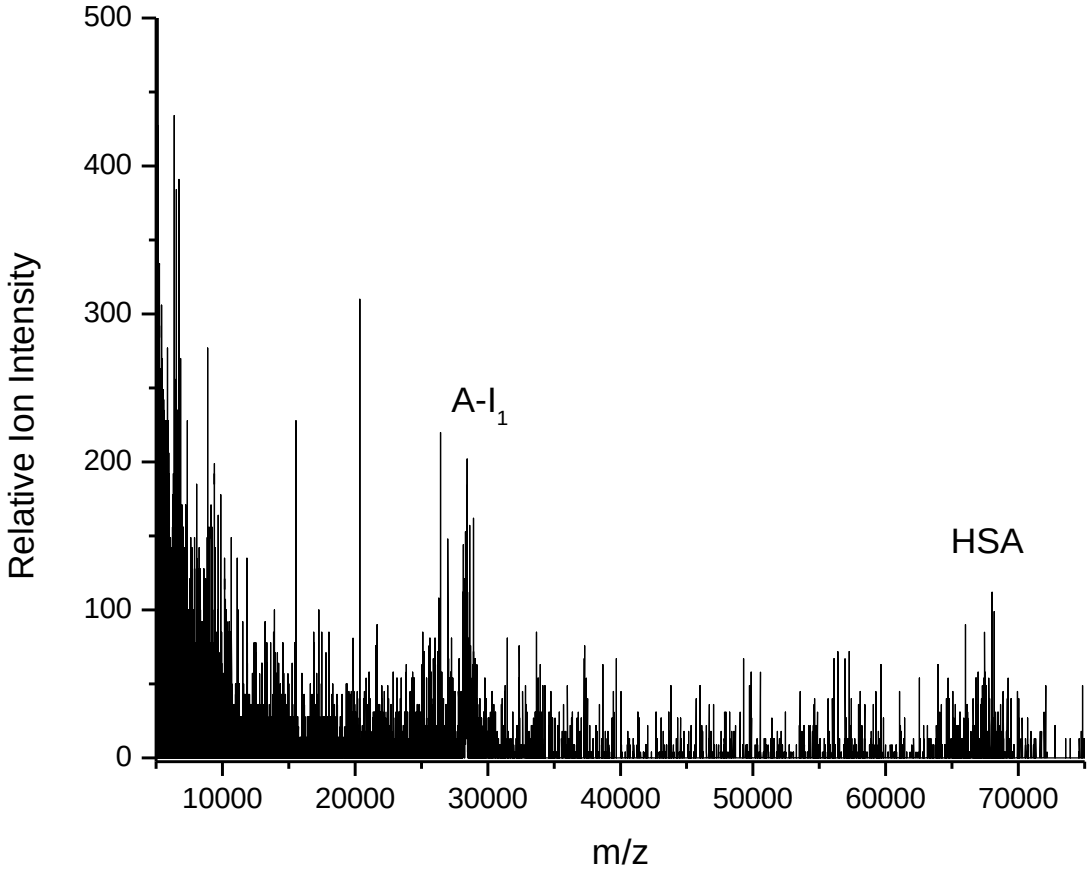

Figure 163. MALDI-MS non HDL spectra from CAD patient 170.

Table 137. Identification of apolipoproteins in the non HDL fraction from CAD patient 170.

Identification	Mass (Da)
ApoA-I_1	28479.85
HSA	67487.64

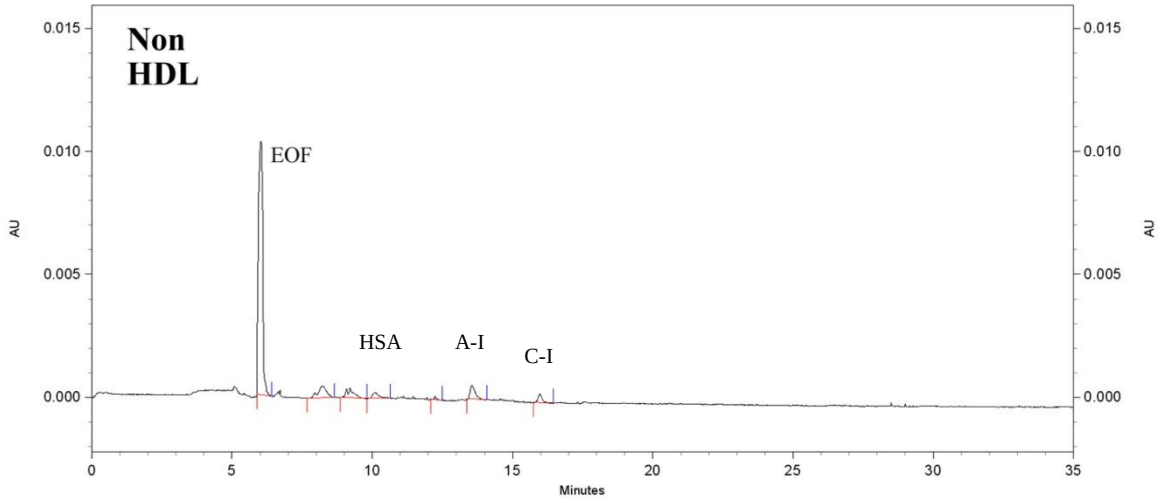

Figure 164. Electropherogram of the non HDL fraction from CAD patient 170.

Table 138. CE data for the non HDL fraction from a 200µL serum sample from CAD patient 170.

Protein	Elution Time (min)	Mobility (x $10^{-5}cm^2/Vs$)	CPA	Concentration (mg/dL)
HSA	10.1	-20.073	288	0.29
ApoA-II	12.2	-25.194	25	-------
ApoA-I	13.6	-27.550	410	1.13
ApoC-I	16.0	-30.834	189	0.45

Figure 163 shows the MALDI-MS spectrum for the non HDL subfraction which contained apoA-I_1 and HSA, both poorly resolved and low in relative ion intensity. Table 137 shows the peak masses for this fraction. The CE results for this fraction, shown in Figure 164, detected small peaks corresponding to albumin, apoA-I, and apoC-I.

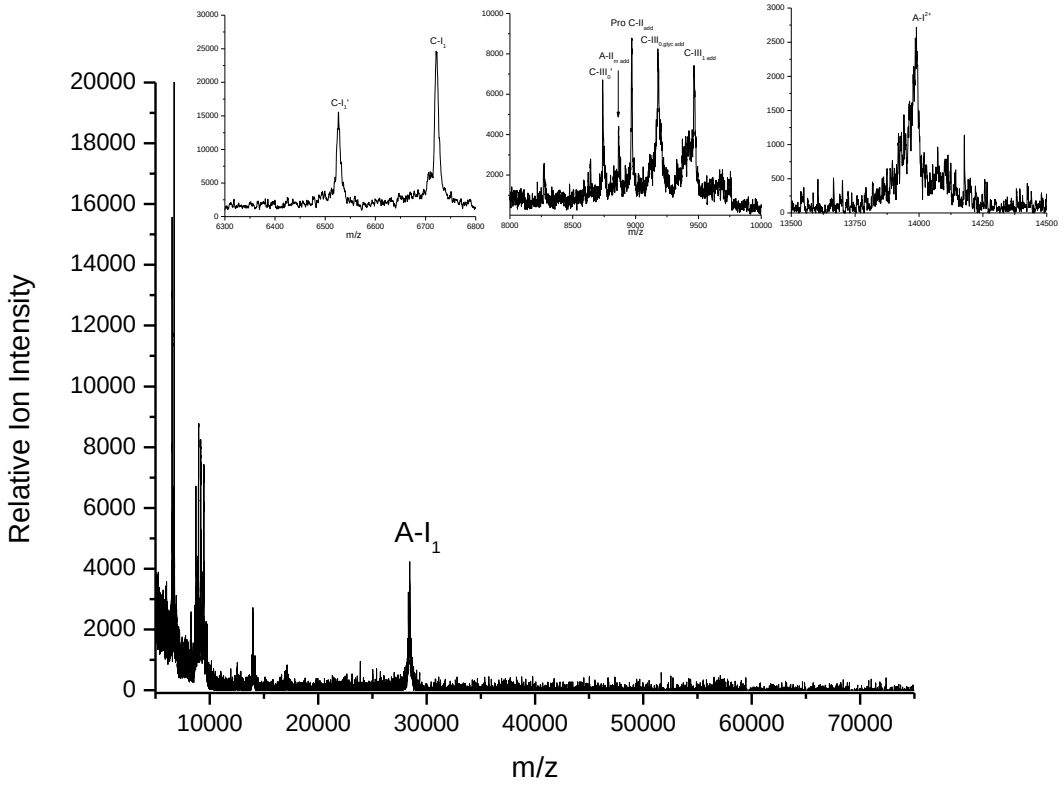

Figure 165. MALDI-MS HDL_2 spectra from CAD patient 170.

Table 139. Identification of apolipoproteins in the HDL_2 fraction from CAD patient 170.

Identification	**Mass (Da)**
ApoC-I_1'	6526.27
ApoC-I_1	6721.89
ApoC-III_0'	8738.28
Pro ApoA-$II_{m\ add}$	8866.18
Pro ApoC-$II_{\ add}$	8973.60
ApoC-$III_{0,glyc\ add}$	9179.79
ApoC-$III_{1\ add}$	9464.72
ApoA-I^{2+}	13900.80
ApoA-I_1	28460.02

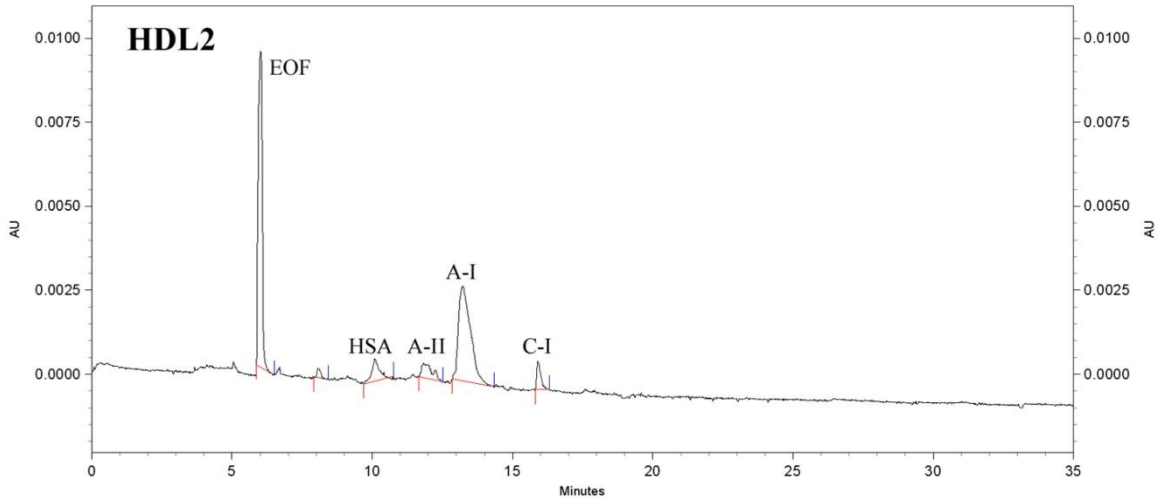

Figure 166. Electropherogram of the HDL_2 fraction from CAD patient 170.

Table 140. CE data for the HDL_2 fraction from a 200µL serum sample from CAD patient 170**.**

Protein	Elution Time (min)	Mobility (x $10^{-5}cm^2/Vs$)	CPA	Concentration (mg/dL)
HSA	10.1	-20.098	988	0.99
ApoA-II	11.8	-24.433	814	-------
ApoA-I	13.2	-27.089	5346	14.8
ApoC-I	15.9	-30.836	450	1.06

The HDL_2 subfraction MALDI-MS spectra, shown in Figure 165, contained apos C-I_1', C-I_1, C-III_0, A-$II_{monomer}$, Pro C-II, C-$III_{0,glyc}$, C-III_1, A-I^{2+}, and A-I_1. Table 139 shows the peak masses for this fraction. The apoC-I peaks were strongly resolved and there appeared to be a shoulder on C-I_1. The 8000 – 10000 *m/z* region was also strongly resolved with high intensity. ApoA-I^{2+} was sharp with splitting near the base. The CE

results from this subfraction, shown in Figure 166 contained peaks corresponding to albumin, apoA-II, A-I, and C-I.

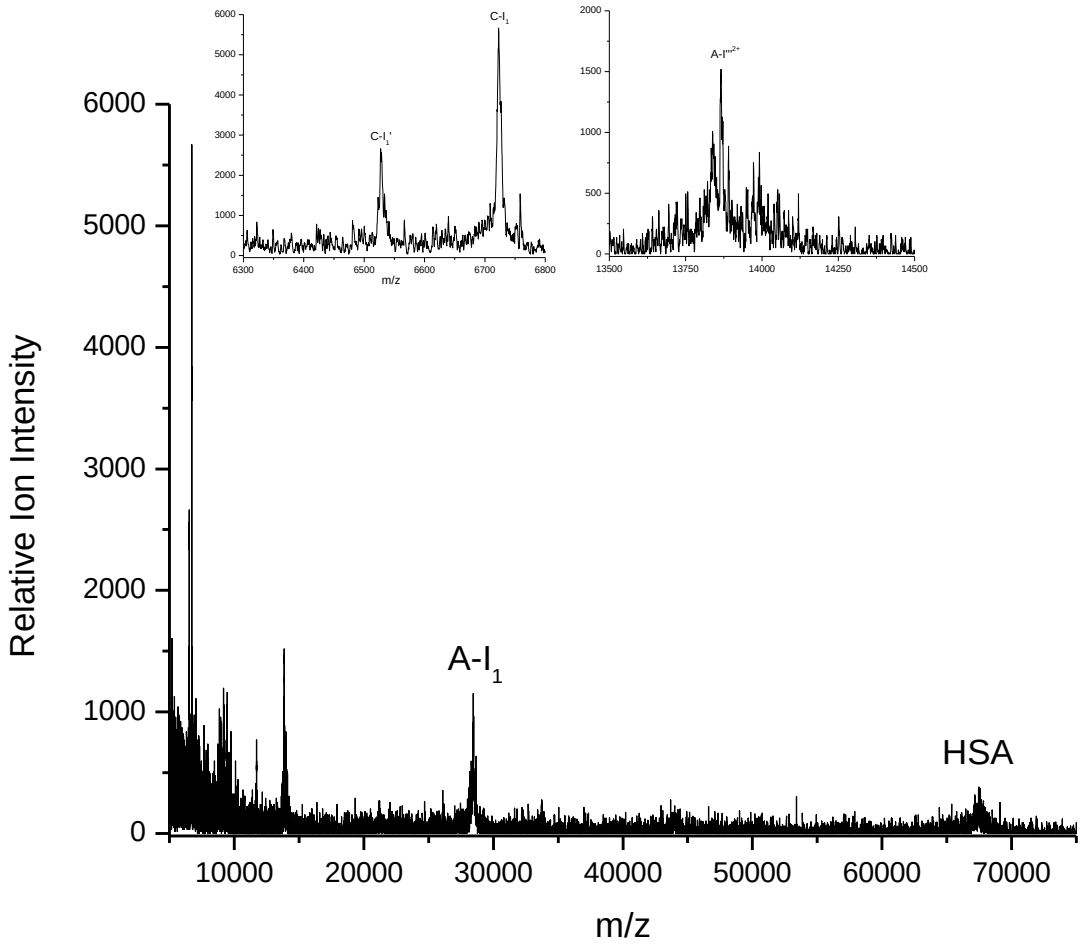

Figure 167. MALDI-MS HDL_3 spectra from CAD patient 170.

Table 141. Identification of apolipoproteins in the HDL_3 fraction from CAD patient 170.

Identification	Mass (Da)
ApoC-I_1'	6528.17
ApoC-I_1	6723.56
ApoA-I'''^{2+}	1366.98
ApoA-I_1	28450.25
HSA	67599.83

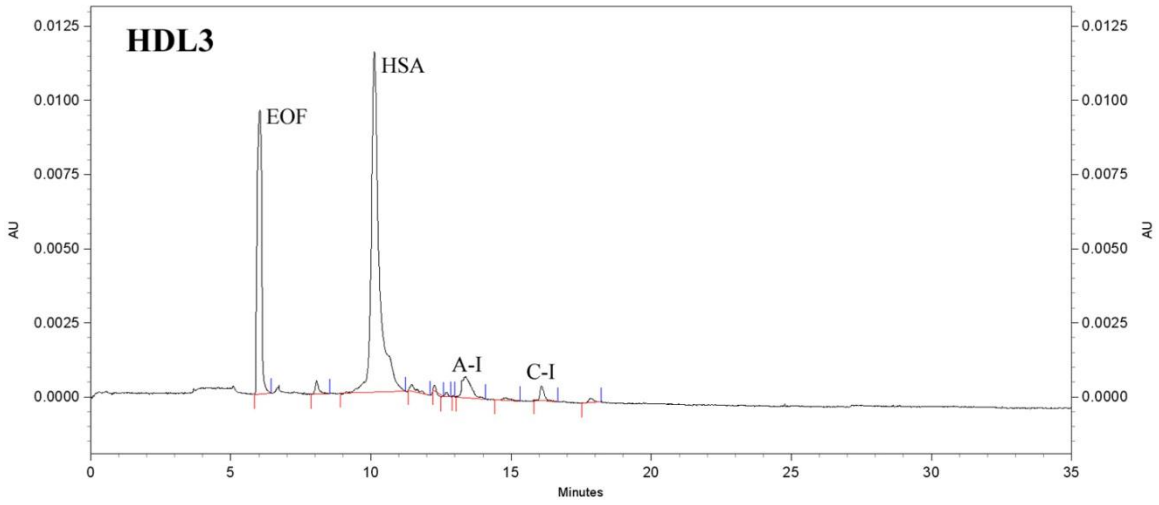

Figure 168. Electropherogram of the HDL_3 fraction from CAD patient 170.

Table 142. CE data for the HDL_3 fraction from a 200µL serum sample from CAD patient 170.

Protein	Elution Time (min)	Mobility (x $10^{-5}cm^2/Vs$)	CPA	Concentration (mg/dL)
HSA	10.1	-20.069	18562	18.59
ApoA-I	13.3	-26.896	1532	4.25
ApoC-I	16.1	-30.895	253	0.60

The HDL_3 subfraction MALDI-MS spectra, shown in Figure 167, contained apos C-I_1', C-I_1, A-I^{2+}, A-I_1, and HSA. Table 141 shows the peak masses for this fraction. The apoC-I peaks were sharp and C-I_1 had a relative ion intensity that was 3 times higher than that of C-I_1'. The CE results, shown in Figure 168 contained albumin, apoA-I, and apoC-I.

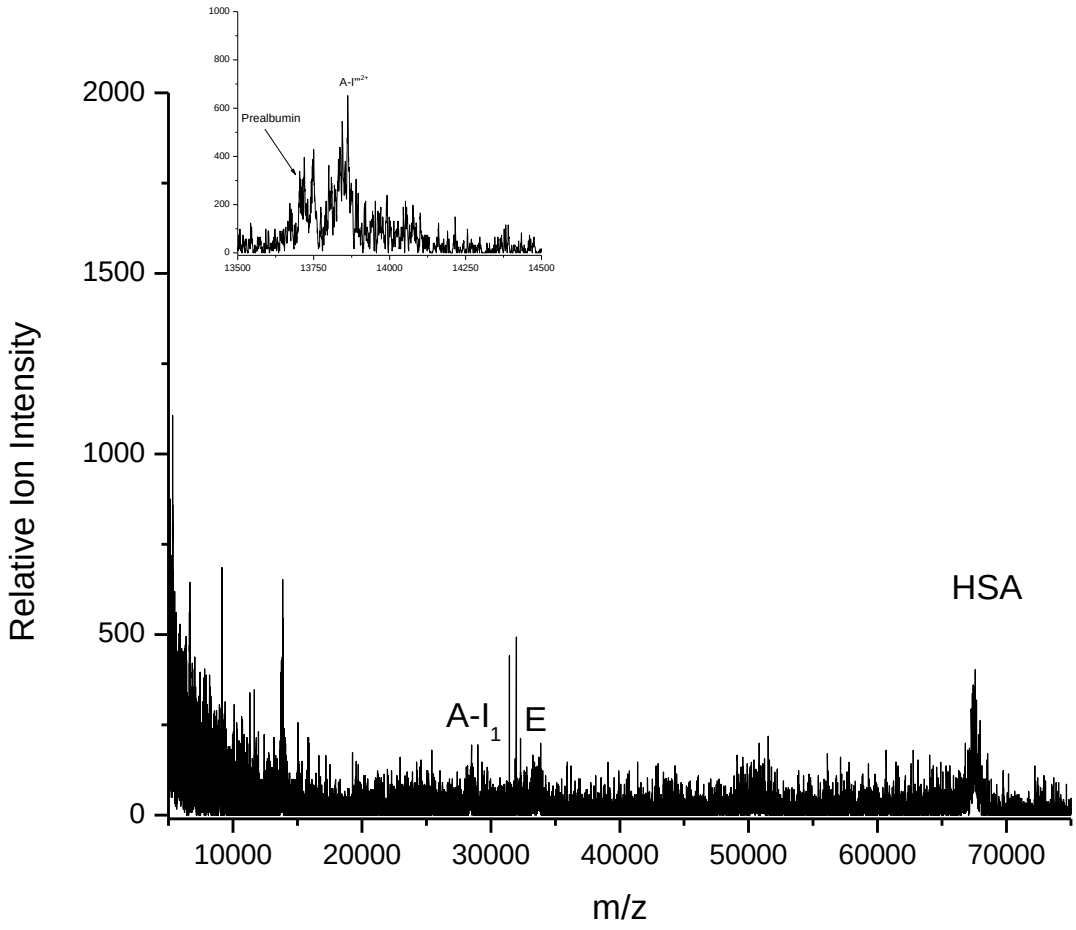

Figure 169. MALDI-MS protein spectra from CAD patient 170.

Table 143. Identification of apolipoproteins in the HDL_2 fraction from CAD patient 146.

Identification	Mass (Da)
Prealbumin	13747.16
ApoA-I'''$^{2+}$	13862.13
ApoA-I_1	28385.77
ApoE	33981.78
HSA	67645.52

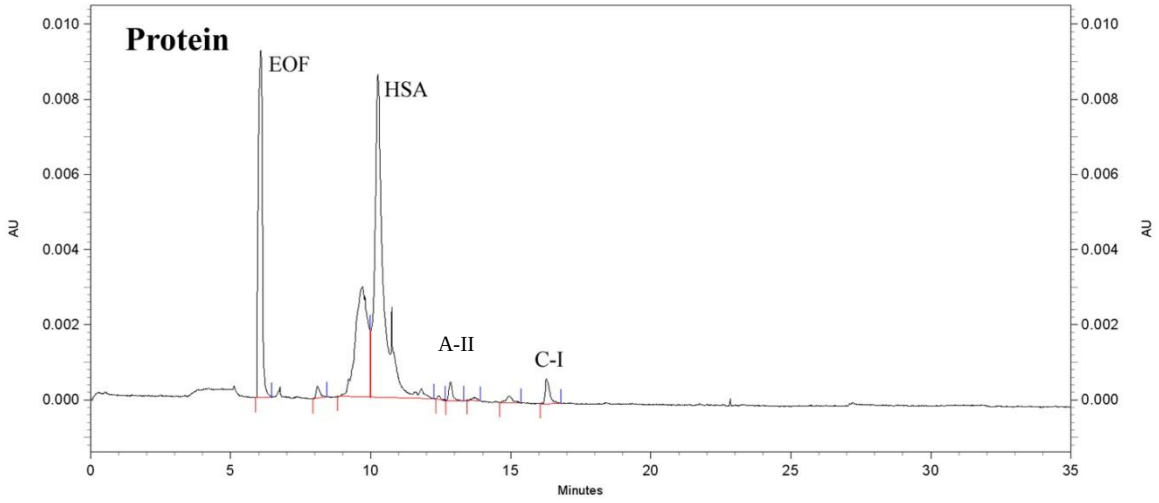

Figure 170. Electropherogram of the protein fraction from CAD patient 170.

Table 144. CE data for the protein fraction from a 200µL serum sample from CAD patient 170.

Protein	Elution Time (min)	Mobility (x $10^{-5}cm^2/Vs$)	CPA	Concentration (mg/dL)
HSA	10.3	-20.205	15119	15.22
ApoA-II	12.9	-25.950	287	-------
ApoA-I	15.0	-29.184	165	0.46
ApoC-I	16.3	-30.770	383	0.90

Table 145. CAD patient 195 medical information

CAD Patient 195	
Age	72 years old
Height	64 inches
Weight	132 lbs.
Gender	Female
Race	Caucasian
Family History of Premature CAD/CAD/PVD	First Degree – No Second Degree – No
Major Risk Factors	Hypertension
Prior or Current History Of:	Angina, CABG, PVD – mesenteric
Current Medications	Statin, Alpha Blocker
Highest LDL	130 - 160mg/dL
Highest TG	< 150mg/dL
Any Prior HDL <35	No
Any Prior Homocysteine >14	No

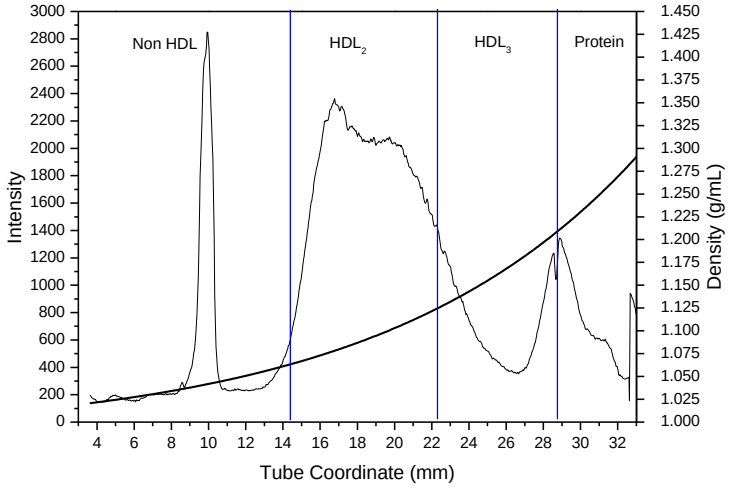

Figure 171. Lipoprotein density profile from CAD patient 195 in a 0.300M solution of Cs_2CdY, spun for 6 hours at 120,000RPM at 5°C after treatment with dextran sulfate.

The protein subfraction MALDI-MS spectra contained prealbumin, apos A-I_1, E, and HSA, shown in Figure 169. Table 143 shows the peak masses for this fraction. Figure 170 shows the CE results for this fraction which contain albumin, apoA-II, apoA-I, and apoC-I.

CAD Patient 195 Discussion

CAD patient 195 whose medical history is presented in Table 145, is a 72 year old Caucasian female who has been diagnosed with CAD, has a family history of premature first and second degree CAD, and suffers from hypertension. Patient 195 has prior and/or current history of angina, coronary artery bypass graft (CABG) surgery, and peripheral vascular disease, and is currently prescribed and taking a statin and alpha blocker. Their highest LDL was between 130 - 160 mg/dL and their highest triglyceride level was below 150 mg/dL. There are no prior levels of HDL below 35mg/dL or homocysteine levels above 14 mg/dL. Patient 195 was a low birth weight infant and has CAD despite elevated HDL levels. Figure 171 shows the Cs_2CdY profile for this subject which contains a broad peak with a shoulder on its denser side.

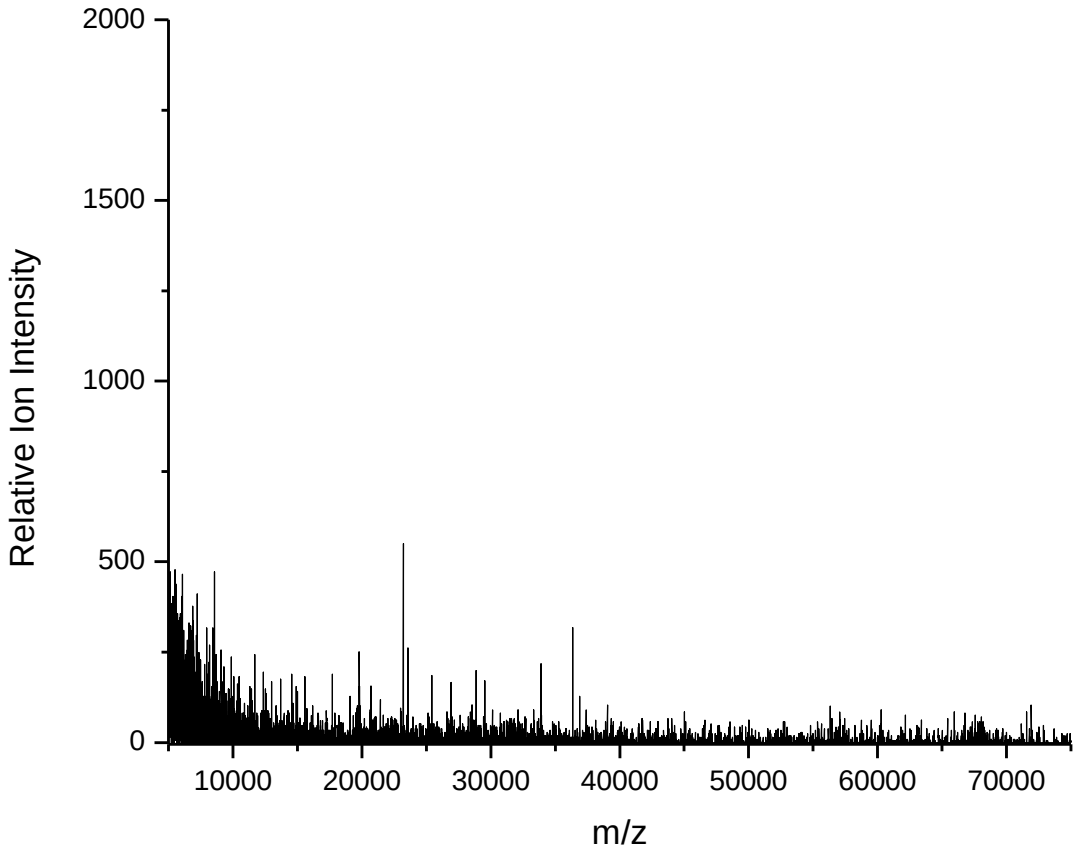

Figure 172. MALDI-MS non HDL spectra from CAD patient 195.

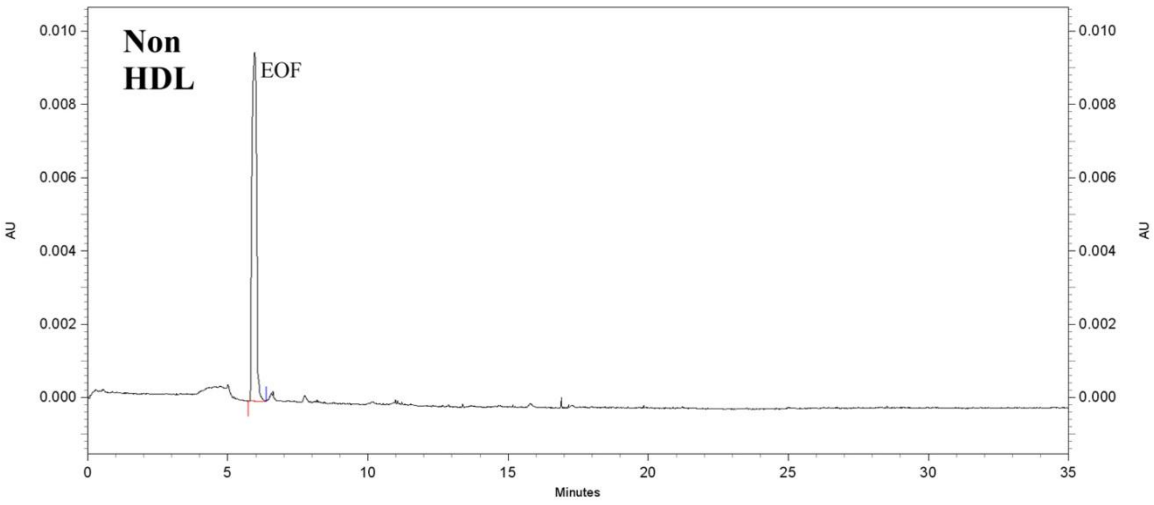

Figure 173. Electropherogram of the non HDL fraction from CAD patient 195.

Figure 172 shows the MALDI-MS spectra for the non HDL subfraction which did not contain any proteins. Comparably, the CE results of this subfraction, shown in Figure 173, did not contain any proteins.

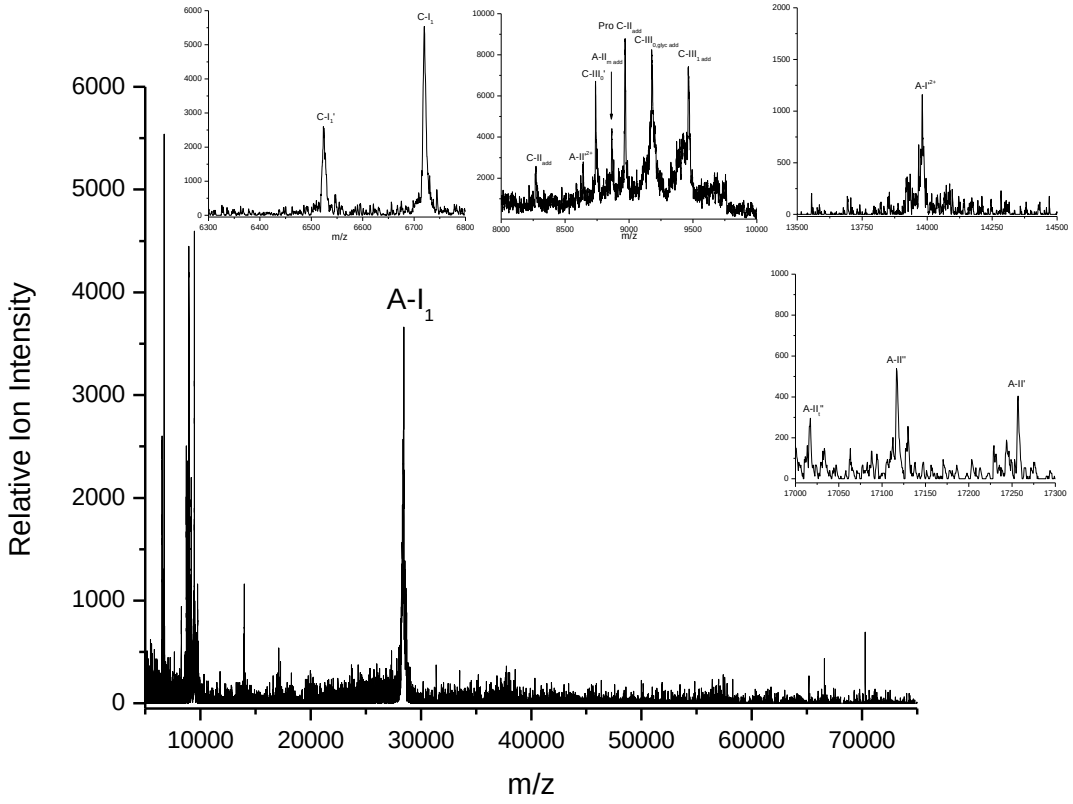

Figure 174. MALDI-MS HDL_2 spectra from CAD patient 195.

Table 146. Identification of apolipoproteins in the HDL_2 fraction from CAD patient 195.

Identification	Mass (Da)
ApoC-I_1'	6524.48
ApoC-I_1	6720.08
ApoC-II_{add}	8271.73
ApoA-II'^{2+}	8647.25
ApoC-III_0'	8738.28
ApoA-$II_{m\ add}$	8866.18
Pro ApoC-II_{add}	8969.05
ApoC-$III_{0,\ glyc\ add}$	9179.79
ApoC-$III_{1\ add}$	9460.63
ApoA-I^{2+}	13981.27

Table 146. (Continued)

Identification	Mass (Da)
ApoA-II_t"	17071.21
ApoA-II"	17116.89
ApoA-II'	17256.85
ApoA-I_1	28439.29

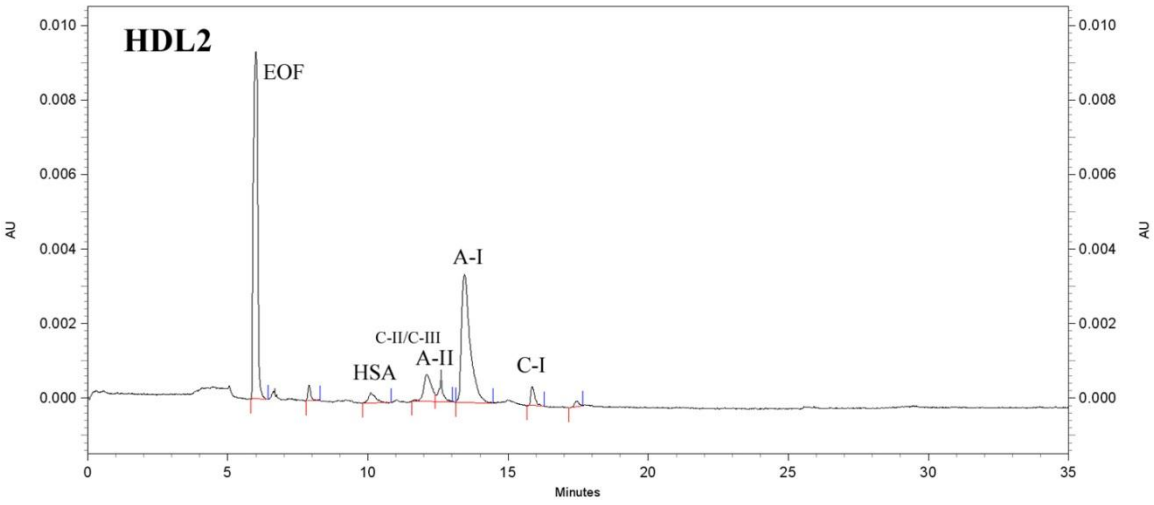

Figure 175. Electropherogram of the HDL_2 fraction from CAD patient 195.

Table 147. CE data for the HDL_2 fraction from a 200µL serum sample from CAD patient 195.

Protein	Elution Time (min)	Mobility (x $10^{-5}cm^2/Vs$)	CPA	Concentration (mg/dL)
HSA	10.1	-20.259	384	0.39
ApoC-III	12.1	-25.122	990	-------
ApoA-II	12.6	-26.125	453	-------
ApoA-I	13.4	-27.579	4566	12.67
ApoC-I	15.9	-30.925	272	0.64
Unidentified	17.5	-32.618	78	-------

The HDL_2 subfraction MALDI-MS spectra, shown in Figure 174, contained apos C-I_1', C-I_1, C-II, A-II^{2+}, C-III_0, C-III_1, A-I^{2+}, A-II, and A-I_1. Table 146 shows the peak masses for this fraction. The apoC-I peaks were sharp and highly resolved as were all other proteins in this fraction. The CE results from this fraction, shown in Figure 175, contained albumin apos C-III, A-II, A-I, C-I, and an unidentified peak.

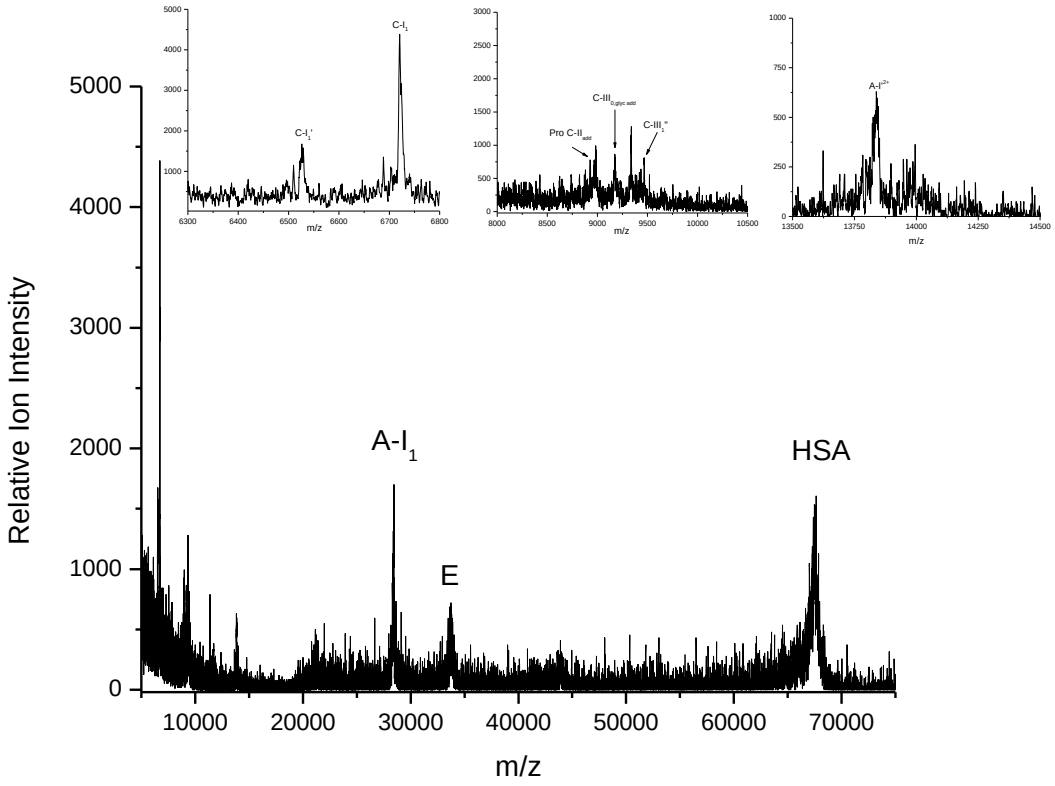

Figure 176. MALDI-MS HDL_3 spectra from CAD patient 195.

Table 148. Identification of apolipoproteins in the HDL_3 fraction from CAD patient 195.

Identification	Mass (Da)
ApoC-I_1'	6526.32
ApoC-I_1	6721.46
Pro ApoC-II_{add}	8984.29
ApoC-$III_{0,\ glyc\ add}$	9175.47

Table 148. (Continued)

Identification	Mass (Da)
ApoC-III$_1$'	9340.46
ApoA-I'$^{2+}$	13986.13
ApoA-I$_1$	28445.32
ApoE	33676.44
HSA	67352.79

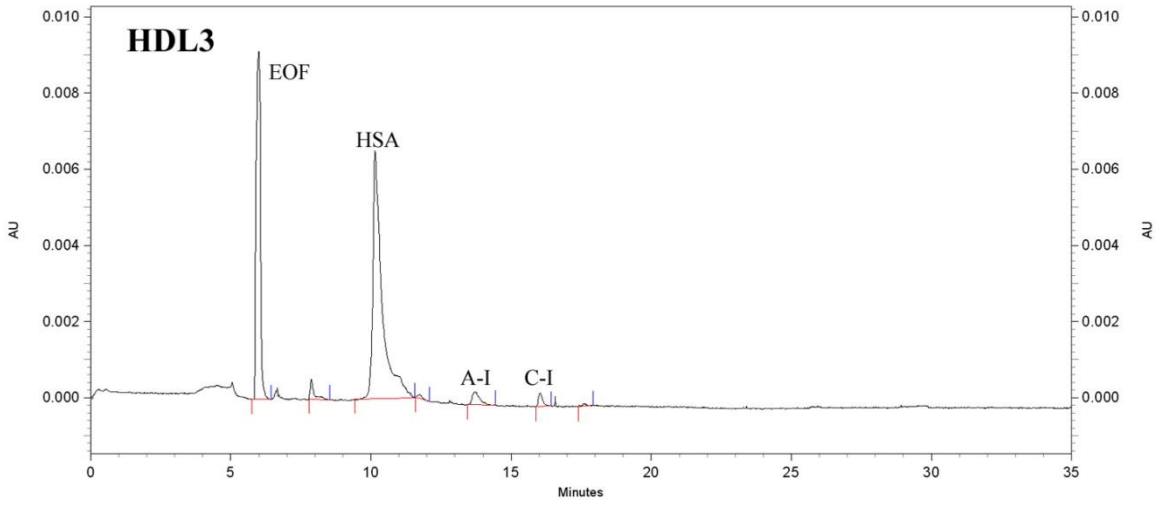

Figure 177. Electropherogram of the HDL$_3$ fraction from CAD patient 195.

Table 149. CE data for the HDL$_3$ fraction from a 200µL serum sample from CAD patient 195.

Protein	Elution Time (min)	Mobility (x 10^{-5}cm^2/Vs)	CPA	Concentration (mg/dL)
HSA	10.2	-20.473	12125	12.21
ApoA-I	13.7	-28.053	373	1.03
ApoC-I	16.0	-31.175	193	0.46

The HDL_3 subfraction MALDI-MS spectra, shown in Figure 176, contained apos C-I_1', C-I_1, Pro C-II, C-$III_{0,glyc}$, C-III_1, A-I^{2+}, A-I_1, E, and HSA. Table 148 shows the peak masses for this fraction. The C-I_1 peak was comparable in intensity to the apoC-I peaks in HDL_2, however, C-I_1', was poorly resolved and very low in intensity. The CE results from this fraction, shown in Figure 177, contained albumin, and apos A-I and C-I.

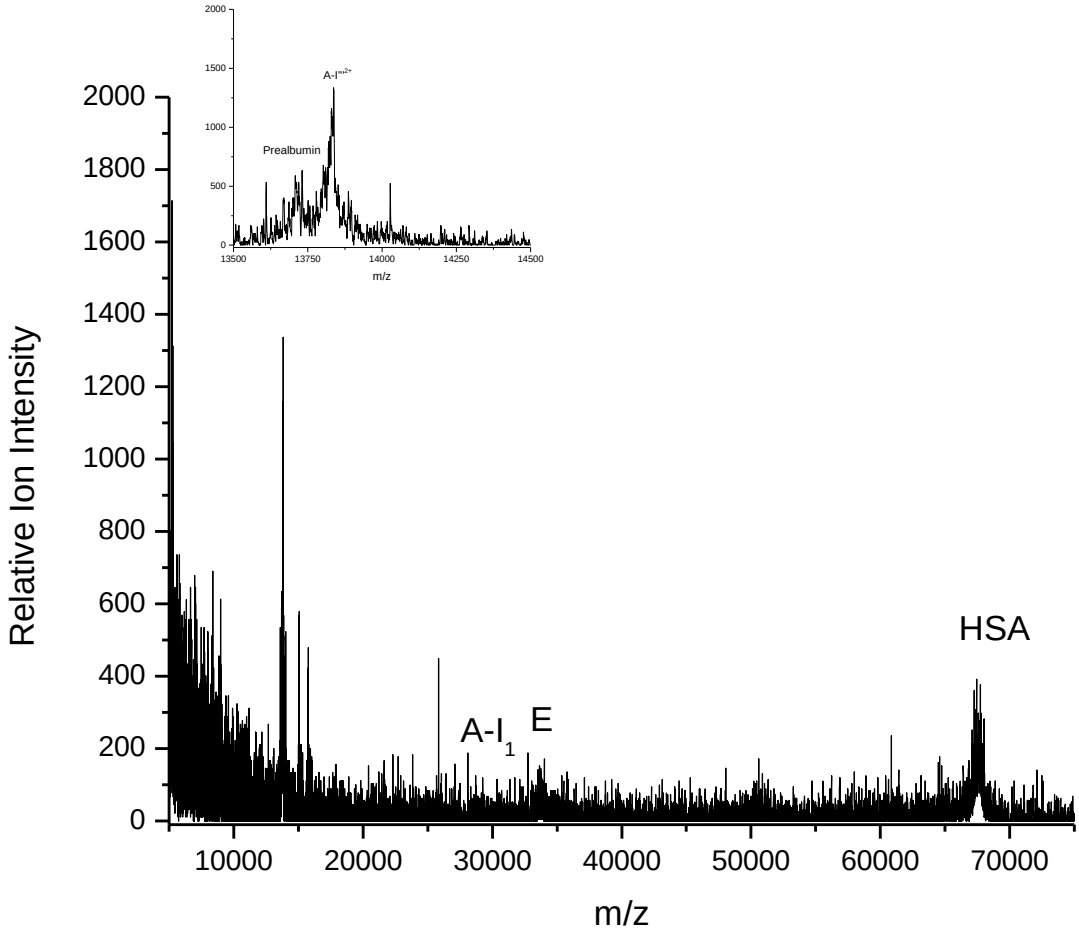

Figure 178. MALDI-MS protein spectra from CAD patient 195.

Table 150. Identification of apolipoproteins in the protein fraction from CAD patient 195.

Identification	Mass (Da)
Prealbumin	13710.35
ApoA-I'''$^{2+}$	13836.88
ApoA-I_1	28513.88
ApoE	33693.56
HSA	67441.09

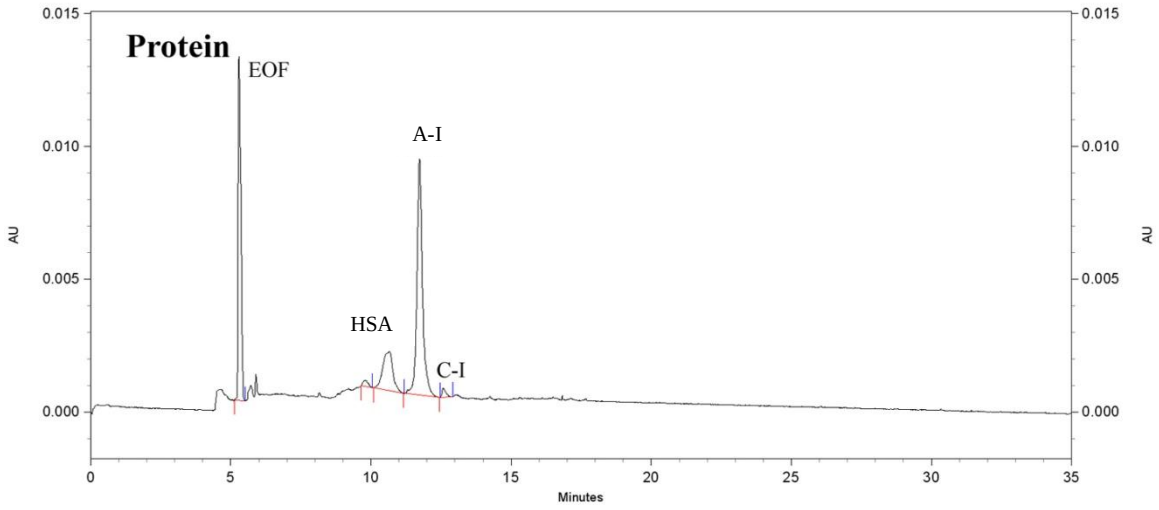

Figure 179. Electropherogram of the protein fraction from CAD patient 195.

Table 151. CE data for the protein fraction from a 200µL serum sample from CAD patient 195.

Protein	Elution Time (min)	Mobility (x $10^{-5}$$cm^2$/Vs)	CPA	Concentration (mg/dL)
HSA	10.7	-28.639	2895	2.91
ApoA-I	11.7	-31.209	8751	24.28
ApoC-I	12.5	-32.890	208	0.49

The protein subfraction MALDI-MS spectra, contained apoA-I^{2+}, A-I_1, and HSA, as shown in Figure 178. Table 150 shows the peak masses for this fraction. The CE results, shown in Figure 179, contained albumin, apoA-I, and apoC-I.

CAD Cohort MALDI-MS Overview Discussion

In analyzing the CAD cohort samples, the major peaks in the non HDL fraction corresponded to: apos C-I_1', C-I_1, C-III, A-I_1, D, and HSA. Patients 49, 84, 143, and 195 contained no detectable peaks in this fraction. ApoA-I_1 was observed in patients 10, 146, and 170 only.

The CAD HDL_2 fractions contained peaks corresponding to C-I_1', C-I_1, C-II, C-III, A-II, SAA_4, A-I_1 and several unidentified peaks. As seen in the HDL_2 fractions from the control cohort, there were no peaks corresponding to human serum albumin in this fraction. Patient 84 contained several unknown peaks in the 10,000 Da mass region which were hypothesized to be related to SAA_1 and or indicative of an acute inflammatory response. ApoA-I_1 intensity was constant throughout all patients. Patients 10, 84, 146, 170 showed an abundance of proteins in the 8000 – 1000 *m/z* range. ApoC-I_1' and apoC-I_1 peaks were overall highly resolved and sharp with the exception of patients 49 and 143 which also contained doublets indicative of oxidative processes.

The CAD HDL_3 fractions contained apos C-I_1', C-I_1, C-II, C-III, A-II, unidentified peaks, prealbumin, SAA_1, A-I_1, E, and HSA. A-I_1 peaks were present in all patients and were primarily of high relative ion intensity with the exception of patients 10, 84, 41, and 146. Differing from the enrichment of proteins observed in the HDL_2 fraction for the 8000 – 10000 *m/z* range, the HDL_3 fraction was not as populated in this region, as also observed in the control cohort. The apoC-I_1' and apoC-I_1 peaks were also lower in intensity in this fraction with doublets observed in patients 146 and 143.

The CAD cohort protein fraction showed peaks corresponding to apos C-I_1', C-I_1, SAA, C-II, A-I_1, E, prealbumin, and human serum albumin. The apoC-I peaks were poorly resolved with low relative ion intensity. There were also several sharp and highly resolved unidentified peaks which consistently appeared in this fraction. The apoA-I_1

peaks were present in half of the patients with relatively low intensity. The albumin peaks in this fraction were generally of high relative ion intensity.

CAD Cohort ApoC-I MALDI-MS Discussion

The most interesting finding following MALDI-MS analysis was the distinct difference in the apoC-I peaks from subfractions in this cohort. This difference was observed in the apparent molecular weight shifting observed in all CAD subfractions as well as the further modifications observed in the splitting of apoC-I peaks in select patients. Tables corresponding to the apoC-I peak masses in the CAD HDL subfractions were presented at the beginning of this section. The average apoC-I peak masses for the non HDL and protein fractions are shown in Tables 152 and 153 respectively.

Table 152. Total CAD cohort Non HDL fraction average apoC-I masses by MALDI.

	CAD Cohort ApoC-I'$_1$	**CAD Cohort ApoC-I$_1$**
Average Mass	6527.18 ± 2.51	6721.61 ± 2.58
Known Mass	6432.50	6630.60
Difference	94.68 ± 2.51	91.01 ± 2.58

Table 153. Total CAD cohort Protein fraction average apoC-I masses by MALDI**.**

	CAD Cohort ApoC-I'$_1$	**CAD Cohort ApoC-I**
Average Mass	6517.13 ± 2.10	6726.61 ± 9.50
Known Mass	6432.50	6630.60
Difference	84.63 ± 2.10	96.01 ± 9.50

Apolipoprotein C-I is composed of 57 amino acids and has a molecular weight of 6630.6 Da as well as a truncated form with a molecular weight of 6432.5 Da. Several mass spectrometry experiments have been carried out which confirm these masses experimentally.[169, 186, 187] Hortin and colleagues at the National Institutes of Health also recently identified apoC-I from human serum with a molecular mass of 6630.6 Da and apoC-I' with a molecular mass of 6432.5 Da.[188]

Post-translational modifications refer to the chemical alteration of proteins following translation including peptide bond cleavage and derivatization of amino acid side chains. Post-translational modifications result in the attachment or addition of biochemical functional groups such as carbohydrates, lipids, phosphates and acetates to amino acids; and may also result in structural changes. The majority of post-translational modifications are introduced by enzymes. These modifications are required for normal biological function of proteins in many instances, although in other cases the role of these modifications is unknown and perhaps detrimental. Approximately, one-third of proteins from mammalian cells are phosphorylated.[189] Phosphorylation is the most highly occurring and physiologically significant reversible regulatory modification. Protein kinases and phosphatases control cell growth, metabolism, division, motility, and differentiation, through selective phosphorylation at plural sites, and dephosphorylation of proteins.[190, 189, 191] Phosphorylation of intracellular proteins serves an important role in signal transduction and as a result, the regulation of intracellular physiological processes.[192, 193] Since mass spectrometry measures molecular mass, it is invaluable for detecting and characterizing covalent post-translational modifications that involve mass changes to amino acids. Protein phosphorylation is detected by an increase in amino acid residue mass of +80 Da. This mass shift reflects the addition of HPO_3 to serine, threonine, tyrosine and also histidine.[194] Acetylation is useful as well in cellular regulation including DNA recognition, protein-protein interaction, and protein stability.[195] Acetylation of lysine and serine residues is detected by a characteristic mass shift of +42.01 Da.[194] Cysteine residues, which are involved in cell proliferation, differentiation, and apoptosis, can be oxidized to form sulfenic acid (R-SOH), sulfinic acid ($R\text{-}SO_2H$), and sulfonic acid ($R\text{-}SO_3H$) respectively, which are detected by mass shifts of +16, +32, and +48 Da.[194] The oxidation of methionine plays a large role in oxidative stress, as well as protein stability, and may undergo a two-electron oxidation to methionine sulfoxide.[196] This oxidation results in a mass shifting of +16Da.[197] Additionally, hydroxylation of proline, as well as tyrosine, tryptophan, and phenylalanine residues results in a mass shifting of +16Da.[198] Sulfonation is another

post-translational modification which occurs as a result of enzymatic modification of proteins. Sulfonation can occur through several linkage types including esters and anhydrides (*O*-sulfonation), amides, and thioesters (*N*-sulfonation). The effects of sulfation of threonine and serine residues results in a mass shift of +80 Da.[199] The effects of sulfation of tyrosine also results in a mass shift of +80 Da.[200]

ApoC-I contains a total of 57 amino acids, and does not contain tyrosine, cysteine, or histidine residues.[108] The mass shifting observed following the analysis of the CAD cohort contained an average mass of +90 Da. Considering the amino acid composition of apoC-I, it is possible that this shifting may be a result of post-translational modifications including phosphorylation, sulfonation, hydroxylation, and oxidation. If phosphorylation is responsible for the mass shifting, ApoC-I contains 7 serine and 3 threonine (2 in C-I') residues which may undergo this particular modification. Phosphorylation results in the addition of a phosphate molecule to a polar R group of an amino acid residue. This in turn can transform a hydrophobic portion of a protein in to a polar hydrophilic portion. It can also introduce a conformational change in the structure of the protein through interaction with other protein residues. Phosphorylation may explain the ability of apoC-I to stimulate protein kinases in apoptosis. Additionally, apoC-I contains 7 serine and 3 threonine residues which may undergo sulfonation. In sulfonation, a sulfonic acid group is added to an amino acid in place of a hydrogen atom. Additionally, the presence of doublet peaks with mass differences of 16 Da could indicate the influences of oxidation and hydroxylation. ApoC-I contains 1 methionine residue which may be oxidized to methionine sulfoxide. ApoC-I also contains 3 phenylalanine, 1 tryptophan, and 1 proline residues which could undergo hydroxylation.

Isoforms of C apolipoproteins have been identified in biological samples as a result of glycosylation and deglycosylation and proteolytic activity at the post-translational levels.[166, 167, 168] The truncated apoC-I isoform apoC-I' was first identified by Bondarenko and colleagues and lacks Thr-Pro residues from the N terminus.[169] In 2006, Wroblewski and colleagues identified a functional polymorphism of apoC-I

detected by mass spectrometry.[170] This polymorphism was found only in individuals of American Indian or Mexican ancestry. Tandem mass spectrometry showed the alteration to consist of a T45S variation which forms part of the lipid interacting surface of apoC-I. The Wroblewski study reported the first case of a structural variant of apoC-I as well as some protein properties that suggest the functional significance of this residue change. The individuals in this study showing the polymorphism had apoC-I doublets for each of the two forms.

Adduct formation corresponds to the attachment of matrix molecules to analyte ions and presents difficulties in MALDI-MS analyses.[201, 202] Adducts complicate spectra and reduce the intensities of ions of interest. The matrix sinapinic acid (3,5-dimethoxy-4-hydroxycinnamic acid) was used for MALDI-MS analysis and is specifically useful in the analysis of proteins in the mass range of apoC-I and other serum apolipoproteins. This matrix is commonly used with the dried droplet method and results in rhomboid crystals. Loboda and colleagues recently investigated adduct formation in MALDI.[203] There are two theories of adduct formation which include incomplete cluster evaporation and poisoning. Incomplete evaporation of analyte-matrix clusters is the assumption upon which the first theory is based. Poisoning refers to adduct formation as analyte ions go through the dense plume of matrix molecules. Though the study did not incorporate the matrix sinapinic acid it was observed that with matrices DHB and ferulic acid, matrix adduct formation in MALDI at elevated pressure occurred due to collisions of analyte ions with a dense plume of matrix molecules. It was also observed that by using smaller laser spots, smaller plumes can be generated, resulting in reduced matrix adduct formation without changing other experimental conditions. It is highly unlikely that the shifting observed in the CAD cohort was due to matrix adducts. Sinapinic acid adducts would predominately be observed with mass shifts corresponding to the addition of sodium or potassium ions which collectively and individually have lower masses than the adducts observed in the CAD apoC-I peaks. Additionally, the effect of matrix adducts would be expected to be observed in all samples and not solely the CAD samples since both cohorts were prepared identically.

Mass spectrometry enabled an in-depth investigation of the HDL subfractions from human serum samples following DGU. In both patient cohorts consisting of control individuals and those with coronary artery disease, a distinct difference was observed in the apoC-I region of the MALDI spectra. In all samples of the control cohort, it was observed that both forms of apoC-I contained peaks which corresponded to the known masses of these proteins. The control patients had apolipoprotein peaks that were extremely close to the known masses of the respective apolipoproteins. Such closeness of the peaks in the control cohort to their known calculated masses indicated that there were no interactions between the apolipoproteins and the heavy metal density gradient that might alter the weights of the proteins and likewise no fragmentation or damage to the apolipoproteins caused by solid phase extraction. The closeness of the peak masses to the known masses also demonstrated the mass accuracy of the instrumentation.

In all samples of the CAD cohort it was observed that apoC-I forms contained peaks with greater masses than the known calculated masses. Such a finding indicated post-translational modifications occurring in the CAD cohort which may be linked to CAD, as this diagnosis was the distinguishing difference between the two cohorts. Mass spectral analysis of HDL serum fractions allowed the identification of the isoform distribution of apoC-I peaks. This study has demonstrated the existence of isoforms of apoC-I and further variability in the isoform pattern in subjects within the CAD cohort.

The observation of new isoforms of apoC-I in the mass spectra of subjects with CAD compared to those without CAD is a significant finding that may explain some of the unique functional properties of HDL. In the identification of the apoC-I adduct, apoC-I_1' had a mass difference of 89.97 ± 2.78 Da and apoC-I_1 had a mass difference of 89.87 ± 2.09 Da which are probably due to the attachment of the same adduct. It is possible that the adduct corresponds to phosphorylation of apoC-I' and C-I, which is known to be accompanied by a comparable mass shift.[169] Post-translational modifications such as phosphorylation, are part of common mechanisms for controlling protein behavior such as enzyme activation and inhibition. Interestingly, HDL

subclasses enriched in apoC-I as well as apoC-I itself have been shown to induce apoptosis in human aortic smooth muscle cells through activation of the neutral sphingomyelinase (N-SMase) pathway generating ceramide a key signaling molecule that regulates apoptosis. It is hypothesized that apoC-I activates the N-SMase pathway by the stimulation of membrane bound protein kinases. The observation that post translational modifications had occurred in the apoC-I and C-I' peaks in the CAD patients, further supports the hypothesis that apoC-I is potentially atherogenic. An alternative hypothesis is that the approximately +90Da mass shift observed may be an acidic form of apoC-I due to oxidation, with a methionine residue converted to methionine sulfoxide, as seen in the recent and comparable results obtained in apes.[171] Likewise, it is important to note that the oxidation of apoC-I in certain CAD individuals, was seen predominately in the more buoyant and larger HDL_2 subclass of HDL. As the distinguishing characteristic between the two cohorts of individuals was the presence or absence of CAD, it is hypothesized that the presence of arterial plaque plays a significant role in the modification observed. The adduct may be due to the interaction of apoC-I and apoC-I' with foam cells or macrophages on the arterial wall. An additional hypothesis is that the shifting observed in the CAD cohort may be the result of a genetic mutation(s) that may compromise the functionality of apoC-I.[204] The results obtained from MALDI-MS further support the hypothesis that apoC-I is a probable biomarker for CAD as suggested by many research studies.

Interestingly, one patient, patient 49, who has not been diagnosed with CAD despite having a family history of the disease, and having apoptotic HDL was included in this study. This patient's MALDI-MS apoC-I spectra corresponded with those in the CAD cohort and showed a mass shift. This result suggests that this analysis may be an initial screening that could indicate the future development of CAD and serve as a biomarker for CAD in this individual, as its MALDI spectra showed characteristics as seen in the CAD cohort and even displayed evidence of further modifications beyond the mass shift. If a mutation of the apoC-I gene is involved in this modification, it is likely that if the site of mutation is involved in the LCAT and CETP activity of apoC-I within the HDL

system, its role in lipoprotein metabolism may be compromised contributing to atherogenic or dysfunctional forms of HDL.

CAD Cohort ApoA-I_1 MALDI-MS Discussion

The CAD cohort apoA-I peaks were observed in detail in the mass range spanning 27,000 – 30,000m/z. As also seen in the control cohort, upon closer inspection it was observed that the peak in this mass range was shifted. Due to this shift, this apolipoprotein peak was designated as apoA-I_1. The masses of apoA-I_1 peaks were averaged and the standard deviation was calculated at the 95% confidence level. For the CAD cohort the average apoA-I_1 mass for all serum fractions was 28466.00 ± 32.09 Da, which corresponded to a mass increase of approximately 387Da. The average apoA-I_1 mass for the non HDL subfraction was 28462.54 ± 102.96 Da, which was 384Da higher than the known mass of apoA-I. The average apoA-I_1 mass for the HDL_2 and HDL_3 fractions were 28461.62 ± 24.21 Da and 28477.16 ± 92.75 Da, which corresponded to mass differences of 383Da and 398 Da respectively. The average apoA-I_1 mass for the protein fraction was 28452.53 ± 25.12 Da, which was approximately 374Da higher than the known mass of apoA-I.

As both cohorts showed comparable mass shifting of apoA-I, it is likely that this modification is due to biological variables such as those described in the control apoA-I_1 discussion which alone may or may not pose a risk to CAD and or its development. In both patient cohorts consisting of control individuals and those with CAD, a consistent mass shift was observed in the apoA-I region of the MALDI-MS spectra. In all samples of the control and CAD cohorts, it was observed that apoA-I contained peaks with greater masses than the known mass of this protein. Such a finding suggests potential sample preparation influences on apoA-I mass. Additionally, the shift may be due to post-translational modifications occurring in the CAD cohort which may be linked to CAD in the CAD cohort, and possibly protected by other HDL associated proteins in the control cohort which also showed this shift despite being free of CAD.

CAD Cohort CE Analysis Discussion

The observed elution order of peaks in the electropherograms was: EOF marker, human serum albumin, apoC-II/apoC-III, apoA-II, apoA-I, and apoC-I. Human serum albumin, has a larger molecular weight than HDL apolipoproteins, which resulted in its lower mobility. ApoC-I is the smallest protein in molecular mass which resulted in its relatively high mobility. There were few striking differences between serum non HDL, HDL_2, HDL_3, and protein subfractions for the two patient cohorts. The composition of each individual subfraction in regards to apolipoprotein composition and peak areas remained relatively consistent over both patient cohorts. Both samples contained a greater ratio of apoA-I to apoC-I in the more buoyant HDL_2 fraction. ApoA-I was most abundant in the HDL_2 subfractions in both samples. The CAD cohort showed more comparable apoA-I concentrations between the HDL_2 and HDL_3 fractions than the control cohort. ApoC-I was most abundant in the HDL_3 subfraction. The ratio of apoA-I to apoC-I was observed to be higher in the HDL_2 subfraction as also observed in the control cohort. The average corrected peak area values for each fraction are shown in Table 165 for the CAD cohort.

Albumin was most abundant in the HDL_3 subfraction followed by the bottom or protein fraction. Human serum albumin is not a structural part of HDL particles, however, it was commonly detected in HDL_3 fractions after preparative ultracentrifugation. Human serum albumin has the capacity to bind cholesterol as well as free fatty acids in the blood stream. It is likely that albumin was also attached to lipoprotein particles prior to purification, which may have contributed to the peak shape variability observed in the lipoprotein profiles.

In the CAD cohort, apoA-I had the highest mobility in the non HDL fraction and the lowest mobility in the HDL_3 fraction. ApoC-I had the highest mobility in the protein fraction and lowest in the HDL_2 subfraction. Human serum albumin had the highest mobility in the non HDL fraction and lowest in the protein fraction though both albumin and apoC-I had constant mobilities that were comparable to their corresponding commercial standards. Overall, the fluctuations in mobilities were consistent across both

cohorts, and may be influenced by a number of factors, the most pertinent of which may be the presence of other sample constituents and contaminants. The average electrophoretic mobility values for each fraction are shown in Table 154 for the CAD cohort.

Table 154. Average electrophoretic mobilities for the non HDL, HDL_2, HDL_3, and protein fractions from 200µL serum samples from the CAD cohort.

Serum Fraction	Average ApoA-I Mobility	Average ApoC-I Mobility	Average HSA Mobility
Non HDL	-28.029 ± 1.239	-31.206 ± 0.236	-20.295 ± 0.314
HDL_2	-28.018 ± 0.603	-31.099 ± 0.159	-20.224 ± 0.308
HDL_3	-27.416 ± 1.875	-31.123 ± 0.305	-20.261 ± 0.590
Protein	-27.499 ± 1.709	-31.293 ± 0.874	-20.146 ± 1.216
Overall Average	-27.422 ± 1.516	-31.215 ± 0.425	-20.864 ± 0.969

Overall, the MALDI-MS data correlated fairly well with capillary electrophoresis with the exception of HDL_2 fractions which consistently showed detectable human serum albumin peaks by CE while consistently showing no detectable human serum albumin by MALDI-MS. The control patients did not show apoA-I in the protein fraction and likewise, the CAD patients were less likely to have any detectable apolipoprotein peaks in the non HDL fraction. The consistent observation that CE fractions containing human serum albumin did not contain albumin by MS indicated that the proteins identified as human serum albumin by CE based upon their electrophoretic mobilities were most likely misidentified. As MALDI-MS is a more sensitive analytical technique, it is highly possible that the true identity of serum components can be measured more confidently by MALDI-MS.

The corrected peak areas and concentrations of apolipoproteins reported, were lower than normal serum concentrations for apos A-I and C-I, with apoA-I having substantially low concentrations. Such values are likely the result of dextran sulfate precipitation as apolipoproteins are also present in the apoB-containing lipoproteins, sample loss following DGU, sample excision, delipidation and desalting, and Speed-Vac evaporation. The most probable explanation for such loss is likely attributed to solid phase extraction, it is likely that apos are retained in the stationary phase. Quantitation using the current methodology will require additional research and development beyond the scope of this study.

Table 155. Clinical studies result summary

Patient	ApoC-I'	ApoC-I	Oxidation	SAA_1	Unknowns	Risk Factors	Medical
1-NonCAD							
3-NonCAD				HDL_3	HDL_3		
7-NonCAD	Low in HDL_3						
13-NonCAD	Low in HDL_3					Hypertension	
14-NonCAD							
16-NonCAD						Hypertension	
24-NonCAD						Hypertension	
25-NonCAD	Low in HDL_2 Nearly depleted in HDL_3			HDL_3		Hypertension	
49	Modified Nearly depleted in HDL_2 and HDL_3	Modified		HDL_3 Protein		Family History	
10-CAD	Modified	Modified Nearly Depleted in HDL_3 and Protein	non-HDL	non-HDL	HDL_3 Protein		Stent, Angina, Angioplasty
41-CAD	Modified Nearly depleted in Protein	Modified Nearly depleted in Protein		Protein	Protein	Hypertension Tobacco	Stent, Angina, Angioplasty

Table 155. (Continued)

Patient	ApoC-I'	ApoC-I	Oxidation	SAA_1	Unknowns	Risk Factors	Medical
84-CAD	Modified	Modified			HDL_2 Protein	Hypertension Diabetes Tobacco Family History	Stent, Angina, Angioplasty, Congestive Heart Failure
143-CAD	Modified Oxidized in HDL_2 and HDL_3	Modified Oxidized in HDL_2	HDL_2 HDL_3			Hypertension	
146-CAD	Modified	Modified			Protein	Hypertension	
170-CAD	Modified	Modified				Hypertension Tobacco	
195-CAD	Modified Nearly depleted in HDL_3	Modified				Hypertension	Angina, CABG

Collaborative Studies

The collaborative studies, served to further assist in the characterization and elucidation of serum subfraction composition. Likewise, these collaborations provided information that was useful in determining the biological functions of a novel atherogenic HDL phenotype in a group of adults with CAD. Clinical lipid levels were provided by Scott & White Hospital (Temple, TX), apoptosis levels were provided by the Chatterjee Laboratory at Johns Hopkins University (Baltimore, MD), and CETP and PLTP transfer rates were provided by Roar Biomedical (New York, NY).

Patient Lipid Levels

Lipid levels were analyzed by standard methods in the Clinical Chemistry Laboratory at Scott & White Hospital (Temple, TX). Lipid levels are included in the traditional risk factors for CAD and include total cholesterol, triglycerides, high density lipoprotein cholesterol (HDL-C), and low density lipoprotein cholesterol (LDL-C).

High and low density lipoprotein cholesterol levels along with triglyceride, and Lipoprotein(a) levels cumulatively comprise the total cholesterol count which is obtained through blood testing. Total cholesterol levels <200 mg/dL are desirable and put individuals at relatively low risk of heart disease. Total cholesterol levels ranging between 200 – 239 mg/dL are categorized as borderline to high risk and may require medication, while total cholesterol levels >240 mg/dL are considered high risk and are associated with twice the risk of heart disease.

High HDL-C levels are desired due to their atheroprotective benefits. Low HDL-C levels, identified as <40 mg/dL for men and <50 mg/dL for women, put individuals at greater risk for heart disease. The average levels for men range from 40 – 50 mg/dL and for women from 50 – 60mg/dL. An HDL cholesterol level ≥60 mg/dL provides protection against heart disease.

The lower an individual's LDL cholesterol, the lower their risk of heart attack and stroke. Levels <100 mg/dL are optimal while levels ranging from 100 – 129 mg/dL are near and or above optimal. LDL cholesterol levels ranging from 130 – 159 mg/dL

are borderline high. LDL cholesterol levels ranging between 160 – 189 mg/dL are considered high, while levels ≥190 mg/dL are extremely high.

Triglyceride is a form of fat, and oftentimes, individuals with high triglyceride levels have high total cholesterol levels including high LDL-C levels and low HDL-C levels. Many individuals have high triglyceride levels due to obesity, physical inactivity, alcohol consumption, smoking, and/or diet. Triglyceride levels <150 mg/dL are considered normal while levels between 150 – 199 mg/dL are considered borderline. Triglyceride levels between 200 – 499 mg/dL are high with levels >500 mg/dL considered very high.

The control cohort patient lipid levels are shown in Table 156 in addition to the true mean CETP values at the 95% confidence level. The total cholesterol levels range from 135 – 226 mg/dL, with a cohort average total cholesterol of 184.43 ± 28 mg/dL. Patients 3 and 13 have levels above 200 mg/dL which put them at borderline high risk. Their risk however also depends on other risk factors and their measurements in those other areas. The triglyceride levels for the control patient cohort range from 49 – 124 mg/dL, with a cohort average of 86.43 ± 25 mg/dL. All patients have normal levels which are classified as below 150mg/dL. The HDL-C levels range from 61 – 89 mg/dL, with a cohort average of 74.29 ± 9 mg/dL. All levels are above 60 mg/dL, which regardless of gender is optimal for a reduced risk of heart disease. The LDL-C levels range from 55 – 130 mg/dL, with a cohort average 91.86 ± 23 mg/dL. As seen with the total cholesterol levels, there are a few patients whose levels are in the near to above optimal range, including patients 3, 13, and 14, whose levels are 130 mg/dL, 115 mg/dL, and 108 mg/dL, respectively.

Table 156. Control patient cohort lipid levels.

Patient	Total Cholesterol (mg/dL)	Triglycerides (mg/dL)	HDL-C (mg/dL)	LDL-C (mg/dL)
1	155	94	62	74
3	226	124	71	130
7	185	70	76	95

Table 156. (Continued)

Patient	Total Cholesterol (mg/dL)	Triglycerides (mg/dL)	HDL-C (mg/dL)	LDL-C (mg/dL)
14	**194**	**124**	**61**	**108**
16	**135**	**49**	**70**	**55**
24	**151**	**60**	**64**	**75**
25	**173**	**97**	**89**	**65**
Average	**183**	**86**	**74**	**92**
Standard Deviation	**34**	**30**	**11**	**28**
True Mean	**183 ± 28**	**86 ± 25**	**74 ± 9**	**92 ± 23**

The CAD cohort patient lipid levels are shown in Table 157. The total cholesterol levels range from 168 – 205 mg/dL with a cohort average of 183.57 ± 19 mg/dL, and with the highest HDL-C levels being lower than the highest HDL-C levels in the control cohort. Patients 41, 146, and 195 have levels in the 200mg/dL range however. The triglyceride levels for the CAD patient cohort were slightly higher than the control cohort, ranging from 69 – 155mg/dL, with a cohort average of 111.86 ± 26 mg/dL. Patient 10 is the only patient whose triglyceride level is borderline high. The HDL-C levels range from 56 – 108 mg/dL, with a cohort average of 83.86 ± 17 mg/dL. Patient 41 has levels in the upper 50s however none of the patients show extremely low values. Patients 146 and 195 show HDL cholesterol levels above 100 mg/dL. The LDL cholesterol levels range from 53 – 120 mg/dL which are lower than those observed from the control cohort, with a cohort average of 81.29 ± 19 mg/dL. There are two patients whose levels are in the near to above optimal range, including patients 41, and 49, whose levels are 120 mg/dL and 115 mg/dL.

Table 157. CAD patient cohort lipid levels.

Patient	Total Cholesterol (mg/dL)	Triglycerides (mg/dL)	HDL-C (mg/dL)	LDL-C (mg/dL)
10	168	155	84	53
41	204	140	56	120

Table 157. (Continued)

Patient	Total Cholesterol (mg/dL)	Triglycerides (mg/dL)	HDL-C (mg/dL)	LDL-C (mg/dL)
84	180	95	78	89
146	**205**	**106**	**102**	**82**
170	**161**	**108**	**69**	**70**
195	**206**	**110**	**108**	**82**
Average	**184**	**112**	**84**	**81**
Standard Deviation	**21**	**28**	**18**	**21**
True Mean	**184 ±19**	**112 ± 26**	**84 ± 17**	**81 ± 19**

Patient 49, whose lipid levels are shown in Figure 158; has total cholesterol that is comparable to both cohort averages and within the desirable range. Their triglycerides are higher than both cohort averages yet still normal by definition. Their HDL-C levels are lower than both cohort averages yet in the desirable range. Lastly, their LDL-C levels are in the near and or above optimal range.

Table 158. Patient 49 lipid levels.

Patient	Total Cholesterol (mg/dL)	Triglycerides (mg/dL)	HDL-C (mg/dL)	LDL-C (mg/dL)
49	184	74	57	116

In regards to the CAD cohort lipid levels, particularly the HDL-C levels, many of the CAD patients have high HDL-C levels. It is this occurrence of accelerated CAD in patients despite high HDL-C and normal lipid levels that is at the center of the atherogenic HDL investigation. It is hypothesized that despite high serum levels of HDL-C, at the metabolic level, there are functional and structural errors preventing HDL from adequately shuttling cholesterol to the liver. The closeness of both cohort lipid

levels also further support the fact that CAD diagnosis based upon coronary angiography is the distinguishing difference between these two groups of patients.

Smooth Muscle Cell Apoptosis

Immunoaffinity chromatography was performed using anti-apoC-I microbeads in order to obtain apoC-I depleted serum subfractions and apoC-I enriched serum as described in the methods chapter. The apoptosis analyses reported here were performed to investigate the hypothesis that apoptotic effects of HDL on aortic smooth muscle cells were attributed to apoC-I enriched HDL.

Immunospecific DGU was utilized to investigate the differential effects of the apoC-I depleted and enriched lipoproteins on the aortic smooth muscle cell cultures. Aortic smooth muscle cells play a critical role in preventing the progression and complications of atherosclerosis, by providing a supportive structural role as part of the fibrous cap that sequesters the lipid core and prevents the rupture of atherosclerotic plaque.[205] The results shown in Figure 180 compare both the commercial procedure (CP) and in-laboratory procedure (LP) described in the methods chapter. Minimal apoptosis was observed with apoC-I depleted HDL subfractions. In contrast, apoC-I enriched whole serum released from the immunoaffinity chromatography beads caused a 15 - 20% increase in aortic smooth muscle cell apoptosis. Figure 180 shows the results obtained from the apoptosis samples which used serum from CAD patient 10. The first two bars correspond to apoC-I depleted HDL_2 and HDL_3 respectively using the in-laboratory method described in the methods chapter. There were less than 5% apoptotic cells in these apoC-I depleted HDL subfractions. The third and fourth bars correspond to the apoC-I depleted HDL_2 and HDL_3 respectively using the commercial method described in the methods chapter. There was a further decrease in the percent of apoptotic cells using the commercial method that correlated to roughly 1% apoptotic cells, showing a slightly greater efficiency with the commercial microbeads compared to the in-laboratory conjugated microbeads. Lastly, the fifth and sixth bars correspond to the apoC-I enriched unfractionated serum corresponding to the in-laboratory and

commercial methods respectively. There was an increase in the number of apoptotic cells when treated with recovered apoC-I enriched serum, roughly 17% of apoptotic cells from the in-laboratory method and roughly 20% apoptotic cells from the commercial method. As also seen with the depleted samples from the two methods, the recovered apoC-I enriched serum from the commercial method was shown to be more efficient in recovering apoC-I from serum. The results of the preliminary studies with CAD patient 10, showed a direct relationship between apoptosis and apoC-I enriched HDL. Such a relationship was also observed by Kolmakova and colleagues in their apoptosis studies.[106]

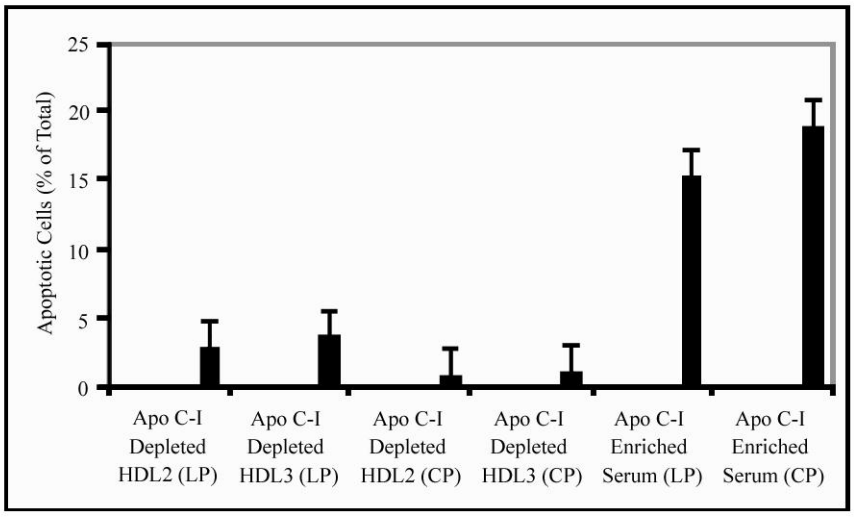

Figure 180. Apoptosis results following the treatment of aortic smooth muscle cell cultures with apoC-I enriched and depleted serum from CAD patient 10 using both in-laboratory (LP) and commercial (CP) immunoprecipitation procedures.

Following the preliminary apoptosis results presented above, it was apparent that there was a direct correlation between apoptosis and apoC-I enrichment. The next step involved assessing the apoptosis levels of patients with and without CAD, to identify

any further relationships. Fractionated serum was submitted to Johns Hopkins to assess aortic smooth muscle cell apoptosis levels.

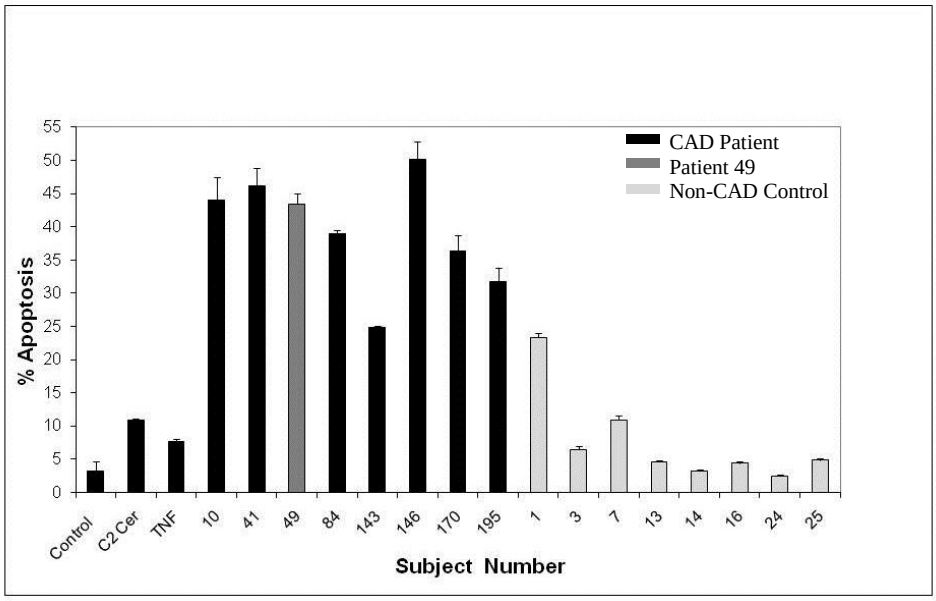

Figure 181. Apoptosis results following the treatment of aortic smooth muscle cell cultures with CAD (black), non-CAD (light grey) and patient 49 (dark grey) non-HDL, HDL_2, HDL_3, and protein subfractions.

Figure 181 shows the aortic smooth muscle cell apoptosis levels induced by serum from each patient included in this study. There was a distinct difference in apoptosis between the two cohorts, with the CAD cohort having substantially higher levels. It was observed that CAD patient 146 induced the greatest percentage of apoptosis with approximately 50% apoptosis. The CAD patients 10, 41, 84 also induced nearly as high of a percentage as patient 146, with values ranging between 40 – 45% apoptosis. Of the CAD cohort patient 143 induced the least percentage of apoptosis, with approximately 25%. In the control cohort, it was observed that overall, there were lower apoptosis levels compared to the CAD cohort. Patient 1 induced the greatest percentage of apoptosis of the cohort with approximately 25% apoptosis. The MALDI-

MS analysis of patient 1 identified the presence of the inflammatory marker, SAA_1, which may contribute to the apoptosis induced by this subject. The lowest percentage of apoptosis was induced by patient 24 who induced approximately 2% apoptosis. Additionally, patient 49 induced a substantially high percentage of apoptosis which was comparable to the degree of apoptosis observed in the CAD cohort patients.

The preliminary results from the apoptosis study with CAD patient 10 showed a direct correlation between apoptosis of aortic smooth muscle cells and the concentration of apoC-I. Similarly, the results obtained showing substantially greater apoptosis percentages amongst the CAD cohort, further support the idea that these patients are inducing such apoptosis due to their apoC-I composition as these subjects all contained the apoC-I isoforms. It is highly probably that apoC-I in individuals with CAD is modified in a way that is detrimental to the arterial wall. Previous apoptosis studies involving apoC-I enriched HDL from infant chord blood showed substantial apoptosis and provided key insight into the mechanisms by which this occurs.[206] It was based upon these previous findings by Kolmakova and colleagues that experiments were carried out in order to ascertain the role of apoC-I in this process. In previous experiments investigating apoC-I in apoptosis, it was observed that commercial apoC-I and apoC-I enriched HDL from low birth weight infants induced apoptosis 5 to 25 fold, compared to control cells, and apoC-I-poor HDL. More importantly, however, it was seen that the mechanism of action by apoC-I was mediated through the recruitment of neutral sphingomyelinase (N-SMase), generating ceramide and activating cytochrome c release as well as caspase. It is hypothesized that this mechanism may contribute to unstable plaque that is more susceptible to rupture, leading to thrombosis, myocardial infarction, and death. It is also possibly that the adducts consistently observed in the mass spectra of CAD patients influence the stimulation of one or more membrane bound protein kinases by apoC-I which in turn activates neutral sphingomyelinase in human aortic smooth muscle cells.

Transfer Protein Assays

Cholesteryl ester transfer protein (CETP) and phospholipid transfer protein (PLTP) activity were measured by collaborators at Roar Biomedical Inc. (New York, NY) utilizing a commercial assay on both patient cohorts. The intravascular metabolism of lipid components of HDL is regulated by enzymes such as cholesteryl ester transfer protein (CETP) and phospholipid transfer protein (PLTP). Consequently, HDL lipids represent complex mixtures of multiple molecular species of phospholipids, cholesteryl esters, triacylglycerols, and partial glycerides which differ in their fatty acid composition, in addition to free cholesterol and lipophilic vitamins. The abundance of individual molecular species of cholesteryl ester in HDL reflects esterification of free cholesterol by LCAT, but equal removal of HDL cholesteryl ester by cellular receptors, primarily by scavenger receptor class B type 1 (SR-B1), and by CETP, which transfers cholesteryl ester to apoB-containing particles including VLDL, VLDL remnants, and LDL in exchange for triglycerides.

Cholesteryl Ester Transfer Protein Assay

Cholesteryl ester transfer protein (CETP), transfers neutral lipids from HDL to VLDL and is present in human serum. CETP plays an important role in lipoprotein metabolism and influences the reverse cholesterol transport pathway. As key determinants of core lipid abundance and composition, LCAT and CETP activities regulate the maturation of nascent HDL to spherical particles, and thereby modulate HDL heterogeneity and function. The Roar CETP Activity Assay is useful for measuring the CETP activity in human serum. The Roar CETP Activity Assay Kit uses a proprietary substrate that enables the detection of CETP-mediated transfer of neutral lipid from the substrate to a physiological acceptor. The transfer activity results in an increase in fluorescence intensity and is further described in the methods chapter. For the CETP assay, a standard curve was prepared by making serial dilutions of the donor molecule in isopropanol and subsequently recording the fluorescence intensity of each

dilution, using isopropanol alone as a blank. The standard curve for the CETP assay is shown in Figure 182.

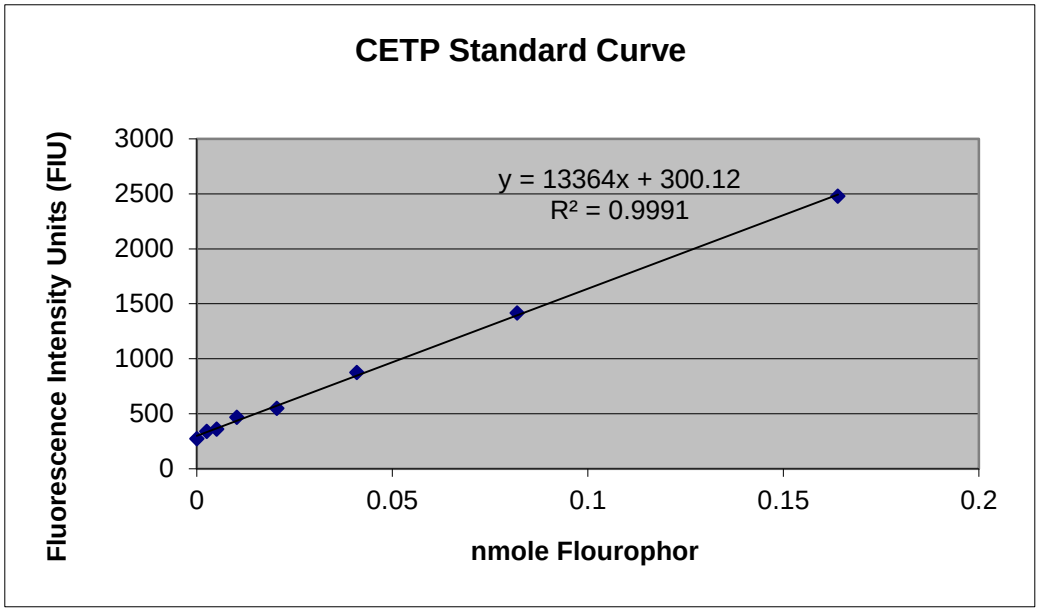

Figure 182. CETP standard curve.

The fluorescence intensity values of the standard curve were applied directly to the results to express activity of the plasma sample as described in the methods chapter. The results from the CETP activity assay are shown in Tables 159 and 160 in addition to the true mean CETP values at the 95% confidence level.

Table 159. CETP assay results for the control cohort

Patient	pMoles Transferred	pMoles transferred/µL/hr	Average FIU	Transferred FIU
1	104	69	3550	1686
3	115	77	3707	1843
7	133	89	3943	2079
13	92	61	3389	1525
14	143	96	4081	2217

Table 160. (Continued)

Patient	pMoles Transferred	pMoles transferred/µL/hr	Average FIU	Transferred FIU
16	135	90	3975	2111
24	170	113	4431	2567
25	128	85	3869	2005
Average	128	85	3868	2004
Standard Deviation	24	16	324	324
True Mean	128 ± 20	85 ± 14	3868 ± 271	2004 ± 271

In the control cohort, there was an average of 128 ± 20 pMoles transferred, 85 ± 14 pMoles transferred/all/hr, 3868 ± 271 average fluorescence intensity units, and 2004 ± 271 transferred fluorescence intensity units. The highest CETP activity was observed in patient 24, who had a transfer rate of 113 pMoles/µL/hour and the lowest CETP activity was observed in patient 13 who had a transfer rate of 61 pMoles/µL/hour.

Table 161. CETP assay results for the CAD cohort

Patient	pMoles Transferred	pMoles transferred/µL/hr	Average FIU	Transferred FIU
10	104	69	3550	1686
41	137	91	3991	2127
49	128	85	3871	2007
84	54	36	2887	1023
143	138	92	4005	2141
146	147	98	4125	2261
170	92	61	3395	1531
195	48	32	2811	947
Average	106	71	3579	1715
Standard Deviation	39	26	512	512
True Mean	106 ± 32	71 ± 21	3579 ± 429	1715 ± 429

In the CAD cohort, there was an average of 106 ± 32 pMoles transferred, 71 ± 21 pMoles transferred/µL/hr, 3579 ± 429 fluorescence intensity units, and 1715 ± 429 fluorescence intensity units transferred. It was seen that the highest CETP activity was observed in patient 146, who had a transfer rate of 98 pMoles/µL/hour and the lowest CETP activity was observed in patient 195 who had a transfer rate of 32 pMoles/µL/hour. It is worth noting that patient 195, who had the lowest CETP activity was also a low birth weight infant and possesses apoC-I enriched HDL. It is known that apoC-I is an inhibitor of CETP and this inhibition may be responsible for the substantially lower CETP transfer rate observed from patient 195. Compared to the control cohort, the CAD cohort had slightly lower average CETP activity, as this cohort contained unanimous apoC-I isoforms, there may be a direct correlation between their lower CETP rates and apoC-I composition. Interestingly, research has shown a link between low CETP activity and protection from CAD. It is probable that the CETP lower activity observed in the CAD cohort, is an attempt by the body to attenuate plaque progression.

Ex Vivo Cholesteryl Ester Transfer Protein Assay

The Roar Ex Vivo CETP Activity Assay is useful for evaluating non-reversible and reversible inhibitors on plasma CETP activity. The assay is not affected by changes in HDL concentration or other endogenous lipoproteins. The difference between the RB-EVAK and RB-CETP is that with the EVAK assay, the concentration of serum is 200µL with 5µL substrate compared to 0.5µL serum in 200µL substrate with the RB-CETP assay. The EVAK dilutes serum less, and when reversible inhibitors are present the EVAK is the preferred assay. The standard curve used for this assay is shown in Figure 183. The results for the patient samples from this assay are shown in Tables 161 and 162 in addition to the true mean CETP values at the 95% confidence level.

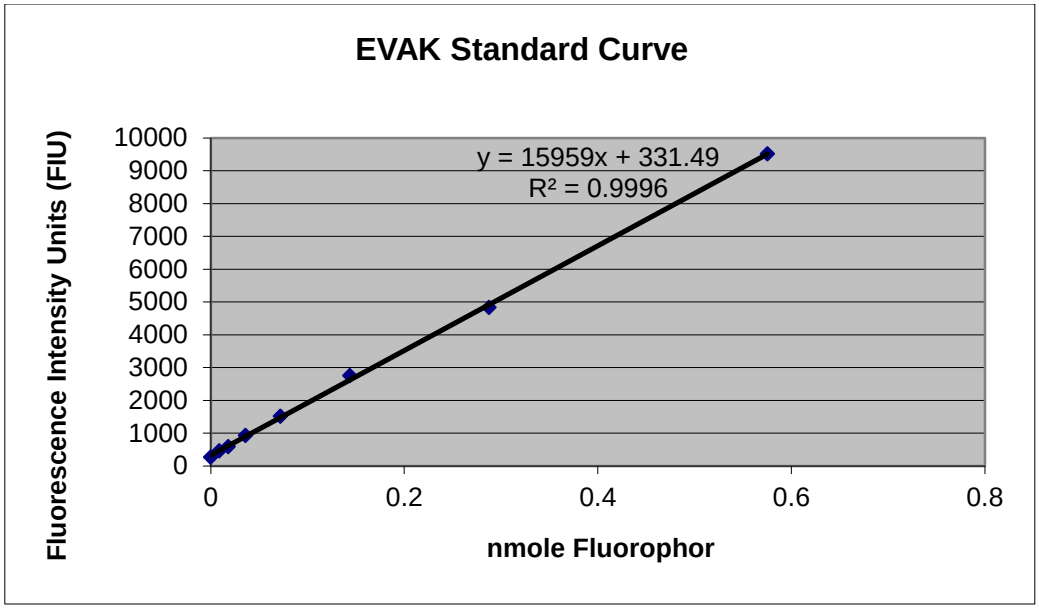

Figure 183. EVAK standard curve.

Table 162. EVAK results for the control cohort.

Patient	pMoles Transferred	pMoles transferred/µL/hr	Average FIU	Transferred FIU
1	84	9	8006	1669
3	104	12	7489	1987
7	90	10	8000	1768
13	87	10	8315	1722
14	129	14	7724	2396
16	139	15	8099	2544
24	11	1	10187	512
25	98	11	8311	1902
Average	93	10	8266	1813
Standard Deviation	39	4	824	614
True Mean	93 ± 32	10 ± 4	8266 ± 689	1813 ± 513

The control cohort had an average 93 ± 32 pMoles transferred, 10 ± 4 pMoles transferred/µL/hr, 8266 ± 689 fluorescence intensity units, and 1813 ± 513 transferred fluorescence intensity units. The highest rate was observed in patient 16 with a rate of 15 pMoles transferred/µL/hr. The lowest rate was observed in patient 24 with a rate of 1 pMoles transferred/µL/hr.

Table 163. EVAK results for the CAD cohort.

Patient	pMoles Transferred	pMoles transferred/µL/hr	Average FIU	Transferred FIU
10	50	6	6256	1137
41	56	6	13335	1224
49	100	11	7407	1931
84	52	6	6605	1154
143	90	10	7445	1760
146	135	15	8535	2484
170	176	20	14755	3134
195	29	3	5776	795
Average	86	10	8764	1702
Standard Deviation	29	3	5776	795
True Mean	86 ± 42	10 ± 5	8764 ± 3387	1702 ± 792

The CAD cohort had an average 86 ± 42 pMoles transferred, 10 ± 5 pMoles transferred/µL/hr, 8764 ± 3387 fluorescence intensity units, and 1702 ± 792 transferred fluorescence intensity units. The highest rate was observed in patient 170 with a rate of 20 pMoles/transferred/µL/hr. The lowest rate was observed in patient 195 with a rate of 3 pMoles transferred/µL/hr. The EVAK assay provides a 96% serum volume analysis as it does not dilute serum to the extent of the CETP assay. This large percentage of undiluted serum results in the inclusion of all factors that may affect the CETP at physiological concentration, in addition to reversible inhibitors such as apoC-I. Interestingly, patient 195 maintained the lowest CETP transfer rate in the CAD cohort

with the EVAK assay which is not affected by changes in HDL concentration or other endogenous lipoproteins.

Recent studies have supported an interest in CETP inhibition *in vivo* by means of either anti-CETP immunotherapy, antisense oligoneluceotides, or specific pharmacological inhibitors.[207, 208, 209] Studies have also shown that small anti-CETP molecules in human populations demonstrate that CETP inhibition markedly increases HDL-C levels and also decreases LDL-C levels.[58, 210, 211] In addition to intervention studies utilizing exogenous substances, studies have shown that plasma CETP levels can be modulated by endogenous factors including the apolipoprotein content of lipoproteins in circulation.[212, 213, 214] ApoC-I has been identified as a potent inhibitor of CETP activity,[215] and unlike other apolipoprotein inhibitors this candidate has been shown to have the ability to decrease CETP activity *in vivo* using mouse models.[98, 102] ApoC-I can suppress CETP-mediated lipid transfer in a concentration dependent manner.[215] Thus variation in apoC-I concentration may be a determinant of neutral lipid exchange in human plasma. Though it is known that apoC-I is a major physiological inhibitor of CETP in plasma, the molecular mechanism of the blockade remains under investigation. The transfer reaction that takes place involving CETP is a complex reaction consisting of at least two rate determining steps. In the first step, CETP binds to lipoproteins through electrostatic interactions with negative charges localized at the lipoprotein surface.[216, 217] Next, following a CETP conformational change, one neutral lipid molecule binds to a hydrophobic site in the C-terminus of the protein prior to being transferred to an electron acceptor.[218, 219] Studies have reported mainly two ways by which the CETP-mediated transfer reaction is blocked. CETP inhibition may be a result of insufficient or excessive binding between CETP and the lipoprotein surface, as it has been shown that both weak[217, 220] and strong[217, 219] CETP-lipoprotein interactions significantly inhibit the lipid transfer reaction. Another way by which CETP may be inhibited is through the blockade of the neutral lipid binding site, resulting in abnormal production of irreversibly associated CETP-lipoprotein complexes.[221, 222] Dumont and colleagues recently studied the effect of apoC-I on the lipid transfer process and indicated that the inhibitory

property of apoC-I is in a direct link with its electrostatic charge properties and its ability to produce significant changes in CETP-lipoprotein interactions.[223] In all cases the addition of apoC-I was accompanied by a marked inhibition of the lipid transfer reaction. It was determined that CETP inhibition by HDL is the consequence of a direct and specific property of apoC-I, because apoC-I-poor HDL displayed a much weaker ability to block the lipid transfer reaction in the HDL concentration ranges studied. Additionally, it appeared that the inhibitory effect of human apoC-I is a direct consequence of its unique electrostatic properties that lead to alteration of the HDL-CETP interactions. The elucidation of the molecular mechanism of CETP inhibition by apoC-I may help identify new mechanisms of CETP blockade. Kinetic studies have shown that the CETP reaction in plasma is dependent on the amount and the specific activity of CETP, as well as on the concentrations and properties of lipoprotein substrates such as HDL.[224, 225] Dumont and colleagues observed that the inhibitory potential of apoC-I is dependent on the amount of HDL and not CETP added.[223] These observations suggest that apoC-I may inhibit CETP through its ability to modify the HDL substrate, rather than through a specific blockade of the CETP molecule. *In vitro* studies examining the electrostatic properties of apoC-I showed that apoC-I is able to produce a significant change in HDL electronegativity which is recognized today as a leading factor in determining the strength of CETP-HDL interactions and the velocity of CETP transfer activity.[226] Overall, it appears as though the inhibition of CETP activity by apoC-I depends in part on the electrostatic properties of apoC-I which have the ability to shift HDL toward lower electronegativity. It is very likely that apoC-I mediated alteration in the binding of CETP to lipoproteins may result in fewer cholesteryl ester transfers in human plasma.

Phospholipid Transfer Protein Assay

The content of phospholipid molecular species in the HDL particle surface can be modulated by transfer or exchange with cell membranes and lipoprotein facilitated by PLTP, and by the actions of plasma and lipoprotein-associated phospholipases, HL, and

EL. The Roar PLTP Activity Assay Kit also includes proprietary substrates to detect PLTP mediated transfer of the fluorescent substrate and is performed similarly to the CETP assay. For the PLTP assay, a standard curve was prepared by making serial dilutions of the donor molecule in isopropanol and subsequently recording the fluorescence intensity of each dilution, using isopropanol alone as a blank. The standard curve for the PLTP Assay is shown in Figure 184.

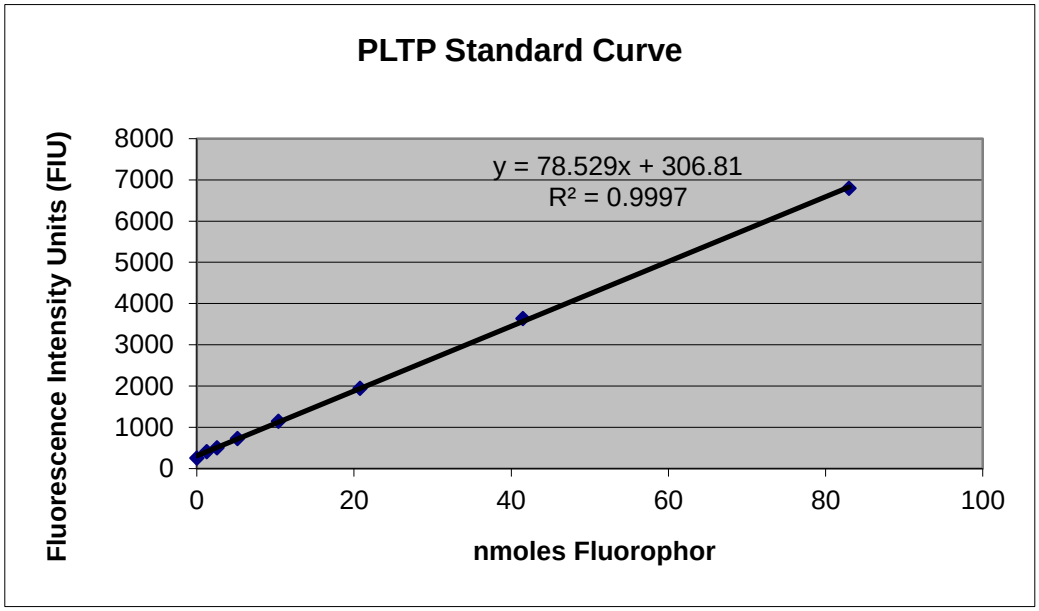

Figure 184. PLTP standard curve.

The fluorescence intensity values of the standard curve were applied directly to the results to express activity of the plasma sample as described in the methods chapter. The results of the PLTP assay are shown in Tables 163 and 164 in addition to the true mean CETP values at the 95% confidence level.

Table 164. PLTP assay results for the control cohort

Patient	pMoles Transferred	pMoles transferred/µL/hr	Average FIU	Transferred FIU
1	14.3	11.4	2525	1435
3	17.6	14.1	2789	1699
7	16.3	13	2686	1596
13	21.4	17.2	3092	2002
14	13.5	10.8	2462	1372
16	11.1	8.9	2274	1184
24	16.9	13.5	2733	1643
25	13.4	10.8	2461	1371
Average	15.6	12.5	2628	1538
Standard Deviation	3.2	2.6	253	253
True Mean	15.6 ± 2.7	12.5 ± 2.1	2628 ± 211	1538 ± 211

The control cohort had an average 15.6 ± 2.7 pMoles transferred, 12.5 ± 2.1 pMoles transferred/µL/hr, 2628 ± 211 fluorescence intensity units, and 1538 ± 211 transferred fluorescence intensity units. The highest PLTP rate was observed in patient 13 with a rate of 17.2 pMoles transferred/µL/hr. The lowest rate was observed in patient 16 with a rate of 8.9 pMoles transferred/µL/hr.

Table 165. PLTP assay results for the CAD cohort

Patient	pMoles Transferred	pMoles transferred/µL/hr	Average FIU	Transferred FIU
10	23.7	18.9	3267	2177
41	23.3	18.6	3238	2148
49	12.7	10.1	2400	1310
84	12.7	10.2	2405	1315
143	12.3	9.8	2369	1279
146	26.3	21	3475	2385
170	27	21.6	3539	2439
195	12.3	9.8	2367	1277
Average	19	15	2883	1791

Table 166. (Continued)

Patient	pMoles Transferred	pMoles transferred/µL/hr	Average FIU	Transferred FIU
Standard Deviation	6.8	5.5	541	539
True Mean	19 ± 5.7	15 ± 4.6	2883 ± 452	1791 ± 451

The CAD cohort had an average 19 ± 5.7 pMoles transferred, 15 ± 4.6 pMoles transferred/µL/hr, 2883 ± 452 fluorescence intensity units, and 1791 ± 451 transferred fluorescence intensity units. The highest PLTP rate was observed in patient 170 with a rate of 21.6 pMoles transferred/µL/hr. The lowest PLTP rate was observed in patients 195 and 143 with a rate of 9.8 pMoles transferred/µL/hr.

The influence of transfer protein rates on CAD risk is complex and it has been shown that both increased and decreased rates of PLTP pose risk in human studies.[227, 228, 229] The importance of this transfer protein centers around its function in mediating the transfer and exchange of phospholipids between lipoproteins[230, 231] and its role in the conversion of HDL in a time and concentration dependent manner.[232, 233] PLTP can mediate the conversion of HDL into larger and smaller particles[234, 235] and generate the efficient and preferred cholesterol acceptor, pre-β HDL, in the process.[236] Other notable functions which also affect CAD risk and overall health include the ability of PLTP to bind and transfer unesterified cholesterol[237, 238] and α-tocopherol[239] among lipoprotein particles and cells. α-Tocopherol is the most potent antioxidant form of vitamin E, and circulates in plasma bound to lipoproteins playing a major role in preventing lipoprotein oxidation and maintaining endothelial function.[85, 240, 241, 242] Interestingly, this protein can also alter the anti-oxidative potentials of lipoprotein particles.[239] Recently it was reported that PLTP was increased in patients with systemic and acute inflammatory response[243, 244] associating PLTP with inflammatory activity. This relationship between inflammation and PLTP is significant since there is supporting evidence regarding the relationship between inflammation and atherogenesis.[245] Additionally, PLTP has been implicated in human atherosclerosis, where it has been detected both on macrophage

foam cells and on the extracellular matrix.[246] Consistent with this implication, increased presence of PLTP has been found in arterial smooth muscle cells and macrophages in atherosclerotic lesions and is increased with cholesterol loading of macrophages.[238] PLTP activity has been shown to increase in conjunction with other independent risk factors for CAD such as cigarette smoking[247, 248] excessive alcohol intake[249] and over consumption of the diterpenes present in filtered coffee.[247]

Similar to the results from both cohorts included in this study showing slightly higher PLTP levels in the CAD cohort, Schlitt and colleagues also studied PLTP rates in CAD and control subjects.[229] This study demonstrated for the first time that plasma PLTP levels were higher in CAD subjects than controls, and this difference was found to be independent of other risk factors. Many possible explanations may result in the relationship between plasma PLTP activity and CAD. One possible explanation is that high PLTP activity may decrease HDL concentrations in line with this possibility, overexpression of PLTP in mouse models have been shown to decrease HDL levels. [250] A second explanation for the PLTP and CAD relationship is that high PLTP activity may increase TRL concentrations. Previous studies with mice have demonstrated that PLTP deficiency in mice resulted in reduced production and levels of TRL and a decrease in atherosclerosis.[251] Thirdly, high PLTP activity may provide a state of prolipoprotein oxidation. Recent work has shown a significant increase in vitamin E content of VLDL and LDL in PLTP deficient mice compared to normal PLTP activity control mice.[252, 253] Thus it is highly probable that PLTP activity in CAD subjects may promote TRL oxidation. Lastly, high plasma PLTP activity may transfer more oxidized phospholipids from TRL to HDL, which may subsequently become less protective against atherosclerosis than normal HDL. Studies supporting this hypothesis have shown that PLTP deficient mice have decreased ability of HDL to inhibit LDL oxidation in artery wall cell cultures.[229] Further studies investigating PLTP will be needed as recent studies have been mainly hypothesis generating and not proving. The finding that PLTP activity is a risk factor for CAD will need to be confirmed by prospective studies. If proven,

PLTP activity may serve as a therapeutic target and be identified as a biomarker for CAD.

CHAPTER IV

CONCLUSIONS

Density gradient ultracentrifugation, capillary electrophoresis, and MALDI-MS, were used to assess two cohorts of serum samples obtained from CAD patients and non-CAD control patients. These methods collectively provided significant clinical information regarding human serum subfractions and their corresponding apolipoproteins, including apolipoprotein composition, electrophoretic mobilities, molecular weights, post-translational modifications, and isoforms.

Methods for obtaining accurate serum high density lipoprotein subfractions using DGU were investigated and improved. This was accomplished through the modification and correction of the defined cut points previously used to obtain the HDL subfractions. Excised serum fractions were re-spun following gravimetric density determination to determine where these cut fractions would appear on the lipoprotein density profile. Upon re-spinning it was discovered that samples were minimally contaminated with neighboring fractions. The excised fractions however, did possess the correct densities despite the minimal contamination. The fact that the subfractions were obtained using a heavy metal solute system, demonstrated feasibility, accuracy, and precision of the method. The dense protein or bottom fraction of the serum sample was found to be composed of HDL_3 and protein in some patients. This fraction contained a volume of less than 60µL and was below the seam of the polycarbonate UC tube making adequate UC separation of this fraction difficult. In the future, it would be beneficial to invest in a longer UC rotor in order to utilize longer UC tubes to achieve a complete and improved separation of this particular region. Likewise, modification of the concentration of the heavy metal Cs_2CdY density gradient solute may also provide a better separation of the HDL subclasses and perhaps even obtain baseline resolution within the HDL subclasses.

Methods for the secondary analysis of subfractions were also developed through the use of commercial apolipoprotein standards. The solid phase extraction protocol with the C_{18} cartridge for delipidation and desalting of the lipoprotein fraction was investigated. Four 100µL 0.1% TFA in acetonitrile elutions were collected to ensure high recovery of the apolipoproteins and verified by MALDI-MS analysis. It was found that only the first 100µL elution contained analytes. In the future, it would be beneficial to investigate other methods of delipidation that would remove more human serum albumin from the samples prior to secondary analysis as this protein was found in substantial quantities in the HDL fractions.

Capillary electrophoresis was used to analyze the serum subfractions from the two patient cohorts and to confirm the elution pattern following solid phase extraction. The protein compositions of the four individual serum subfractions were uniform throughout the patient samples and cohorts. The electrophoretic mobilities of the apolipoproteins were observed for the two cohorts and various serum subfractions. The electrophoretic mobility of apoA-I fluctuated minimally depending on the serum fraction and other sample constituents. There were also no distinct differences observed between the two patient cohorts in terms of electrophoretic mobilities and peak shapes. In the future it would be beneficial to explore the use of larger serum volumes for capillary electrophoresis analysis to better visualize less abundant apolipoproteins and to enable quantitation of apolipoproteins.

Serum fractions were analyzed by MALDI-MS as a qualitative analytical method. Increased sensitivity and resolution were obtained using the Voyager STR instrument. MALDI-MS analysis provided the most valuable information regarding apoC-I. It was observed in the CAD patient samples from every serum subfraction analyzed, that there was a shift in the mass to charge ratio corresponding to apoC-I and apoC-I′, the truncated form of the protein. This shift was approximately 90amu higher than the known mass of this protein, and was not observed in any of the control patient samples, whose apoC-I and apoC-I′ peaks were at the known masses for these two proteins. In addition to the shifting, some of the CAD patients demonstrated further

modifications indicative of oxidative processes. One patient, who did not have diagnosed CAD, displayed MALDI-MS spectra identical to those in the CAD cohort; such a spectral pattern suggests that this individual will develop CAD in the future. These observations strongly supported the hypothesis that some forms of apoC-I are potentially atherogenic. In the future, it would be beneficial to fragment the apoC-I peaks to identify the modifications to this protein as there was variation in the masses of the CAD cohort apoC-I peaks.

The bottom or protein fraction was analyzed by the methodologies described previously to evaluate any loss of apolipoproteins during the ultracentrifugation spin especially considering the contamination of the protein fraction with HDL_3. The capillary electrophoresis and MALDI-MS results of this fraction indicated that it was composed predominantly of human serum albumin. However, apoA-I and apoC-I were also detected in the mass spectra of some CAD patient protein fractions. It was hypothesized that the apolipoproteins present in this fraction were from mixing with the HDL_3 fraction; however, they could also be from apolipoproteins present in the free form or as nascent HDL. Based on the analysis, however, very minimal loss of apolipoproteins occurred during the ultracentrifugation spin.

HDL enriched in apoC-I is an emerging risk factor for CAD. Some subjects with this risk factor have elevated HDL-cholesterol levels and were initially perceived to have a lower risk of CAD based upon their lipid levels. In collaborative studies with Johns Hopkins, it was observed that apoC-I enriched HDL fractions and apoC-I enriched serum induced apoptosis of aortic smooth muscle cells. Interestingly, these apoC-I enriched biological samples were from a CAD patient with the modified apoC-I mass peaks. It is probable that this modification may in turn be influencing the stimulation of one or more membrane bound protein kinases which in turn activate the neutral sphingomyelinase pathway inducing apoptosis of human aortic smooth muscle cells and could be due to a genetic mutation that could compromise apoC-I function.

Transfer protein tests were performed for both cohorts of patients. Cholesteryl ester transfer protein (CETP) rates were lower in the CAD cohort compared to the

control cohort. The CAD patient with the lowest of all CETP transfer rates was also a low birth weight infant with apoC-I enriched HDL. This finding correlated with the known fact that apoC-I is an inhibitor of CETP. It is unknown, however, whether this inhibition contributes to CAD development or is a protective response to halt or decrease CAD development. Phospholipid transfer protein (PLTP) rates were also assessed from the two cohorts and resulted in higher transfer rates in the CAD cohort.

Overall, the wide array of methods utilized provided information that was frequently supported by the other methods. Analyzing the serum subfractions from two cohorts of clinically different patients enabled a closer look into the composition of HDL serum subfractions. Novel apoC-I isoforms were identified through MALDI-MS analysis in all CAD cohort patients. This modified protein also proved to be apoptotic in collaborative clinical studies. Through the incorporation of several methods and studies, it was elucidated that apoC-I has the capability of being modified post-translationally and subsequently influences apoptosis of aortic smooth muscle cells, ultimately leading to the destabilization of atherosclerotic plaque and acceleration of CAD.

REFERENCES

1 Heron, M.; Hoyert, D.; Murphy, S.; Xu, Kochanek, K.; Tejada-Vera, B. *National Vital Statistics Reports*, **2006,** *57.*

2 Wilson, P.; Abbot, R.; Castelli, W. *Arteriosclerosis,* **1988,** *8,* 737.

3 deGoma, E.; deGoma, R.; Rader, D. *J. Am. Coll. Cardiol.* **2008,** *51,* 2199 – 2211.

4 Executive Summary of the Third Report of the National Cholesterol Education Program (NCEP) Expert Panel on Detection, Evaluation, and Treatment of High Blood Cholesterol in Adults (Adult Treatment Panel III). *JAMA*¸ **2001,** *285,* 2486 – 2497.

5 Linsel-Nitschke, P.; Tall, A. *Nature Rev.* **2005,** *4,* 193.

6 Chapman, M.; Assmann, G.; Fruchart, J-C.; Shepherd, J.; Sitori, C. *Curr. Med. Res. Opin.* **2004,** *20,* 1953 – 1268.

7 *High-Density Lipoproteins: From Basic Biology to Clinical Aspects,* Christopher Fielding, editor. Wiley-VCH Verlag GmbH & Co. KGaA, Weinheim, **2007**

8 Brewer, H.; Remaley, A.; Neufeld, E.; Basso, F.; Joyce, C. *Arteriosler. Thromb. Vasc. Biol.* **2004,** *24,* 1755.

9 Toth, P.; *Drugs* (Adis International), pp.1363-1379, **2010**

10 Barter, P; Nicholls, S.; Rye, K.; Anantharamaiah G.; Navab, M.; Fogelman, A. *Circ. Res.* **2004,** *95,* 764 – 772.

11 Mineo, C.; Deguchi, H.; Griffin, J.; Shaul, P. *Circ. Res.* **2006,** *98,* 1352 – 1364.

12 Navab, M.; Hama, S.; Cooke, C.; Anantharamaiah, G.; Chaddha, M.; Jin, L.; Subbanagounder, G.; Faull, K.; Reddy, S.; Miller, N.; Fogelman, A. *J. Lipid Res.* **2000,** *41,* 1481.

13 Kontush, A.; Chapman, M. *Nature* **2006,** *6,* 144 – 153.

14 Navab, M.; Berliner, J.; Subbanagounder, G.; Hama, S.; Lusis, A.; Castellani, L.; Reddy, S.; Shih, D.; Shi, W.; Watson, A.; et al. *J. Lipid Res.,* **2004,** *45,* 993 – 1007.

15 Van Lenten, B.; Navab, M.; Shih, D.; Fogelman, A.; Lusis, A *Trends Cardiovasc. Med.* **2001,** *11,* 155 – 161.

16 Ansell, B. *Am. J. Cardiol.* **2007,** *11,* 3N – 9N.

17 Ansell, B.; Watson, K.; Fogelman, A.; Navab, M.; Fonarow, G. *Am. J. Cardiol.* **2005,** *46,* 1792 – 1798.

18 Nofer, J.; Kehrel, B.; Fobker, M.; Levkau, B.; Assmann, G.; von Eckardstein, A. *Atherosclerosis,* **2002,** *161,* 1 - 16.

19 Yuhanna, I.; Zhu, Y.; Cox, B.; Hahner, L.; Osborne-Lawrence, S.; Marcel, Y.; Anderson, R.; Mendelsohn, M.; Hobbs, H.; Shaul, P. *Nature Med.* **2001,** *7,* 855.

20 Calabresi, L.; Gomaraschi, M.; Franceschini, G. *Arterioscler. Thromb. Vasc. Biol.* **2003,** *23,* 1724 – 1731.

21 Singh, I.; Shishehbor, M.; Ansell, B. *JAMA.,* **2007,** *298,* 786 - 798.

22 Florentin, M.; Liberopoulos, E.; Wierzbicki, A.; Mikhailidis, D. *Curr. Opin. Lipidol.* **2003,** *14,* 159 – 163.

23 Robbesyn, F.; Garcia, V.; Auge, N.; Vieira, O.; Frisach, M.; Salvayre, R.; Negre -Salvayre, A. *FASEB J.,* **2003,** *17,* 743 – 745.

24 Sugano, M.; Tsuchida, K.; Makino, N. *Biochem. Biophys. Res. Commun.* **2000,** *272,* 872 – 876.

25 Drew, B.; Fidge, N.; Gallon-Beumier, G.; Kemp, B.; Kingwell, B. *Proc. Natl. Acad. Sci. USA,* **2004,** *101,* 6999 – 7004.

26 Nofer, J.; van der Gie, M.; Tolle, M.; Wolinska, I.; von Wnuck Lipinski, K.; Baba, H.; Tietge, U.; Godecke, A.; Ishii, I.; Kleuser, B, et al., *J. Clin. Investig.,* **2004,** *113,* 569 – 581.

27 Chen, L.; Mehta, J. *Life Sci.,* **1994,** *55,* 1815 – 1821.

28 Arking, D.; Atzmon, G.; Arking, A.; Barzilai, N.; Dietz, H. *Circ. Res.*, **2005,** *96,* 412 – 418.

29 Barzilai, N.; Atzmon, G.; Schechter, C.; Schaefer, E.; Cupples, A.; Lipton, R.; Cheng, S.; Shuldiner, A. *JAMA,* **2003,** *290,* 2030 – 2040.

30 van der Steeg, W.; Holme, I.; Boekholdt, S.; Larsen, M.; Lindal, C.; Stroes, E.; Tikkanen, M.; Wareham, N.; Faergeman, O.; Olsson, A.; Pedersen, T.; Khaw, K -T.; Kastelein, J. *J. Am. Coll. Cardiol.* **2008,** *51,* 634 – 642.

31 Duffy, D.; Rader, D. *Nature* **2009,** *6,* 455 – 463.

32 Cuchel, M.; Rader, D. *Arterioscler. Thromb. Vasc. Biol.* **2003,** *23,* 1710 – 1712.

33 Borggreve, S.; Hillege, H.; Wolffenbuttel, B.; et al. *J. Clin. Endocrinol. Metabl.* **2006,** *91,* 3382 – 3388.

34 Barter, P.; Caulfied, M.; Eriksson, M.; et al. *N. Engl. J. Med.* **2007,** *357,* 2109 – 2122.

35 Rader, D. *N. Engl. J. Med.* **2007,** *357,* 2180 – 2183.

36 Kastelein, J.; van Leuven, S.; Burgess, L.; et al. *N. Engl. J. Med.* **2007,** *356,* 1620 – 1630.

37 Nissen, S.; Tardif, J.; Nicholls, S.; et al. *N. Engl. J. Med.* **2007,** *356,* 1304 – 1316.

38 Ansell, B.; Navab, M; Hama, S.; et al. *Circulation,* **2003,** *108,* 2751 – 2756.

39 Ansell, B.; Fonarow, G.; Fogelman, A. *Curr. Atheroscler. Rep.* **2006,** *8,* 405 – 411.

40 Navab, M.; Nantharamaiah, G.; Reddy, S.; Van Lenten, B.; Ansell, B.; Hama, S.; Hough, G.; Bachini, E.; Grijalva, V.; Wagner, A.; Shaposhnik, Z.; Fogelman, A. *Ann. Med.* **2005,** *37,* 1 – 6.

41 Fogelman, A. *Nat. Med.* **2004,** *10,* 902 – 904.

42 Rader, D. *J. Clin. Invest.* **2006,** *116,* 3090 – 3100.

43 Duffy, D.; Rader, D. *Circulation* **2006,** *113,* 1140 – 1150.

44 Brown, B.; et al. *N. Engl. J. Med.* **2001,** *345,* 1583 – 1592.

45 Taylor, A.; Sullenberger, L.; Lee, H.; Lee, J.; Grace, K. *Circulation,* **2004,** *110,* 3512 – 3517.

46 Meyers, C.; Kamanna, V.; Kashvap, M. *Curr. Opin. Lipidol.* **2004,** *15,* 659 – 665.

47 Lewis, G.; Rader, D. *Circ. Res.* **2005,** *96,* 1221 – 1232.

48 Brown, M.; Inazu, A.; Hesler, C.; Agellon, L.; ;Mann, C.; Whitlock, M.; Marcel, Y.; Milne, R.; Koizumi, J.; Mabuchi, H.; Takeda, R.; Tall, A. *Nature,* **1989,** *342,* 448 – 451.

49 Inazu, A.; Brown, M.; Hesler, C.; Agellon, L.; Koizumi, J.; Takata, K.; Maruhama, Y.; Mabuchi, H.; Tall, A. *N. Engl. J. Med.* **1990,** *323,* 1234 – 1238.

50 Hovingh, G.; Hutten, B.; Holleboom, A.; Petersen, W.; Rol, P.; Stalenhoef, A.; Zwinderman, A.; de Groot, E.; Kastelein, J.; Kuivenhoven, J. *Circulation,* **2005,** *112,* 879 – 884.

51 [No authors listed] *Circulation,* **2000,** *102,* 21 – 27.

52 Keech, A.; Simes, R.; Barter, P.; Best, J.; Scott, R.; Taskinen, M.; Forder, P.; Pillai, A.; Davis, T.; Glasziou, P.; Drury, P.; Kesaniemi, Y.; Sullivan, D.; Hunt, D.; Colman, P.; d'Emden, M.; Whiting, M.; Ehnholm, C.; Laakso, M. *Lancet,* **2005,** *366,* 1849 – 1861.

53 Birjmohun, R.; Hutten, B.; Kastelein, J.; Stroes, E. *J. Am. Coll. Cardiol.* **2005,** *45,* 185 – 197.

54 Thompson, M. *Nature Clin. Pract. Cardiovasc. Med.* **2004,** *1,* 84 – 89.

55 Chiesa, G.; Sirtori, C.; *Curr. Opin. Lipidol.* **2003,** *14,* 159 – 163.

56 Navab, M.; Anantharamaiah, G.; Reddy, S.; Hama, S.; Hough, G.; Grijalva, V.; Wagner, A.; Frank, J.; Datta, G.; Garber, D.; Fogelman, A. *Circulation,* **2004,** *109,* 3215 – 3220.

57 Brousseau, M.; Diffenderfer, M.; Millar, J.; Nartsupha, C.; Asztalos, B.; Welty, F.; Wolfe, M.; Rudling, M.; Björkhem, I.; Angelin, B.; Mancuso, J.; Digenio, A.; Rader, D.; Schaefer, E. *Arterioscler. Thromb. Vasc. Biol.* **2005,** *25,* 1057 – 1064.

58 Brousseau, M.; Schaefer, E.; Wolfe, M.; Bloedon, L.; Digenio, A.; Clark, R.; Mancuso, J; Rader, D. *N. Engl. J. Med.* **2004,** *350,* 1505 – 1515.

59 Navab, M.; Anantharamaiah, G.; Hama, S.; Hough, G.; Reddy, S.; Frank, J.; Garber, D.; Handattu, S.; Fogelman, A. *Arterioscler. Thromb. Vasc. Biol.* **2005,** *25,* 1426 – 1432.

60 Kang, P.; Izumo, S.; *TRENDS in Molecular Medicine* **2003,** *9,* 177 – 182.

61 Rich, T.; Watson, C.; Wyllie, A.; *Nat. Cell. Biol.* **1999,** *1,* E69 – E71.

62 Savill, J.; Fadok, V. *Nature* **2000,** *407,* 784 – 788.

63 Lee, Y.; Gustafsson, A.; *Apoptosis*, **2009,** *14,* 536 - 548

64 Aharinejad, S.; Andrukhova, O.; Lucas, T., et al *N. Engl. J. Med.* **1996,** *335,* 1182 – 1189.

65 Bryant, D.; Becker, L., Richardson, J., et al *Circulation,* **1998,** *97,* 1375 – 1381.

66 Sayen, M.; Gustafsson, A.; Sussman, M.; et al *Am. J.Physiol. Cell Physiol* **2003,** *284,* C562 – C570.

67 Wang, J.; Silva, J.; Gustafsson, et al N. *Proc. Natl. Acad. Sci*, **2001,** *98,* 4038 - 4043

68 Green, D.R.; Reed, J.C.; *Science* **1998,** *281,* 1322 – 1326.

69 Ashkenazi, A.; Dixit, V.; *Science* **1998,** *281,* 1305 – 1308.

70 Lund-Katz, S.; Liu, L.; Thuahnai, S.; Phillips, M. *Front. Bioscien.* **2003,** *8,* 1044 –1054.

71 Havel, R. ; Eder, H.; Bragdon, J.; *J. Clin. Invest.* **1955,** *34,* 1345 – 1353.

72 Lindgren, F.; Elliott, H.; Gofman, J. *J. Phys. Colloid. Chem.* **1951,** *44,* 80 – 93.

73 Kontush, A.; Chapman, M. *Nat. Clin. Pract. Cardiovasc. Med.* **2006,** *3,* 144 – 153.

74 Kontush, A.; Therond, P.; Zerrad, A.; et al. *Arterioscler. Throb. Vasc. Biol.* **2007,** *27,* 1843 – 1849.

75 Tailleux, A.; Fruchart, J. *Crit. Rev. Clin. Lab Sci.* **1996,** *33,* 163 – 201.

76 Cheung, M.; Brown, B.; Wolf, A.; Albers. J. *J. Lipid Re.* **1991,** *32,* 383 – 394.

77 Asztalos, B.; Horvath, K.; McNamara, J.; et al. *Atherosclerosis*, **2002,** *164,* 361 – 369.

78 Johansson, J.; Carlson, L.; Landou, C.; Hamsten, A. *Arterioscler. Thromb.* **1991,** *11,* 174 – 182.

79 Johnson, J., Ph.D. Dissertation, Texas A&M University, College Station, 2008.

80 Cavelier, C.; Lorenzi, I.; Rohrer, L.; von Eckardstein, A.; *Biochim. Biophys. Acta*, **2006,** *1761,* 655 – 666.

81 Sviridov, D.; Miyazaki, O.; Theodore, K.; Hoang, A.; Fukamachi, I.; Nestel, P. *Arterioscler. Thromb. Vasc. Biol.* **2002,** *22,* 1482 – 1488.

82 Kuivenhoven, J.; Pritchard, H.; Hill, J.; Fohlich, J.; Assman, G.; Kastelein, J. *J. Lipid Res.* **1997,** *38,* 191 – 205.

83 Trigatti, B.; Krieger, M.; Rogotti, A. *Arteriosler. Thromb. Vasc. Biol.* **2003,** *23,* 1732 – 1738.

84 de Grooth, G.; Klerkx, A.; Stroes, E.; Stalenhoef, A.; Kastelein, J.; Kuivenhoven, J. *J. Lipid Res.* **2004,** *45,* 1967 – 1974.

85 Huuskonen, J.; Olkkonen, V.; Jauhiainen, M.; Ehnholm, C. *Atherosclerosis*, **2001,** *155,* 269 – 281.

86 Ishida, T.; Choi, S.; Kundu, R.; Hirata, K.; Rubin, E.; Cooper, A.; Quertermous, T. *J. Clin. Invest.* **2003,** *111,* 347 – 355.

87 Kumpula, L.; Kumpula, J.; Taskinen, M.-R.; Jauhiainen, M.; Kaski, K.; Ala -Korpela, M. *Chem. Phys. Lipids.* **2008,** *155,* 57.

88 Rezaee, F.; Casetta, B.; Levels, J.; Speijer, D.; Meijers, J. *Proteomics*, **2006,** *6,* 721 – 730.

89 Fidge, N. H.; Nestel, P. J.; Ishikawa, T.; Reardon, M.; Billington, T.; **1980,** 29, 643 – 653.

90 Zhang, Y.; Zanotti, I.; Reilly, M.; Glick, J.; Rothblat, G.; Rader, D. *Circulation,* **2003,** *108,* 661 – 663.

91 Plump, A.; Scott, C.; Breslow, J. *Proc. Natl. Acad. Sci.* **1994,** *91,* 9607 – 9611.

92 Tangirala, R.; Tsukamoto, K.; Chun, S.; Usher, D.; Puré, E.; Rader, D. *Circulation,* **1999,** *100,* 1816 – 1822.

93 Nanjee, M.; Doran, J.; Lerch, P.; Miller, N. *Arterioscler. Thromb. Vasc. Biol.* **1999,** *19,* 979 – 989.

94 Nanjee, M.; Doran, J.; Lerch, P.; Miller, N. *J. Lipid Res.* **2001,** *42,* 1586 – 1593.

95 Garber, D.; Datta, G.; Chaddha, M.; Palgunachari, M.; Harna, S.; Navab, M.; Fogelman, A.; Segrest, J.; Anantharamaiah, G. *J. Lipid Res.* **2001,** *42,* 545 - 552.

96 Curry, M. D.; McConathy, W. J.; Fesmire, J. D.; Alaupovic, P.; *Clin. Chem.* **1981,** *27,* 543 – 548.

97 Knott, T.J.; Robertson, M.E.; Priestley, L.M.; Wallis, S.; Scott, J. *Nucleic Acids Res,* **1984,** *12,* 3909 – 3915.

98 Gautier, T.; Masson, D.; De Barros, J. P.; Athias, A.; Gambert, P.; Aunis, D.; Metz-Boutigue, M.H.; Lagrost, L.; *J. Biol. Chem.* **2000,** *275,* 37504 – 37509.

99 Segrest, J.P.; Morrisett, J. D.; Jackson, R. L.; Gotto, A. M. FEBS Lett. *38,* **1974,** 274.

100 Liu, M.; Subbaiah, P.V. *Biochim Biophys Acta* **1993,** *1168*,144-152.

101 Steyrer, E.; Kostner, G. M. *Biochim Biophys Acta* **1988,** *958,* 484-491.

102 Gautier, T.; Masson, D.; Jong, M. C.; Duverneuil, L.; Le Guern, N.; Deckert, V.; Pais de Barros, J.P.; Dumont, L.; Bataille, A.; Zak, Z.; Jiang, X. C.; Tall, A. R.; Havekes, L. M.; Lagrost, L.; *J. Biol. Chem.* **2002,** *277,* 31354 – 31363.

103 Kushwaha, R. S.; Hasan, S. Q.; McGill, H. C. Jr.; Getz, G. S.; Dunham, R. G.; Kanda, P. *J. Lipid Res.* **1993,** *34,* 1285 – 1297.

104 Kwiterovich, P.O. Jr.; Cockrill, S.L.; Virgil, D.G.; Garrett, E.S.; Otvos, J.; Knight-Gibson, C.; Alalupovic, P.; Forte, T.; Zhang, L.; Farwig, Z.N.; Macfarlane, R.D.; *JAMA*, **2005,** *293,* 1891 - 899.

105 Godfrey, K.M.; Barker, D.J.; *Am. J. Clin. Nutr.* **2000,** *71,* 1344S - 1352S.

106 Kolmakova, A.; Kwiterovich, P.; Virgil, D.; Alauopovic, P.; Knight-Gibson, C.; Martin, S.F.; *J. Lipid Res.**1993,** 34,* 1285 – 1297.

107 Buchko, G.; Rozek, A.; Zhong, Q.; Cushley, R. *Pept. Res.* **1995,** *2*, 86 – 94.

108 Shulman, R.; Herbert, P.; Wehrly, K.; Fredrickson, D. *J. Biol. Chem.* **1975,** *1*, 182 – 190.

109 Segrest, J.P.; DeLoof, H.; Dohlman, J.G.; Brouilette, C.G.; Anantharamaiah, G.M. *Proteins: Struct. Funct. Genet.* **1990,** *8*, 103-117.

110 Segrest, J.P.; Jones, M.K.; de Loof, H.; Brouillette, C.G.; Venkatachalapathi, Y.V.; Anantharamaiah, G.M. *J. Lipid Res.* **1992,** *33*, 141-166.

111 Rozek, A.; Buchko, G.; Kanda, P.; Cushleyi, R. *Protein Science*, **1997,** *6*, 1858 – 1868.

112 Davidson, P.J.; Norton, P.; Wallis, S.C.; Gill, L.; Cook, M.; Willamson, R.; Humphries, S.R.; *Biochem Biophys Res Comm.*, **1986,** *136*, 876 – 884.

113 Myklebost, O.; Rogne, S. *Hum Gen* **1986,** *73*, 286 – 289.

114 Lauer, S.; Walker, D.; Elshourbagy, N.A.; Reardon, C.A.; Levy-Wilson, B.; Taylor, J.M. *J. Biol. Chem.* **1988,** *263*, 7277 – 7286.

115 Simonet, W.S.; Bucay, N.; Lauer, S.J.; Taylor, J.M.; *J. Biol. Chem.* **1995,** *270* , 26278 – 26281.

116 Dumon, M.F.; Clerc, M.; *Clin Chim Acta* **1986,** *157*, 239-248.

117 Xu, Y.; L.;Berglund, R.; Ramakrishnan, R.; Mayeux, R.; Ngai, C.; Holleran, S.; Tycko, B.; Leff, T.; Shachter, N.S. *J. Lipid Res*, **1999,** *40*, 50 – 58.

118 Berbee, J.F.P.; van der Hoogt, C.C.; Sundararaman, D.; Havekes, L.; Rensen, P.C. *J. Lipid Res.* **2005,** *46*, 297 – 306.

119 Jonas, A.; *Biochim. Biopys. Acta.* **2000,** *1529*, 245 – 256.

120 Rader, D.; Ikewai, K.; Duverger, N.; Schmidt, H.; Pritchard, H.; Frohlich, J.; Clerch, M.; Dumon, M.;J Fairwell, T.; Zech, L. *J. Clin. Invest.* **1994,** *93*, 321 – 330.

121 Hoeg, J.; Santamarina-Fojo, S.; Bérard, A.; Cornhill, J.; Herderic, E.; Feldman, S.; Haudenschild, C.; Vaisman, B.; Hoyt, R.; Demosky, S.; Kauffman, R.; Hazel, C.; Marcovina, S.; Brewer, H. *Circulation*, **1996,** *93*, 11448 – 11453.

122 Foger, B.; Chase, M.; Amar, M.; Vaisman, B.; Shamburek, R.; Paigen, B.; Fruchart-Najib, J.; Paiz, J.; Kock, C.; Hoyt, R.; Brewer, H.; Santamarina-Fojo, S. *J. Biol. Chem.* **1999,** *274,* 36912 – 36920.

123 Barter, P.; Brewer, H.; Chapman, M.; Hennekens, C.; Rader, C.; Tall, A. *Arterioscler. Thromb. Vasc. Biol.* **2003,** *23,* 160 – 167.

124 Tato, F.; Vega, G.L.; Grundy, S.M.; *Arterioscler. Thromb. Vasc. Biol.* **1997,** *17,* 56.

125 McPherson, R.; Mann, C.J.; Tall, A.R.; Hogue, M.; Martin, L.; Milne, R.W.; Marcel, Y.L. *Arterioscler. Thromb.* **1991,** *11,* 797.

126 Agerholm-Larsoen, B.; Nordestgaard, B.G.; Steffensen, R.; Jensen, G.; Tybjaerg -Hansen, A. *Circulation,* **2000,** *101,* 1907.

127 Tall, A.R. *Annu. Rev. Nutr.* **1998,** *18,* 297.

128 Lagrost, L.; Athias, A.; Gambert, P.; Lallemant, C. *J. Lipid Res.* **1994,** *35,* 825.

129 Qin, S.; Kawano, K.; Bruce, C.; Lin, M.; Bisgaier, C.L.; Tall, A.R.; Jiang, X.C. *J. Lipid Res.* **2000,** *41,* 269.

130 Hailman, E.; Albers, J.; Wolfbauer, G.; Tu, A.-T.; Wright, S.D. *J. Biol. Chem.* **1996,** *271,* 172.

131 Settasatian, N.; Duong, M.; Curtiss, L.K.; Ehnhholm, C.; Jauhiainen, M.; Huuskonen, J.; Rye, K.-A. *J. Biol. Chem.* **2001,** *276,* 26898.

132 Zheng, L.; Nukuna, B.; Brennan, M.; Sun, M.; Goormastic, M.; Settle, M.; Schmitt, D.; Fu, X.; Thomson, L.; Fox, P. et al. *J. Clin. Invest.* **2004,** *114,* 529 – 541.

133 Valiyaveettil, M.; Kar, N.; Ashraf, M., et al. *Blood,* **2008,** *111,* 1962 – 1971.

134 Nagano, Y.; Arai, H.; Kita, T. *Proc. Natl. Acad. Sci,* **1991,** *125,* 39 – 46.

135 Favari, E.; ;Lee, M.; Calabresi, L, et al. *J. Biol. Chem.* **2004,** *279,* 9930 – 9936.

136 Jaross, W.; Eckey, R.; Menschikowski, M. *Eur. J. Clin. Invest.* **2002,** *32,* 383 – 393.

137 Hirowatari, Y.; Tsunoda, Y.; Ogura, Y.; Homma, Y. *Atherosclerosis*, **2009,** *204,* e52 – e57.

138 Yee, M.; Pavitt, D.; Tan, T.; Venkatesan, S.; Godsland, I.; Richmond, W.; Johnston, D. *J. Lipid Res.* **2008,** *49,* 1364 – 1371.

139 Laker, M.F.; *Clin. Endocrinol. Metab.* **1990,** *4,* 693 – 718

140 deLalla, O.; Harold, E.; Gofman, J. *Meth. Biochem. Analysis.* Interscience Publishers Inc., 1954

141 Kane, J.; Kunitake, S. *Lipoproteins in Health in Disease* **1999,** 465 – 471.

142 Skinner, E. In, *Lipoprotein Analysis: A Practical Approach*, Oxford University Press, **1992,** 85 – 118.

143 Hallberg, C.; Haden, M.; Bergstrom, Hansson, G.; Pettersson, K.; Westerlund, C.; Bondkjers, G.; Lindqvist-Ostlund, A.; Camejo, B. *J. Lipid Res.* **2005,**

144 Bergmeier, C.; Siemeier, R.; Gross, W.; *Clin Chem.* **2004,** *50,* 2309 – 2315.

145 Nauck, M.; Warnick, G.; Rifai, N. *Clin. Chem.* **2002,** *48,* 236 – 254.

146 Foreman J.; Karlin, J.; Edelstein, C.; Juhn, D.; Rubenstein, A.; Scanu, A. *J. Lipid Res.* **1977,** *18,* 759 – 767.

147 Cruzado, I.; Cockrill, S.; McNeal, C.; Macfarlane, R. *J. Lipid Res.* **1998,** *39,* 205 –217.

148 Ford, T.; Graham, J.; Rickwood, D. *Anal. Biochem,* **1982,** *123,* 23 – 31.

149 Hosken, B.; Cockrill, S.; Macfarlane, R. *Anal. Chem.* **2005,** *77,* 200 - 207

150 Johnson, J.; Bell, N.; Donahoe, E.; Macfarlane, R. *Anal. Chem.* **2005,** *77,* 7054 – 7061.

151 Ifft, J.; Voet, D.; Vinograd, J. *J. Phys. Chem.* **1961,** *65,* 1138 – 1145.

152 Corthals, G.; Gygi, S.; Aebesold, R.; Patterson, S. *Proteome Research* **2000,** 197 – 227.

153 Patterson, S.; Aebersold, R. *Electrophoreis* **1995,** *16,* 1791 – 1814.

154 Gevaert, K.; Vandekerckhove, J. *Electrophoresis* **2000,** *21,* 1145 – 1154.

155 Strupat, K. *Meth. Enzymol.* **2004,** *405,* 1 – 36.

156 Heller, M.; Stalder, D.; Schlappritzi, E.; Hayn, G.; Matter, U.; Haeberli, A. *Proteomics,* **2005,** *5,* 2619 – 2630.

157 Karlsson, H.; Leanderson, C.; Tagesson, C.; Lindahl, M. *Proteomics,* **2005,** *5,* 551– 565.

158 Karlsson, H.; Lindqvist, H.; Tagesson, C.; Lindahl, M. *J. Proteome Res.* **2006,** *5,* 2685 – 2690.

159 Mancone, C.; Amicone, G.; Fimia, E.; Bravo, M. Piacentini, M.; Tripodi, M.; Alonzi, T. *Proteomics,* **2007,** *6,* 721 – 730.

160 Heinecke, J. *Curr. Opin. Lipidol.* **1997,** *8,* 268 – 274.

161 Bergt, C.; Pennathur, S.; Fu, X.; Byun J.; O'Brien, K.; McDonald, T.; Singh, P.; Anantharamaiah, G.; Chait, A.; Brunzell, J. et al. *Proc. Natl. Acad. Sci.* **2004,** *101,*13032 – 13037.

162 Gaut, J.; Yeh, G.; Tran, H.; Byun, J.; Henderson . J.; Richter, G.; Brennan, M.; Lusis, A.; Belaaouaj, A.; Hotchkiss, R., et al. *Proc. Natl. Acad. Sci.* **2001,** *98,* 11961 – 11966.

163 Daugherty, A.; Dunn, J.; Rateri, D.; Heinecke, J. *J. Clin. Invest.* **1994,** *94,* 437 – 444.

164 Shao, B.; Oda, M.; Bergt, C.; Fu, X.; Green, P.; Brot, N.; Oram J.; Heinecke, J. *J.Biol. Chem.* **2006,** *281,* 9001 – 9004.

165 Shao, B.; Pennathur, S.; Pagani, I.; Oda, M.; Wiztum, J.; Oram, J.; Heinecke, J. *J. Biochem. Molec. Biol.* **2010**

166 Hussain, M.; Zannis, V. *Biochemistry,* **1990,** *29,* 209 – 217.

167 Zannis, V.; McPherson, J.; Goldberger, G.; Karathanasis, S.; Breslow, J. *J. Biol. Chem.* **1984,** *259,* 5495 – 5499.

168 Scanu, A.; Byrne, R.; Edelstein, C. *J. Lipid Res.* **1984,** *25,* 1593 – 1601.

169 Bondarenko, P.; Farwig, Z.; McNeal, C.; Macfarlane, R. *International Journal of Mass Spectrometry,* **2002,** *219,* 671 –680.

170 Wroblewski, M.; Wilson-Grady, J.; Martinez, M.; Kasthuri, R.; McMillan, K.; Flood-Urdangarin, C.; Nelsestuen, G. *FEBS Journal,* **2006,** *273,* 4707 – 4715.

171 Puppione, D.; Ryan, C.; Bassilian S.; Souda, P.; Xiao, X.; Ryder, O.; Whitelegge, J. *Comp. Biochem. Phys.* **2010,** *5,* 73 – 79.

172 Lehmann, R.; ;Liebich, H.; Grubler, G.; ;Voelter, W. *Electrophoresis* **1995,** *16,* 998 – 1001.

173 Schmitz, G.; Mollers, C.; Richter, V. *Electrophoresis* **1997,** *18¸1807 – 1813.*

174 Stocks, J. ; Miller, N. *J. Lipid Res.* **1998,** *39,* 1305 – 1309.

175 Stocks, J. ; Nanjee, M.; Miller, N.; *J. Lipid Res.* **1998,** *39,* 218 – 227.

176 Tadey, T.; Purdy, W. *J. Chromatogr.* **1993,** *652,* 131 – 138.

177 Watkins, L. K.; Bondarenko, P. V.; Barbacci, D. C.; Song, S.; Cockrill, S. L.; Russell, D. H.;Macfarlane, R. D. *J. Chrom. A* **1999,** *183 – 189.*

178 Cruzado, I. D.; Song, S.; Crouse, S. F.; O'Brien, B. C.; Macfarlane, R. D. *Anal. Biochem.* **1996,** *243,* 100 – 109.

179 Cruzado, I. D.; Hu, A. Z.; Macfarlane, R. D. *J. Cap. Elec.* **1996,** *1,* 25 – 29.

180 Warnick, G. R.; Benderson, J.; Albers, J. J. *Clin. Chem.* **1982,** 1379 – 1388.

181 Smith, L, C.; Massey, J. B.; Sparrow, J. T.; Gotto, A. M. Jr.; Pownall, H. J.; *Supramolecular Structure and Function* (G. Pifat and J. N. Herak, eds.), p.210. Plenum, New York, 1983.

182 Barbacci, L.; Ph.D Dissertation, Department of Chemistry, Texas A&M University, College Station, TX, **2000**

183 Nagano, Y.; Arai, H.; Kita, T. *Proc. Natl. ACAD. Sci.* **1991,** *88,* 6457 – 6461.

184 Salmon, S.; Maziere, C.; Auclair, M.; Theron, L.; Santus, R.; Maziere, J. *Biochim. Biophys, Res. Commun.* **1992,** *1125,* 230 – 235.

185 Shao, B.; Chongren, T.; Heinecke, J.; Oram, J. *J. Lipid. Res.* **2010,** *51*, 1849 – 1858.

186 Hortin, G., *Clinical Chemistry*, **2006,** *52*, 1223 – 1237.

187 Johnson, J.; Henriquez, R.; Tichy, S.; Russell, D.; McNeal, C.; Macfarlane, R. International Journal of Mass Spectrometry, **2007,** 268, 227 – 233.

188 Hortin, G.; Remaley, A., *Clinical Proteomics*, **2006,** *2*, 103 – 115.

189 Hubbard, M.J.; Cohen, P. *Trends Biochem. Sci.* **1993,** *18*, 172 – 177.

190 Cohen, P.; *Trends Biochem. Sci.* **1992,** *17*, 408 – 413.

191 Carr, S.; Annan, R.; Huddleston, M. *Methods in Enzym.* **2005,** *405*, 82 – 115.

192 Eck, M.J. *Curr. Biol.* **1995,** *3*, 421 – 429.

193 Pawson, T. *Nature*, **1995,** *373*, 573 – 580.

194 Witze, E.S; Old, W.M; Resing, K.A.; Ahn, N. *Nature Methods*, **2007,** *4*, 798 – 806.

195 Seo, J.; Lee, K.-J. *J. Biochem. Molec. Biol.* **2004,** *37*, 35 – 44.

196 Schoneich, C. *Biochim Biophys Acta*, **2005,** *1703*, 111 – 119.

197 Baldwin, M.; *Molecular & Cellular Proteomics*, **2004,** *3.1*, 1 - 9

198 Vidal, C.; Kirchner, G.; Sewing, K.-F. *J. Amer. Society Mass Spec*, ***1998,*** *9*, 1267 – 1274.

199 Medzihradszky, K.F.; Darula, Z.; Perlson, E.; Fainzilber, M.; Chalkley, R.J.; Ball, H.; Greenbaum, D.; Bogyo, M.; Tyson, D.R.; Bradshaw, R.A. *Mol. Cell Proteomics*, **2004,** *5*, 429 – 440.

200 Medzihradszky, K.F.; Darula, Z.; Perlson, E.; Fainzilber, M.; Chalkley, R.J.; Ball, H.; Greenbaum, D.; Bogyo, M.; Tyson, D.R.; Bradshaw, R.A. *Mol. Cell Proteomics*, **2004,** *5*, 429 – 440.

201 Beavis, R.; Chait, B. *Rapid Commun. Mass. Spectrom.* **1989,** *3*, 432.

202 Beavis, R.; Chait, B. *Anal. Chem.***1990,** *62*, 1836.

203 Loboda, A.; Chernushevich, I. *Internationa Journal of Mass Spectrometry,* **2005,** *240,* 101-105.

204 Moore, D.; McNeal, C.; Macfarlane, R. *Biochem. Biophys. Res. Comm. 2011, 404,* 1034 – 1038.

205 Libby, P.; Ridker, P.; Maseri, A.; *Circulation.* **2002,** *105,* 1135.

206 Kolmakova, A.; ;Kwiterovich, J.; Virgil, D.; Alaupovic, P.; Knight-Gibson, C.; Martin, S.; Chatterjee, S. *Arterioscler. Thromb. Vasc. Biol.* **2004,** *24,* 264.

207 Sugaon, M.; Maikino, N.; Sawada, S.; Otsuka, S.; Watanabe, M.; Okamoto, H.; Kamada, M.; Mitshushima, A. *J. Biol. Chem.* **1998,** *273,* 5033 – 5036.

208 Rittershaus, C.; Miller, D.; Thomas, L.; Picard, M.; Honan, C.; Emmett, C.; Pettey, C.; Adari, H.; Hammond, R.; Beattie, D.; Callow, A.; Marsch, H.; Ryan, U. *Arterioscler. Thromb. Vasc. Biol.* **2000,** *20,* 2106 – 2112.

209 Okamoto, H.; Yonemori, F.; Wakitani, K.; Minowa, T.; Maeda, K.; and Shinkai, H. *Nature,* **2000,** *406,* 203 – 207.

210 De Grooth, G.; Kuivenhoven, J.; Stalenhoef, A.; deGraaf, J.; Zwinderman, A.; Posma, J.; van Tol, A.; Kastelein, J. *Circulation,* **2002,** *105,* 2159 – 2165.

211 Clark, R.; Sutfin, T.; Ruggeri, R.; Willaer, A.; Sugarman, E.; Magnus-Aryitey, G.; Cosgrove, P.; Sand, T.; Wester, R.; Williams, J.; Perlman, M.; Bamberger, M. *Arterioscler. Thromb. Vasc. Biol.* **2004,** *24,* 490 – 497.

212 Guyard-Dangremont, V.; Lagrost, L.; Gambert, P. *J. Lipid Res.* **1994,** *35,* 982 – 992.

213 Cho, K.; Lee, J.; Choi, M.; lCho, J.; Lim, J.; Park, Y. *Biochim. Biophys. Acta.* **1998,** *1391,* 133 – 144.

214 Wang, X.; Driscoll, D.; Morton, R. *J. Biol. Chem.* **1999,** *274,* 1814 – 1820.

215 Gautier, T.; Masson, D.; Pais de Barros, J-P.; Athias, A.; Gambert, P.; Aunis, D.; Metz-Boutigue, M-H.; Lagrost, L. *J. Biol. Chem.* **2000,** *275,* 37504 – 37509.

216 Nishida, H.; Arai, H.; Nishida, T. *J. Biol. Chem.* **1993,** *268,* 16352 – 16360.

217 Masson, D.; Athias, A.; Lagrost, L. *J. Lipid. Res.* **1996,** *37,* 1579 – 1590.

218 Swenson, T.; Broacia, R.; Tall, A. *J. Biol. Chem.* **1998,** *263,* 5150 – 5157.

219 Swenson, T.; Hesler, C.; Brown, M.; Quinet, E.; Trotta, P.; Haslanger, M.; Gaeta, F.; Marcel, Y.; Mine, R.; Tall, A. *J. Biol. Chem.* **1989,** *264,* 14318 – 14326.

220 Tall, A.; *J. Lipid Res.* **1986,** *27,* 361 – 367.

221 Hope, H.; Heuvelman, D.; Duffin, K.; Smith, C.; Zablocki, J.; Schilling, R.; Hegde, S.; Lee, L.; Witherbee, B.; Baganoff, M.; Bruce, C.; Tall, A.; Krul, E.; Glenn, K.; Connolly, D. *J. Lipid Res.* **2000,** *41,* 1604 – 1614.

222 Epps, D.; Greenlee, K.; Harris, J.; Thomas, E.; Castle, C.; Fisher, J.; Hozak, R.; Marchke, C.; Melchior, G.; Kezdy, R.; *Biochemistry,* **1995,** *34,* 12560 – 12569.

223 Dumont, L.; Gautier, T.; Pais de Barros, J-P.; Laplanche, H.; Blache, D.; Ducoroy, P.; Fruchart, J.; Fruchart, J-C.; Gambert, P.; Masson, D.; Lagrost, L. *J. Biol. Chem.* **2005,** *280,* 38108 – 38116.

224 Ihm, J.; Quinn, D.; Bush, S.; Chataing, B.; Harmony, J. *J. Lipid. Res.* **1982,** *23,* 1328 – 1341.

225 Barter, P; Jones, M. *J. Lipid Res.* **1980,** *21,* 238 – 249.

226 Desrumaux, C.; Athias, A.; Masson, D.; Gambert, P.; Lallemant, C.; Lagrost, L. *J.Lipid Res.* **1998,** *39,* 131 – 142.

227 Cheung, M.C.; Wolfbauer, G.; Kennedy, H.; Brown, B.C.; Albers, J.J. *Biochim Biophys Acta* **2001,** *1537,* 117 – 124.

228 Huuskonen, J.; Ekstrom, M.; Tahvanainen, E.; Vainio, A.; Metso, J.; Pussinen, P.; Ehnholm, C.; Olkkonen, V.M.; Ehnholm, C.; Jauhiainen, M.; Hattori, H. *J. Lipid Res.* **2000,** *151,* 451 – 461.

229 Shlitt, A.; Bickel, C.; Thumma, P.; Blankenberg, S.; Rupprecht, H.; Meyer, J.; Jiang, X-C. *Arteriosler. Thromb. Vasc. Biol.* **2003,** *23,* 1857 – 1862.

230 Tall, A.R.; Krumholz, S.; Olivecrona, T.; Deckelbaum, R.J. *J. Lipid Res.* **1985,** *26,* 842 – 851.

231 Tall, A.R.; Abreu, E.; Shuman, J. *J. Biol. Chem.* **1983,** *258,* 2174- 2180.

232 Jauhiainen, M.; Metso, J.; Pahlman, R.; Blomqvist, S.; van Tol, A.; Ehnohlm, C. *J. Biol. Chem.* **1993,** *268,* 4032 – 4036.

233 Tu, A.Y.; Nishida, H.I.; Nishida, T. *J. Biol. Chem.* **1993,** *268,* 23098 – 23105.

234 Albers, J.J.; Wolfbauer, G.; Cheung, M.C.; Day, J.R.; Ching, A.F.; Lok, S.; Tu, A.-Y. *Biochim. Biophys. Acta,* **1995,** *1258,* 27 – 34.

235 Cheung, M.C.; Wolfbauer, G.; Deguchi, H.; Fernadez, J.; Griffin, J.; Albers, J. *Biochim. Biophys. Acta* **2009,** *1791,* 206 – 211.

236 von Eckardstein, A.; Jauhiainen, M.; Huang, Y.; Metso, J.; Langer, C.; Pussinen, P.; Wu, S.; Ehnolm, C.; Assman, G. *Biochim. Biophys. Acta,* **1996,** *1301,* 255 – 262.

237 Nishida, H.I.; Nishida, T. *J. Biol. Chem.* **1997,** *272,* 6959 – 6964.

238 Cheung, M.C.; Brown, B.G.; Larsen, E.K.; Frutkin, A.; O'Brien, K.; Albers, J. *Biochim. Biophys. Acta* **2006,** *1762,* 131 – 137.

239 Desrumaux, C.; Deckert, V.; Athias, A.; Masson, D.; Lizard, G.; Palleau, V.; Gambert, P.; Lagrost, L. *FASEB J.* **1999,** *13,* 883 – 892.

240 Burton, G.W.; Hughes, L.; Ingold, K.U. *J. Amer. Chem. Soc.* **1983,** *105,* 5950 – 5951.

241 Keaney, J.F.; Gaziano, J.M.; Xu, A.; Frei, B.; Curran-Celentano, J.; Shwaery, G.T.; Loscalzo, J.; Vita, J.A. *PNAS* **1993,** *90,* 11880 – 11884.

242 Esterbauer, H.; Waeg, G.; Puhl, H.; Dieber-Rotheneder, M.; Tatzber, F. *EXS* **1992,** *62,* 145 – 157.

243 Barlage, S.; Frohlich, D.; Bottcher, A.; Jauhiainen, M.; Muller, H.P.; Noetzel, F.; Rothe, G.; Schutt, C.; Linke, R.P.; Lackner, K.J.; Ehnholm, C.; Schmitz, G. *J. Lipid Res.* **2001,** *42,* 281- 290.

244 Pussinen, P.J.; Metso, J.; Malle, E.; Bsrlage, S.; Palosuo, T.; Sattler, W.; Schmitz,G.; Jauhiainen, M. *Biochim. Biophys. Acta* **2001,** *1533,* 153 – 163.

245 Ross, R. *N. Engl. J. Med.* **1999,** *340,* 115 – 126.

246 O'Brien, K.D.; Vuletic, S.; McDonald, T.O.; Wolfbauer, G.; Lewis, K.; Tu, A. -Y.; Marcovina, S.; Wight, T.N.; Chait, A.; Albers, J.J. *Circulation* **2003,** *108,* 270 – 274.

247 Dullaart, R.P.; Hoogenberg, K.; Dikkeschei, B.D.; van Tol, A. *Arterioscler. Thromb.* **1994,** *14,* 1581 – 1585.

248 Mero, N.; van Tol, A.; Scheek, L.M.; van Gent, T.; Labeur, C.; Rosseneu, M.; Taskinen, M.R. *J. Lipid Res.* **1998,** *39,* 1493 – 1502.

249 Liinamaa, M.J.; Hannuksela, M.L.; Kesaniemi, Y.A.; Savolainen, M.J. *Arterioscler. Thromb. Vasc. Biol.* ***1997,*** *17,* 2940 – 2947.

250 Van Haperen, R.; van Tol, A.; Vermeulen, P.; Jauhiainen, M.; van Gent, T.; van den Berg, P.; Ehnholm, S.; Grosveld, F.; van der Kamp, A.; de Crom, R. *Arterioscler. Thromb. Vasc. Biol.* **2000,** *20,* 1082 – 1088.

251 Jiang, X.C.; Qin, S.; Qiao, C.; Kawano, K.; Lin, M.; Skold, A.; Xiao, X.; Tall, A.R. *Nat. Med.* **2001,** *7,* 847 – 852.

252 Jiang, X.C.; Qin, S.; Min, L.; Schneider, M.; Tall, A.R.; Lagrost, L. *Circulation* **2001,** 104:II-232.

253 Qin, S.; Tall, A.R.; Jiang, X.C. *Circulation,* **2001,** 104:II-329.

VITA

D'Vesharronne J. Moore graduated *cum laude* from Texas Southern University in May 2006 with a B.S. in chemistry. In the fall of 2006 she joined the Laboratory for Cardiovascular Chemistry under the direction of Dr. Ronald Macfarlane. Her research involved the development of methodologies for the isolation and characterization of high density lipoprotein subfractions using density gradient ultracentrifugation combined with immunoprecipitation, capillary electrophoresis, and mass spectrometry. She defended her research in the spring of 2011 and received her Ph.D. in the spring of 2011.

Her previous undergraduate research experiences include the Texas Southern University NASA University Research Center where she used inductively coupled plasma-mass spectrometry (ICP-MS) to investigate drinking water trace metal contamination; an internship with the NASA Johnson Space Center where she conducted further analyses of local drinking water metal contamination; and an REU internship with the Texas Center for Superconductivity and the University of Houston, where she conducted inorganic crystallographic synthesis of mixed-valent gold bromide perovskites. She presented her research annually at the American Chemical Society (ACS), Texas Academy of Science, and National Organization for the Professional Advancement of Black Chemists and Chemical Engineers (NOBCChE) conferences.

Her teaching experience includes the First Year Chemistry Program at Texas A&M University where from 2006 to 2011, she served as teaching and instructional assistants, taught general chemistry I, II, and engineering chemistry laboratories, developed curriculum and assessments for general chemistry II laboratory courses, and instructed and supervised teaching assistants.

Her awards include the Louis Stokes Alliance for Minority Participation (LSAMP) Scholarship, NASA Texas Space Grant Consortium Scholarship and Fellowship, Texas A&M University Graduate Diversity Fellowship, CenterPoint Energy Scholarship, and Texas A&M University Teaching Excellence Award. In June 2009 she presented her research at the XV International Symposium on Atherosclerosis.

She can be reached at TAMU Chemistry MS 3255 College Station, TX 77843.